NASA Contractor Report 177970

MECHANICAL PROPERTIES TESTING OF CANDIDATE POLYMER MATRIX MATERIALS FOR USE IN HIGH PERFORMANCE COMPOSITES

Richard S. Zimmerman and Donald F. Adams

UNIVERSITY OF WYOMING
Laramie, Wyoming

Grant NAGI-277
December 1985

National Aeronautics and Space Administration

Langley Research Center
Hampton, Virginia 23665

PREFACE

This technical report presents the results of the second year of effort on NASA-Langley Research Grant NAG-1-277. The NASA-Langley Technical Monitor is Dr. Norman J. Johnston of the Materials Division.

All work was performed by the Composite Materials Research Group (CMRG) within the Department of Mechanical Engineering at the University of Wyoming. Co-Principal Investigators were Mr. Richard S. Zimmerman, Staff Engineer, and Dr. Donald F. Adams, Professor.

The finite element micromechanics computer runs were performed by Mr. Jayant M. Mahishi, Ph.D. student. Making major contributions to the program were Edward D. Schafer and Craig H. Johnson, M. S. students, and Eric Q. Lewis, Jeffrey A. Kessler, Thomas A. Ohnstad, and Bruce L. Jahnke, undergraduate students. All are members of the Composite Materials Research Group.

The authors are specially indebted to Dr. Paul Zoller of E. I. duPont de Nemours Co., Wilmington, Delaware, who performed the neat resin bulk modulus measurements reported here. His cooperation is greatly appreciated. The assistance and technical advice of the NASA-Langley Technical Monitor, Dr. Norm Johnston, is likewise greatly appreciated.

Use of commercial products or names of manufacturers in this report does not constitute official endorsement of such products or manufacturers, either expressed or applied, by the National Aeronautics and Space Administration.

TABLE OF CONTENTS

TABLE OF CONTENTS (CONTINUED)

TABLE OF CONTENTS (CONTINUED)

SECTION 1

SUMMARY

This study represents a continuation of NASA-Langley Grant No. NAG-1-277 involving the investigation of unreinforced (neat) resin properties and their relations to composite material properties. This second-year effort was performed in a manner similar to that of the first year [1]. That is, four resin systems were chosen for detailed mechanical property characterization. These four resin systems were Hexcel HX-1504, an epoxy, Narmco 5245-C, a bismaleimide/epoxy blend, American Cyanamid CYCOM 907 (formerly BP 907), a multi-phase epoxy, and Union Carbide ERX-4901A cured with methylenedianaline (MDA), an epoxy. The first two resins listed were chosen as being potential candidates in the ACEE Program. The other two resins were chosen because each possesses a unique material property. All neat resins were supplied in uncured bulk form by NASA-Langley and were cast into various shapes as required to prepare test specimens for use in this study. Resin casting was performed using the same basic techniques developed during the previous five years of work in this area by the CMRG. These processes are discussed in detail in the first-year report [1].

Comprehensive mechanical characterization was completed on all four neat resin systems, at six different environmental conditions. Dry and moisture-saturated specimens were tested at 23°C, 82°C, and 121°C. The first-year study [1] included elevated temperature testing at slightly different temperatures, viz, 23°C, 54°C, and 82°C. The higher temperatures used in the present study were selected to more closely characterize these neat resins near their curing temperatures, to provide a more accurate representation of their stress-strain behavior at elevated

temperatures. Testing performed during the present year included tensile, torsional shear, Iosipescu shear, Single-Edge Notched-Bend (SEN) fracture toughness, coefficient of thermal expansion, and coefficient of moisture expansion tests. These various tests were performed to allow a comprehensive comparison of material properties for all resin systems studied. A linear regression computer curve-fit of the data was also performed for all properties, for all resins, to provide material property input data for the finite element micromechanics computer program. This permitted the prediction of composite material response for any hygrothermal condition desired.

Whenever possible, comparisons were made between all eight resin matrix systems tested to date, i.e., the Hercules 2220-1, 2220-3, and 3502, and the Fibredux 914 epoxies of the first-year study, and the four resins of current interest, viz, Hexcel HX-1504, Narmco 5245-C, American Cyanamid CYCOM 907, and Union Carbide ERX-4901A (MDA). Where appropriate, available data for Hercules 3501-6 epoxy were also utilized. Some of the more important comparisons are summarized here in barchart form in Figures 1 through 4 and in Tables 1 through 6, as discussed in the following paragraphs.

The two ACEE candidate resin systems, the HX-1504 and the 5245-C, performed extremely well overall, at all test conditions, being comparable to the resin systems of the first-year study. Additional tensile testing of the first-year resin systems, at 121°C, was also performed, to permit full comparisons with the present-year resin systems. The CYCOM 907 and ERX-4901A (MDA) were not included in the comparisons in most cases due their special nature of being "laboratory model resins". Properties that were compared for these two resins,

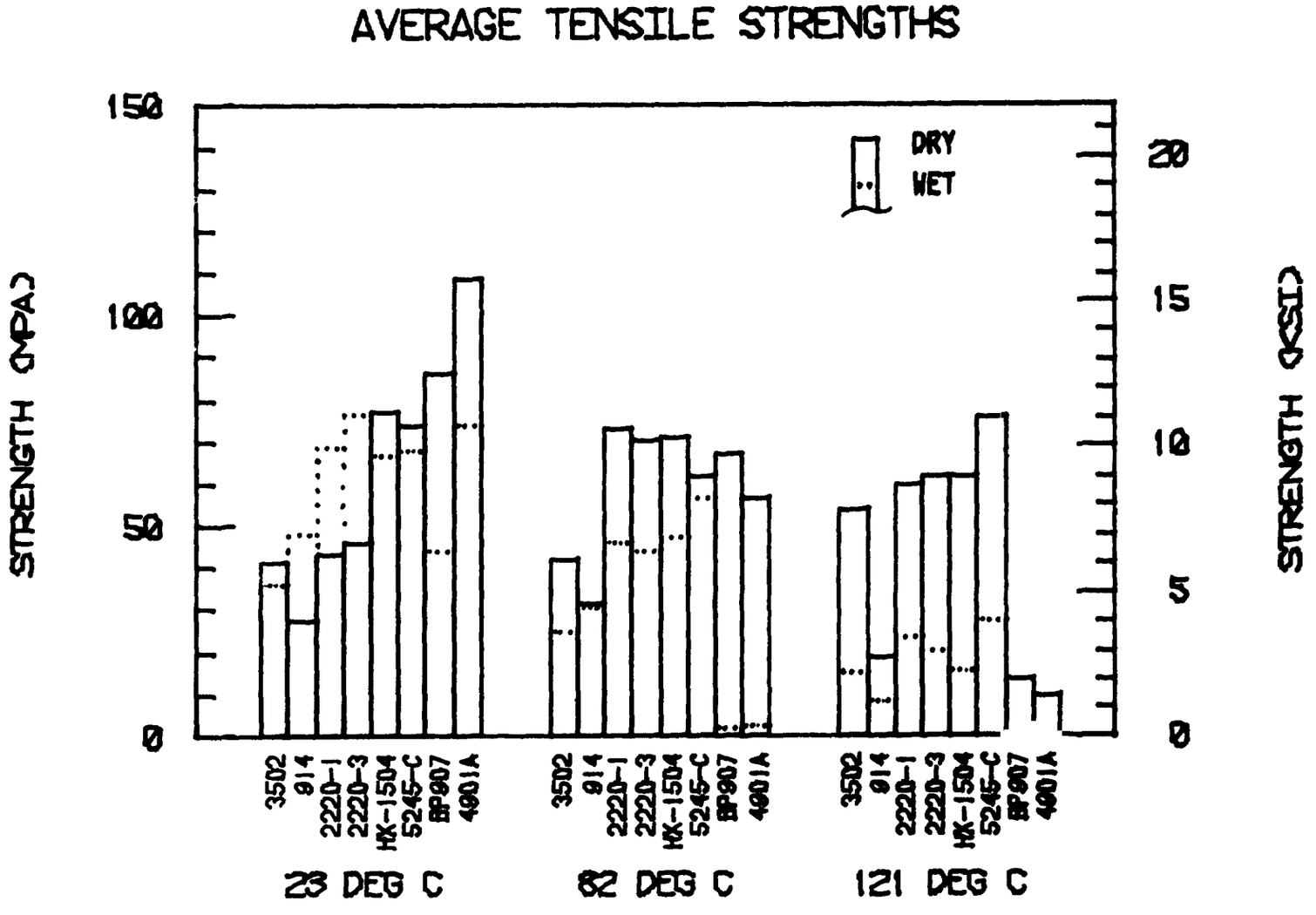

Figure 1. Tensile Strengths of Eight Neat Resins as a Function of Temperature and Moisture Preconditioning (Dry or Saturated).

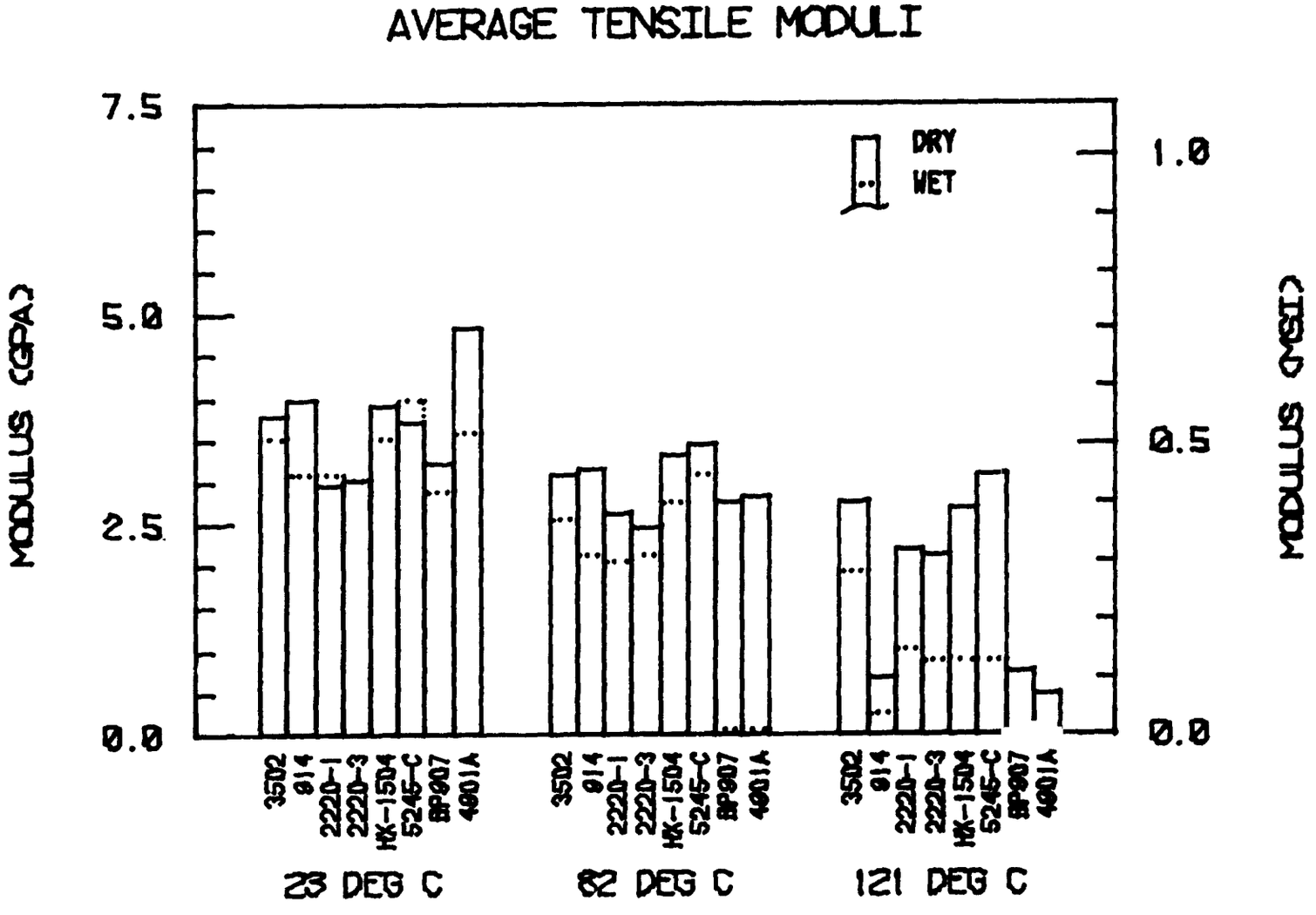

Figure 2. Tensile Moduli of Eight Neat Resins as a Function of Temperature and Moisture Preconditioning (Dry or Saturated).

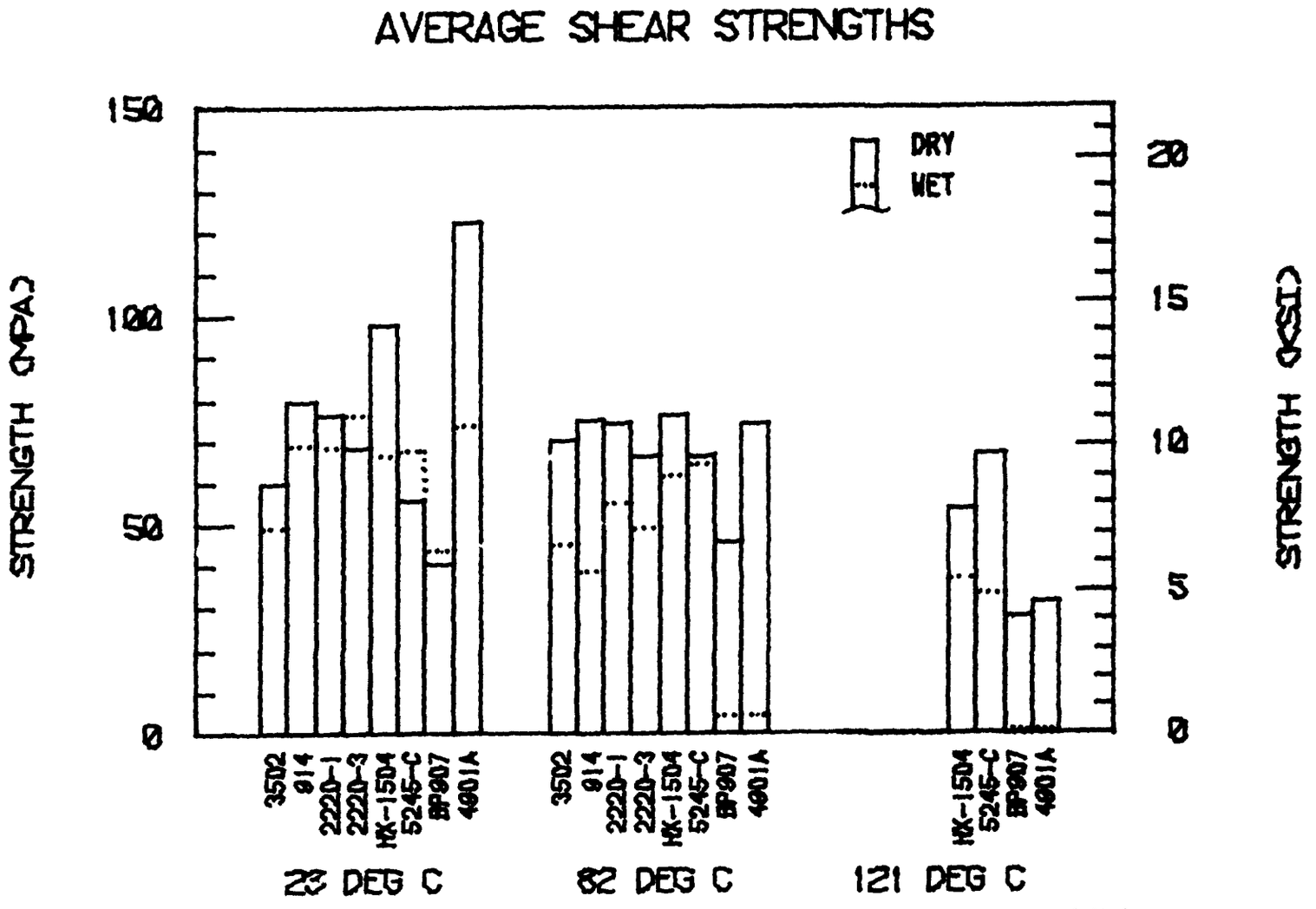

Figure 3. Shear Strengths of Eight Neat Resins as a Function of Temperature and Moisture Preconditioning (Dry or Saturated).

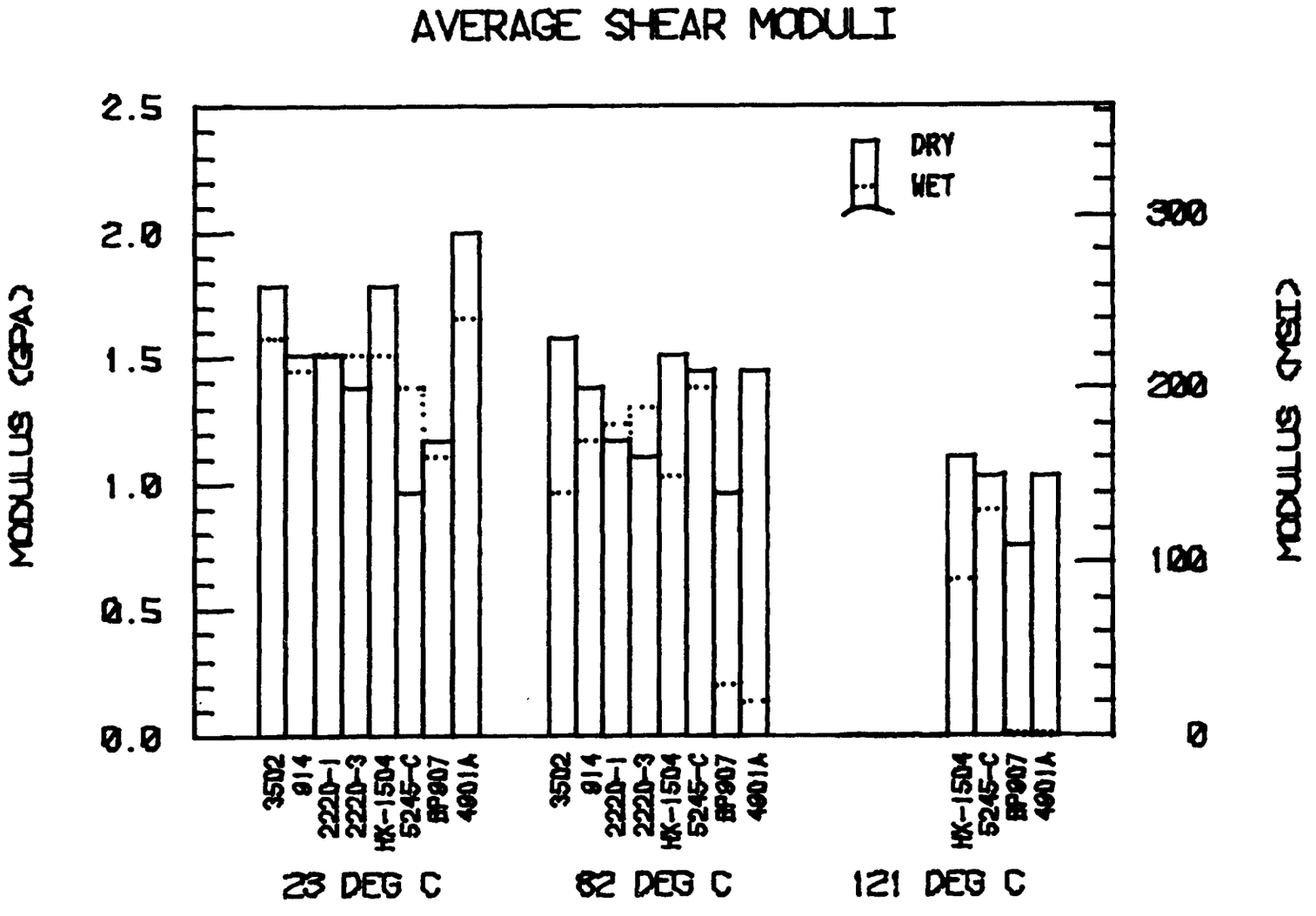

Figure 4. Shear Moduli of Eight Neat Resins as a Function of Temperature and Moisture Preconditioning (Dry or Saturated).

TABLE 1

AVERAGE MATERIAL PROPERTIES FOR EIGHT NEAT RESIN SYSTEMS;
ROOM TEMPERATURE, DRY CONDITION

Neat Resin System	Tensile Strength (MPa)	(ksi)	Shear Strength (MPa)	(ksi)	Young's Modulus (GPa)	(Msi)	Shear Modulus (GPa)	(Msi)	Poisson's Ratio	Coefficient of Thermal Expansion (10^{-6}/°C)
3502	41	6.0	60	8.7	3.8	0.55	1.8	0.26	0.36	50.5
914	28	4.0	80	11.6	4.0	0.58	1.5	0.22	0.36	58.4
2220-1	43	6.3	77	11.1	3.0	0.43	1.5	0.22	0.36	55.6
2220-3	46	6.7	68	9.9	3.0	0.44	1.4	0.20	0.36	53.6
HX-1504	77	11.2	98	14.2	3.9	0.57	1.8	0.26	0.37	50.8
5245-C	74	10.7	56	8.1	3.7	0.54	1.0	0.14	0.39	48.0
907	86	12.5	41	5.9	3.2	0.47	1.2	0.17	0.42	54.8
4901A(MDA)	109	15.8	123	17.8	4.8	0.70	2.0	0.29	0.41	57.8

TABLE 2

AVERAGE MATERIAL PROPERTIES FOR EIGHT NEAT RESIN SYSTEMS;
82°C, DRY CONDITION

Neat Resin System	Tensile Strength (MPa)	(ksi)	Shear Strength (MPa)	(ksi)	Young's Modulus (GPa)	(Msi)	Shear Modulus (GPa)	(Msi)	Poisson's Ratio
3502	42	6.1	70	10.2	3.1	0.45	1.6	0.23	0.37
914	32	4.6	75	10.9	3.2	0.46	1.4	0.20	0.37
2220-1	73	10.6	74	10.8	2.6	0.38	1.2	0.17	0.36
2220-3	70	10.2	65	9.6	2.5	0.36	1.1	0.16	0.35
HX-1504	71	10.3	77	11.1	3.3	0.48	1.5	0.22	0.36
5245-C	62	9.0	66	9.6	3.4	0.50	1.4	0.21	0.40
907	67	9.7	46	6.7	2.8	0.40	1.0	0.14	0.42
4901A(MDA)	57	8.2	74	10.8	2.8	0.41	1.4	0.21	0.44

TABLE 3

AVERAGE MATERIAL PROPERTIES FOR EIGHT NEAT RESIN SYSTEMS;
121°C, DRY CONDITION

Neat Resin System	Tensile Strength (MPa)	(ksi)	Shear Strength (MPa)	(ksi)	Young's Modulus (GPa)	(Msi)	Shear Modulus (GPa)	(Msi)	Poisson's Ratio
3502	54	7.8	*		2.8	0.40	*		0.46
914	19	2.8	*		0.7	0.10	*		0.44
2220-1	60	8.7	*		2.2	0.32	*		0.42
2220-3	62	9.0	*		2.1	0.31	*		0.39
HX-1504	62	9.0	54	7.8	2.7	0.39	1.1	0.16	0.37
5245-C	76	11.0	67	9.7	3.1	0.45	1.0	0.15	0.40
907	1	0.1	1	0.1	2.6	0.38	1.4	0.20	0.41
4901A(MDA)	10	1.4	32	4.6	0.5	0.07	1.0	0.15	0.35

*Property not measured

TABLE 4

ROOM TEMPERATURE, MOISTURE-SATURATED CONDITION

Neat Resin System	Tensile Strength (MPa)	(ksi)	Shear Strength (MPa)	(ksi)	Young's Modulus (GPa)	(Msi)	Shear Modulus (GPa)	(Msi)	Poisson's Ratio	Coefficient of Thermal Expansion (10^{-6}/°C)	Coefficient of Moisture Expansion (10^{-3}/%M)	Equilibrium Moisture Content (%M)
3502	36	5.2	50	7.2	3.5	0.51	1.6	0.23	0.43	55.5	2.70	5.0
914	48	7.0	69	10.0	3.1	0.45	1.4	0.21	0.43	62.6	3.02	7.0
2220-1	68	9.9	68	9.9	3.1	0.45	1.5	0.22	0.41	58.6	2.51	3.8
2220-3	67	9.7	68	9.9	3.1	0.45	1.5	0.22	0.43	57.5	2.96	4.0
HX-1504	51	7.4	66	9.6	3.5	0.51	1.5	0.22	0.40	54.7	2.07	3.8
5245-C	47	6.8	68	9.8	4.0	0.58	1.4	0.20	0.39	50.2	1.52	2.1
907	59	8.4	44	6.4	2.9	0.42	1.1	0.16	0.43	58.0	2.29	5.1
4901A (MDA)	79	11.5	74	10.7	3.6	0.52	1.7	0.24	0.40	60.9	1.55	7.2

TABLE 5

AVERAGE MATERIAL PROPERTIES FOR EIGHT NEAT RESIN SYSTEMS;
82°C, MOISTURE-SATURATED CONDITION

Neat Resin System	Tensile Strength (MPa)	(ksi)	Shear Strength (MPa)	(ksi)	Young's Modulus (GPa)	(Msi)	Shear Modulus (GPa)	(Msi)	Poisson's Ratio
3502	25	3.6	46	6.6	2.6	0.37	1.0	0.14	0.42
914	32	4.6	39	5.6	2.1	0.31	1.2	0.17	0.40
2220-1	46	6.7	55	8.0	2.1	0.30	1.2	0.18	0.43
2220-3	44	6.4	50	7.2	2.1	0.31	1.3	0.19	0.47
HX-1504	48	6.9	62	9.0	2.8	0.40	1.0	0.15	0.41
5245-C	57	8.2	65	9.4	3.1	0.45	1.4	0.20	0.42
907	2	0.3	5	0.7	0.1	0.01	0.2	0.03	0.43
4901A(MDA)	3	0.4	5	0.7	0.1	0.01	0.1	0.02	0.42

TABLE 6

AVERAGE MATERIAL PROPERTIES FOR EIGHT NEAT RESIN SYSTEMS;
121°C, MOISTURE-SATURATED CONDITION

Neat Resin System	Tensile Strength (MPa)	(ksi)	Shear Strength (MPa)	(ksi)	Young's Modulus (GPa)	(Msi)	Shear Modulus (GPa)	(Msi)	Poisson's Ratio
3502	15	2.2	*		1.9	0.28	*		0.45
914	8	1.2	*		0.3	0.04	*		0.49
2220-1	23	3.4	*		1.0	0.15	*		0.49
2220-3	21	3.0	*		0.9	0.13	*		0.49
HX-1504	16	2.3	37	5.4	0.9	0.13	6.8	0.98	0.49
5245-C	28	4.0	34	4.9	0.9	0.13	0.9	0.13	0.49
907**									
4901A(MDA)**									

*Properties not measured

**Material not tested due to highly degraded properties at this environmental condition

however, were fracture toughness for the CYCOM 907 and Young's modulus for the ERX-4901A (MDA). These comparisons did demonstrate that these specific properties of these model resin systems were higher than for the ACEE resin systems, as expected. The "model resins" rapidly deteriorated, however, when exposed to moisture saturation and elevated temperature conditions, as also expected.

The tensile strengths recorded during the current study (Figure 1) were similar to those of the two Hercules 2220 systems of the first year. All of these were stronger than the Hercules 3502 and the Ciba-Geigy Fibredux 914. Possible reasons, are that these resins are actually stronger, and/or that these resins are tougher and therefore less susceptible to inherent defects in the test specimens, as will be discussed in detail in Section 6.

The ERX-4901A (MDA) exhibited the highest room temperature, dry Young's modulus of any of the resins tested to date (see Figure 2). However, at 82°C, dry its modulus was comparable to those of the other systems, and at 121°C, dry its modulus was much lower than that of all but the Fibredux 914. In the presence of moisture, it was no stiffer than the other systems even at room temperature. The two ACEE resins tested in the present effort, viz, the HX-1504 and the 5245-C, exhibited good elevated temperature stiffness retention in the dry condition, although the 3502 was superior at the 121°C, wet condition.

Shear strengths for the neat resins tested here were comparable to the first-year results (Figure 3). Shear testing was performed utilizing torsion rod specimens for all resin systems except the CYCOM 907 epoxy. The Iosipescu shear test was used for this one resin system due to the difficulty in casting void free test specimens in the round dogbone

shape used in the torsion test. The Iosipescu shear test method uses a flat specimen, which can be cast more reliably. The Iosipescu shear test has only recently been adapted by the CMRG for use with neat resins; it provided reasonable shear modulus values but lower than expected shear strengths. Work is continuing on improving results for neat resins using this test method. Complete shear test results are included in Section 3.

The room temperature, dry shear modulus of the ERX-4901A (MDA) was high, consistent with the Young's modulus results, but likewise fell dramatically at the elevated temperatures in the presence of moisture (see Figure 4). The Narmco 5245-C bismaleimide/epoxy exhibited an anomalously low shear modulus in the room temperature, dry condition, but otherwise was comparable in performing to the WX-1504.

As observed during the first-year study [1] also, the isotropic relation between E, ν, and G was not satisfied, providing further evidence that these polymers do not respond to mechanical loadings in an isotropic manner. Limited bulk modulus data available confirmed these results.

Single-Edge Notched-Bend (SEN) fracture toughness testing was also performed on the four neat resin systems chosen for this study. Discussions with Dr. Donald Hunston of the National Bureau of Standards, Dr. William Jones of Texas Tech University, and Dr. Willard Bascom of Hercules Inc. were held to try to improve current testing techniques and, therefore, achieve better results than achieved in the first-year fracture toughness testing [1]. However, more work is needed to optimize this test method and permit reasonable uniformity of results between investigators. The major obstacle to uniformity appears to be the sensitivity of the variety of methods of inducing a crack at the root of

the notch currently being used by various investigators. Of the three methods attempted as part of the present study, a razor blade cooled in liquid nitrogen and then tapped into the notch to sharpen it appears to be the most satisfactory. The other two methods of crack initiation, a room temperature razor blade tap and slicing of the neat resin at a temperature above its glass transition temperature (T_g), were less acceptable because of lack of consistency and the added thermal excursion required for the resin, respectfully.

Results from this fracture testing indicated that the CYCOM 907 achieved the highest toughness, as expected. The measured toughness of the 5245-C was much less than that of the CYCOM 907, but twice that of the HX-1504 and ERX-4901A at room temperature. Complete results are given in Section 3 of this report.

Coefficient of thermal expansion (CTE) testing was performed on both dry and moisture-saturated specimens. The CTE for all neat resins was measured over a temperature range from -40°C to +121°C, using a glass tube dilatometer and an LVDT monitored by a microprocessor. A linear increase in CTE with temperature over this range was recorded, with an increase in CTE for all resins after moisture saturation.

Coefficient of moisture expansion (CME) testing was also performed on all four neat resin systems, from dry to full saturation at 65°C. A minimum of six replicates of each material were tested, to provide a reasonable basis for CME values. The equilibrium moisture level for each resin system was also determined; values ranged from 2.1 weight percent for the 5245-C to 7.2 weight percent for the ERX-4901A (MDA). The HX-1504 stabilized at 3.8 weight percent and the CYCOM 907 at 5.1 weight percent moisture absorption. A more detailed discussion of the thermal

and moisture expansion testing is included in Section 3.

Scanning electron microscopy (SEM) was performed on randomly selected failed test specimens to correlate with the first-year observations of fracture features exhibited by various matrix materials. The current SEM results are presented in Section 4 and Appendix D of this report. These supplement the large catalog of SEM photographs taken last year and documented in Reference [1]. All are thus available for future studies of the fracture methodology seen in unreinforced resin systems.

Micromechanics predictions of composite material response were performed using as input data the neat resin matrix experimental data generated in this program. Predictions are also included for the four matrix materials of the first-year study, plus Hercules 3501-6 epoxy. Hercules AS4 high strength graphite fiber was modeled; fiber data were taken from the literature. Unidirectional composite material response was predicted and will be subsequently correlated with experimental data to be generated during a planned continuation effort. These predictions are given in Section 5.

Additional discussion and conclusions are included in Section 6 of this report. Appendix A contains tables of individual test specimen results for all tests. Individual stress-strain curves are presented in Appendix B. Fracture surfaces of the neat resin fracture toughness specimens are shown in the photographs of Appendix C.

SECTION 2

INTRODUCTION

This report presents the results of the second year of a continuing study of unreinforced (neat) polymer resin systems being considered primarily for use in aerospace applications. The program was initiated due to the need for material property data on relatively new resin systems being evaluated for the Aircraft Energy Efficiency (ACEE) program. Composite materials are being fabricated and evaluated by commercial airframe manufacturers, but it was deemed desirable to develop a technique to evaluate the many new matrix materials continually becoming available without going through the effort of prepregging and fabricating composites. This shortcut allows the more rapid and more cost effective evaluation of new matrix materials.

New polymer systems are continually being developed to fill the need for tough, strong, and stiff matrix materials for use in high performance composite material systems. These candidates must be screened carefully to determine their potential usefulness in aerospace applications.

The Composite Materials Research Group (CMRG) at the University of Wyoming has been active in the mechanical properties characterization of candidate polymer matrices for a number of years, as discussed in Reference [1]. The development of methods of fabricating unreinforced (neat) polymers into test specimens has evolved into a well-defined processing capability. This capability, along with extensive composite materials testing experience, has permitted the extensive screening accomplished during the initial two years of the present NASA-Langley Grant study, the first-year results being reported in Reference [1].

A total of eight polymer matrix systems have now been comprehensively characterized in tension and shear. These eight neat resin systems include Hercules 3502, 2220-1, and 2220-3, Ciba-Geigy Fibredux 914, Hexcel HX-1504, Narmco 5245-C, American Cyanamid CYCOM 907, and Union Carbide ERX-4901A (MDA). Also measured were the coefficients of thermal expansion and moisture expansion and a small amount of neat resin fracture toughness testing has also been performed.

Data were already available prior to the first-year study for Hercules 3501-6 epoxy [5,6]; these have also been used here whenever appropriate. After characterizing the unreinforced resin, a finite element micromechanics analysis can be used to predict composite performance at various environmental conditions. This numerical model has proven to be quite accurate in its predictions in several previous programs [2-6]. However, correlations with experimental data have not yet been possible in the present program due to the lack of available composites data. To resolve this problem, test data will be generated for some of the composite systems during the next year of effort at the University of Wyoming. This will provide the correlation and verification needed to use with confidence the micromechanics analysis as it is intended, for predicting composite material response when experimental data are not available. These predictions will save time and effort by foregoing the preparation and testing of composites until an attractive resin candidate is identified.

The first-year grant [1] involved the first four resin systems listed above. The present (second-year) grant included the other four resins. Of these latter four matrices, the Hexcel HX-1504 and Narmco 5245-C have been chosen by airframe manufacturers as candidates for the

Aircraft Energy Efficiency (ACEE) Program. The American Cyanamid CYCOM 907 and Union Carbide ERX-4901A(MDA) were chosen for the present study because of their promise as laboratory "model resin" systems. A "model" system is defined here as a material possessing a desired property not commonly exhibited by matrices in current use. The characteristic of CYCOM 907 of particular interest is good fracture toughness in neat resin and composite forms. The ERX-4901A(MDA) has a relatively high Young's modulus of 4.83 GPa (0.70 Msi), which is of interest in compression loading applications where fiber microbuckling is a consideration. This resin may improve the compressive strength of the composite by providing a greater degree of lateral support to the fiber because of its higher stiffness. Both of these "model" resin systems have serious weaknesses also, however, which would limit their use in most practical applications, as will be addressed in this report.

SECTION 3

EXPERIMENTAL RESULTS

3.1 Introduction

A comprehensive test program was completed for the four unreinforced (neat) resin systems identified in Sections 1 and 2. Table 7 indicates the test matrix with accompanying environmental conditions; a total of six combinations of temperature and moisture environmental conditions were used in the mechanical testing. Specimens were cast into test configurations from bulk resin. Dry test specimens were stored in dessicators; specimens designated for wet testing were suspended over distilled water at 74°C in sealed containers until fully moisture-saturated. Periodic weighings of these specimens were performed to monitor weight gain versus time and thus determine when moisture saturation was achieved.

All static testing was performed using an Instron Model 1125 electromechanical universal testing machine. A BEMCO Model FTU 3.8 environmental chamber was used to maintain the desired elevated test temperatures. A Hewlett-Packard Model 21MX-E mini-computer was used to record and reduce all data. A CDC Cyber 730/760 computer was used to generate all plots of material properties and groupings of stress-strain plots.

3.2 Cure Cycles for Neat Resins

The four neat resins tested in the current year were cast using the same types of steel molds used during the first-year program [1]. Recommended cure cycles for each resin system were obtained from the respective manufacturers to ensure that proper cures were obtained. An intermediate temperature initial gel was performed in the steel molds

TABLE 7

NEAT RESIN TEST MATRIX

Test Method	Moisture Condition	Test Temperature 23°C	82°C	121°C
Tension	Dry	5	5	5
	Moisture-Saturated	5	5	5
				30 total
Shear	Dry	5	5	5
	Moisture-Saturated	5	5	5
				30 total
Fracture Toughness	Dry	5	5	5
	Moisture-Saturated	5	5	5
				30 total
Coefficient of Thermal Expansion	Dry	6	-40°C to 121°C	
	Moisture-Saturated	6	-40°C to 121°C	
				6 total
Coefficient of Moisture Expansion	98%RH	65°C, Dry to Saturation		
				6 total
		102 Specimens of Each Resin System		

Total for Four Resin Systems -- 408 Specimens

before the final cure to minimize thermal stresses in the cured specimens.

The cure cycle for the HX-1504 included 20-30 minutes under 20-24 in. Hg vacuum at 93°C, followed by an initial cure temperature of 120°C for 5 hours. A final cure of 3 hours at 177°C was performed in an air circulating oven after the specimens had been removed from the molds.

Cure for the 5245-C included 30-40 minutes under 20-24 in. Hg vacuum at 100°C, followed by an initial cure of 5 hours at 120°C. A final cure of 3 hours at 177°C was performed in an air circulating oven after the specimens had been removed from the molds.

The CYCOM 907 was subjected to the 20-24 in. Hg vacuum at 100°C for 45-60 minutes before curing for 5 hours at 130°C. A final cure of 3 hours at 177°C was performed in an air circulating oven after the specimens had been removed from the molds.

The ERX-4901A(MDA) was formulated at 65°-75°C by mixing 42 grams of 4,4 methylenedianaline (MDA) curing agent per each 100 grams of ERX-4901A epoxy. The mixture was stirred under a fume hood until the curing agent was dissolved. After 15-20 minutes in vacuum at 50°C, an initial cure at 90°C for 7 hours was performed. Then an intermediate 4-hour cure at 120°C was imposed before the final cure of 10 hours at 160°C was performed. The final cure was in an air circulating oven after the specimens had been removed from the molds.

3.3 Tensile Test Results

Engineering constants measured included Young's modulus, E, Poisson's ratio, ν, ultimate stress, σ_u, and ultimate strain, ϵ_u. Complete stress-strain curves to failure were recorded. All individual stress-strain curves and test results are included in the Appendix.

Summary tables are included in Section 1.

A standard dogbone-shaped specimen was used for all tensile testing. The specimens were 152 mm (6 in.) long by 7.6 mm (0.3 in) wide in the gage section by 2.5 mm (0.1 in.) thick. Each specimen was instrumented with an extensometer to measure axial strain and thus generate a complete stress-strain curve. A second extensometer was used to measure transverse strain for each test. Poisson's ratio was then calculated from the measured longitudinal and transverse strains. Figure 5 shows the extensometer arrangement used on each tensile specimen.

Figure 6 is a bar graph of the average tensile strengths of the four neat resins at the three test temperatures. The dry strength values are represented by the thin horizontal bars and the moisture-saturated strengths by the heavy bars. The groups of bars represent from left to right, Hexcel HX-1504, Narmco 5245-C, Cycom 907, and Union Carbide ERX-4901A(MDA), as indicated.

Dry tensile strengths at room temperature for all the resin systems were greater than 70 MPa (10 ksi). In fact, the average strength of the ERX-4901A(MDA) was measured to be greater than 100 MPa (15 ksi). This is a very high measured strength for a neat (unreinforced) epoxy. As test temperature was increased, tensile strengths typically decreased, except for the 5245-C, which increased to its highest strength at the 121°C test temperature. This could be due to the bismaleimide constituent in the 5245-C formulation, which would be expected to have better high temperature properties than the epoxies tested. The CYCOM 907 and ERX-4901A(MDA) fell to below 14 MPa (2 ksi) at the 121°C test temperature, after performing reasonably well at the 23°C (room temperature) and 82°C temperatures. The tensile strength of the HX-1504 decreased

Figure 5. Typical Arrangement of a Longitudinal and a Transverse Extensometer on a Neat Resin Tension Specimen.

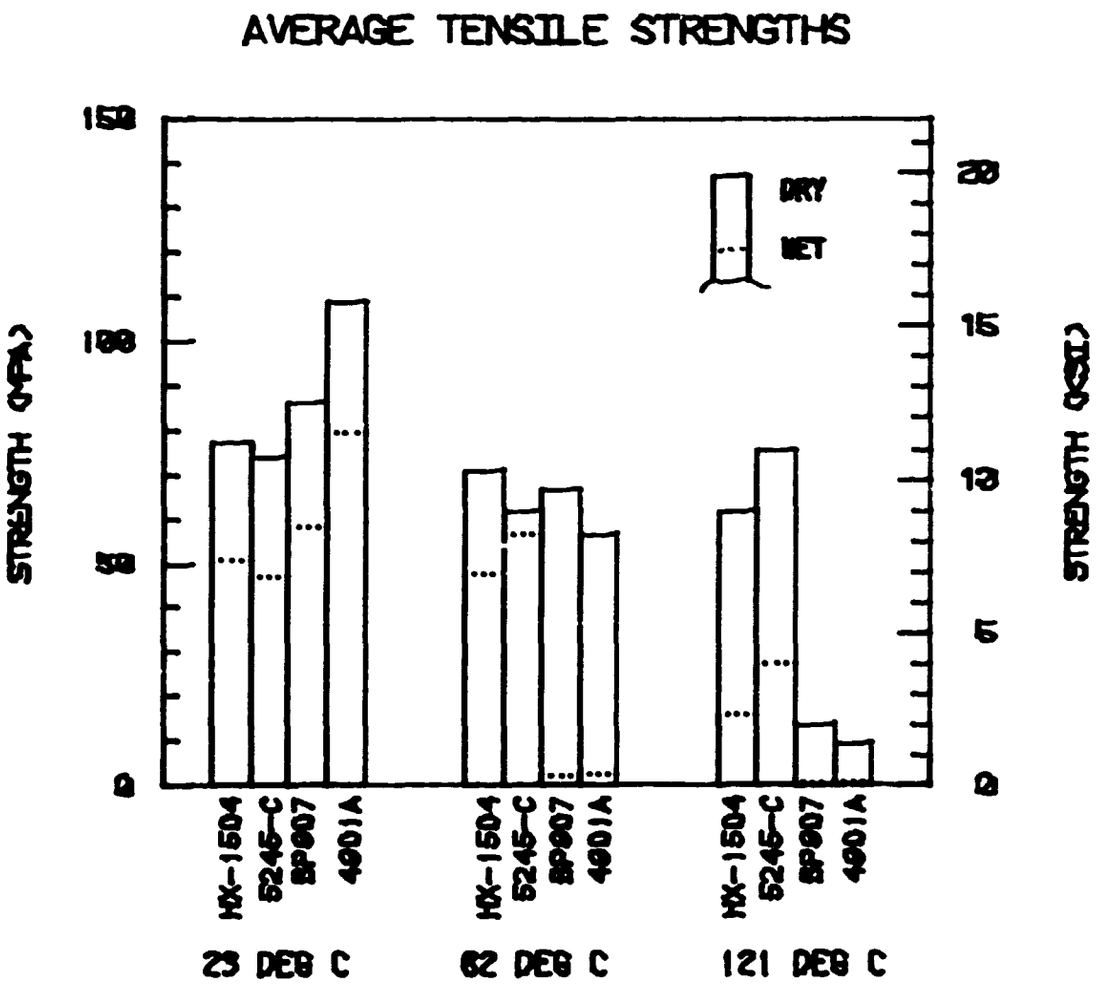

Figure 6. Average Tensile Strengths of the Four Neat Resin Systems Tested, as a Function of Test Temperature and Moisture Content.

only slightly with increasing temperature.

Tensile moduli averages are plotted in Figure 7. The HX-1504 and 5245-C ACEE resins retained their tensile stiffness well at all three test temperatures while the stiffnesses of the ERX-4901A(MDA) and CYCOM 907 fell to very low levels at the 121°C temperature. The ERX-4901A(MDA) exhibited a 4.8 GPa (0.7 Msi) tensile modulus at the room temperature, dry condition, which is high for a neat resin.

Figure 8 shows a typical failed tensile specimen. Most specimens failed straight across the gage section in the manner shown, which is different from failures seen in the resins tested during the prior program [1]. Failures in the earlier resin systems typically included a missing triangular chip from one side of the specimen [1]. Resins tested here failed without breaking any small pieces from the specimens during fracture. Figure 9 shows two ERX-4901A(MDA) specimens, one before testing (top) and one after testing (bottom). The ERX-4901A(MDA) when tested at 121°C stretched dramatically but did not fracture. Ripples can be seen in the surface of the tested specimen, indicating a "necking" process such as seen in ductile metals at high elongations. The elevated temperature strength of this resin was quite low, as was the modulus. The CYCOM 907 behaved similarly at the 121°C temperature.

The room temperature strength of all four neat resins dropped approximately the same amount after moisture-saturation. The HX-1504 and 5245-C moisture-saturated strengths at 82°C were similar to their 23°C values, but fell to below 35 MPa (5 ksi) at the 121°C test temperature. The 5245-C bismaleimide/epoxy blend exhibited the highest strength retention of the four resin systems at the 121°C test temperature, for both the dry and wet conditions.

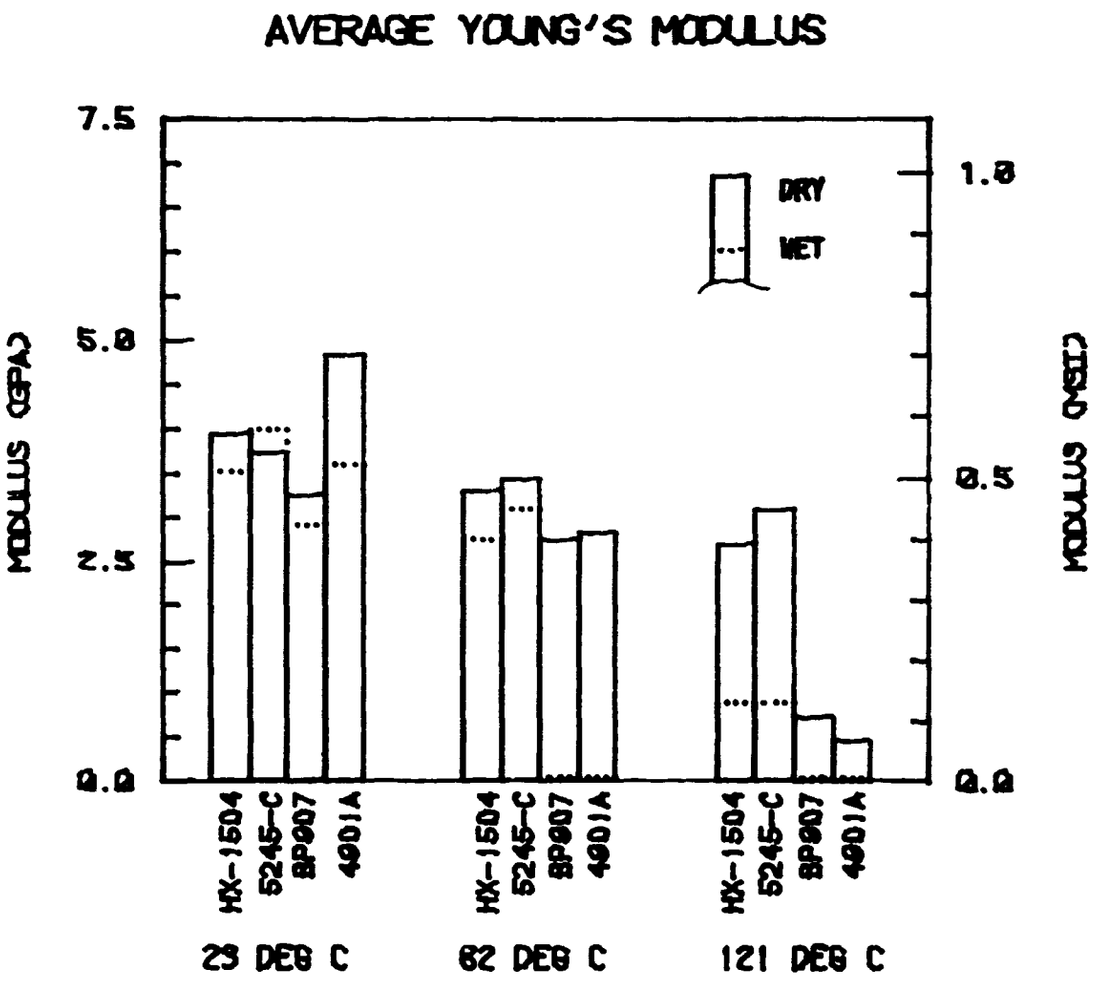

Figure 7. Average Tensile Moduli of the Four Neat Resin Systems Tested, as a Function of Test Temperature and Moisture Content.

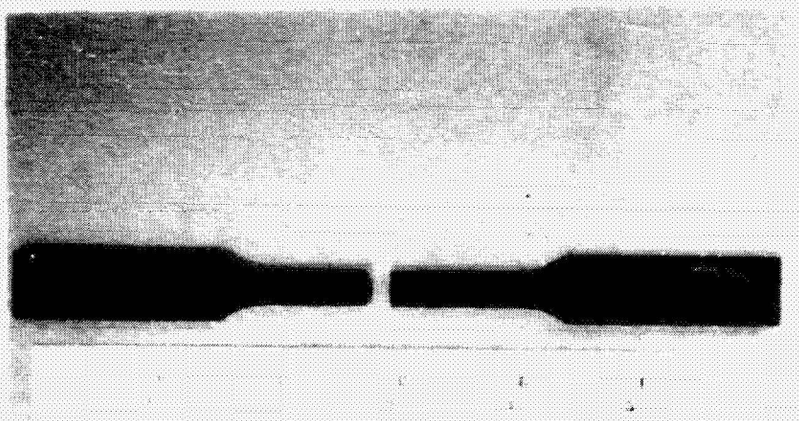

Figure 8. Failed 5245-C Tension Specimen Tested at 121°C, Dry. It Will Be Noted That the Failure is Straight Across the Specimen.

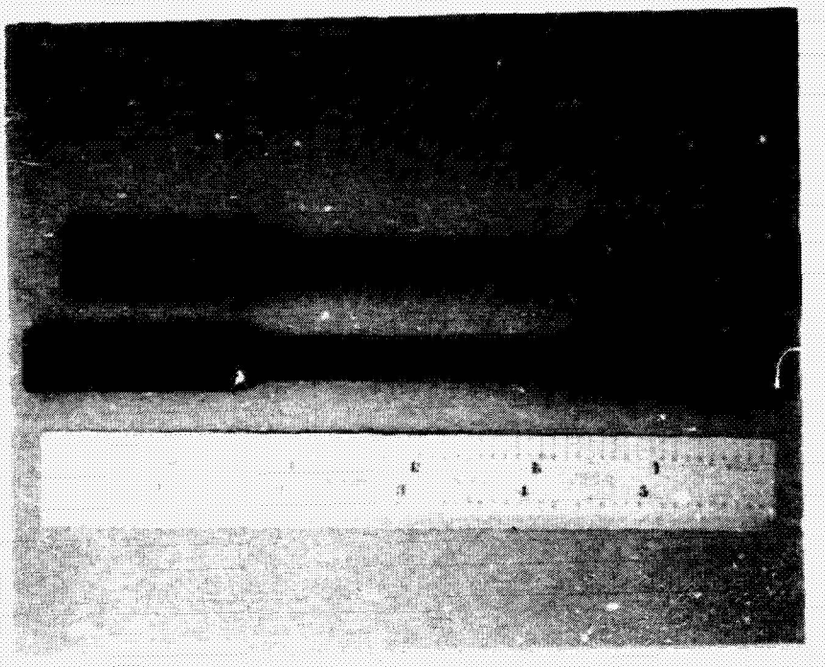

Figure 9. ERX-4901A(MDA) Tensile Specimens: Untested Specimen (Top) and Specimen After Testing at 121°C, Dry Conditions (Bottom). The Increase in Specimen Length and Surface Appearance After Testing Will Be Noted.

Moisture-saturated resin tensile strength averages are also shown in the barchart of Figure 6. The average strength of three of the resins was about the same at room temperature, with the ERX-4901A(MDA) being somewhat higher than the other three material systems. A moisture degradation effect is quite evident for all resin systems. The CYCOM 907 and ERX-4901A(MDA) strengths fell to less than 7 MPa (1 ksi) at the 82°C test temperature, thus they were not tested at 121°C. These two "model system" resins have very poor hot, wet tensile strength properties at and above 82°C.

Figure 7 shows the moisture-saturated tensile moduli for the four resin systems. As previously noted, the moisture-saturation (wet) values are displayed using a thick horizontal bar in the bar chart. Values are about equal to the dry values at room temperature, but decrease much more at the elevated test temperatures. The room temperature tensile modulus of the 5245-C is indicated to have increased slightly after moisture-saturation. However, this small increase may be due the experimental scatter rather than any physical phenomenon. The CYCOM 907 and ERX-4901A(MDA) were not tested at 121°C in the wet condition since the values at 82°C were so low as to be barely measurable.

Figure 10 shows two CYCOM 907 tensile specimens for comparison. The specimen at the bottom of the photograph was tested at 82°C in the moisture-saturated condition. Comparison of its length with that of the untested specimen at the top of the photograph indicates almost 5 mm (0.2 in.) of stretching. The rippling of the surface is not as evident as that seen in Figure 9 for the ERX-4901A(MDA) dry material.

3.4 Shear Test Results

All shear testing was performed using an Instron Model 1125 univer-

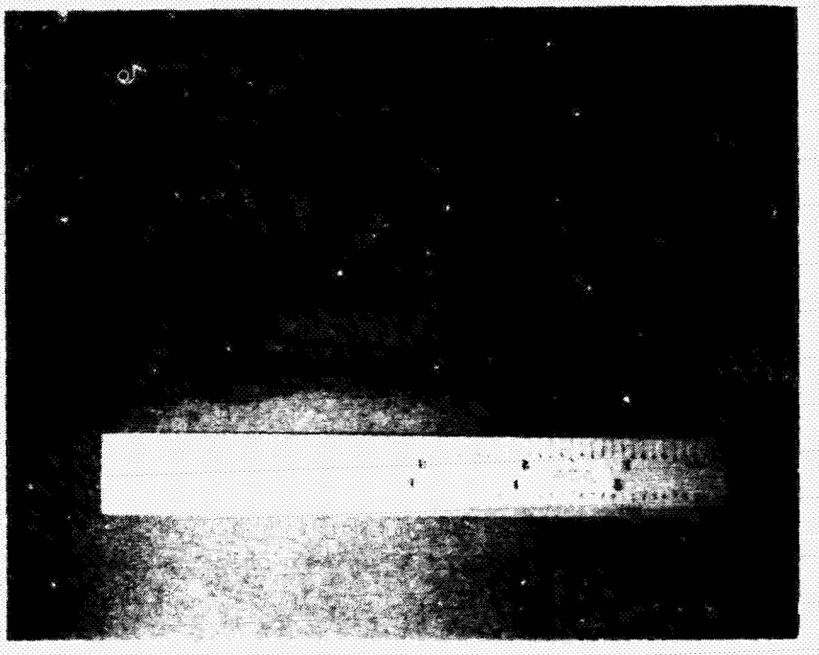

Figure 10. CYCOM 907 Tensile Specimens: Untested Specimen (Top) and Specimen After Testing at 82°C, Wet Conditions (Bottom). The Increase in Specimen Length After Testing Will Be Noted.

sal testing machine. Three of the four resin systems were tested using a round dogbone-shaped specimen in torsion. The fourth system, the CYCOM 907, was never successfully cast into this round configuration, and was tested using an Iosipescu shear test configuration. The CYCOM 907 could not be cast into the round dogbone shape because of its high viscosity. All attempts resulted in entrapping many air pockets, making the specimens unusable. Additional flat specimens were then cast to make Iosipescu shear test specimens. The Iosipescu shear test uses a flat rectangular specimen with a 90° machined notch on both sides [7-9]. Figure 11 shows the specimen configuration and loading used for this test method. This test works very well for composite materials but has some drawbacks when testing unreinforced resins. Stress concentrations near the inner load points sometimes prevent a good measure of shear strength in neat resins. Shear strengths for the CYCOM 907 reported here are, therefore, possibly somewhat lower than might be expected for this material at the lower test temperatures. At the higher test temperatures, this stress concentration effect is reduced by the plastic deformation of the epoxy, resulting in a reasonable measure of shear strength. Shear modulus, however, is measured reasonably well at the lower temperatures using a strain gage rosette. Recent improvements in the test fixture design [10] should provide better results in future neat resin shear testing.

The shear modulus for the round specimens was measured utilizing the rotometer also used in the first-year program. Its description and use are discussed in detail in the first-year report [1]. It uses two pairs of LVDT's to measure the rotations of two cams attached to the specimen. The differential rotation of the two cams is then converted to

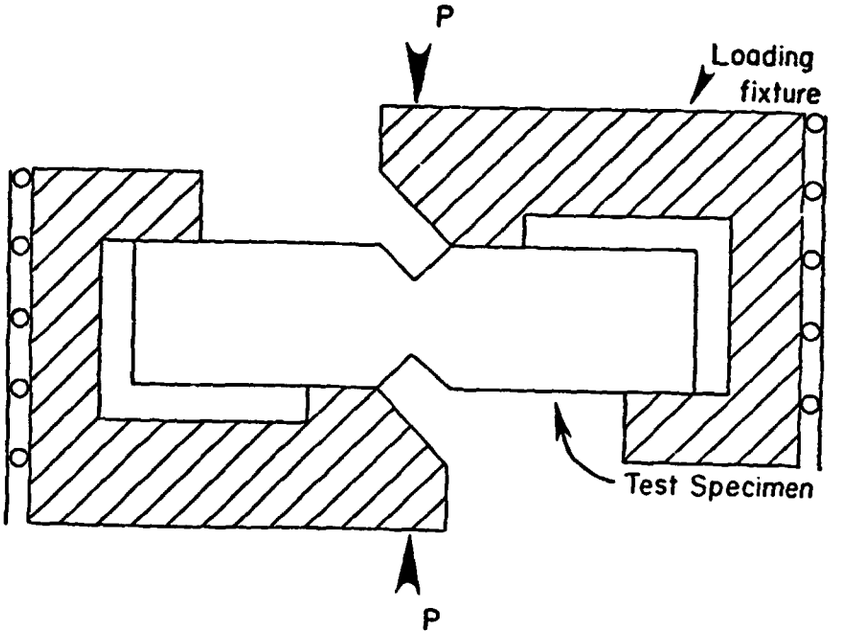

Figure 1?. Schematic of Loading Fixture for the Iosipescu Shear Test.

shear strain directly for use in shear modulus calculations. Figure 12 shows the rotometer test setup with the four LVDT's and two cams attached to a neat resin specimen.

Shear strength averages for dry and moisture-saturated tests are plotted in Figure 13. There was a wide variation in values among the four resin systems tested. For example, the room temperature, dry shear strengths ranged from 117 MPa (17 ksi) to only 41 MPa (6 ksi). The ERX-4901A(MDA) epoxy averaged over 117 MPa (17 ksi) shear strength at room temperature in the dry condition, but fell rapidly to about 35 MPa (5 ksi) at the 121°C test temperature. The HX-1504 averaged nearly 100 MPa (14 ksi) at room temperature, but fell to nearly 55 MPa (8 ksi) at the 121°C test temperature. The 5245-C bismaleimide/epoxy blend registered equal shear strengths at all test temperatures, probably due to the influence of the bismaleimide constituent which has better high temperature properties than the epoxies. The CYCOM 907 epoxy shear strengths reported may not be fully representative of the material performance at the 23°C test temperature due to the load point stress concentrations noted earlier in the discussion of the Iosipescu shear test. The strength values at 82°C and 121°C, at 45 MPa (6.5 ksi) and 4 28 MPa (4 ksi), respectively, probably are representative of the CYCOM 907, however. The stress concentration encountered in the Iosipescu shear test fixture used is blunted significantly at elevated temperatures.

Moisture-saturated shear strength averages plotted in Figure 13 indicate a drastic degradation of the HX-1504 and ERX-4901A(MDA) resins, but not of the 5245-C or 907. The HX-1504 and 5245-C neat resins per-

formed almost identically at all temperatures when wet. The ERX-4901A(MDA) shear strength was comparable to that of the 1504 and 5245-C at the room temperature, wet condition, but degraded extremely

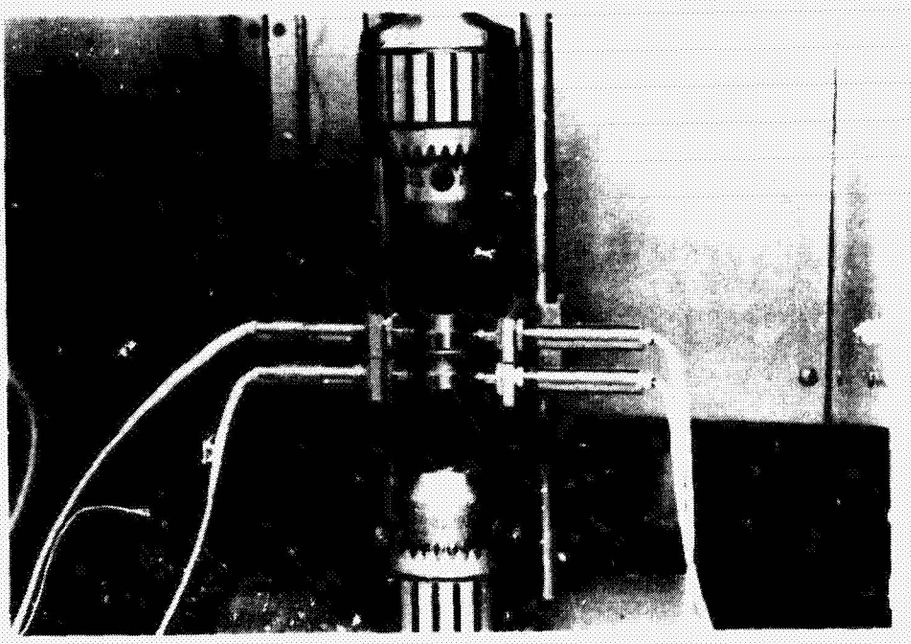

Figure 12. Rotometer Test Fixture Showing LVDT and Cam Arrangement for Measuring Shear Strain in a Torsion Test.

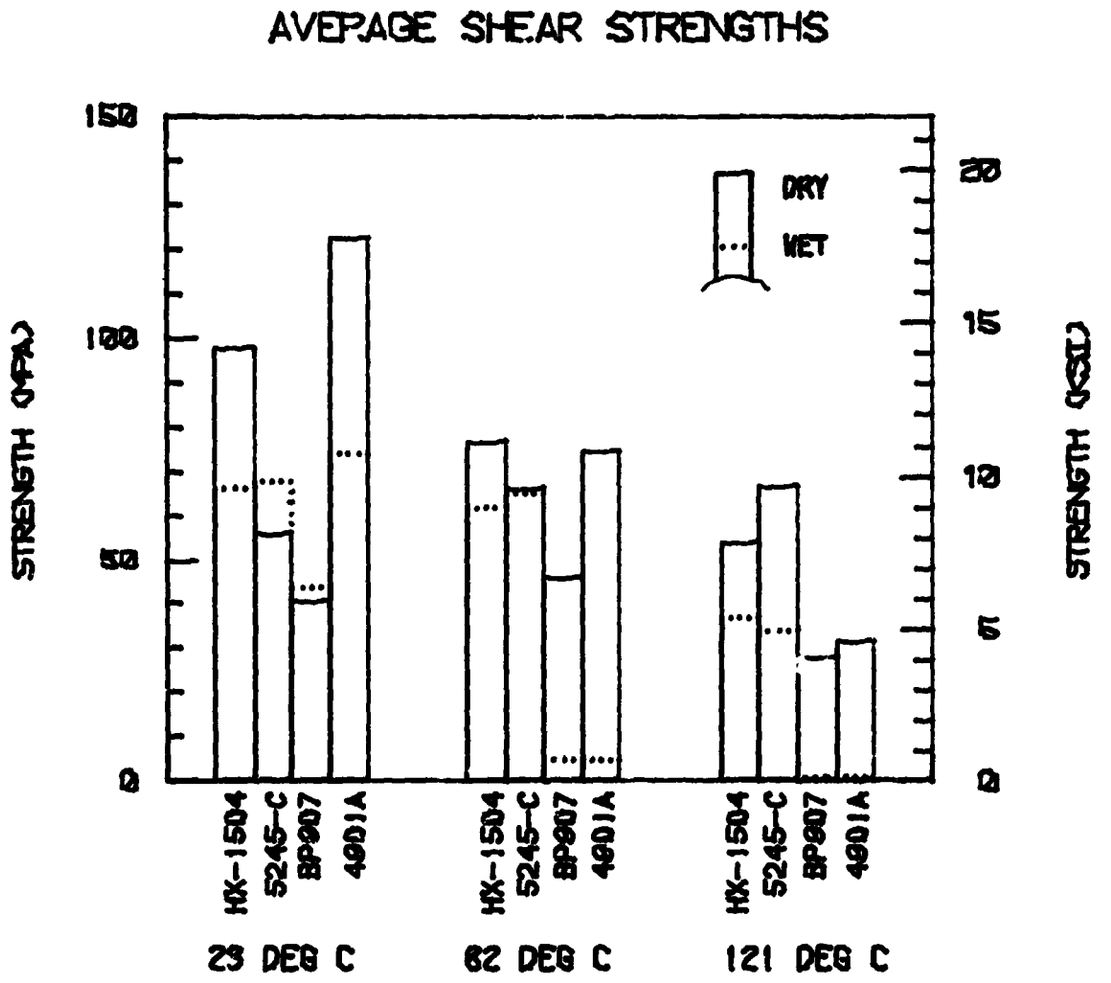

Figure 13. Average Shear Strengths of the Four Neat Resin Systems Tested, as a Function of Test Temperature and Moisture Content.

rapidly to a very low level at 82°C. The 5245-C exhibited a slightly higher room temperature shear strength when wet than when dry. The ERX-4901A(MDA) shear strength at the room temperature, wet condition was less than two-thirds the dry value, showing the extremely deleterious effect of moisture on this particular epoxy system. The HX-1504 also degraded to about two-thirds of its dry shear strength value when moisture-saturated at room temperature. The 5245-C bismaleimide/epoxy exhibited only about 50 percent of its dry strength at 121°C when moisture-saturated, whereas the HX-1504 retained almost two-thirds of its shear strength at 121°C when wet. The CYCOM 907 room temperature shear strength is probably not indicative of the material and should be higher because of the stress concentration present in the Iosipescu test specimen. However, its shear strength at 82°C, although very low, is definitely indicative of its true strength because the specimens did not fail catastrophically, only deforming plastically. Neither the CYCOM 907 nor the ERX-4901A(MDA) were tested at 121°C, wet since the shear strength values were already below 7 MPa (1 ksi) at the 82°C test temperature. At 121°C, the dry shear strengths of the 907 and ERX-4901A(MDA) were comparable to the wet shear strengths of the HX-1504 and 5245-C.

Figure 14 displays in barchart form the average shear moduli for the four resin systems, dry and wet. The ERX-4901A(MDA) and HX-1504 shear moduli were fairly close to each other at all three temperatures when tested dry. The 5245-C exhibited the lowest shear modulus at room temperature in the dry condition, but it is possible that this is not an accurate value for this matrix system. Some additional testing should perhaps be done to verify the values reported here. There was some

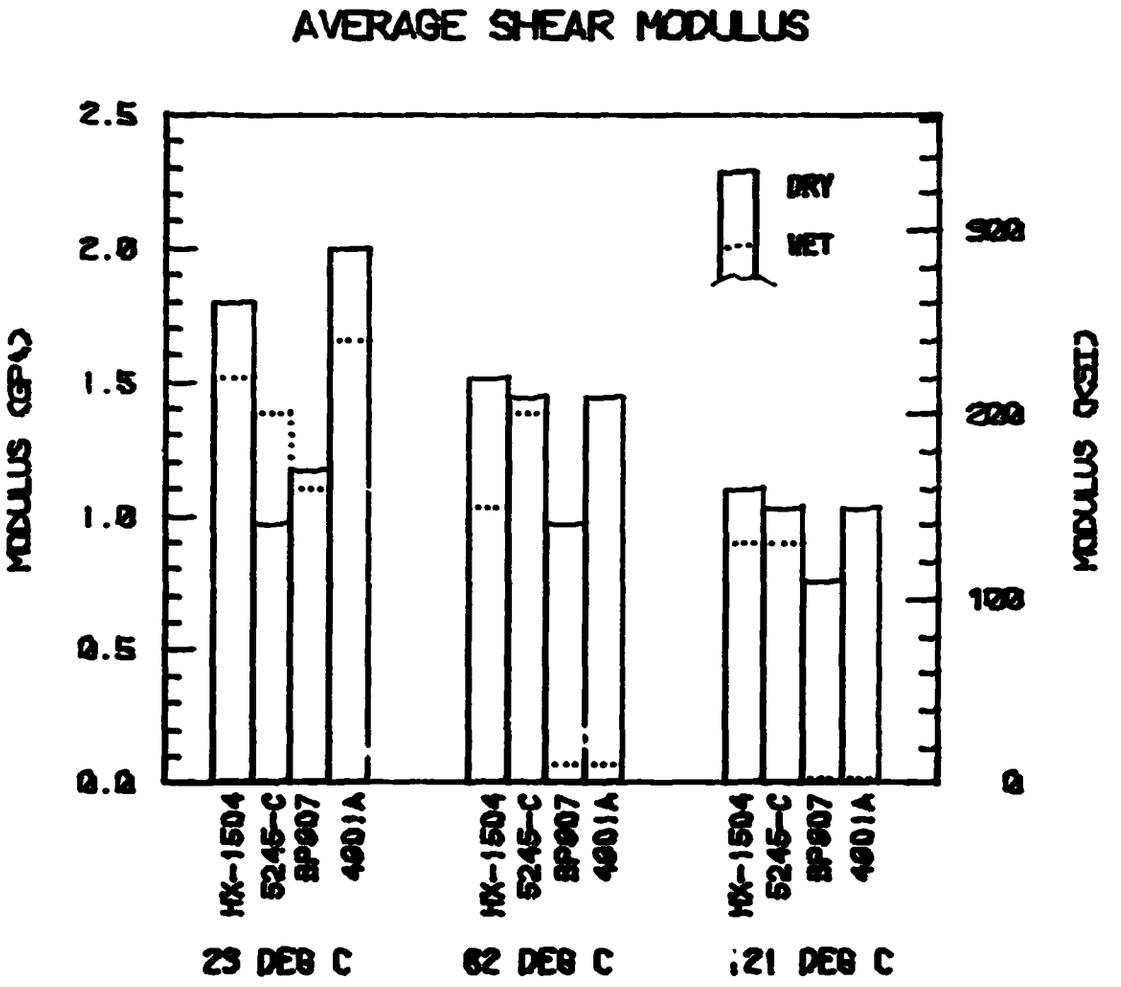

Figure 14. Average Shear Moduli of the Four Neat Resin Systems Tested, as a Function of Test Temperature and Moisture Content.

slippage in the test fixture when testing some of these specimens, which could have affected the results for this one resin system. The problem was corrected for all subsequent torsion testing.

Figure 14 also shows the moisture-saturated shear moduli for the four resin systems tested. The HX-1504 and 5245-C performed reasonably well, with the 5245-C maintaining a slightly higher shear modulus at the elevated temperatures when wet. The ERX-4901A modulus was initially higher than the two ACEE resins, but fell dramatically at the 82°C temperature and was, therefore, not even tested at 121°C wet. The CYCOM 907 at room temperature exhibited a reasonable shear modulus for this lower stiffness material, but it fell to a very low level at the 82°C temperature, in a manner similar to that of the ERX-4901A(MDA). Likewise, the 907 was not tested at the 121°C temperature, wet condition. The 907 and ERX-4901A(MDA) dry shear moduli were comparable to the HX-1504 and 5245-C wet and dry shear moduli at the 121°C test temperature.

Figure 15 shows a typical failed HX-1504 neat resin torsion specimen, with an untested specimen included for comparison. The ends of the failed specimen are placed at the approximate distance for the original length, thereby indicating the missing section. Small pieces were ejected at high velocity during the violent fracture. Figure 16 is a failed ERX-4901A(MDA) torsion specimen tested at the 121°C, dry condition. A straight line was drawn along the specimen axis prior to testing to allow a visual record of the amount of twist exhibited by this resin at this test temperature. As shown here, almost 180 degrees of rotation was imposed prior to suspending the test, without fracture. Extensive plastic flow was observed in all ERX-4901A(MDA) specimens at

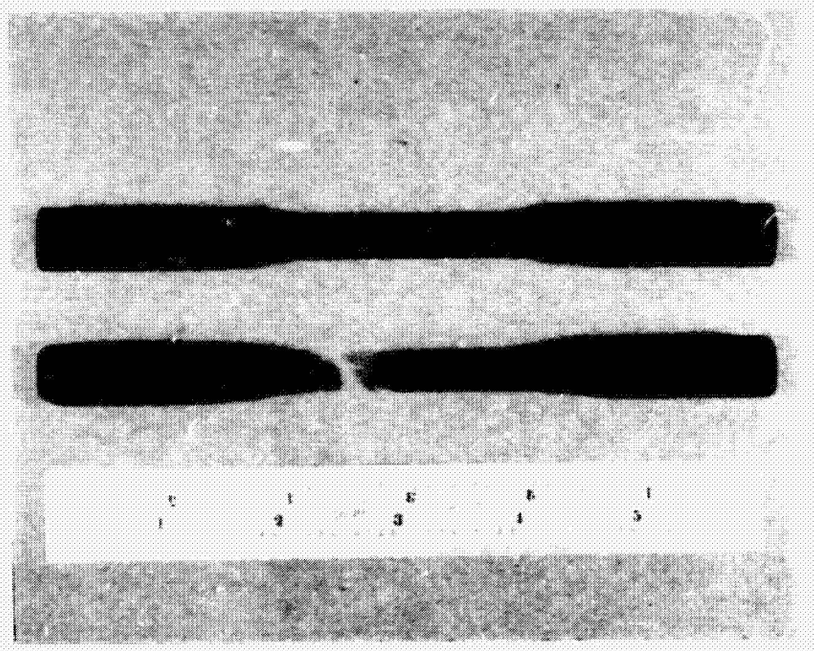

Figure 15. Untested Specimen HX-1504 Torsion (Top) and Failed Specimen (Bottom) Tested at the 121°C, Dry Condition.

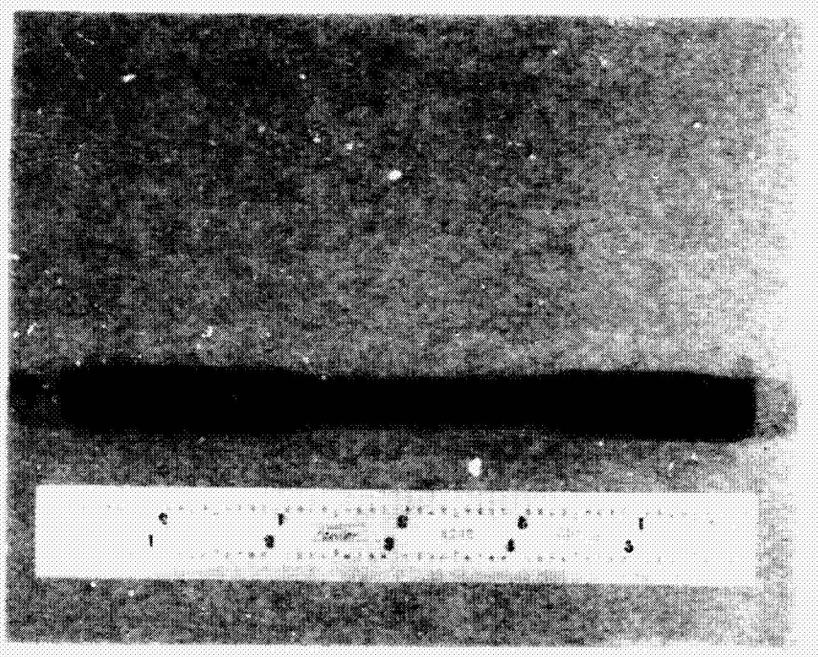

Figure 16. Failed ERX-4901A(MDA) Torsion Specimen Tested at the 121°C, Dry Condition, the Total Twist Being Indicated by the Deformation of the Initially Straight Line Drawn Along the Axis.

this test condition.

Figure 17 shows a failed CYCOM 907 Iosipescu specimen tested at the 23°C, dry condition. The inside right and inside left load points were very close to the fracture paths of the specimen, probably accounting for the locations of these fractures. The location of the strain gage between the notches can also be seen in this photograph. Elevated temperature, wet testing at 82°C yielded failures such as that seen in Figure 18. No gross fracture has occurred, but a distinct lateral translation of the right half of the specimen relative to the left half can be seen, as well as the distortion of the strain gage due to shear loading.

Figure 19 shows a failed HX-1504 torsion specimen tested at 121°C, wet. There is much less material missing than was observed in the 23°C and 82°C, wet testing. That is, a less brittle failure is indicated in the specimen of Figure 19. Likewise, this failure is much less brittle than that indicated previously in Figure 15 for the same material tested in the 121°C, dry condition. A classic torsion failure of a brittle material is nevertheless obvious in Figure 19. The failure surface is at a 45 degree angle, suggesting that failure occurred on the plane of maximum tensile stress.

A typical failure of a CYCOM 907 Iosipescu shear test specimen is shown in Figure 20. This specimen was tested at 23°C, wet and failed in three distinct pieces, similar to the dry specimen failures (see Figure 17). No fracture was obtained for the CYCOM 907 at the 82°C, wet test condition, however. The specimen deformed plastically at this elevated temperature, wet condition and the test was suspended after gross deformation occurred.

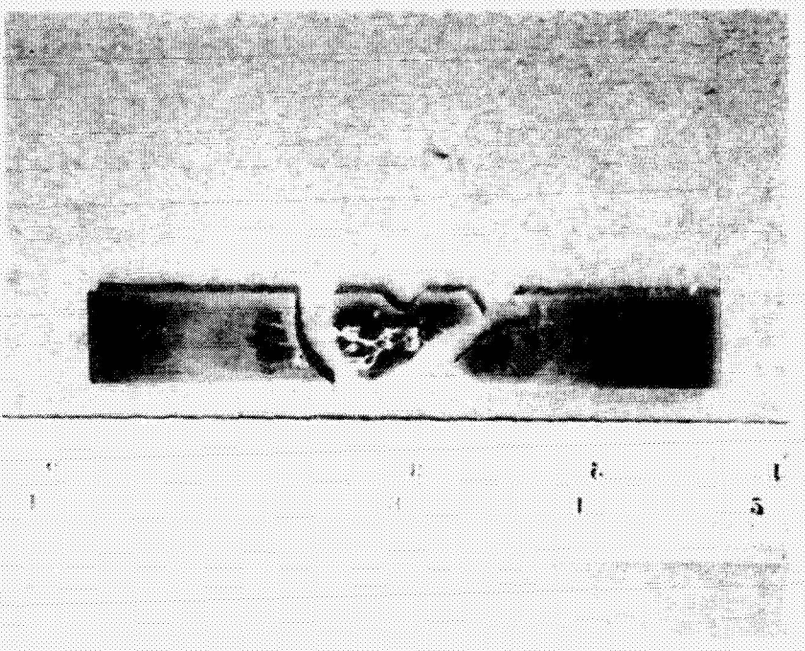

Figure 17. Failed CYCOM 907 Iosipescu Shear Specimen Tested at the 23°C, Dry Condition.

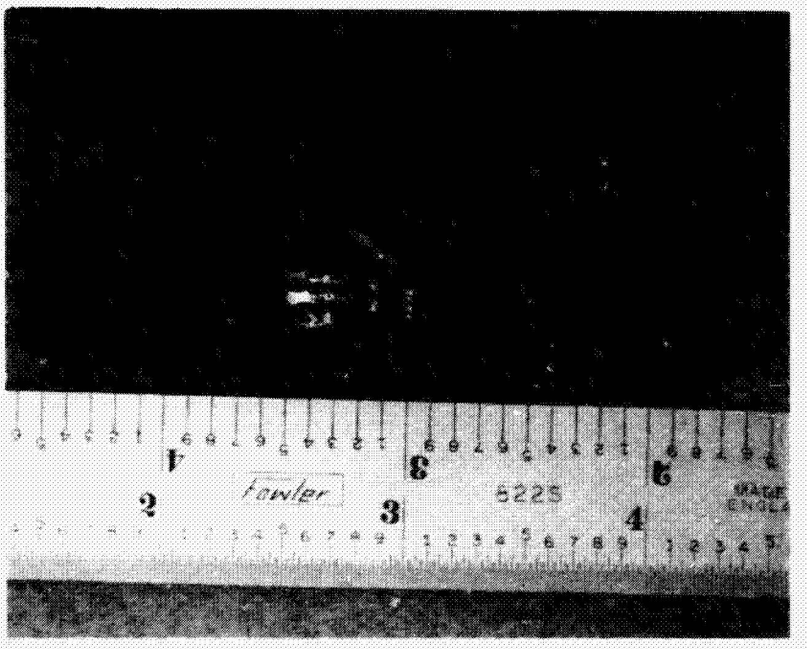

Figure 18. Failed CYCOM 907 Iosipescu Shear Specimen Tested at the 82°C, Dry Condition. Excessive Transverse (Shear) Deformation Across the Notches Will Be Noted.

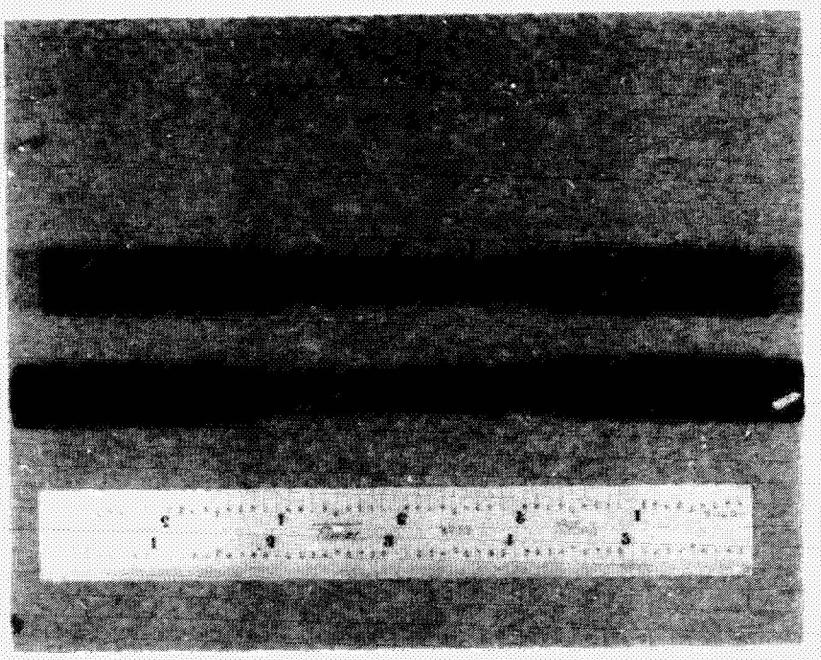

Figure 19. Untested HX-1504 Torsion Specimen (Top) and Failed Specimen (Bottom) Tested at the 121°C, Wet Condition, Showing the Characteristic Helical Fracture Surfaces Observed.

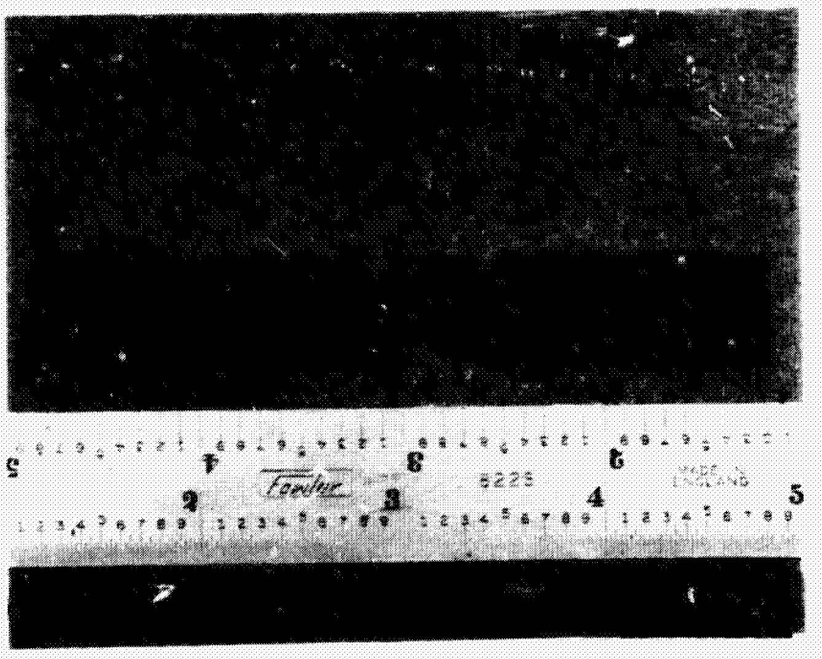

Figure 20. Failed CYCOM 907 Iosipescu Shear Specimen Tested at 23°C, Wet, Showing a Characteristic Three-Piece Failure.

3.5 Relations Between Elastic Constants

As in the first-year program [1], the lack of satisfaction of the isotropic relation [11]

$$G = \frac{E}{2(1 + \nu)} \tag{1}$$

was apparent. Results for all eight matrix materials are summarized in Table 8. The data for the first four materials are reported from Table 2 of Reference [1]. The occasional differences between the values listed in Table 8 and those of Reference [1] are due to the data errors corrected since Reference [1] was published, or round-off differences due to converting to S.I. units here.

As can be seen in Table 8, the values of shear modulus G calculated from Eq. (1) using values of Young's modulus E and Poisson's ratio ν measured in the uniaxial tensile tests are generally lower than the measured values of G (using the solid rod torsion test; or the Iosipescu shear test in the case of the CYCOM 907 epoxy, as previously discussed). The scatter in the data for the four matrix materials of the present study is greater than that observed previously, even though with even more testing experience and at least as much care, it might be expected that less scatter should be present. One possible explanation is that the current resin systems are much different from one another than the previous four systems were. For example, the Narmco 5245-C exhibited a negative percent difference (i.e., the calculated value of G was higher than the measured value) for three of the six environmental conditions, being the only resin system to exhibit such a response. Two of these negative percentages were low, i.e., -7 percent and -4 percent. The value of -40 percent at the 23°C, dry condition was due to the

TABLE 8

Measured Versus Calculated Shear Moduli
for Eight Neat Resin Systems

Neat Resin System	Measured Young's Modulus (GPa)	Measured Poisson's Ratio	Measured Shear Modulus (GPa)	Calculated Shear Modulus (GPa)	$\frac{G_{meas}-G_{calc}}{G_{meas}}$ (percent)
23°C, Dry					
Hercules 3502	3.65	0 36	1.79	1.34	25
Fibredux 914	4.02	0.36	1.52	1.48	3
Hercules 2220-1	3.15	0.36	1.52	1.16	24
Hercules 2220-3	3.17	0.36	1.38	1.17	16
Hexcel HX-1504	3.86	0.369	1.79	1.41	21
Narmco 5245-C	3.74	0.387	0.96	1.35	-40
CYCOM 907	3.26	0.416	1.18	1.15	3
ERX-4901A(MDA)	4.80	0.408	2.00	1.70	15
54°C, Dry					
Hercules 3502	3.24	0.36	1.59	1.19	25
Fibredux 914	3.37	0.36	1.52	1.24	18
Hercules 2220-1	2.96	0.37	1.38	1.08	22
Hercules 2220-3	2.96	0.36	1.24	1.09	12

TABLE 8 (CONTINUED)

Measured Versus Calculated Shear Moduli
for Eight Neat Resin Systems

Neat Resin System	Measured Young's Modulus (GPa)	Measured Poisson's Ratio	Measured Shear Modulus (GPa)	Calculated Shear Modulus (GPa)	$\frac{G_{meas}-G_{calc}}{G_{meas}}$ (percent)
82°C, Dry					
Hercules 3502	3.10	0.37	1.59	1.13	29
Fibredux 914	3.17	0.37	1.52	1.16	24
Hercules 2220-1	2.62	0.36	1.17	0.96	18
Hercules 2220-3	2.45	0.35	1.10	0.91	17
Hexcel HX-1504	3.31	0.360	1.51	1.22	19
Narmco 5245-C	3.45	0.396	1.45	1.24	15
CYCOM 907	2.76	0.424	0.98	0.97	1
ERX-4901A(MDA)	2.63	0.440	1.45	0.98	32
121°C, Dry					
Hercules 3502	2.76	0.463	--		
Fibredux 914	0.67	0.436	--		
Hercules 2220-1	2.28	0.430	--		
Hercules 2220-3	2.16	0.390	--		
Hexcel HX-1504	2.69	0.367	1.10	0.98	11
Narmco 5245-C	3.10	0.400	1.03	1.11	-7
CYCOM 907	0.83	0.375	0.77	0.30	61
ERX-4901A(MDA)	0.48	0.346	0.90	0.18	80

TABLE 8 (CONTINUED)

Measured Versus Calculated Shear Moduli
for Eight Neat Resin Systems

Neat Resin System	Measured Young's Modulus (GPa)	Measured Poisson's Ratio	Measured Shear Modulus (GPa)	Calculated Shear Modulus (GPa)	$\frac{G_{meas}-G_{calc}}{G_{meas}}$ (percent)
23°C, Moisture-Saturated					
Hercules 3502	3.52	0.43	1.58	1.23	22
Fibredux 914	3.10	0.43	1.45	1.08	25
Hercules 2220-1	3.11	0.41	1.52	1.10	27
Hercules 2220-3	3.03	0.43	1.52	1.06	30
Hexcel HX-1504	3.51	0.396	1.52	1.26	17
Narmco 5245-C	4.00	0.392	1.38	1.44	-4
CYCOM 907	2.90	0.430	1.10	1.01	8
ERX-4901A(MDA)	3.58	0.396	1.65	1.28	22
54°C, Moisture-Saturated					
Hercules 3502	3.03	0.38	1.38	1.10	20
Fibredux 914	2.56	0.42	1.24	0.90	27
Hercules 2220-1	2.56	0.43	1.31	0.90	31
Hercules 2220-3	2.41	0.44	1.24	0.84	32

TABLE 8 (CONTINUED)

Measured Versus Calculated Shear Moduli
for Eight Neat Resin Systems

Neat Resin System	Measured Young's Modulus (GPa)	Measured Poisson's Ratio	Measured Shear Modulus (GPa)	Calculated Shear Modulus (GPa)	$\frac{G_{meas}-G_{calc}}{G_{meas}}$ (percent)
82°C, Moisture-Saturated					
Hercules 3502	2.58	0.42	1.10	1.04	5
Fibredux 914	2.14	0.40	1.17	0.76	35
Hercules 2220-1	2.07	0.43	1.24	0.72	42
Hercules 2220-3	2.14	0.47	1.31	0.73	44
Hexcel HX-1504	2.76	0.410	1.03	0.98	5
Narmco 5245-C	3.10	0.424	1.38	1.09	21
CYCOM 907	0.07	0.518	0.21	0.02	90
ERX-4901A(MDA)	0.07	--	0.16	--	--
121°C, Moisture-Saturated					
Hercules 3502	1.90	0.45	--		
Fibredux 914	0.27	--	--		
Hercules 2220-1	1.02	--	--		
Hercules 2220-3	0.86	--	--		
Hexcel HX-1504	0.89	0.500	0.62	0.30	52
Narmco 5245-C	[illegible]	0.510	0.90	0.30	67
CYCOM 907	--	--	--		
ERX-4901A(MDA)	--	--	--		

abnormally low value of G measured, i.e., 0.96 MPa. At the 82°C, dry condition the measured value of G was 1.45 MPa; at 121°C, dry it was 1.03 MPa. Since the matrix stiffness would normally be expected to decrease with increasing temperature, as typically indicated by the other materials tested, experimental error in the 23°C, dry data is suspected, although none was uncovered.

Rather than focusing on the few anomalies in the data of Table 8, however, it should be emphasized that the trend of the calculated values of G being lower than the measured values is obvious, the average difference being about 20 percent. The differences were roughly comparable between the data of the two years. The differences were again the greatest at the highest test temperatures, for both dry and moisture-saturated conditions. This could be associated with the more pronounced nonlinearity of the material at the higher temperature, or simply due a greater influence of data error associated with measuring smaller values of E and G.

Careful study of the data of Table 8 did not suggest any other clear trends from material to material, or from one test condition to another.

As stated in the prior report [1] also, it should be emphasized that both the tensile test and the shear tests are well established, straightforward techniques, and typically at least five or six replicates were tested to establish the averages given in Table 8. The coefficients of variation were typically less than five percent. Thus, the data are considered to be very reliable. Also, this observation that the isotropic relation of Eq. (1) is not satisfied for neat resins is not new. The present authors reported a similar discrepancy for Hercules

3501-6 epoxy in Reference [12], based upon tests conducted in 1978. Prior to the time, relatively little neat resin specimen fabrication and testing had been done, and it was not known whether the observed discrepancies between E, ν and G were real, or simply due to experimental error, only very limited data being available.

Recently, a brief discussion with E. T. Camponeschi [13] indicated that he and his colleagues have also noted a discrepancy between E, ν and G for Narmco 5208 epoxy, a system similar to the Hercules 3501-6 and 3502 epoxies. No data have yet been published, however.

The present authors are not yet prepared to explain the consistent discrepancy observed. However, it would appear that it is associated with a coupling between shear stresses and normal strains, and possibly between normal stresses and shear strains. The former coupling effect has been observed by the authors in unpublished torsion test results for thin-walled neat resin tubes, and also for solid rods. That is, the applied shear stress induces an axial normal strain in the specimen. This should not occur in an isotropic material, nor in a specially orthotropic material. However, it would in an anisotropic material, this coupling parameter being termed a "coefficient of mutual influence of the first kind" by Lekhnitski [14]. Whether other coupling terms may also exist, e.g., "coefficients of mutual influence of the second kind" and Chentsov coefficients [15], has not been tested by the present authors as of yet. The suggestion is, however, that an ansiotropic constitutive relation may be required to properly define the stress-strain response of polymers such as those utilized here. Obviously, much more work remains to be done in this area.

3.6 Correlations with Bulk Modulus Measurements

Because of the consistent discrepancy between measured values of the shear modulus G and the values calculated using the isotropic relation of Eq. (1), as presented in Section 3.5, it was desired to obtain additional independent data. After discussing the problem with Dr. Paul Zoller of DuPont [16], he agreed to perform bulk modulus measurements on samples of the resin systems. Samples of seven of the eight resin systems were sent to him (a sample of the Union Carbide ERX-4901A(MDA) was not available at the time), along with a sample of Hercules 3501-6 epoxy. To date, Dr. Zoller has tested four of the eight systems provided to him, viz, Hercules 3501-6 and 2220-1, Narmco 5245-C, and Fibredux 914.

Each of the four resin systems was tested at three nominal temperatures, viz, 30°C, 66°C, and 102°C. The actual temperature of each test was provided; temperatures varied only slightly from these nominal values. Thus, only nominal values are reported here. Results of the bulk modulus measurements made at DuPont are given in Table 9.

The isotropic relation for calculating bulk modulus is usually expressed as [11]:

$$K = \frac{E}{3(1 - 2\nu)} \tag{2}$$

where E and ν are the Young's modulus and Poisson's ratio, respectively. Since measurements of E and ν had been made at temperatures other than those used by Dr. Zoller in his bulk modulus tests, the values given in Table 8 were linearly interpolated to give the values listed in Table 9. Then, using Eq. (2), the first column of calculated values of K listed in Table 9, in terms of E and ν, were obtained. As can be seen, the

TABLE 9

MEASURED VERSUS CALCULATED BULK MODULI FOR FOUR NEAT RESIN SYSTEMS

Neat Resin System	Estimated Young's Modulus* (GPa)	Estimated Poisson's Ratio*	Estimated Shear Modulus (GPa)	Measured Bulk Modulus [16] (GPa)	Calculated Bulk Modulus, K, and Percent Deviation from Measured, $K_{meas}-K_{calc}/K_{meas}$ Using E and ν (Eq. 2) K (GPa)	Using E and ν (Eq. 2) Deviation (percent)	Using ν and G (Eq. 5) K (GPa)	Using ν and G (Eq. 5) Deviation (percent)	Using E and G (Eq. 6) K (GPa)	Using E and G (Eq. 6) Deviation (percent)
30°C, Dry										
Hercules 3501-6**	4.13	0.34	1.56	4.79	4.30	10	2.27	53	1.82	62
Fibredux 914	3.87	0.36	1.52	5.54	4.61	17	2.90	48	0.82	85
Hercules 2220-1	3.11	0.36	1.49	4.85	3.70	24	2.84	41	0.85	82
Narmco 5245-C	3.71	0.39	1.02	4.49	5.62	-25	2.94	35	***	--
66°C, Dry										
Hercules 3501-6**	3.40	0.34	1.27	4.39	3.54	19	1.85	58	1.82	59
Fibredux 914	3.28	0.36	1.37	5.20	3.90	25	2.61	50	****	--
Hercules 2220-1	2.81	0.36	1.29	4.31	3.35	22	2.46	43	****	--
Narmco 5245-C	3.53	0.39	1.32	4.29	5.35	-25	3.80	11	1.85	57
102°C, Dry										
Hercules 3501-6**	2.67	0.34	0.99	3.94	2.78	29	1.44	63	1.62	59
Fibredux 914	1.89	0.40	1.05	4.75	3.15	34	3.50	26	****	--
Hercules 2220-1	2.45	0.40	0.66	4.05	4.08	-1	2.20	46	***	--
Narmco 5245-C	3.27	0.40	1.23	4.24	5.45	-29	4.10	3	1.55	63

*Interpolation of data at higher and lower temperatures

**From References [12,17]

***Negative denominator

****Negative numerator

deviations from the measured values of bulk modulus were generally in the range of 20 percent, with the Narmco 5245-C exhibiting irregular response, i.e., the calculated value was higher than the measured value. It will be recalled (see Table 8) that this tended to be the case in the calculations of shear modulus G from E and ν also. Possible reasons are discussed in Section 3.5.

The measured values of E, ν and G for all of the materials tested appear to be reasonable in general, with a very few exceptions, as previously noted. Nevertheless, it is conceivable that either the tensile testing or the shear testing, or both, are being conducted improperly. (This is definitely not suspected, however. For example, identical tests using aluminum give values of E, ν and G which consistently satisfy the isotropic relation of Eq. 1).

The isotropic relation for bulk modulus given in Eq. (2) can be reformulated in terms of ν and G instead, starting with the definition of bulk modulus in terms of the Lame constants λ and G as [11]:

$$K = \lambda - \frac{2}{3} G \tag{3}$$

where $$\lambda = 2G\nu/(1 - 2\nu) \tag{4}$$

and G is the shear modulus.

Substituting Eq. (4) into Eq. (3) gives

$$K = \frac{2}{3} G \left(\frac{5\nu - 1}{1 - 2\nu}\right) \tag{5}$$

Thus, K can be calculated independently of the experimentally measured

value of E. The calculations using Eq. (5) are also listed in Table 9. As can be seen, the predicted values of K are again consistently lower than the measured values. But the deviations are typically about twice as great as when K was calculated from E and ν.

To complete the exercise, ν was then eliminated from the relation used to calculate K. This was done by solving Eq. (1) for ν, and substituting this into Eq. (3), where λ is defined by Eq. (4). The result is

$$K = \frac{G(\frac{5}{3}E - 4G)}{(3G - E)} \tag{6}$$

The values of K calculated using Eq. (6) are presented in the last columns of Table 9. As can be seen, the deviations from the measured values of K were generally greater than when Eq. (5) was used. Another difficulty in using Eq. (6) was that under certain conditions, either the numerator or the denominator was negative. This is physically impossible, of course, since the bulk modulus must be a positive quantity. If the measured values of E and G used are assumed to be reasonably accurate, this calculation is a further indication that the isotropic relation is not valid for these materials.

Poisson's ratio ν is the most difficult property of the three stiffnesses E, ν and G to measure accurately, being the quotient of small strain values and therefore very sensitive to inaccuracies of measurement. The sensitivity of K to errors in ν can be seen by examining Eq. (5). The term in the numerator involves multiplying ν by five, thus amplifying any measured error. Thus, it was anticipated that eliminating dependence on ν in the calculation of K might improve

accuracy. As can be seen, this was not the case.

In summary, a careful study of the bulk modulus results of Table 9 did not suggest any logical trends, other than the fact that the isotropic relation is not satisfied. It is hoped that additional bulk modulus data will become available for additional comparisons. However, indications are that the present data, although somewhat limited in amount, are sufficiently accurate to demonstrate the inconsistency between measured and calculated values of bulk modulus.

3.7 Fracture Toughness Test Results

Neat resin fracture toughness testing was performed on the four neat resins using the Single-Edge Notched-Bend (SEN) test method described in ASTM Standard E399 [18]. All testing was performed using an Instron Model 1125 universal test machine.

Test specimens were cast in the same manner as the tension specimens, being 152 mm (6.0 in) long, 12.7 (0.50 in) wide, and 6.4 mm (0.25 in) thick. Three notches were cut along one edge of each specimen, spaced evenly to allow for three tests of each 15.2 mm (6 in) rectangular piece. An abrasive blade in a metallurgical cut-off saw was used for this notching operation.

Figure 21 shows the three-point bend fixture used to test the fracture toughness specimens. A razor blade cooled in liquid nitrogen was used to start the crack at the tip of the sawcut notch, using a light tap on the razor blade. This method was selected after lengthy discussions with numerous investigators to pick the best crack initiator method. A manual tap on the razor blade was used, and usually provided a satisfactory starter crack. Some specimens were broken due to too hard a tap, but a feel for the proper tapping force on the razor blade was

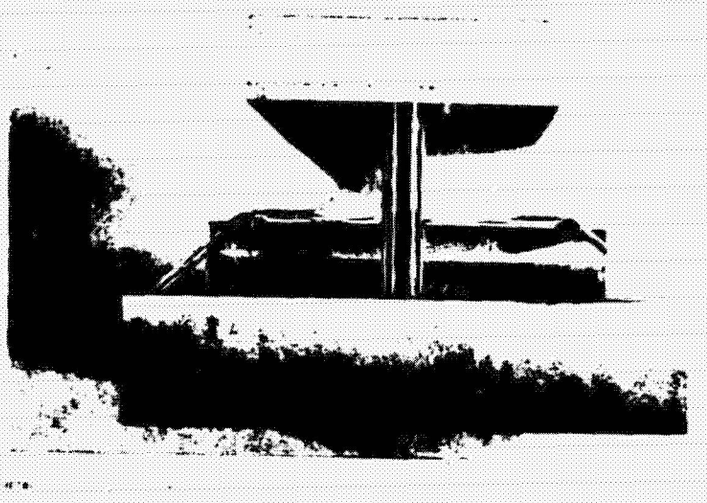

Figure 21. Text Fixture Used in Conducting the Single-Edge Notched-Bend (SEN) Fracture Toughness Testing.

quickly developed.

Figure 22 is a barchart plot of the average critical strain energy release rates (G_{IC}) of the four neat resin systems. Table 10 lists these average values of G_{IC} for the four neat resin systems tested. Three of the four resins exhibited relatively low values when tested dry at all three temperatures. The average value for the CYCOM 907 was above 1300 J/m^2, however, and increased rapidly with increasing temperature. This material was not tested at the 121°C temperature since the toughness was so much higher than the other three resins at the 82°C temperature, and the crack did not propagate at the 82°C temperature. The G_{IC} values reported here are two to four times the values obtained by others for these resins [19] and should therefore only be used for relative comparison purposes. The individual test results are tabulated in the Appendix and indicate the large scatter of the data. Some difficulty is still being encountered in initiating the crack in the SEN test method. These relatively brittle resins make it difficult to initiate adequate cracks without failing the test specimen. Representative test specimens have been sent to NASA-Langley for testing also, to obtain an independent evaluation of the present test procedure.

The 5245-C bismaleimide/epoxy blend remained quite low in toughness even at the high test temperatures when tested dry. In fact, the toughness actually decreased, somewhat. The HX-1504 and ERX-4901A toughness increased slightly as temperature increased.

The critical strain energy release rate averages for the moisture-saturated materials shown in Figure 22 indicate that all four neat resins exhibited higher values when wet than when dry, and these values increased at a much faster rate as temperatures were increased. The

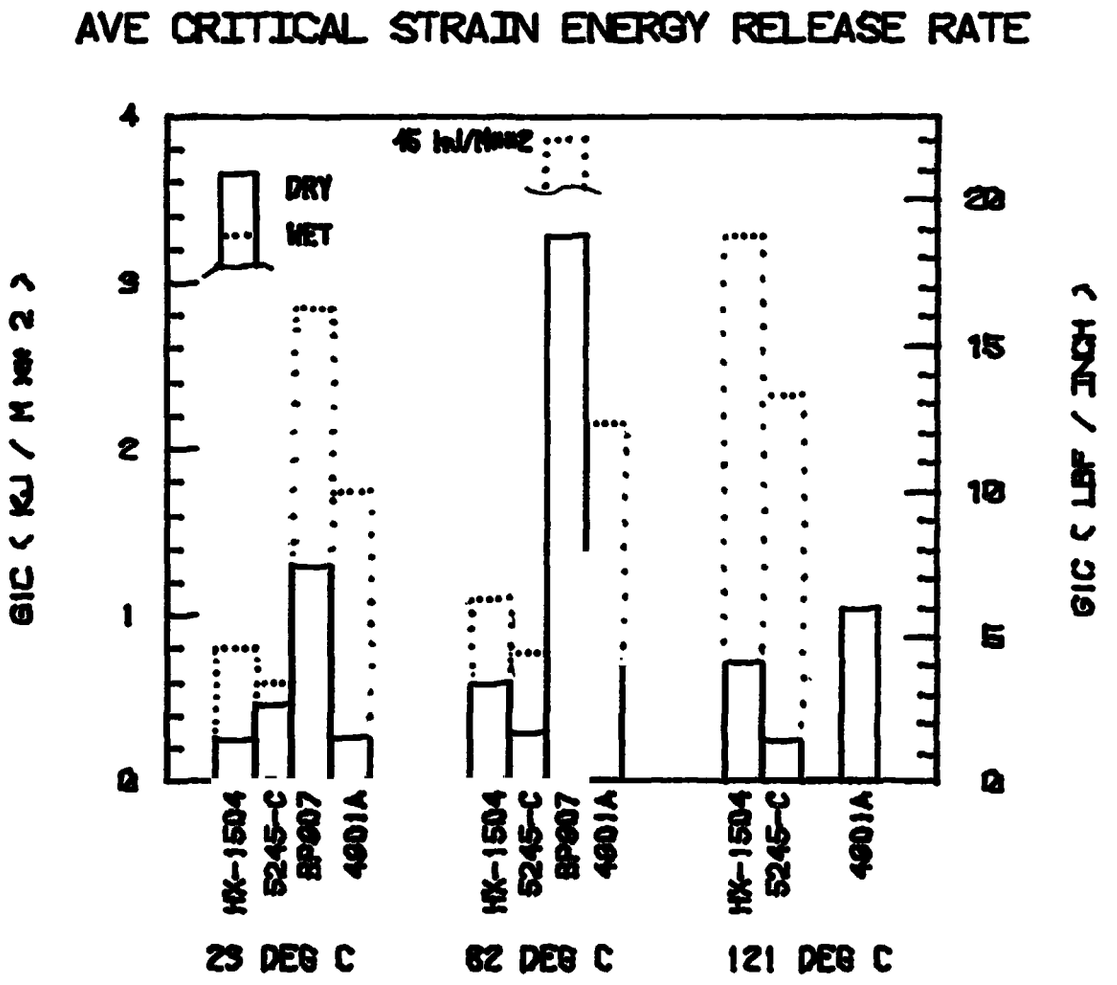

Figure 22. Average Critical Strain Energy Release Rate of the Four Neat Resin Systems Tested, as a Function of Test Temperature and Moisture Content.

TABLE 10

AVERAGE CRITICAL STRAIN ENERGY RELEASE RATES
FOR THE FOUR NEAT RESIN SYSTEMS TESTED

Neat Resin System	Test Temperature (°C)	Critical Strain Energy Release Rate G_{IC} (J/m^2) Dry	Wet
HX-1504	23	253	803
	82	590	1100
	121	727	3280
5245-C	23	470	592
	82	298	782
	121	258	2325
CYCOM 907	23	1293	2840
	82	3286	45062
	121	--	--
ERX-4901A(MDA)	23	276	1753
	82	716	2150
	121	1040	--

CYCOM 907 average at the room temperature, wet condition was similar to the value obtained at the 82°C, dry condition, and it rapidly increased to a value of 45 kJ/m^2 at the 82°C, wet condition. This average value was well above those of the other resins, as indicated in Figure 22. The HX-1504 and 5245-C behaved similar to each other, and after being below 1 kJ/m^2 at room temperature, increased to nearly 3 kJ/m^2 at the 121°C temperature when tested wet. The toughness of the ERX-4901A(MDA) increased by a factor of five due to moisture absorption at room temperature, and by a factor of three at the 82°C temperature. No testing was performed on the CYCOM 907 and ERX-4901A(MDA) at the 121°C, wet condition because of the rapid deterioration of these systems under these environmental conditions.

Figures C1 through C14 of Appendix C present optical photographs of various fracture surfaces obtained for the four neat resins tested during the present study. Figures C1 through C3 show fracture surfaces of the HX-1504 at the three test temperatures. The machined notch in the SEN specimen is at the top in these three photographs. Some evidence of crack propagation and arrest can be seen in each photograph.

Figures C4 through C6 are photographs of the 5245-C bismaleimide/ epoxy SEN fracture specimens. The machined notch is at the right. Only by close inspection can any evidence be seen of the crack arresting in this material at room temperature and 82°C. Two bands can be seen in the 121°C specimen, indicating crack arrest may have also occurred in the 5245-C material.

The CYCOM 907 SEN specimen fracture surfaces shown in Figures C7 and C8 of Appendix C, representing tests at room temperature and 82°C, respectively, show no evidence of crack arrest. A specimen tested at

121°C is shown in both Figures C9 and C10. The crack propagated and then arrested some distance from the end of the notch. The specimens at this test condition did not fail catastrophically, but rather deformed until they touched the test fixture after deflecting about 2 mm. Figure C9, a side view of the notch in the SEN specimen, shows the distance the crack propagated into the specimen. Figure C10 shows the open crack at the end of the notch to be much more visible than immediately after the razor blade tap, due to being spread by the bending action of the test.

Figure C11 shows virtually no evidence of crack arrest in the ERX-4901A(MDA) epoxy at room temperature. Some crazing can be seen in the area of the notch end. This crazing was seen in many SEN fractures and is thought to have been caused by insufficient razor tapping force and, therefore, an insufficient initial crack front for proper fracture.

The center of the photograph of Figure C12 shows some evidence of crack arrest. An area of horizontal lines starts which might point to a region of crack arrest.

Figures C13 and C14 are photographs of the ERX-4901A(MDA) epoxy tested at the 121°C, dry condition. Similar behavior to that of the CYCOM 907 is seen at this test condition. The crack propagated and then arrested when the specimen deformed the 2 mm to touch the fixture. The precrack is open, indicating a proper razor tap prior to the test.

3.8 Coefficient of Thermal Expansion Results

Multiple specimens of each resin system were used to measure average coefficients of thermal expansion (CTE). Testing was performed using a quartz tube dilatometer and an LVDT to measure the change in length of the test specimen. Control of the test chamber temperature and acquisition of data was performed by a North Star microprocessor. Data

storage was accomplished using a 5 1/4" floppy disk drive. Testing was performed between -40°C and 120°C, on both dry and wet specimens. Table 11 lists the average values of CTE for the HX 1504, 5245-C, CYCOM 907, and ERX-4901A(MDA). The values were essentially constant over this temperature range. The 5245-C exhibited the lowest CTE of the four systems when tested dry, while the ERX-4901A(MDA) had the highest CTE values. The CTE of all four material systems increased with moisture saturation, as indicated in Table 11.

TABLE 11

AVERAGE COEFFICIENTS OF THERMAL EXPANSION OF THE FOUR NEAT RESIN SYSTEMS TESTED

Resin System	Coefficient of Thermal Expansion, CTE (10^{-6}/°C) Dry	Moisture-Saturated
HX-1504	50.8	54.7
5245-C	48.0	50.2
CYCOM 907	54.8	58.0
ERX-4901A(MDA)	57.8	60.9

3.9 Coefficient of Moisture Expansion Results

Coefficient of moisture expansion (CME) measurements were conducted for each of the four resin systems, from dry to saturation at 65°C. Distilled water in moisture chambers was used to develop the 98 percent relative humidity used for all testing. The CMRG automated moisture expansion test facility was used to perform these CME tests [6]. Two identical specimens are used for the CME measurements. Both specimens are surface ground to a thickness of 0.9 mm (0.035 in) after cutting

into 70 mm x 70 mm (2.75 in x 2.75 in) square pieces. This large square specimen with a very small thickness is used to allow the assumption of one-dimensional diffusion during the moisture saturation process (i.e., edge effects are negligible). An electronic balance is used to measure the weight gain as a function of time of one of the specimens in the test chamber while a quartz tube dilatometer and LVDT are used to measure the in-plane linear expansion of the other specimen simultaneously in the same chamber. Using these two parameters, the strain with respect to percent moisture absorption is then calculated and the numerous data points are then curve-fit using a linear regression analysis. The resulting equation for CME then can be used in the micromechanics computer program as input data to model moisture effects on composite materials. Average CME values and percent weight gains at moisture saturation are given in Table 12 for the four neat resin systems.

TABLE 12

AVERAGE COEFFICIENTS OF MOISTURE EXPANSION AND MOISTURE SATURATION WEIGHT GAINS FOR THE FOUR NEAT RESIN SYSTEMS TESTED

Resin System	Coefficient of Moisture Expansion, CME (10^{-3}/%M)	Moisture Saturation Weight Gain (%M)
HX-1504	2.07	3.8
5245-C	1.52	2.1
CYCOM 907	2.29	5.1
ERX-4901A(MDA)	1.55	7.2

SECTION 4

SCANNING ELECTRON MICROSCOPY

4.1 Introduction

Scanning electron microscopy (SEM) has been a valuable tool in the cataloging and understanding of fracture mechanisms associated with fiber-reinforced composites for many years. The Composite Materials Research Group (CMRG) has utilized the SEM over the past 12 years to study composite material fractures, and the past five years for the study of neat resin fractures. The SEM provides a large depth of field at high magnification and is thus much more valuable in the study of rough fracture surfaces than the optical microscope. Magnifications from 10X to 500X are particularly useful when examining neat resin fractures, but magnifications from 1000X to 5000X are sometimes meaningful.

A JEOL-35C scanning electron microscope was used for all of the work of the present study. This instrument has a magnification range from 10X to 180,000X, a depth of field of 30μ at 1000X, and a resolution of 60Å.

4.2 Specimen Preparation

A total of 27 failed specimens were mounted for examination. Fewer specimens were viewed during this second-year than in the first year [1]. The large volume of photographs taken during the prior year provide a good representation of neat resin fracture surfaces in general, and the preliminary SEM studies performed this year indicated very similar features. Thus, only an overview of the neat resin fracture surfaces observed will be presented here, since similar features were seen in the detailed SEM study completed last year.

A Bueller No. 4150 silicon carbide cutoff blade was used to cut the

SEM specimens from representative failed test specimens. All specimens were then cleaned in an ultrasonic cleaning tank to remove any surface debris. Duco cement was used to bond the SEM specimens to the one-inch diameter brass mounting disks. A silver conducting paint was then applied around the bond line to ensure a good conducting path from the specimen to the brass disk. Finally, gold was vapor-deposited on all specimens to make them electrically conductive and preclude the accumulation of electrons on the fracture surface when the specimen is exposed to the electron beam in the SEM, which causes flaring and hence a poor viewing image.

4.3 Explanation of SEM Photographs

Specimens representing several test conditions for each resin type were viewed and photographed. Representative photographs are presented in Appendix D. A description of each SEM photograph is included below each figure caption, with a brief discussion included to interpret the features shown in that SEM photograph.

The photographic system of the SEM records information directly across the bottom of each SEM photograph. Referring to Figure D1 of Appendix D as a typical example, the caption reads:

25KV X50 0100 100.0U UW84

The interpretation is as follows:

25 KV	election beam accelerating voltage, in kilovolts
X50	magnification
0100	photograph number
100.0U	length of scale bar, in microns
UW84	the SEM unit identification number, i.e., University of Wyoming and the current year, 1984.

The specimen numbering system is summarized here for convenience. A typical specimen identification is divided into three sets of characters. For example, the specimen number in Figure D1 is LTDJ26. This is interpreted as follows:

L	identifies the program, NASA-Langley neat resin testing
TDJ	identifies the specimen type, environmental condition, and resin system
26	identifies the test temperature and specimen number

The complete set of codes for all specimens tested is as follows:

Type of Mechanical Test

T	Tension
S	Torsional Shear
I	Iosipescu Shear
F	Fracture Toughness

Specimen Conditioning

D	Dry
W	Moisture-Saturated (Wet)

Resin System

J	HX-1504
O	5245-C
P	CYCOM 907
Q	ERX-4901A(MDA)

Test Temperature and Specimen Number

00-09	Room Temperature
10-19	82°C
20-29	121°C

This code is slightly different from the one used in the first-year

study [1]; it was changed to simplify the identification of specimens. From five to eight specimens were tested at each condition.

4.4 Neat Resin Tension

One dry and one moisture-saturated neat resin specimen of each resin system was studied in the SEM. Similar fracture surface features as seen previously [1] were seen in the neat resins studied during this year. A failure initiation site could be identified in most cases, located in the smooth zone of the fracture. A transition area outside the smooth zone separated it from a rough zone thought to be the last region to fracture at failure.

The SEM photographs of Figures D1 through D16 of Appendix D are a small sampling of the fracture surfaces for tensile failure surfaces. Descriptions are given at the bottom of each photograph, directly under the figure caption, to allow the reading of the description while viewing the photograph.

4.5 Neat Resin Shear

Both dry and moisture-saturated specimens were examined in the SEM. The photographs of Figures D17 through D28 of Appendix D give representative views of failure surfaces seen in the four neat resin systems studied. Features shown are similar to ones seen in the first-year study [1], with the shear surfaces being similar in appearance to the tension fracture surfaces. Some swirling can be seen in some of the torsion failures, caused by the torsion loading used in those tests. The Iosipescu specimen shown in Figure D26 shows some shear lacerations near the upper notch area, which is characteristic for this test method.

4.6 Neat Resin Fracture Toughness

A number of neat resin fracture toughness specimen surfaces were

also studied in the SEM. One specimen at each condition was viewed and photographed to identify surface feature characteristics for the four neat resins tested. Typical photographs are included in Figures D29 through D41 of Appendix D. The sawcut notch can usually be seen at the left side of each photograph. Very small ridges can also be seen in most of the photographs where the crack probably propagated slowly before failing in an unstable manner. Many of the Single-Edge Notched-Bend (SEN) specimens failed via an unstable crack propagation. As test temperature or moisture level increased, some evidence of crack arrest and then further crack growth was seen. The CYCOM 907 and ERX-4901A (MDA) properties degraded so dramatically at the high temperatures and moisture levels that the specimens never fractured before deflecting enough to touch the test fixture, at which point the test was stopped.

SECTION 5

MICROMECHANICS PREDICTIONS OF COMPOSITE RESPONSE

5.1 Introduction

The philosophy and purpose of developing a micromechanics prediction capability, and details of the finite element analysis methodology used, were presented in detail in the first-year report [1]. Thus, this discussion will not be repeated here. One important addition has been made to the analysis during the past year, however. The longitudinal shear loading capability [5,17,20] utilized in the first-year study has now been combined with a crack initiation and propagation capability [21-24]. Thus, it is now possible to study patterns of crack propagation induced under any combination of mechanical and hygrothermal loadings. This also extends the micromechanics analysis capability one step closer to the ultimate goal of being able to accurately predict unidirectional composite strength. Strengths can, in fact, be predicted now using the present analysis, as will be demonstrated in the next subsections. However, there is still insufficient unidirectional composite experimental data available covering enough different fiber/matrix material combinations and test conditions to permit an adequate correlation of micromechanics predictions with actual data. That is, to date, sufficient correlations have been attempted (see, for example, Reference [17] as well as the result presented here) to indicate significant promise, but not enough to be conclusive.

One recognized problem area is the selection or development of a suitable failure criterion. More composites test data must become available before much more can be done in this area. Thus, in generating the present numerical results, a maximum normal stress failure criterion

has been used for axial and transverse tensile loadings, and an octahedral shear failure criterion for longitudinal shear loadings. Obviously it would be desireable to develop a universal failure criterion applicable to all loading conditions.

5.2 Constituent Material Properties

As in the first-year study [1], a graphite/epoxy composite was modeled, assuming a fiber volume of 60 percent. The circular fibers were assumed to be packed in a square array, the finite element grid model being as presented in Figure 63 of Reference [1].

5.2.1 Fiber Properties

A Hercules AS4 graphite fiber was modeled; the assumed properties are listed in Table 13. These are the same graphite fiber properties used in generating the micromechanics predictions of the first-year study. Again the transverse normal strength and the axial and in-plane shear strengths of the fiber were assumed to be arbitrarily high values, to insure that the fiber did not fail in these modes.

5.2.2 Matrix Properties

The measured properties of the four matrix materials of the present study, viz, Hexcel HX-1504, Narmco 5245-C, American Cyanamid CYCOM 907, and Union Carbide ERX-4901A(MDA), were reported in Section 3, actual stress-strain curves being included in Appendix B. For use in the micromechanics analysis, it is necessary to average the typically five to seven individual stress-strain curves at each given test condition into a single curve. As described previously [1], this is done using a Richard-Blacklock curve-fit relation [28]. Since tests were conducted on both dry and moisture-saturated specimens at three different temperatures, viz, 23°C, 82°C, and 121°C, this averaging results in six curves

TABLE 13

HERCULES AS4 GRAPHITE FIBER PROPERTIES [25]

Longitudinal Modulus, E_ℓ	235 GPa	(34 Msi)
Transverse Modulus*, E_t	14 GPa	(2 Msi)
Major Poisson's Ratio*, $\nu_{\ell t}$	0.20	
In-Plane Poisson's Ratio*, ν_{tt}	0.25	
Longitudinal Shear Modulus*, $G_{\ell t}$	28 GPa	(4 Msi)
In-Plane Shear Modulus**, G_{tt}	5.5 GPa	(0.8 Msi)
Coefficient of Longitudinal Thermal Expansion, α_ℓ	-0.36×10^{-6}/°C	
Coefficient of Transverse Thermal Expansion*, α_t	18×10^{-6}/°C	
Longitudinal Tensile Strength, σ_ℓ^u	3.59 GPa	(520 ksi)
Transverse Tensile Strength*, σ_t^u	0.35 GPa	(50 ksi)

*Estimated (see References [26,27]

**Calculated, $G_{tt} = E_t/2(1 + \nu_{tt})$

for each resin system, for each of the two loading conditions, i.e., axial tension or shear (solid rod torsion or Iosipescu). Since, as discussed in detail in Sections 3.5 and 3.6, these matrix materials do not exhibit classical isotropic response, different results will be obtained depending upon whether the tensile or the shear data are used in the micromechanics analysis. Based upon prior experience, and consistent with the first-year work [1], the shear stress-strain curves have been used here. However, both tensile and shear data will be presented here, for future reference

For sake of completeness, the tensile stress-strain curves and the shear stress-strain curves for the four matrix materials tested in the first-year study, viz, Hercules 3502, Hercules 2220-1, Hercules 2220-3, and Ciba-Geigy Fibredux 914, are included here also, as Figures 23 through 26. These are Figures 64 through 67 of Reference [1]. The curves for dry specimens are shown as solid lines, the moisture-saturated results as dashed lines. The curves for each condition decrease in order with increasing temperature.

Since predicted results will also be presented for the Hercules 3501-6 epoxy tested several years ago in another program [29], its average tensile and shear stress-strain curves are given in Figure 27. Values of E, ν and G for this matrix material were given in Table 9 also, at different temperatures. Complete data for the Hercules 3501-6 epoxy can be found in References [12,17].

Tensile and shear stress-strain curves are presented for each of the four matrix materials tested in the present study in Figures 28 through 31. Property values were also given in Tables 1 through 6 of Section 1. As can be seen, the shear stress-strain curves exhibit some

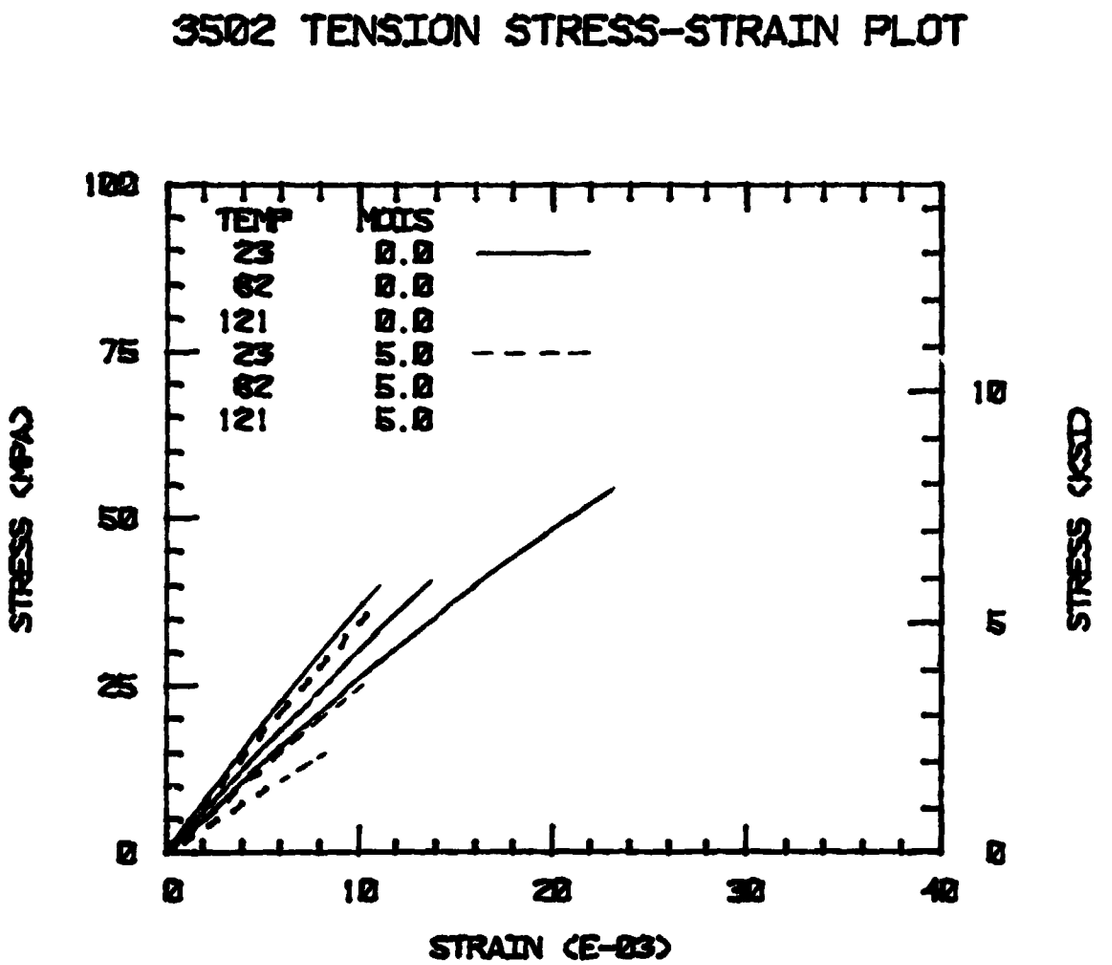

a) tensile data

Figure 23. Hercules 3502 Neat Resin Stress-Strain Curves, Dry (solid lines) and Moisture-Saturated (dashed lines), at Three Test Temperatures.

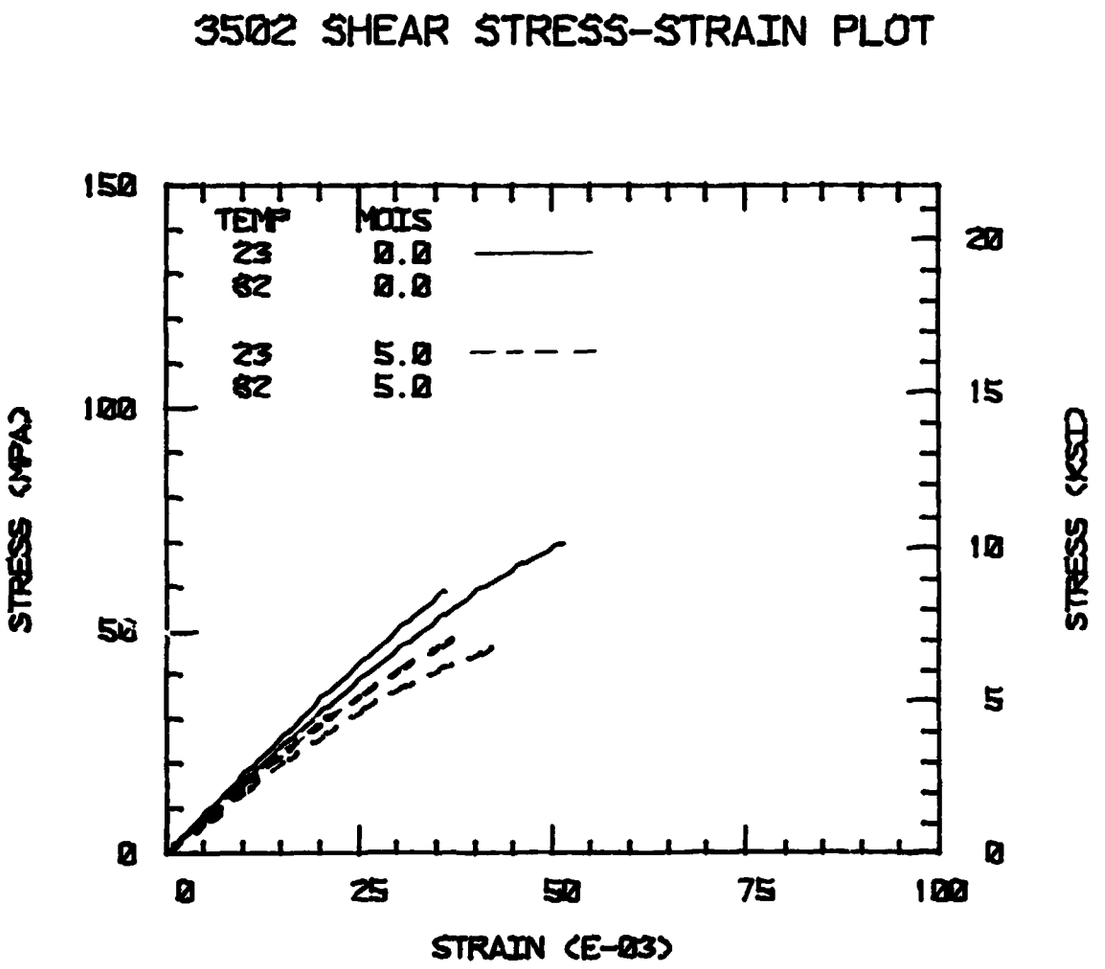

b) shear data

Figure 23 (continued). Hercules 3502 Neat Resin Stress-Strain Curves, Dry (solid lines) and Moisture-Saturated (dashed lines), at Three Test Temperatures.

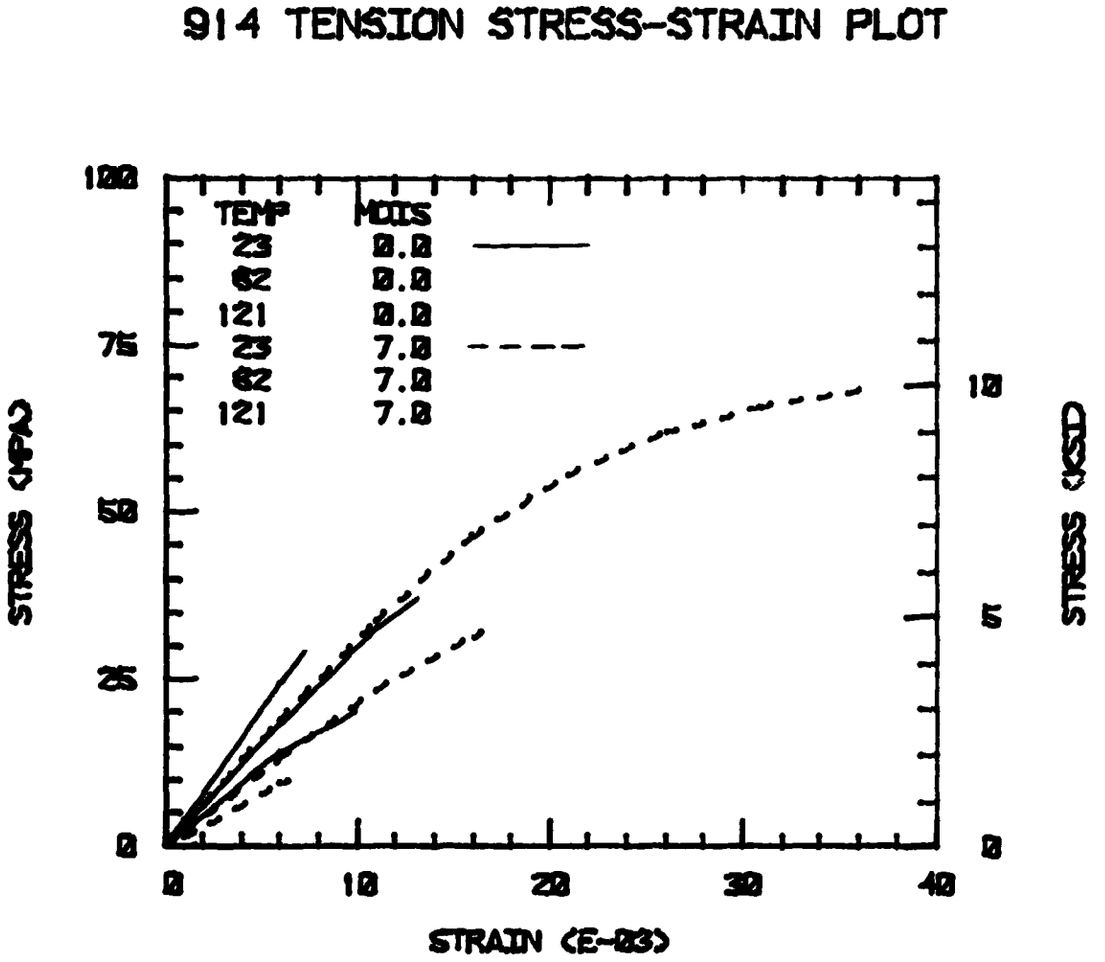

a) tensile data

Figure 24. Ciba Geigy Fibredux 914 Neat Resin Stress-Strain Curves, Dry (solid lines) and Moisture-Saturated (dashed lines), at Three Test Temperatures.

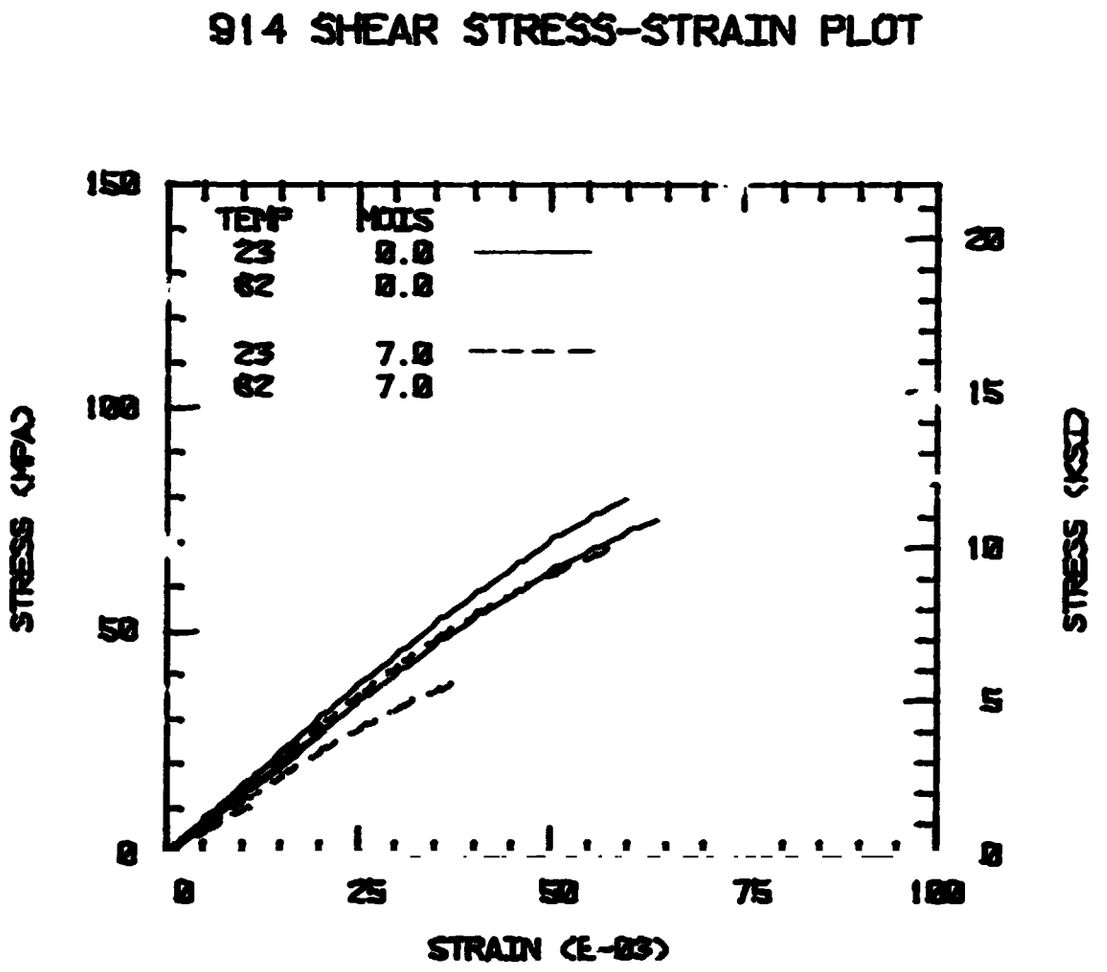

b) shear data

Figure 24 (continued). Ciba Geigy Fibredux 914 Neat Resin Stress-Strain Curves, Dry (solid lines) and Moisture-Saturated (dashed lines), at Three Test Temperatures.

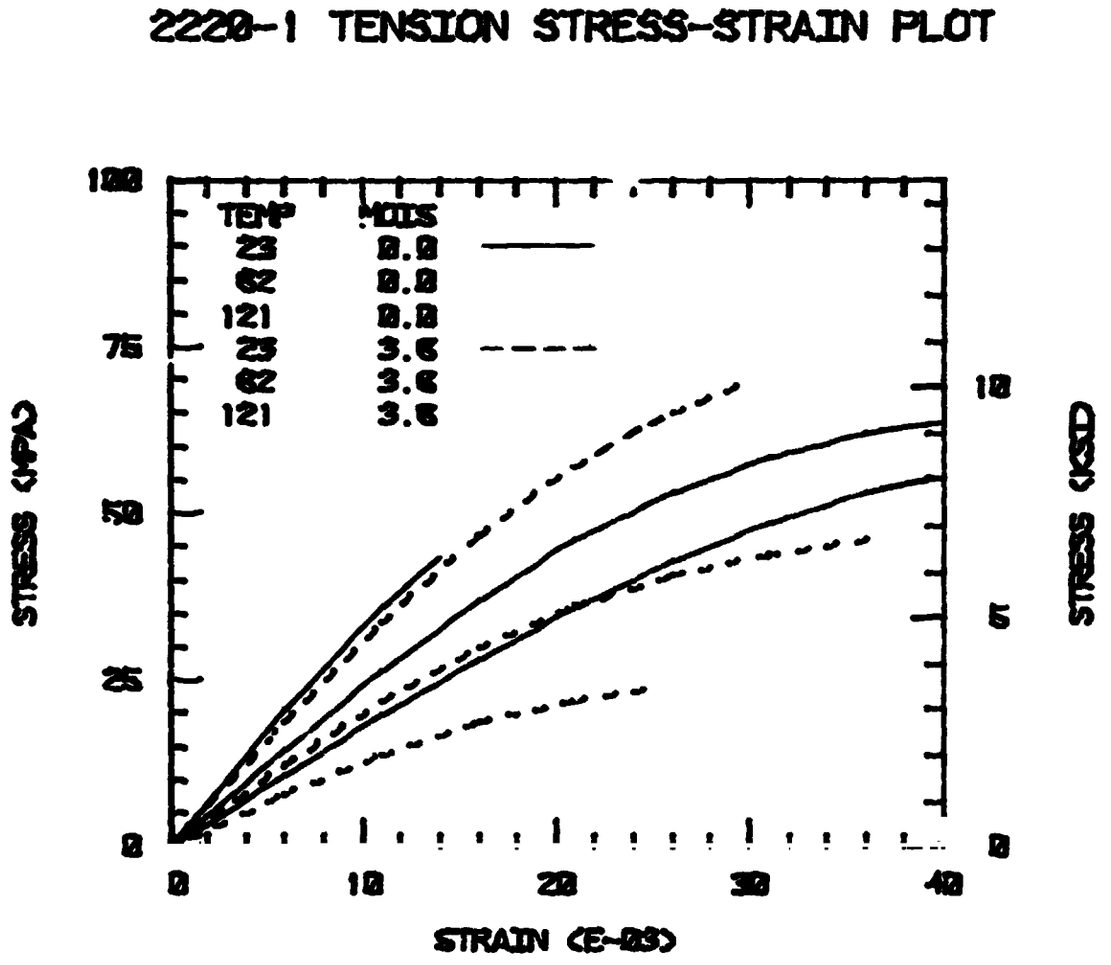

a) tensile data

Figure 25. Hercules 2220-1 Neat Resin Stress-Strain Curves, Dry (solid lines) and Moisture-Saturated (dashed lines), at Three Test Temperatures.

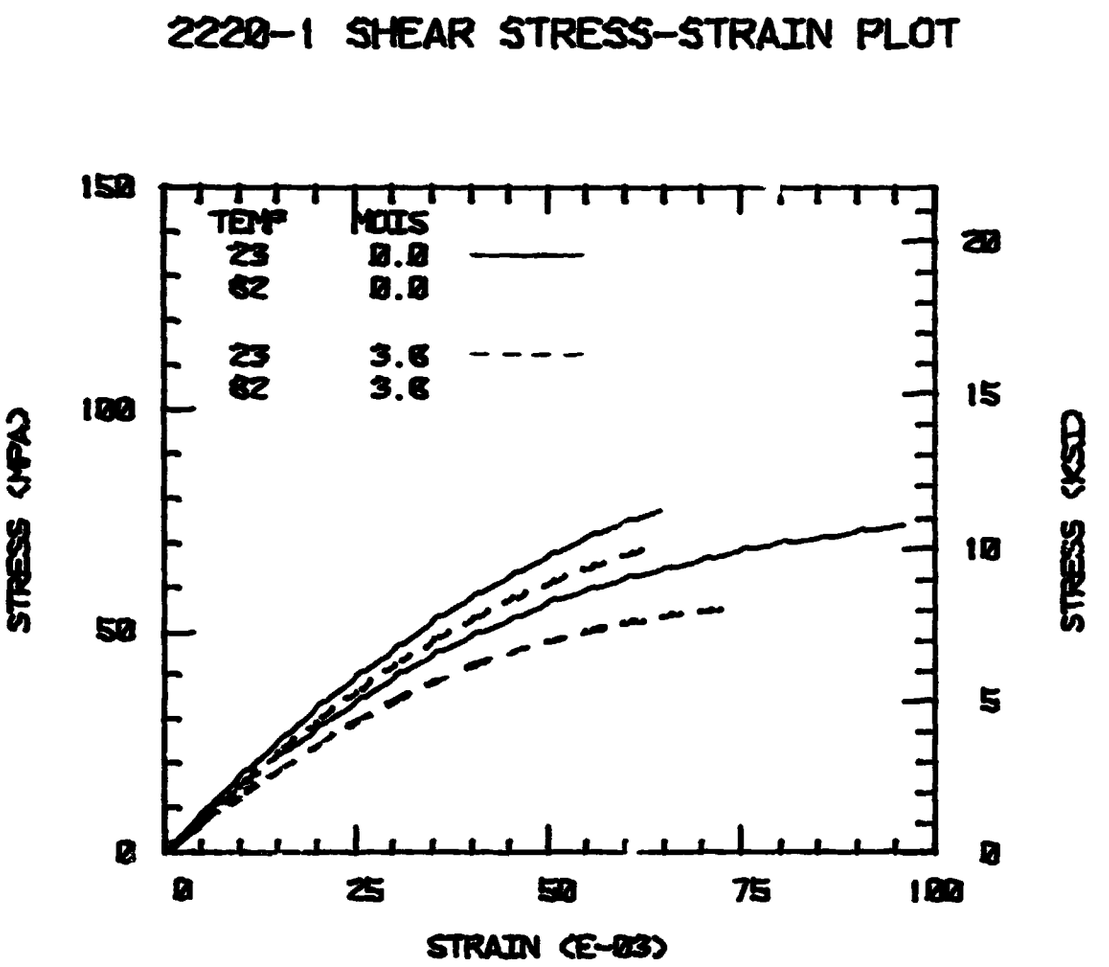

b) shear data

Figure 25 (continued). Hercules 2220-1 Neat Resin Stress-Strain Curves, Dry (solid lines) and Moisture-Saturated (dashed lines), at Three Test Temperatures.

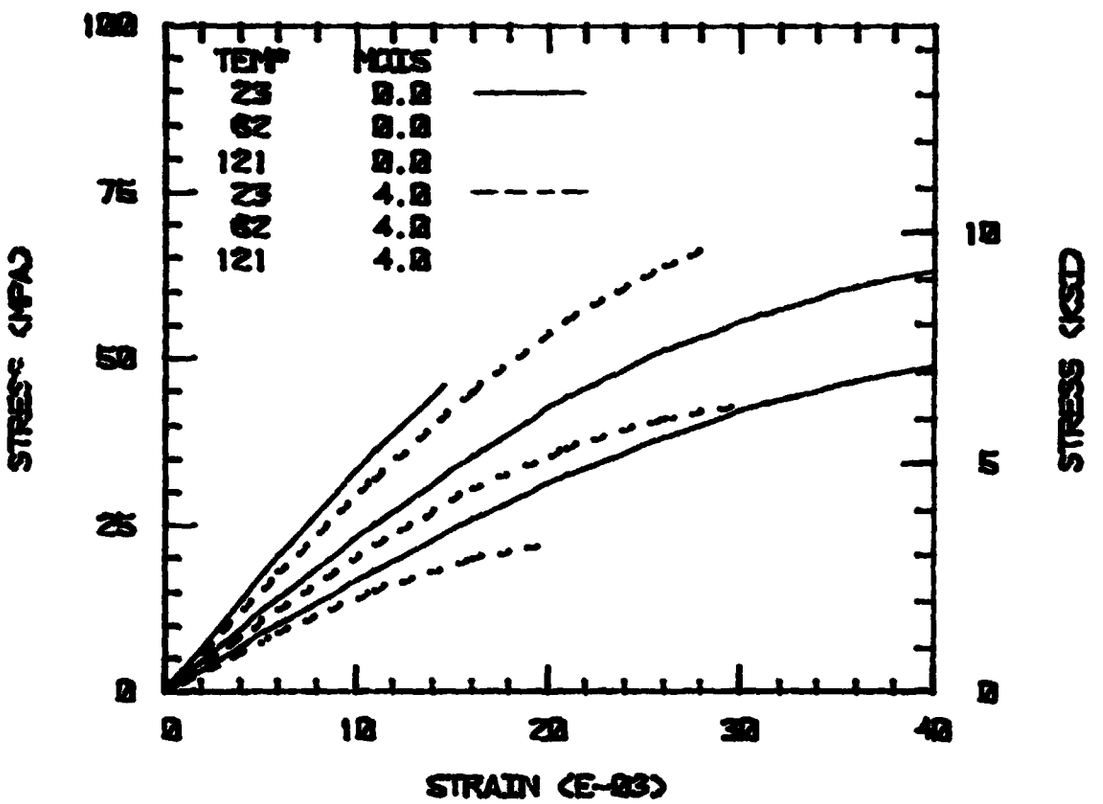

a) tensile data

Figure 26. Hercules 2220-3 Neat Resin Stress-Strain Curves, Dry (solid lines) and Moisture-Saturated (dashed lines), at Three Test Temperatures.

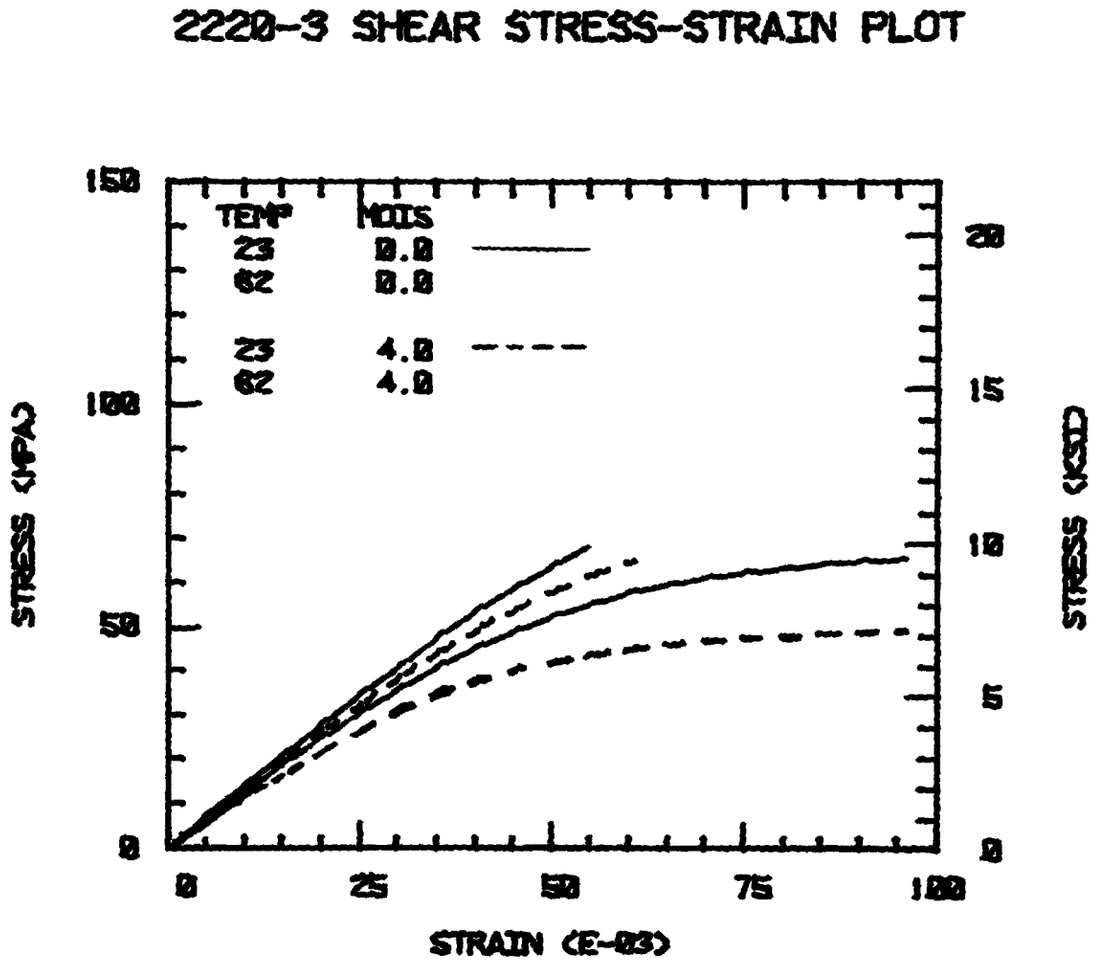

b) shear data

Figure 26 (continued). Hercules 2220-3 Neat Resin Stress-Strain Curves, Dry (solid lines) and Moisture-Saturated (dashed lines), at Three Test Temperatures.

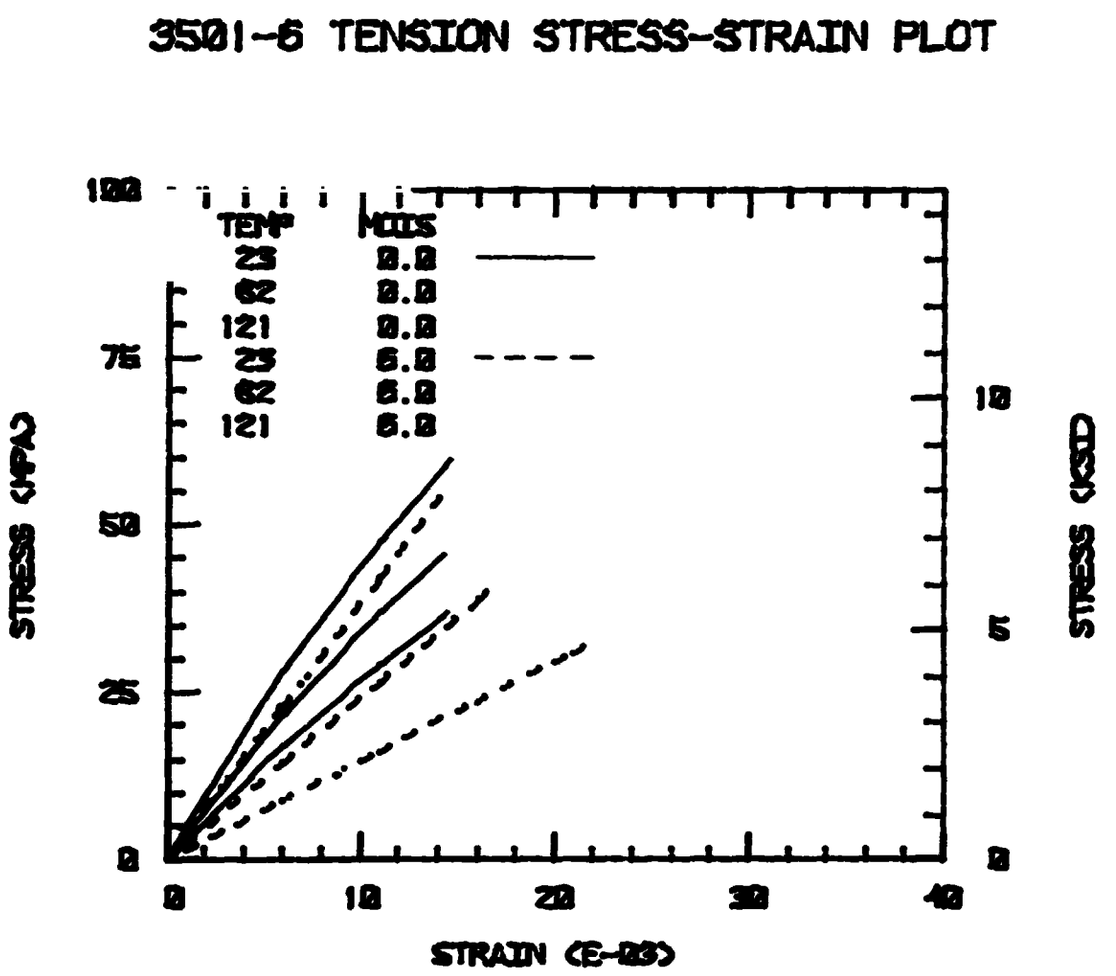

a) tensile data

Figure 27. Hercules 3501-6 Neat Resin Stress-Strain Curves, Dry (solid lines) and Moisture-Saturated (dashed lines), at Three Test Temperatures.

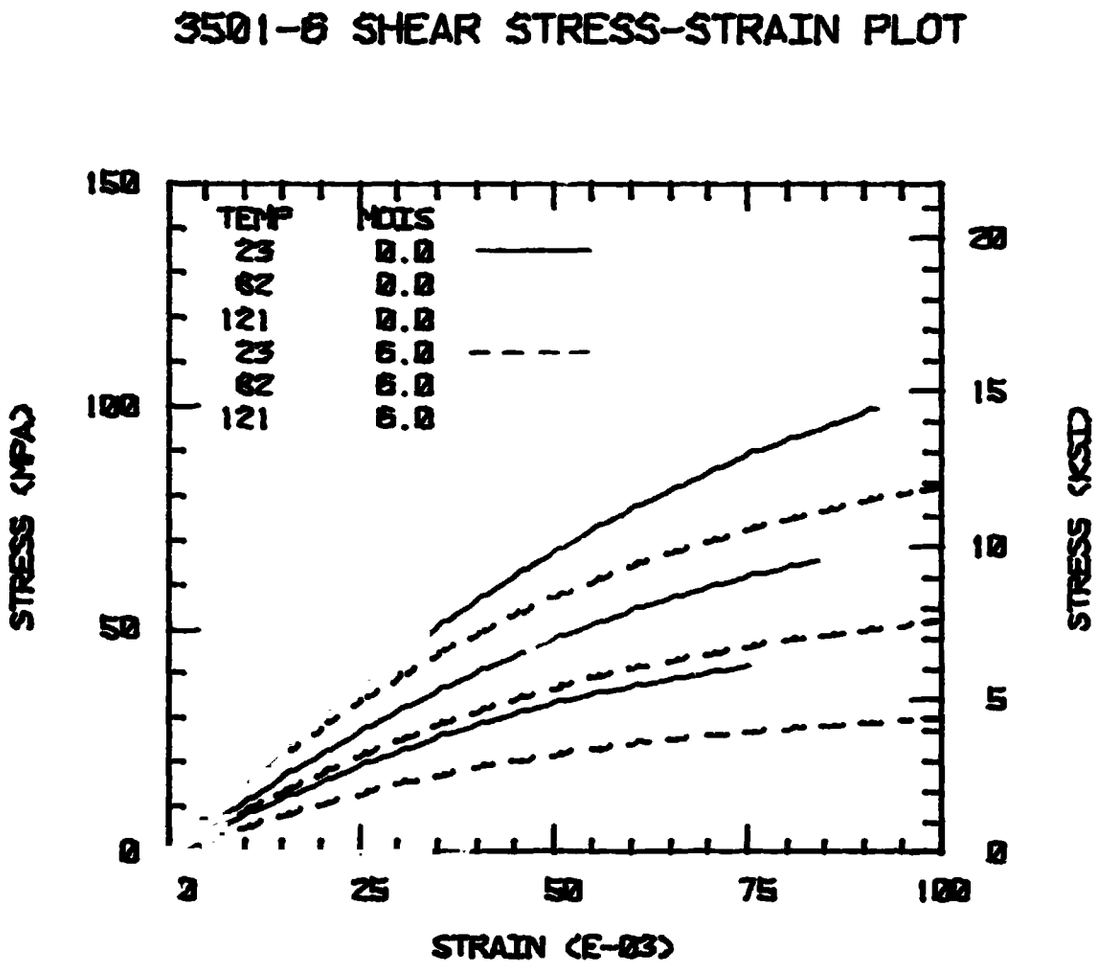

b) shear data

Figure 27 (continued). Hercules 3501-6 Neat Resin Stress-Strain Curves, Dry (solid lines) and Moisture-Saturated (dashed lines), at Three Test Temperatures.

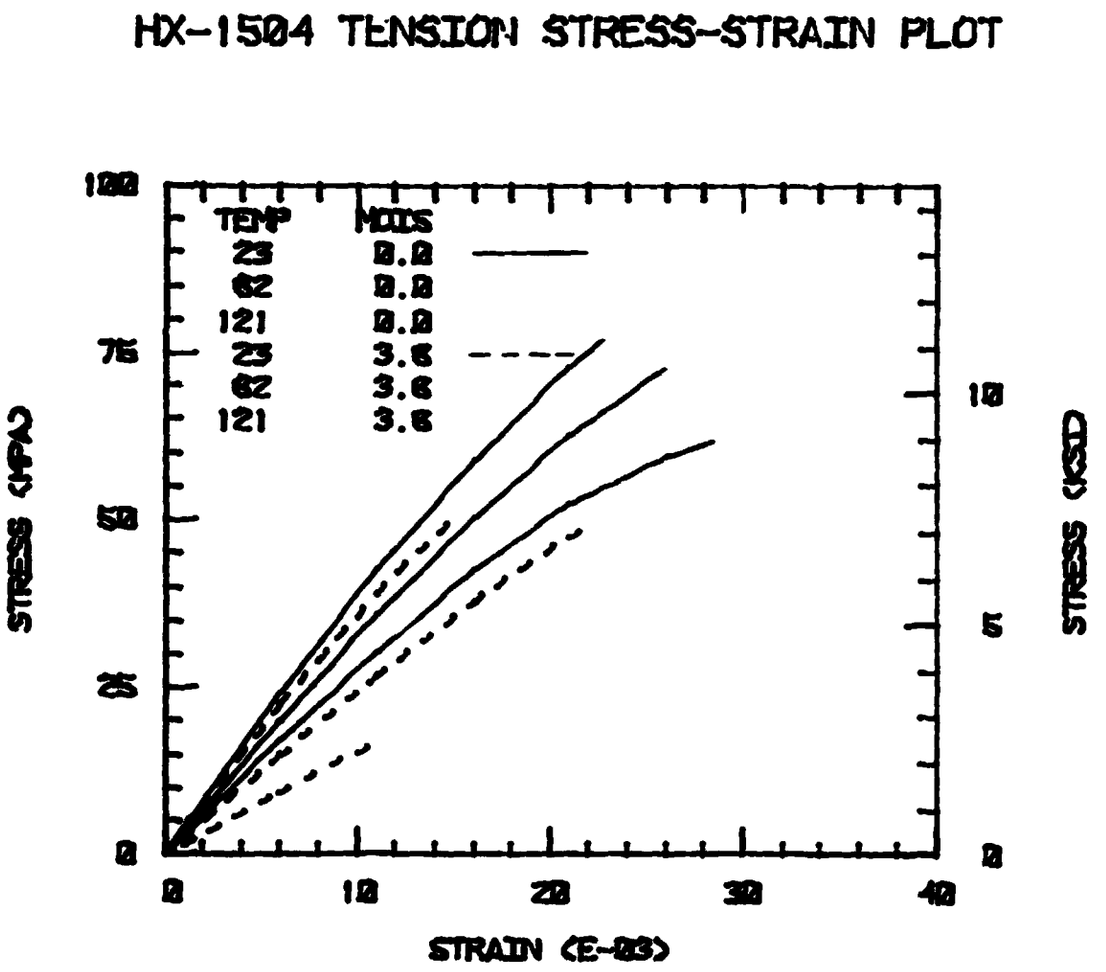

a) tensile data

Figure 28. Hexcel HX-1504 Neat Resin Shear Stress-Strain Curves, Dry (solid lines) and Moisture-Saturated (dashed lines), at Three Test Temperatures.

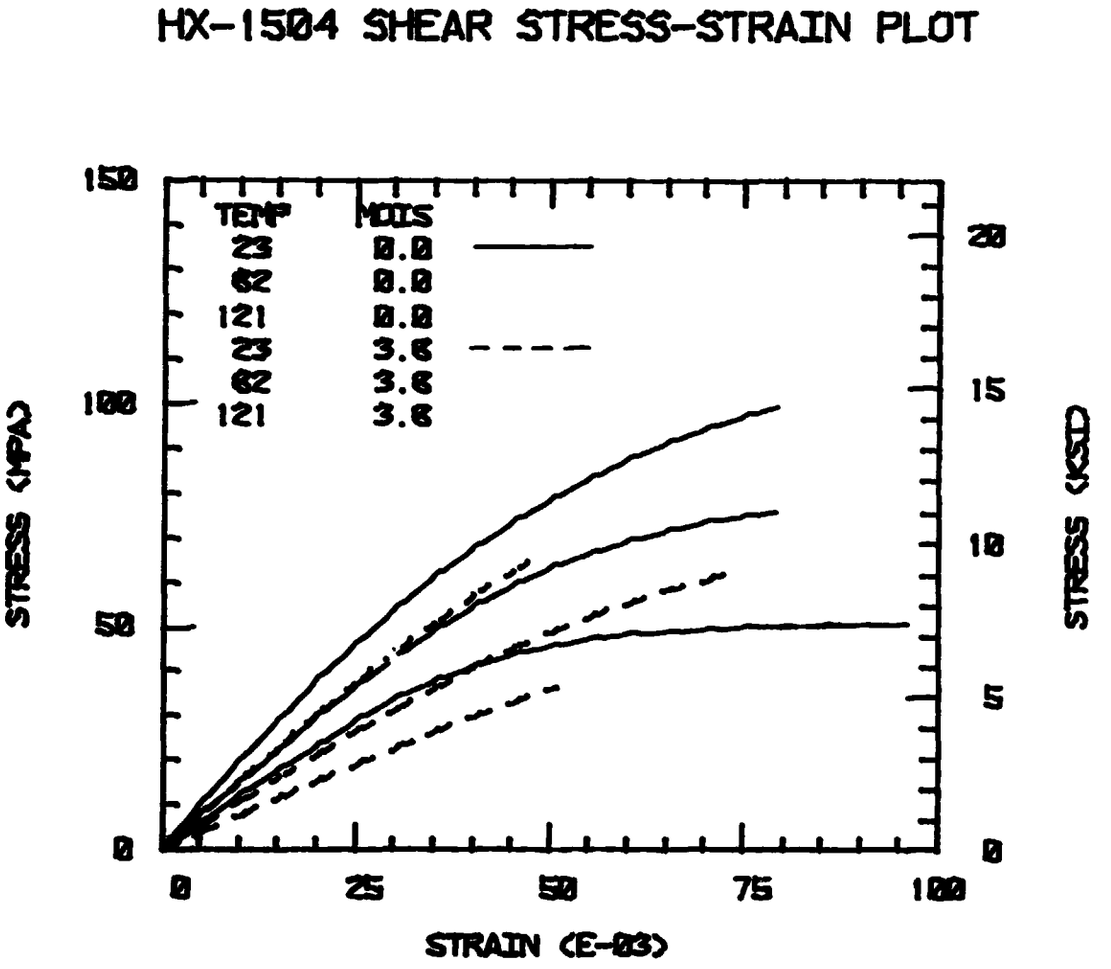

b) shear data

Figure 28 (continued). Hexcel HX-1504 Neat Resin Shear Stress-Strain Curves, Dry (solid lines) and Moisture-Saturated (dashed lines), at Three Test Temperatures.

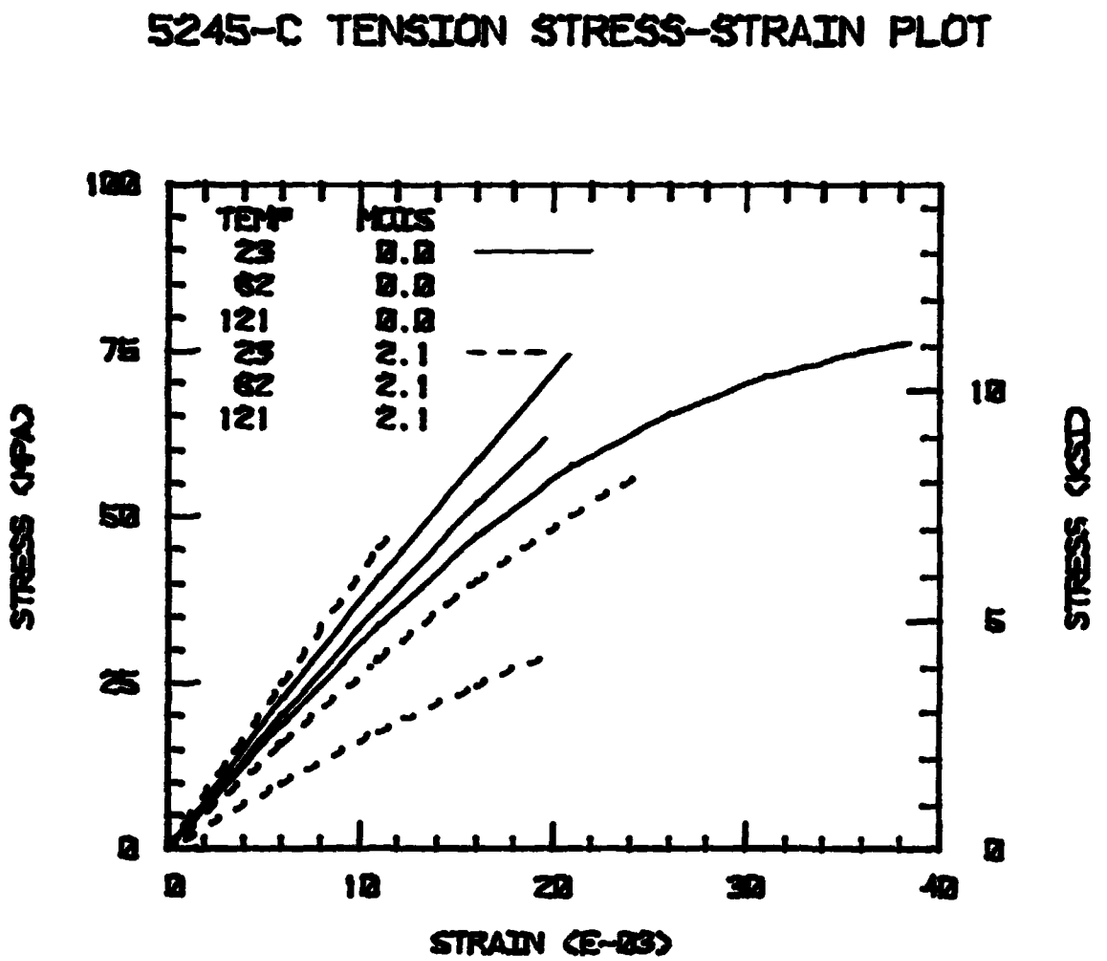

a) tensile data

Figure 29. Narmco 5245-C Neat Resin Shear Stress-Strain Curves, Dry (solid lines) and Moisture-Saturated (dashed lines), at Three Test Temperatures.

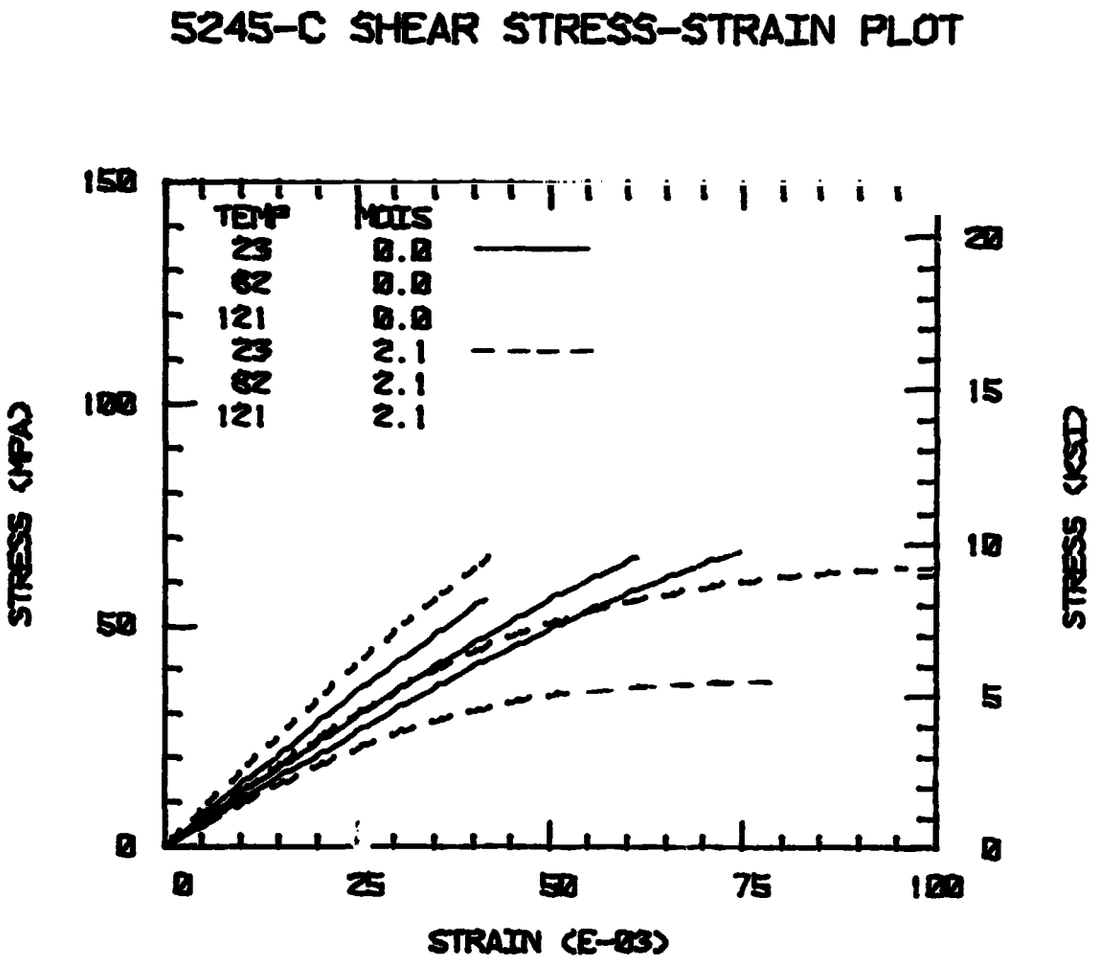

b) shear data

Figure 29 (continued). Narmco 5245-C Neat Resin Shear Stress-Strain Curves, Dry (solid lines) and Moisture-Saturated (dashed lines), at Three Test Temperatures.

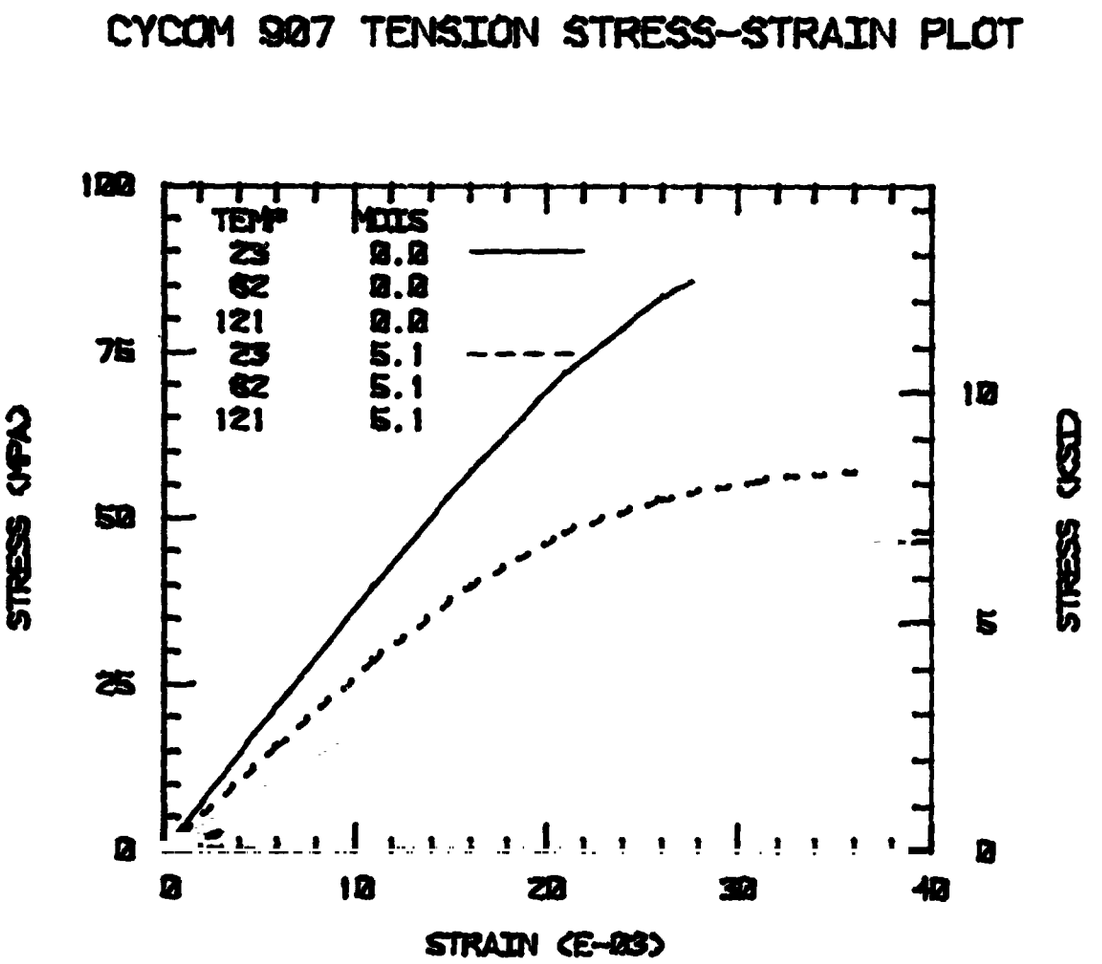

a) tensile data

Figure 30. American Cyanamid CYCOM 907 Neat Resin Stress-Strain Curves, Dry (solid lines) and Moisture-Saturated (dashed lines), at Three Test Temperatures.

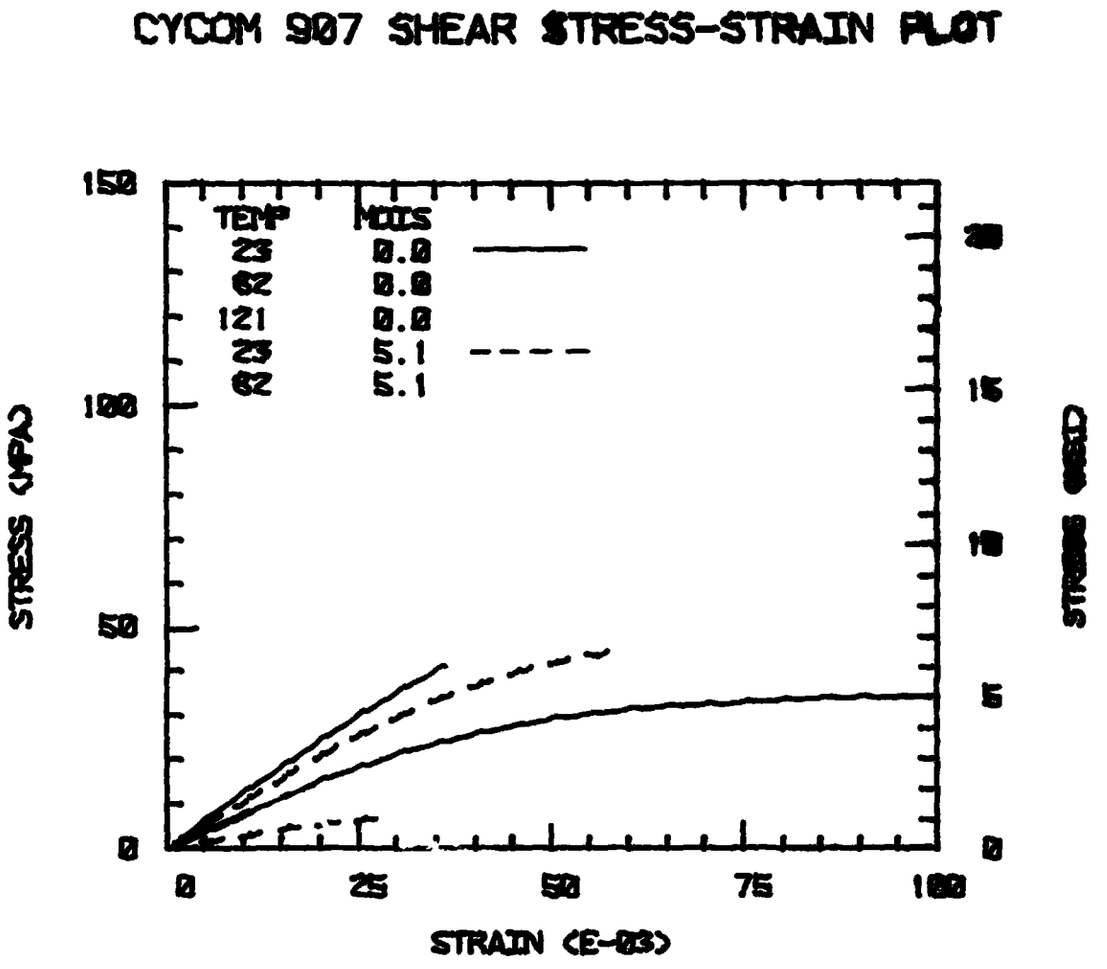

b) shear data

Figure 30 (continued). American Cyanamid CYCOM 907 Neat Resin Stress-Strain Curves, Dry (solid lines) and Moisture-Saturated (dashed lines), at Three Test Temperatures.

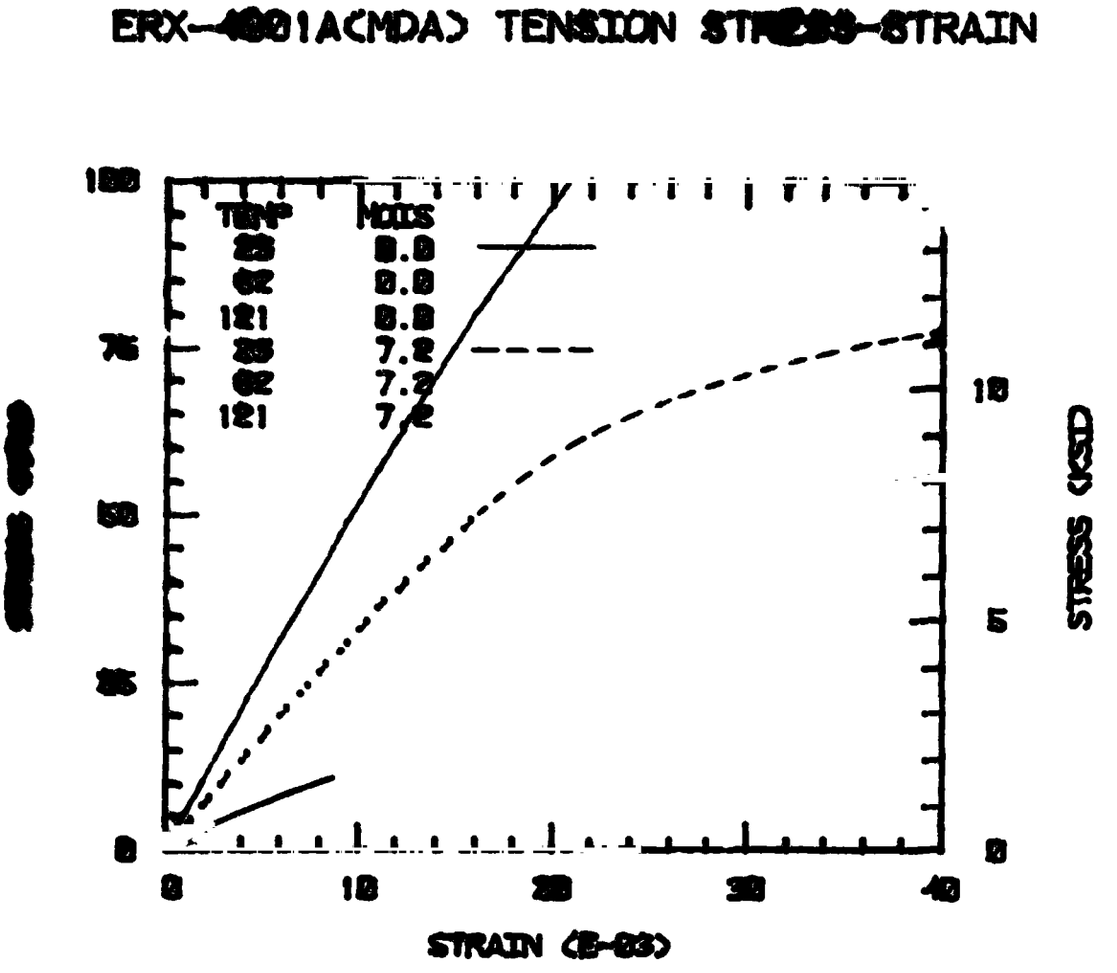

a) tensile data

Figure 31. Union Carbide ERX-4901 (MDA) Neat Resin Stress-Strain Curves, Dry (solid lines) and Moisture-Saturated (dashed lines), at Three Test Temperatures.

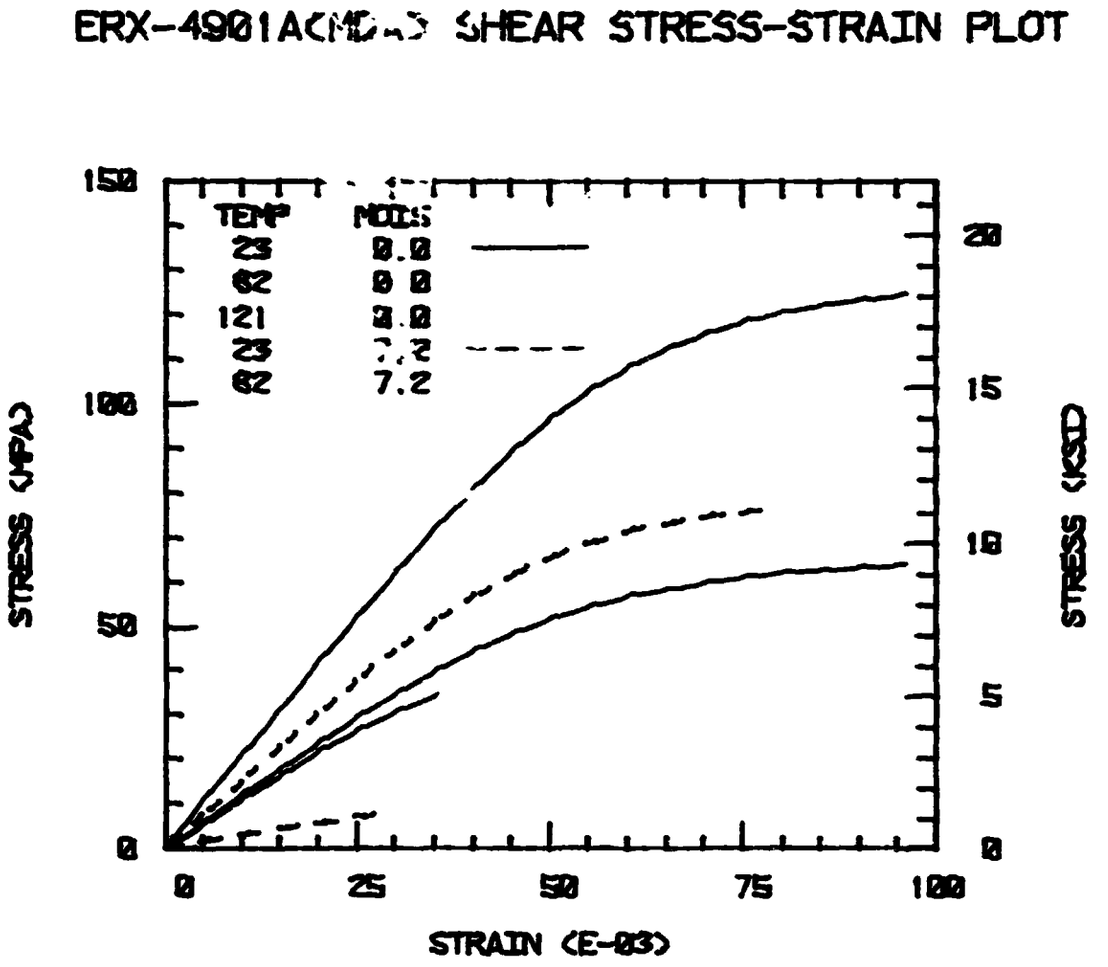

b) shear data

Figure 31 (continued). Union Carbide ERX-4901 (MDA) Neat Resin Stress-Strain Curves, Dry (solid lines) and Moisture-Saturated (dashed lines), at Three Test Temperatures.

C-2

degree of nonlinearity.

Since the tensile data of Figures 23 through 31 are all plotted to the same scale, and the shear data are also plotted to the same scale, they can be used to make qualitative comparisons of the nine matrix materials to be discussed here, quantitative data being given in Tables 1 through 6 of Section 1, Table 9 of Section 3, and the tables of Appendix A.

These data are actually used in the form of octahedral shear stress-octahedral shear strain relations in the micromechanics analysis. Thus it is necessary to convert the data to this form. Sample plots of octahedral shear stress-octahedral shear strain for the four matrix materials of the first year were presented in Figure 76 of Reference [1]. These plots only differ from the uniaxial tensile and shear data presented here in Figures 23 through 31 by appropriate constant factors. Thus, the general shapes of the curves are unchanged.

In theory, if octahedral shear (distortional energy) is a valid representation of multiaxial stress state effects, then either uniaxial tensile or shear data, when converted to octahedral values, should give the same results. The purpose of Figure 76 Reference [1] was to present the data from both types of test on the same plots, for the two environmental extremes, i.e., room temperature, dry (RTD) and elevated temperature, wet (ETW) conditions. As was seen, the tensile tests appeared to result in premature failures, which was most pronounced for the less ductile Hercules 3502 and Fibredux 914 epoxies. However, the data for the Hercules 2220 systems both indicated that if premature tensile failures had not occurred, the tensile data probably would not have followed the shear data. This difference has been observed previously

also [12,29], and is as yet unexplained. For the present predictions of composite response, only the neat epoxy data generated from the shear tests will be utilized, as previously stated.

As the shear stress-strain response of the matrix materials is nonlinear, it is necessary to input the entire stress-strain curve into the micromechanics analysis. This is done by using a three-parameter experimental equation of the form first suggested by Richard and Blacklock [28], i.e.,

$$\tau = \frac{G\gamma}{\left[1 + \left|\frac{G\gamma}{\tau_o}\right|^n\right]^{\frac{1}{n}}} \tag{7}$$

where

G = initial shear modulus

n = curvature parameter

τ_o = asymptotic shear stress value

γ = shear strain

The three parameters, G, n, and τ_o describe the stress-strain response of the epoxy in a particular temperature and moisture environment. By then using regression techniques, each parameter may be described as a polynomial function in temperature and moisture by using equations of the form

$$P = C_1T^2 + C_2T + C_3M + C_4TM + C_5 \tag{8}$$

where P = property of interest (e.g., G, n, τ_o, etc)

$C_1 - C_5$ = regression coefficients for that property.

Therefore, the entire shear stress-strain response, as a function

of temperature and moisture, can be expressed for each of the matrix materials represented by the families of curves in Figures 23 through 31 in terms of Eq. (7), by evaluating the regression coefficients for G, n, and τ_o in Eq. (8). These coefficients for the nine matrix materials of interest here are presented in Tables 14 through 22. The experimentally determined yield and ultimate shear strengths, τ_y and τ_u, respectively, are also presented in the same manner, for use in the yield and failure criteria. Yield in all cases was based upon an octahedral shear criterion. For longitudinal shear loadings, τ_u was used in the octahedral shear failure criterion. For transverse tensile loadings, an ultimate normal stress σ_u was calculated from the relation $\sigma_u = \sqrt{3}\tau_u$, for use in the maximum principal stress failure criterion. The actual values of σ_u as measured were actually somewhat lower than $\sqrt{3}\tau_u$, as can be seen by comparing Figures 1 and 3. The measured values of σ_u were felt to be low, however, as previously discussed. Also, by assuming σ_u to be a function of τ_u, only shear test data were used, making the transverse tensile and longitudinal shear loading predictions mutually consistent. Units of modulus and stress in Tables 14 through 22 are psi, as indicated. These can be converted to S.I. units (Pa) by multiplying by 6.8947×10^3.

Although neat resin tensile data were not used in generating the present micromechanics analysis results (except for Poisson's ratio ν, which is required as input along with the shear properties), these data are also included in Tables 14 through 22 for future reference. The values E, n, and σ_o replace G, n, and τ_o, respectively, in the Richard-Blacklock curve-fit equation, i.e., Eq. (7), in calculating the tensile stress σ as a function of tensile strain ε.

TABLE 14

HERCULES 3502 NEAT RESIN MATRIX MATERIAL PROPERTIES EXPRESSED AS FUNCTIONS OF TEMPERATURE AND MOISTURE (T in °C, M in Wt. %)

$$\text{Property} = C_1T^2 + C_2T + C_3M + C_4TM + C_5$$

Property	C_1	C_2	C_3	C_4	C_5
Shear Data					
G (psi)	0	-3.39×10^{2}	-6.61×10^{3}	0	2.58×10^{5}
n	0	0	-1.00×10^{-1}	0	3.00
τ_o (psi)	0	-3.39×10^{1}	-1.05×10^{3}	0	1.68×10^{4}
τ_y (psi)	0	-1.66×10^{1}	-6.71×10^{2}	0	5.55×10^{3}
τ_u (psi)	0	1.94×10^{1}	-6.78×10^{1}	0	8.44×10^{3}
Tensile Data					
E (psi)	0	-1.71×10^{3}	-2.51×10^{3}	-1.66×10^{2}	5.91×10^{5}
n	0	0	0	0	3.00
σ_o (psi)	0	0	2.08×10^{2}	-1.02×10^{1}	1.10×10^{4}
σ_y (psi)	0	-1.69×10^{1}	0	0	3.90×10^{3}
σ_u (psi)	0	0	1.21×10^{2}	0	4.88×10^{3}
ν	0	0	0.01	0	0.36
Temperature and Moisture Data					
α ($°C^{-1}$)	0	0	0	0	5.05×10^{-5}
β ($\%M^{-1}$)	0	0	0	0	2.70×10^{-3}

TABLE 15

CIBA-GEIGY FIBREDUX 914 NEAT RESIN MATRIX MATERIAL PROPERTIES EXPRESSED AS FUNCTIONS OF TEMPERATURE AND MOISTURE (T in °C, M in Wt. %)

$$\text{Property} = C_1T^2 + C_2T + C_3M + C_4TM + C_5$$

Property	C_1	C_2	C_3	C_4	C_5
Shear Data					
G (psi)	0	-3.39×10^{2}	-2.93×10^{2}	-4.84×10^{1}	2.28×10^{5}
n	0	0	0	0	3.00
τ_o (psi)	0	-3.39×10^{1}	-4.23×10^{2}	-7.30	1.78×10^{4}
τ_y (psi)	0	-1.66×10^{1}	-3.43×10^{2}	-1.51×10^{-1}	5.55×10^{3}
τ_u (psi)	0	-9.11×10^{1}	-4.19×10^{2}	5.70	1.41×10^{4}
Tensile Data					
E (psi)	0	-2.39×10^{3}	-1.83×10^{4}	0	6.47×10^{5}
n	0	0	0	0	3.00
σ_o (psi)	0	-1.37×10^{2}	-1.18×10^{3}	0	2.06×10^{4}
σ_y (psi)	0	-1.66×10^{1}	2.82×10^{1}	0	3.55×10^{3}
σ_u (psi)	0	1.76×10^{1}	5.53×10^{2}	0	3.31×10^{3}
ν	0	0	4.30×10^{-3}	0	0.36
Temperature and Moisture Data					
α ($°C^{-1}$)	0	0	0	0	5.84×10^{-5}
β ($\%M^{-1}$)	0	0	0	0	3.02×10^{-3}

TABLE 16

HERCULES 2220-1 NEAT RESIN MATRIX MATERIAL PROPERTIES EXPRESSED AS FUNCTIONS OF TEMPERATURE AND MOISTURE (T in °C, M in Wt. %)

$$\text{Property} = C_1T^2 + C_2T + C_3M + C_4TM + C_5$$

Property	C_1	C_2	C_3	C_4	C_5
Shear Data					
G (psi)	0	-5.17×10^{2}	-7.25×10^{3}	-4.53×10^{1}	2.57×10^{5}
n	0	0	1.03×10^{1}	0	2.00
τ_o (psi)	0	-5.78×10^{1}	-9.79×10^{2}	0	1.73×10^{4}
τ_y (psi)	0	-1.72×10^{1}	-1.91×10^{2}	0	5.25×10^{3}
τ_u (psi)	0	0	-1.00×10^{2}	0	1.13×10^{4}
Tensile Data					
E (psi)	0	-2.38×10^{3}	-7.64×10^{3}	-8.76×10^{1}	5.50×10^{5}
n	0	0	-7.89×10^{-2}	0	3.00
σ_o (psi)	0	0	8.85×10^{2}	-2.00×10^{1}	1.11×10^{4}
σ_y (psi)	0	0	2.96×10^{2}	0	2.00×10^{3}
σ_u (psi)	0	7.36×10^{1}	1.76×10^{3}	-3.36×10^{1}	4.43×10^{3}
ν	0	0	1.05×10^{-2}	0	0.36
Temperature and Moisture Data					
α ($°C^{-1}$)	0	0	0	0	5.56×10^{-5}
β ($\%M^{-1}$)	0	0	0	0	2.96×10^{-3}

TABLE 17

HERCULES 2220-3 NEAT RESIN MATRIX MATERIAL PROPERTIES EXPRESSED AS FUNCTIONS OF TEMPERATURE AND MOISTURE (T in °C, M in Wt. %)

$$\text{Property} = C_1T^2 + C_2T + C_3M + C_4TM + C_5$$

Property	C_1	C_2	C_3	C_4	C_5
Shear Data					
G (psi)	0	-3.33×10^{2}	-1.88×10^{3}	-4.31×10^{1}	2.11×10^{5}
n	0	0	0	0	3.00
τ_o (psi)	0	-7.69×10^{1}	-5.95×10^{2}	0	1.64×10^{4}
τ_y (psi)	0	-1.66×10^{1}	-2.63×10^{2}	0	5.55×10^{3}
τ_u (psi)	0	-1.29×10^{1}	2.55×10^{2}	0	1.07×10^{4}
Tensile Data					
E (psi)	0	-2.53×10^{3}	-1.75×10^{4}	7.89×10^{1}	5.54×10^{5}
n	0	0	1.25×10^{-1}	0	2.50
σ_o (psi)	0	-5.08×10^{1}	-2.63×10^{2}	0	1.52×10^{4}
σ_y (psi)	0	0	3.50×10^{2}	0	3.00×10^{3}
σ_u (psi)	0	6.07×10^{1}	1.54×10^{3}	-2.90×10^{1}	5.11×10^{3}
ν	0	0	0.02	0	0.36
Temperature and Moisture Data					
α ($°C^{-1}$)	0	0	0	0	5.36×10^{-5}
β ($\%M^{-1}$)	0	0	0	0	2.51×10^{-3}

TABLE 18

HERCULES 3501-6 NEAT RESIN MATRIX MATERIAL PROPERTIES EXPRESSED AS FUNCTIONS OF TEMPERATURE AND MOISTURE (T in °C, M in Wt. %)

$$\text{Property} = C_1T^2 + C_2T + C_3M + C_4TM + C_5$$

Property	C_1	C_2	C_3	C_4	C_5
Shear Data					
G (psi)	0	-1.14×10^{3}	-2.49×10^{3}	0	2.60×10^{5}
n	0	2.56×10^{-3}	2.78×10^{-3}	1.65×10^{-4}	1.54
τ_o (psi)	0	-1.50×10^{2}	-1.36×10^{3}	0	2.67×10^{4}
τ_y (psi)	0	-3.19×10^{1}	-3.94×10^{2}	0	6.18×10^{3}
τ_u (psi)	0	-8.73×10^{1}	-6.03×10^{2}	0	1.67×10^{4}
Tensile Data					
E (psi)	0	-3.19×10^{3}	-3.14×10^{4}	-4.72×10^{1}	8.24×10^{5}
n	0	7.43×10^{-4}	2.02×10^{-2}	-3.37×10^{-4}	9.97×10^{-1}
σ_o (psi)	0	-1.22×10^{2}	-3.17×10^{2}	-3.02×10^{5}	4.34×10^{4}
σ_y (psi)	0	-2.56×10^{1}	-4.27×10^{2}	0	5.58×10^{3}
σ_u (psi)	0	-3.47×10^{1}	-1.48×10^{2}	0	9.63×10^{3}
ν	0	0	0	0	0.34
Temperature and Moisture Data					
α ($°C^{-1}$)	0	0	0	0	3.83×10^{-5}
β ($\%M^{-1}$)	0	0	0	0	3.20×10^{-3}

TABLE 19

HEXCEL HX-1504 NEAT RESIN MATRIX MATERIAL PROPERTIES EXPRESSED AS FUNCTIONS OF TEMPERATURE AND MOISTURE (T in °C, M in Wt. %)

$$\text{Property} = C_1T^2 + C_2T + C_3M + C_4TM + C_5$$

Property	C_1	C_2	C_3	C_4	C_5
Shear Data					
G (psi)	0	-1.18×10^{3}	-2.26×10^{4}	0	3.16×10^{5}
n	0	2.01×10^{-2}	3.99×10^{-1}	-5.30×10^{-3}	1.48
τ_o (psi)	0	-1.17×10^{2}	-1.71×10^{3}	0	2.17×10^{4}
τ_y (psi)	0	-1.07×10^{1}	-1.65×10^{2}	0	5.14×10^{3}
τ_u (psi)	0	-6.43×10^{1}	-1.28×10^{3}	0	1.59×10^{4}
Tensile Data					
E (psi)	0	-1.91×10^{3}	-6.79×10^{2}	-3.99×10^{2}	6.40×10^{5}
n	0	1.41×10^{-2}	-4.91×10^{-2}	1.23×10^{-3}	1.44
σ_o (psi)	0	-1.23×10^{2}	-9.60×10^{2}	0	2.57×10^{4}
σ_y (psi)	0	0	1.74×10^{2}	0	4.00×10^{3}
σ_u (psi)	0	-2.19×10^{1}	-6.91×10^{2}	0	1.18×10^{4}
ν	0	0	0	0	0.37
Temperature and Moisture Data					
α ($°C^{-1}$)	0	0	1.03×10^{-6}	0	5.08×10^{-5}
β ($\%M^{-1}$)	0	0	0	0	2.07×10^{-3}

TABLE 20

NARMCO 5245-C NEAT RESIN MATRIX MATERIAL PROPERTIES EXPRESSED AS FUNCTIONS OF TEMPERATURE AND MOISTURE (T in °C, M in Wt. %)

$$\text{Property} = C_1T^2 + C_2T + C_3M + C_4TM + C_5$$

Property	C_1	C_2	C_3	C_4	C_5
Shear Data					
G (psi)	0	-5.35×10^{2}	2.61×10^{4}	-2.62×10^{2}	2.17×10^{5}
n	0	0	8.89×10^{-2}	-2.23×10^{-3}	3.00
τ_o (psi)	0	-3.22×10^{1}	9.19×10^{1}	-3.14×10^{1}	1.74×10^{4}
τ_y (psi)	0	-4.03×10^{1}	-2.40×10^{3}	1.92×10^{1}	7.03×10^{3}
τ_u (psi)	0	1.71×10^{1}	1.76×10^{3}	-3.03×10^{1}	7.85×10^{3}
Tensile Data					
E (psi)	0	-8.99×10^{2}	6.07×10^{4}	-1.35×10^{3}	5.64×10^{5}
n	0	0	8.89×10^{-2}	-2.23×10^{-3}	3.00
σ_o (psi)	0	-9.13×10^{1}	-4.55×10^{2}	-1.50×10^{1}	2.32×10^{4}
σ_y (psi)	0	-2.15×10^{1}	-6.65×10^{2}	0	6.29×10^{3}
σ_u (psi)	0	0	-9.12×10^{2}	-1.23×10^{1}	1.01×10^{4}
ν	0	0	0	0	0.39
Temperature and Moisture Data					
α ($°C^{-1}$)	0	0	0	0	6.03×10^{-5}
β ($\%M^{-1}$)	0	0	0	0	1.55×10^{-3}

TABLE 21

AMERICAN CYANAMID CYCOM 907 NEAT RESIN MATRIX MATERIAL PROPERTIES
EXPRESSED AS FUNCTIONS OF TEMPERATURE AND MOISTURE
(T in °C, M in Wt. %)

$$\text{Property} = C_1T^2 + C_2T + C_3M + C_4TM + C_5$$

Property	C_1	C_2	C_3	C_4	C_5
Shear Data					
G (psi)	0	-2.10×10^{3}	-2.11×10^{-2}	-1.38×10^{2}	2.24×10^{5}
n	0	-1.58×10^{-2}	6.63×10^{2}	-3.82×10^{-3}	3.37
τ_o (psi)	0	-1.32×10^{1}	-4.35×10^{2}	0	1.29×10^{4}
τ_y (psi)	0	-1.88×10^{1}	-1.66×10^{2}	0	3.75×10^{3}
τ_u (psi)	0	-8.91×10^{1}	-1.39×10^{2}	0	9.63×10^{3}
Tensile Data					
E (psi)	2.13×10^{1}	-6.94×10^{3}	-3.00×10^{4}	5.38×10^{1}	6.77×10^{5}
n	0	-1.33×10^{-2}	3.58×10^{-2}	-2.35×10^{-3}	4.31
σ_o (psi)	0	-1.74×10^{2}	-1.45×10^{3}	0	1.89×10^{4}
σ^y (psi)	0	-2.81×10^{1}	-4.55×10^{2}	0	5.12×10^{3}
σ^y_u (psi)	0	-1.42×10^{2}	-1.30×10^{3}	0	1.66×10^{4}
ν^u	0	0	0	0	0.42
Temperature and Moisture Data					
α ($°C^{-1}$)	0	0	1.16×10^{-6}	0	4.88×10^{-5}
β ($\%M^{-1}$)	0	0	0	0	2.29×10^{-3}

TABLE 22

UNION CARBIDE ERX-4901A(MDA) NEAT RESIN MATRIX MATERIAL PROPERTIES EXPRESSED AS FUNCTIONS OF TEMPERATURE AND MOISTURE

(T in °C, M in Wt. %)

$$\text{Property} = C_1T^2 + C_2T + C_3M + C_4TM + C_5$$

Property	C_1	C_2	C_3	C_4	C_5
Shear Data					
G (psi)	0	-4.18×10^{3}	-9.38×10^{3}	-1.00×10^{2}	3.90×10^{5}
n	0	-3.92×10^{-2}	7.26×10^{-2}	-4.90×10^{-3}	4.92
τ_o (psi)	0	-2.27×10^{2}	-1.08×10^{3}	0	2.36×10^{4}
τ_y (psi)	0	-4.96×10^{2}	-5.11×10^{2}	0	8.41×10^{3}
τ_u (psi)	0	-2.15×10^{2}	-1.24×10^{3}	0	2.30×10^{4}
Tensile Data					
E (psi)	3.76×10^{1}	-1.15×10^{4}	-4.12×10^{4}	1.77×10^{2}	1.00×10^{6}
	1.11×10^{-4}	-1.57×10^{-2}	4.54×10^{-2}	-2.67×10^{-3}	3.37
(psi)	0	-3.41×10^{2}	-1.77×10^{3}	1.16×10^{1}	3.02×10^{4}
σ^{y} (psi)	0	-4.49×10^{1}	-2.07×10^{2}	0	6.22×10^{3}
σ^{y}_{u} (psi)	0	-2.55×10^{2}	-8.94×10^{2}	0	2.20×10^{4}
ν^{u}	0	0	0	0	0.41
Temperature and Moisture Data					
α ($°C^{-1}$)	0	0	0	0	6.03×10^{-5}
β ($\%M^{-1}$)	0	0	0	0	1.55×10^{-3}

Also required as input to the micromechanics analysis are the coefficients of thermal expansion α and moisture expansion β of the matrix materials. These properties are also included in Tables 14 through 22. As noted in the results of the first-year study also, the coefficients of thermal expansion α of the present matrix materials were found to be relatively constant with temperature, and only slightly higher for the material in the moisture-saturated state than when tested dry. The coefficients of moisture expansion β were assumed to be constant as inputs to the analysis. The neat resin matrix material properties as presented in functional form in Tables 14 through 22 should be very convenient for use by other investigators needing the various properties of these polymer systems at any temperature and moisture condition. As will be noted, although the experimental data were fit as a function of C, T^2, the regression coefficient C, was negligibly small.

5.3 Predicted Unidirectional Composite Response

In the first-year report [1], a detailed presentation of predicted internal stress states in the matrix of the four materials considered was included. Since unidirectional composite experimental data are still not available at the end of this second-year effort for use in comparing predicted versus measured composite response, further stress state plots of this type will not be presented here. The previously presented results [1] adequately indicate the predictive capabilities available. It is expected that composite properties will be measured for at least some of these material systems during the next-year study. At that time, additional micromechanics predictions of stress states will be presented.

Since the crack initiation and propagation capability was not used in the first-year study, being a recent development as discussed in Section 5.1, these predictions will be presented here, along with predicted unidirectional composite stress-strain curves to failure. All nine matrix materials for which properties were presented in Figures 23 through 31 and Tables 14 through 22 will be included, even though only four were actually tested in the present second-year study; these results are not yet available anywhere else, having been generated as part of the present study.

As previously stated, a square array of continuous Hercules AS4 graphite fibers [25], of circular cross section in a 60 volume percent unidirectional composite, has been assumed as representing a typical composite. These are the same conditions as assumed in the first-year study [1]. However, the analysis is fully capable of handling other geometric and/or material configurations as well, e.g., noncircular fibers, hexagonal or random fiber packing arrays, etc. Also as in the first-year report [1], results were generated only for uniaxial loadings, viz, longitudinal tension, transverse tension, and longitudinal shear. No compressive loadings or multiaxial loading combinations were included, although the present analysis is fully capable of modeling any type or combination of mechanical and hygrothermal loadings simultaneously.

Results will be presented here for the same four hygrothermal conditions assumed in Reference [1], viz, room temperature (21°C), dry (RTD), elevated temperature (100°C), dry (ETD), room temperature, wet (RTW), and elevated temperature, wet (ETW), where wet implies the fully moisture-saturated condition of the matrix. Values for the eight mater-

ials tested for NASA-Langley to data were listed in Table 4 of Section 1. These are repeated here in Table 23, for convenience, along with the corresponding value assumed here for the Hercules 3501-6 epoxy (see References [6,26] for more information on this epoxy matrix material).

Results for the longitudinal tensile loadings will not be presented here since they were not particularly interesting. The composite stress-strain curves were linear to failure, as expected since this is a fiber-dominated loading mode. Thus, the stress-strain plots also did not vary measurably from one matrix material to another, since all incorporated the same Hercules AS4 graphite fiber. Typically, the matrix yielded, then failed (a maximum principal stress failure criterion was used), with relatively little crack propagation. Composite failure was then dictated by fiber failure.

In future analyses, a three-dimensional finite element analysis will be used so that influences of broken fibers, matrix defects, etc. can be modeled.

5.3.1 Transverse Tensile and Longitudinal Shear Strengths

The micromechanics predictions of transverse tensile strength and longitudinal shear strength are presented in Table 24. As previously discussed, these strength predictions are highly dependent on the failure criterion assumed, and the input stress-strain response of the matrix material. As unidirectional composite strength data become available for these materials, it will be possible to modify the present assumptions as appropriate to fit the experimental data. In the meantime, however, these predicted strengths can be used to compare the various composite materials, since they are all based upon the same assumptions.

TABLE 23

MOISTURE SATURATION EQUILIBRIUM WEIGHT GAINS FOR NINE NEAT RESIN MATRIX MATERIALS

Neat Resin System	Equilibrium Moisture Content (weight percent, %M)
Hercules 3502	5.0
Fibredux 914	7.0
Hercules 2220-1	3.8
Hercules 2220-3	4.0
Hercules 3501-6	6.0
Hexcel HX-1504	3.8
Narmco 5245-C	2.1
CYCOM 907	5.1
ERX-4901A(MDA)	7.2

The trends can be visualized more readily by plotting the data of Table 24 in barchart form, as in Figures 32 and 33. Figure 32 is a plot of the predicted transverse tensile strengths. It will be noted that in many cases the predicted strength is higher at 100°C, dry than at room temperature, dry conditions. This is because the curing residual stresses are relieved somewhat as the temperature is raised back up toward the 177°C cure temperature (60°C in the case of the Union Carbide ERX-4901A(MDA) matrix composite). Moisture-induced matrix swelling also tends to offset the thermal stresses. Thus, the room temperature, wet strength is predicted to be greater than the room temperature, dry strength for some fiber-matrix combinations. This is not universally true, however, as the strength of some matrix materials is degraded significantly after moisture absorption, as indicated in Figures 1 and 3 of Section 1. This moisture degradation is more severe at elevated temperatures. Thus, the hot, wet strengths tend to be lower than the room temperature, dry strengths.

Some apparent anomalies can be seen in the data of Table 24 and Figure 32. For example, the room temperature, dry transverse tensile strength of the Fibredux 914 composite appears to be abnormally low. Likewise, the corresponding strength of the CYCOM 907 composite is predicted to be very high. These prediction can be explained by the various interactions of input properties in the analysis. Whether they agree with actual measured composite material strengths will only be known when experimental data become available.

Figure 33 is a plot of the predicted shear strengths listed in Table 24. Since the cooldown from the cure temperature induces high normal stresses rather than shear stresses, the predicted 100°C, dry

TABLE 24

SUMMARY OF PREDICTED STRENGTHS OF NINE AS4 GRAPHITE FIBER-REINFORCED UNIDIRECTIONAL COMPOSITES

(Fiber Volume = 60 Percent)

Matrix Material and Environment	Transverse Tensile Strength $\bar{\sigma}_{2}^{ult}$ (MPa)	(ksi)	Longitudinal Shear Strength $\bar{\tau}_{12}^{ult}$ (MPa)	(ksi)
Hercules 3502				
RT, Dry	25	3.6	58	8.3
100°C, Dry	41	6.0	71	10.3
RT, Wet (5.0%M)	20	2.9	34	4.9
100°C, Wet (5.0%M)	10	1.5	19	2.7
Fibredux 914				
RT, Dry	7	1.0	77	11.2
100°C, Dry	31	4.5	46	6.7
RT, Wet (7.0%M)	20	2.8	30	4.4
100°C, Wet (7.0%M)	13	1.9	13	1.8
Hercules 2220-1				
RT, Dry	41	6.0	74	10.7
100°C, Dry	72	10.4	69	10.0
RT, Wet (3.8%M)	54	7.9	69	10.0
100°C, Wet (3.8%M)	33	4.8	51	7.4
Hercules 2220-3				
RT, Dry	41	5.9	66	9.5
100°C, Dry	68	9.8	75	10.9
RT, Wet (4.0%M)	57	8.3	71	10.3
100°C, Wet (4.0%M)	30	4.4	33	4.7
Hercules 3501-6				
RJ, Dry	61	8.9	85	12.4
100°C, Dry	41	6.0	64	9.3
RJ, Wet (6.0%M)	31	4.4	68	9.8
100°C, Wet (6.0%M)	14	2.0	21	3.0

TABLE 24 (CONTINUED)

SUMMARY OF PREDICTED STRENGTHS OF NINE AS4 GRAPHITE FIBER-REINFORCED UNIDIRECTIONAL COMPOSITES

(Fiber Volume = 60 Percent)

Matrix Material and Environment	Transverse Tensile Strength $\bar{\sigma}_2^{ult}$		Longitudinal Shear Strength $\bar{\tau}_{12}^{ult}$	
	(MPa)	(ksi)	(MPa)	(ksi)
Hexcel HX-1504				
RT, Dry	74	10.8	72	10.4
100°C, Dry	69	10.0	72	10.5
RT, Wet (3.8%M)	47	6.8	71	10.4
100°C, Wet (3.8%M)	32	5.0	46	6.7
Narmco 5245-C				
RT, Dry	66	9.6	61	8.8
100°C, Dry	62	8.9	65	9.4
RT, Wet (2.1%M)	55	8.0	71	10.3
100°C, Wet (2.1%M)	35	5.1	41	5.9
CYCOM 907				
RT, Dry	82	12.0	54	7.9
100°C, Dry	41	6.0	38	5.5
RT, Wet (5.1%M)	45	6.6	32	4.7
100°C, Wet (5.1%M)	13	1.9	--	--
ERX-4901A(MDA)				
RT, Dry	109	15.8	114	16.5
100°C, Dry	41	5.9	52	7.5
RT, Wet (7.2%M)	56	8.2	58	8.4
100°C, Wet (7.2%M)	7	1.0	9	1.3

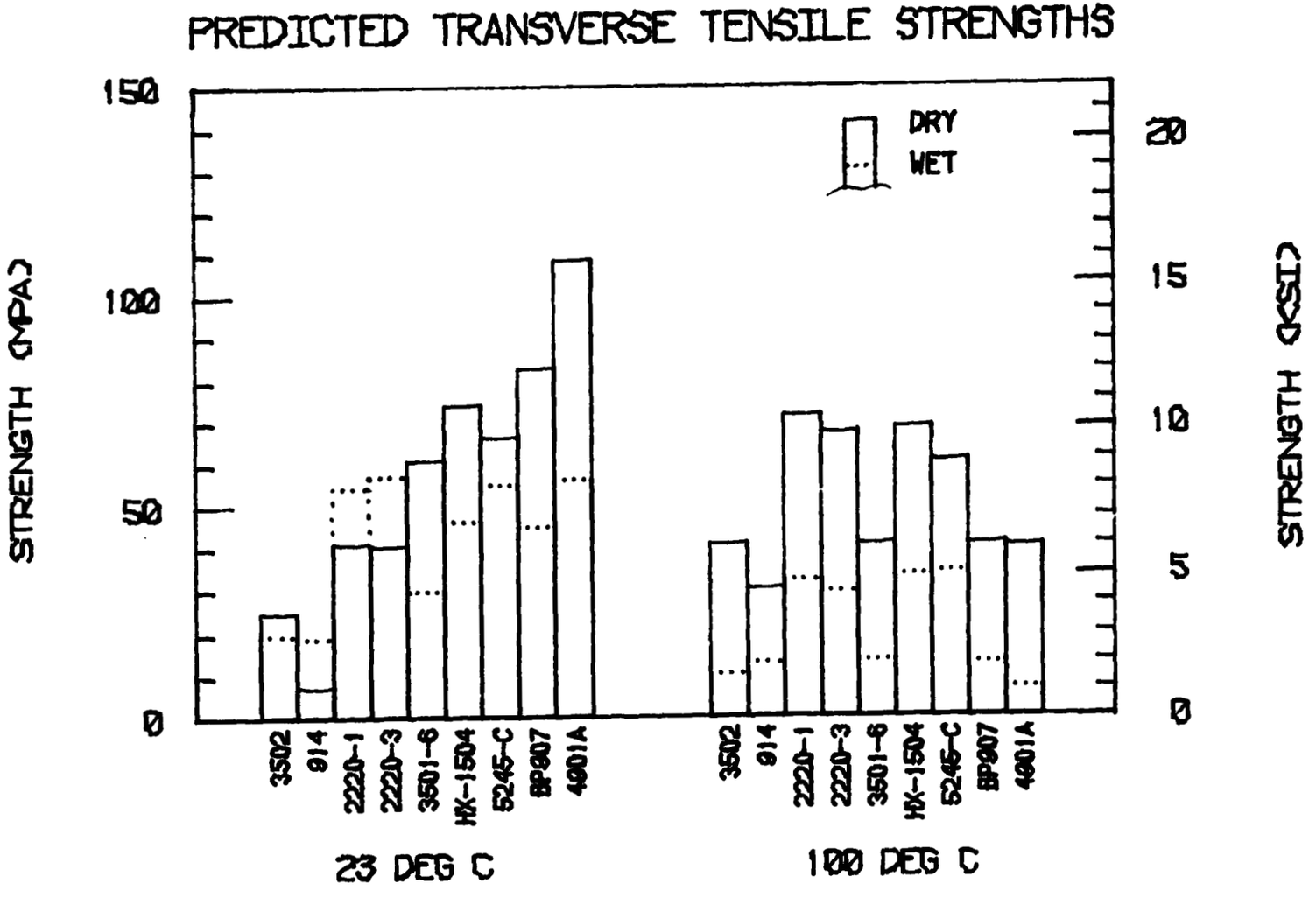

Figure 32. Predicted Transverse Tensile Strengths of Nine AS4 Graphite/Epoxy Unidirectional Composites (V_f = 60 percent) as a Function of Temperature and Moisture Content.

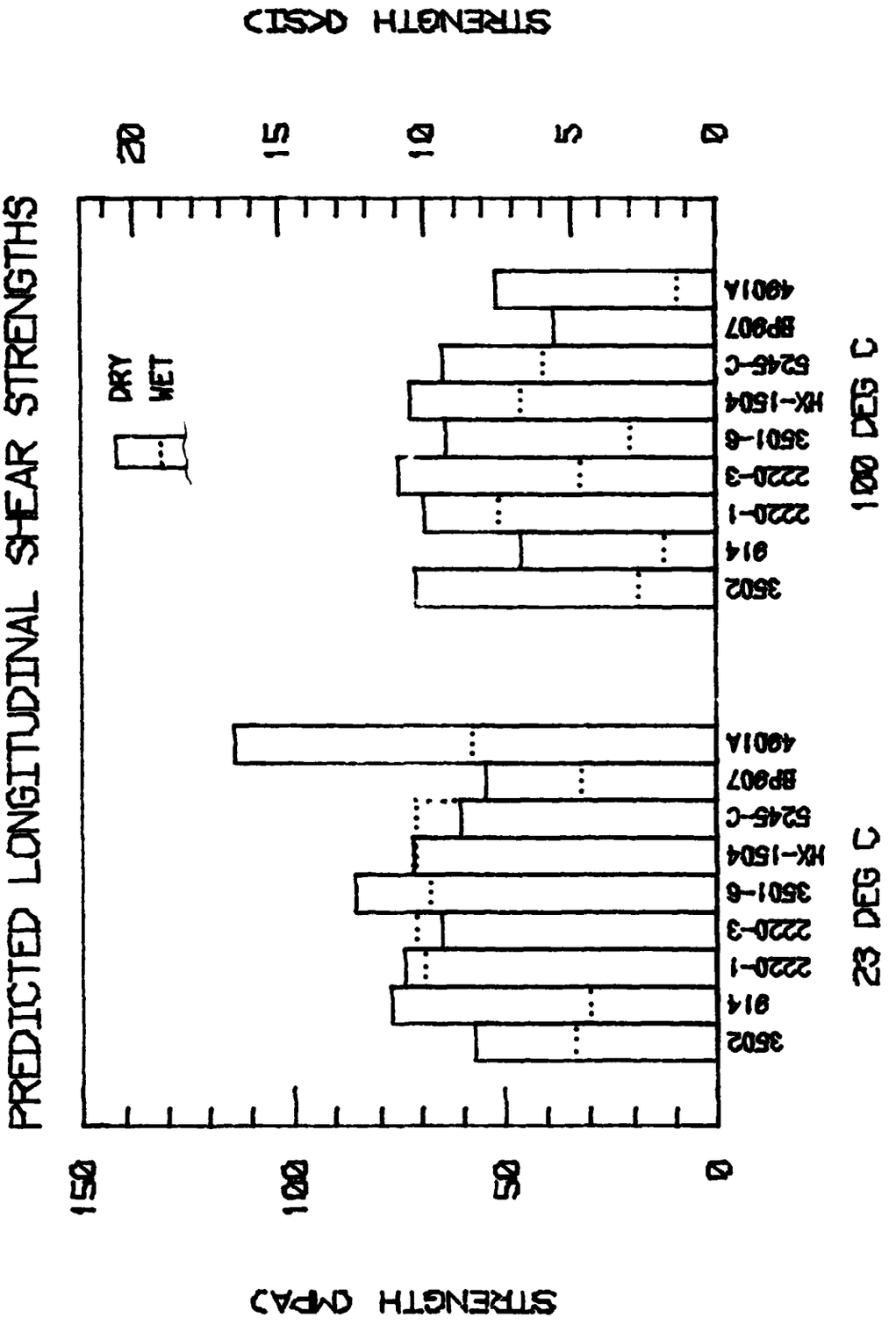

Figure 33. Predicted Longitudinal Shear Strengths of Nine AS4 Graphite/Epoxy Unidirectional Composites (V_f = 60 percent) as a Function of Temperature and Moisture Content.

shear strengths are not generally higher than the room temperature, dry values, unlike for the transverse tensil- loading. The shear strength reduction with increasing temperature (see Figure 3) dominates in most cases.

The very high predicted shear strength of the ERX-4901A(MDA) matrix composite will also be noted in Figure 33. This is of course due to the high measured shear strength of this matrix at the room temperature, dry condition (see Figure 3). The same reasoning applies in explaining its drastic loss in shear strength at the 100°C, wet condition.

Obviously, much comparative information can be obtained from Table 24 and Figures 32 and 33.

5.3.2 Transverse Normal and Longitudinal Shear Stiffnesses

The micromechanical predictions of transverse modulus and shear modulus are given in Table 25, and presented in barchart form in Figures 34 and 35. Most of these predicted values are not significantly influenced by the current uncertainties which affect strength predictions, i. ., yield and strength criteria and the form of the nonlinear matrix stress-strain response. Also, it has been demonstrated many times that the current micromechanics analysis can predict bulk properties such as moduli, Poisson's ratios, and coefficients of thermal expansion and moisture expansion very accurately. (See, for example, References [2,3,5,6,12,17,21,26] of those previously cited in this report.) Thus, most of the predicted stiffnesses presented in Table 25 and Figures 34 and 35 can be compared with a high level of confidence, even with the lack of correlating experimental data. The exceptions arise when the analysis predicts local crack initiation and propagation in the matrix during cooldown from the cure temperature, or after moisture absorption.

TABLE 25

SUMMARY OF PREDICTED STIFFNESS PROPERTIES OF NINE AS4 GRAPHITE FIBER-REINFORCED UNIDIRECTIONAL COMPOSITES

(Fiber Volume = 60 Percent)

Matrix Material and Environment	Transverse Modulus E_{22} (GPa)	(Msi)	Shear Modulus G_{12} (GPa)	(Msi)
Hercules 3502				
RT, Dry	8.58	1.25	5.47	0.79
100°C, Dry	7.68	1.11	4.99	0.72
RT, Wet (5.0%M)	3.16	0.45	4.87	0.71
100°C, Wet (5.0%M)	1.69	0.24	4.36	0.63
Fibredux 914				
RT, Dry	5.80	0.84	4.93	0.71
100°C, Dry	4.96	0.72	4.43	0.64
RT, Wet (7.0%M)	3.74	0.54	4.76	0.69
100°C, Wet (7.0%M)	2.22	0.32	0.35	0.05
Hercules 2220-1				
RT, Dry	8.23	1.19	5.39	0.78
100°C, Dry	6.57	0.95	4.65	0.67
RT, Wet (3.8%M)	8.24	1.20	4.83	0.70
100°C, Wet (3.8%M)	4.75	0.69	3.78	0.55
Hercules 2220-3				
RT, Dry	8.29	1.20	4.62	0.67
100°C, Dry	6.45	0.94	4.11	0.60
RT, Wet (4.0%M)	8.76	1.27	4.40	0.64
100°C, Wet (4.0%M)	5.59	0.81	3.61	0.52
Hercules 3501-6				
RT, Dry	9.84	1.43	5.21	0.76
100°C, Dry	8.23	1.19	3.47	0.50
RT, Wet (6.0%M)	4.39	0.64	4.86	0.71
100°C, Wet (6.0%M)	1.30	0.19	2.72	0.39

TABLE 25 (CONTINUED)

SUMMARY OF PREDICTED STIFFNESS PROPERTIES OF NINE AS4 GRAPHITE FIBER-REINFORCED UNIDIRECTIONAL COMPOSITES

(Fiber Volume = 60 Percent)

Matrix Material and Environment	Transverse Modulus E_{22} (GPa)	(Msi)	Shear Modulus G_{12} (GPa)	(Msi)
Hexcel HX-1504				
RT, Dry	9.04	1.31	6.15	0.89
100°C, Dry	8.05	1.17	4.49	0.65
RT, Wet (3.8%M)	8.95	1.30	4.66	0.68
100°C, Wet (3.8%M)	6.00	0.87	2.90	0.42
Narmco 5245-C				
RT, Dry	8.99	1.30	4.65	0.67
100°C, Dry	8.48	1.23	3.83	0.56
RT, Wet (2.1%M)	9.48	1.38	5.43	0.79
100°C, Wet (2.1%M)	8.31	1.21	3.81	0.55
CYCOM 907				
RT, Dry	9.38	1.36	4.23	0.61
100°C, Dry	5.79	0.84	2.63	0.38
RT, Wet (5.1%M)	7.18	1.04	3.53	0.51
100°C, Wet (5.1%M)	0.26	0.04	--	--
ERX-4901A(MDA)				
RT, Dry	10.65	1.54	6.47	0.94
100°C, Dry	6.11	0.89	3.78	0.55
RT, Wet (7.2%M)	8.24	1.19	5.06	0.73
100°C, Wet (7.2%M)	0.06	0.01	0.05	0.01

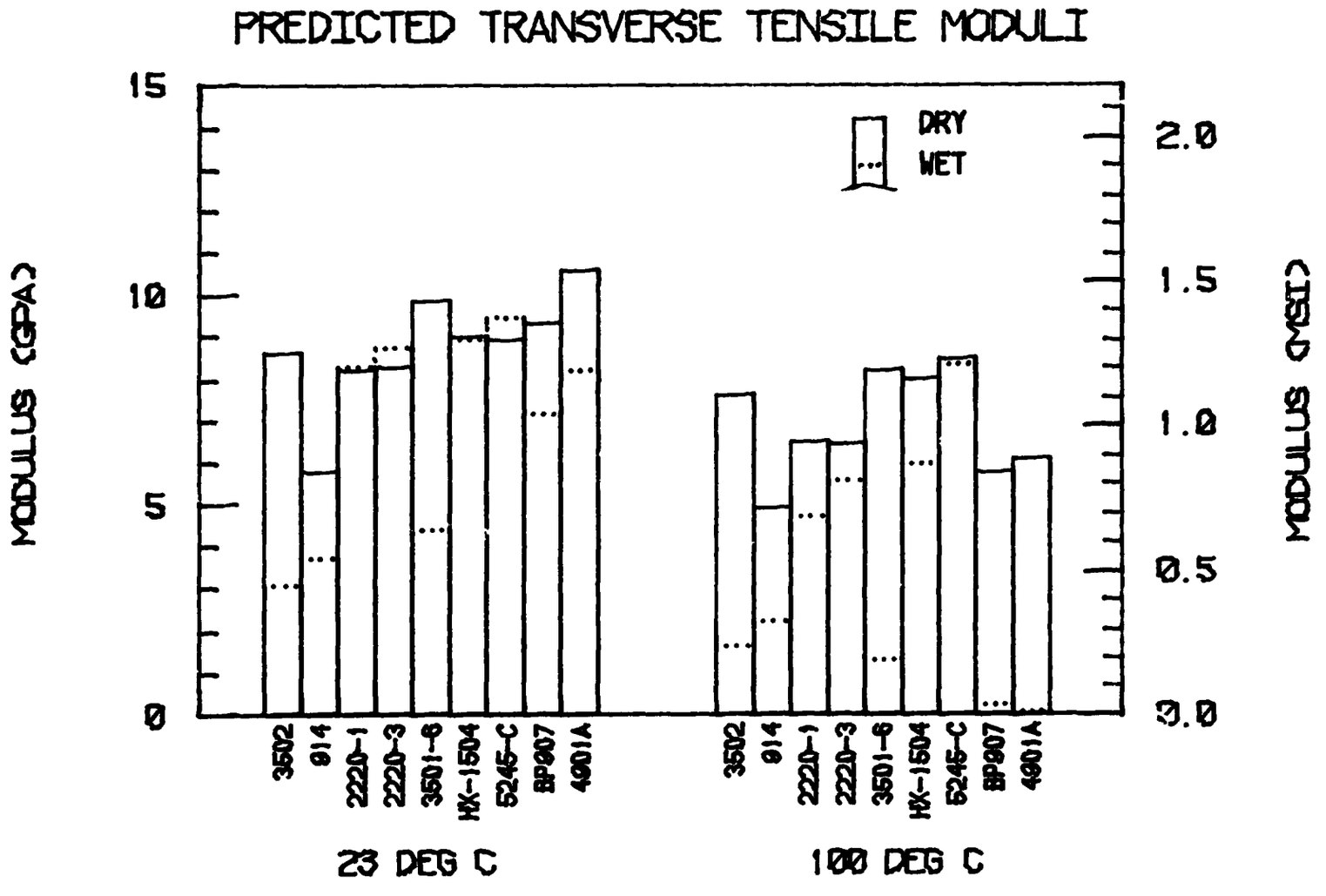

Figure 34. Predicted Transverse Modulus of Nine AS4 Graphite/Epoxy Unidirectional Composites (V_f = 60 percent) as a Function of Temperature and Moisture Content.

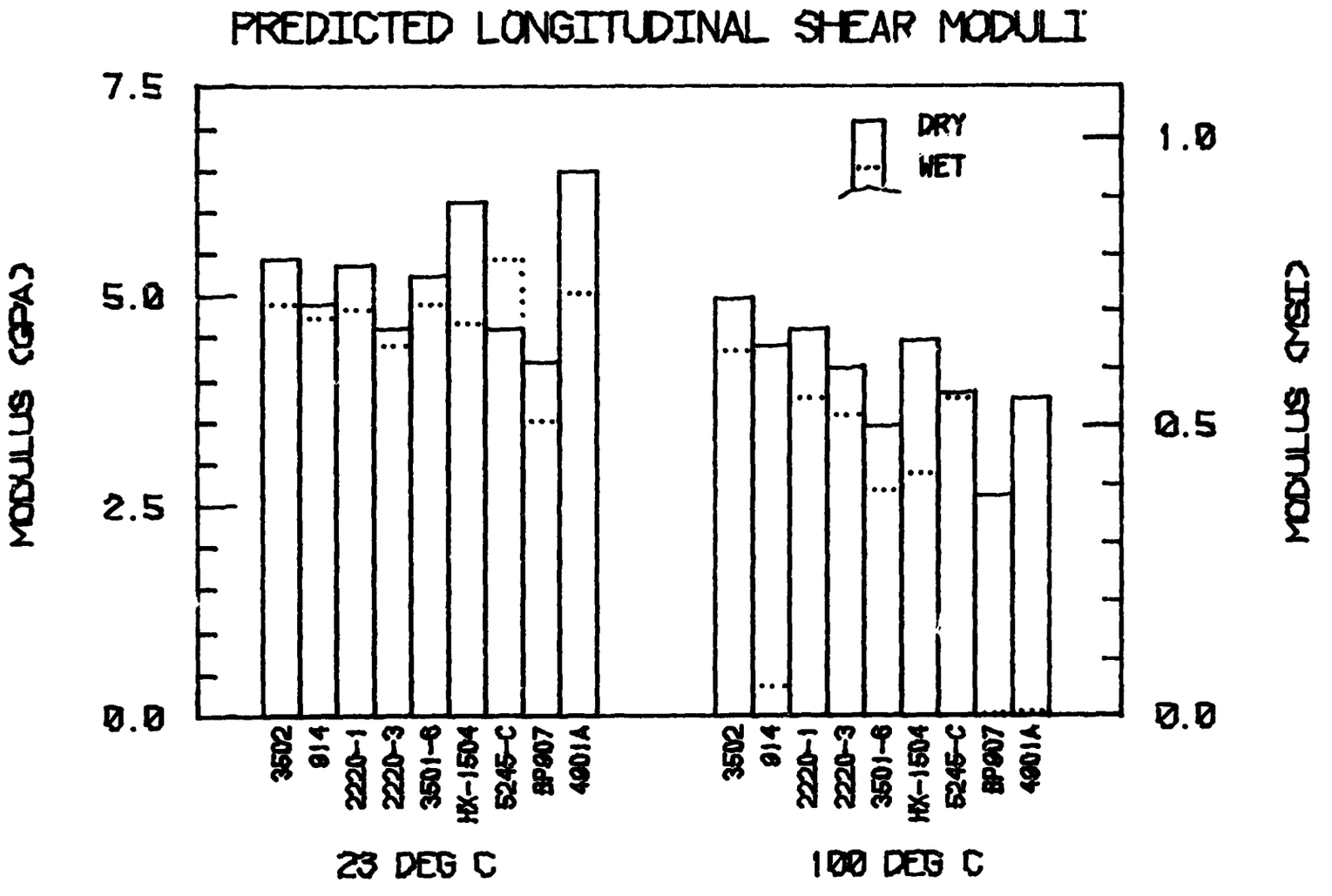

Figure 35. Predicted Longitudinal Shear Modulus of Nine AS4 Graphite/Epoxy Unidirectional Composites (V_f = 60 percent) as a Function of Temperature and Moisture Content.

This is obviously dictated by the failure criterion and matrix stress-strain response assumed.

Plots of yield zones and crack patterns will be presented in the following sections. As will be seen, however, it was the AS4/3502 in the moisture-saturated condition (at both room temperature and 100°C), the AS4/914 at all environmental conditions and the AS4/3501-6 in the moisture-saturated condition (at both room temperature and 100°C) that did exhibit matrix cracking prior to mechanical loading. Also, some other systems did exhibit matrix cracking prior to mechanical loading. Also, some other systems did exhibit extensive yielding prior to mechanical loading even though they did not crack, and some of these began to crack even in the first loading increment. This extensive yielding and crack initiation prior to mechanical loading lowers the stiffness of the composite.

These influences on the transverse modulus (Table 25 and Figure 34) will be considered first. It will be noted that the transverse modulus of the AS4/914 composite is relatively low at all environmental conditions, due to the extensive hygrothermal cracking induced. Likewise, the AS4/3502 and the AS4/3501-6 composite transverse moduli in the moisture-saturated condition are also low, even though the dry values are as high as those of the other composites. Of course, the very low transverse modulus values of both the AS4/CYCOM 907 and the AS4/ERX-4901A(MDA) composites in the hot, wet condition are due to the extreme loss of stiffness of these matrix materials at this condition (see Tables 5 and 6 and Figure 2 of Section 1). These were selected by NASA as model systems, as previously discussed, and were known t degrade at the hot, wet condition.

It is interesting that the Hercules 3502, the baseline matrix material of the first-year study [1], and the Hercules 3501-6, a widely used matrix material in current aerospace structures, are predicted to not perform as well in the moisture-saturated condition as the four other matrix materials not mentioned above, i.e., Hercules 2220-1 and 2220-3, Hexcel HX-1504, and Narmco 5245-C. That is, it is encouraging that these newer, "toughened" matrix materials are predicted to offer improved composite properties.

The longitudinal shear modulus is not as strongly influenced by gross yielding and cracking of the matrix, as indicated in Table 25 and Figure 35, for essentially the same reasons as the shear strength is not, as previously discussed. As for transverse tensile modulus, the very low values of longitudinal shear modulus for the AS4/CYCOM 907 and AS4/ERX-4901A(MDA) composites at the hot, wet condition is due to the loss of matrix stiffness. However, in the case of the AS4/914 composite, the loss of shear modulus at this condition is due to the almost complete crack propagation around the fiber-matrix interface during cooldown and subsequent moisture absorption. Of course, both the transverse tensile strength and the longitudinal shear strength were degraded severely also, as indicated previously in Table 24 and Figures 32 and 33.

5.3.3 Thermal and Moisture Exparsion Coefficients

Unidirectional composite properties which are much less often experimentally determined than strengths or stiffnesses, but which are also needed in design as well as analysis, are the coefficients of thermal expansion and coefficients of moisture expansion. The micro-mechanics analysis is capable of predicting these properties whenever an

increment of temperature or moisture, respectively, is applied.

Results for the nine resin-matrix composites being considered here are presented in Table 26. Thermal expansion values are not given for the room temperature, wet condition since an increment of temperature was not applied after the moisture was added. This could readily be done, however, if these data were needed. Likewise, values of moisture expansion are only included in Table 26 for the room temperature, wet condition. For the 100°C, wet condition, the moisture was added at room temperature, then the temperature was incremented up to 100°C. Again, an increment of moisture could be added at 100°C, if it is desired to determine the moisture expansion coefficients at this temperature.

The predicted values of the coefficients of thermal expansion and coefficients of moisture expansion can actually be a function of the failure criterion used. If the particular failure criterion selected results in crack initiation and propagation during cooldown and/or during moisture absorption, then the matrix material becomes effectively less stiff. This in turn influences the fiber-matrix interaction during an increment of temperature or moisture. In the present case a maximum normal stress failure criterion was used for tensile loading, and an octahedral shear criterion for shear loading, and computer runs were initiated from the cure temperature, dry stress-free state in both cases. Thus, when cracking did occur prior to mechanical loading, as will be discussed in the next sections, slightly different values of α and β were obtained. The values listed in Table 18 are those corresponding to the minimum cracking condition. As experimental data become available, it will be possible to correlate these differences in predictions with the actual data, and infer the correct condition. In

TABLE 26

SUMMARY OF PREDICTED THERMAL AND MOISTURE EXPANSION PROPERTIES OF NINE AS4 GRAPHITE FIBER-REINFORCED UNIDIRECTIONAL COMPOSITES

(Fiber Volume = 60 Percent)

Matrix Material and Environment	Coefficients of Thermal Expansion (10^{-6}°C)		Coefficients of Moisture Expansion (10^{-3}/%M)	
	α_{11}	α_{22}	β_{11}	β_{22}
Hercules 3502				
RT, Dry	0.196	37.0	-	-
100°C, Dry	0.123	36.3	-	-
RT, Wet (5.0%M)	-	-	0.030	1.46
100°C, Wet (5.0%M)	0.059	39.6	-	-
Fibredux 914				
RT, Dry	0.050	40.9	-	-
100°C, Dry	0.045	40.6	-	-
RT, Wet (7.0%M)			0.013	0.59
100°C, Wet (7.0%M)	0.019	38.7	-	-
Hercules 2220-1				
RT, Dry	0.390	39.9	-	-
100°C, Dry	0.355	39.4	-	-
RT, Wet (3.8%M)	-	-	0.031	1.57
100°C, Wet (3.8%M)	0.073	41.9	-	-
Hercules 2220-3				
RT, Dry	0.274	38.3	-	-
100°C, Dry	0.223	38.1	-	-
RT, Wet (4.0%M)	-	-	0.034	1.40
100°C, Wet (4.0%M)	0.090	41.8	-	-
Hercules 3501-6				
RT, Dry	0.222	32.4	-	-
100°C, Dry	0.102	35.2	-	-
RT, Wet (6.0%M)	-	-	0.033	1.65
100°C, Wet (6.0%M)	0.099	45.1	-	-

TABLE 26 (CONTINUED)

SUMMARY OF PREDICTED THERMAL AND MOISTURE EXPANSION PROPERTIES OF NIS AS4 GRAPHITE FIBER-REINFORCED UNIDIRECTIONAL COMPOSITES

(Fiber Volume = 60 Percent)

Matrix Material and Environment	Coefficients of Thermal Expansion (10^{-6}/°C)		Coefficients of Moisture Expansion (10^{-3}/%M)	
	α_{11}	α_{22}	β_{11}	β_{22}
Hexcel HX-1504				
RT, Dry	0.241	37.7	-	-
100°C, Dry	0.185	37.4	-	-
RT, Wet (3.8%M)	-	-	0.029	1.07
100°C, Wet (3.8%M)	0.027	38.9	-	-
Narmco 5245-C				
RT, Dry	0.210	36.5	-	-
100°C, Dry	0.173	36.4	-	-
RT, Wet (2.1%M)	-	-	0.024	0.82
100°C, Wet (2.1%M)	0.212	37.6	-	-
CYCOM 907				
RT, Dry	0.070	37.7	-	-
100°C, Dry	0.075	37.2	-	-
RT, Wet (5.1%M)	-	-	0.019	1.28
100°C, Wet (5.1%M)	0.347	52.1	-	-
ERX-4901A(MDA)				
RT, Dry	0.684	44.9	-	-
100°C, Dry	0.301	43.8	-	-
RT, Wet (7.2%M)	-	-	0.017	0.87
100°C, Wet (7.2%M)	0.362	50.0	-	-

the meantime, the values listed in Table 26 are offered as general trends.

It should be noted that the predicted values of moisture expansion were much less sensitive to matrix cracking than the values of thermal expansion.

5.4 Predicted Stress-Strain Curves and Crack Propagation Patterns

Micromechanics predictions of unidirectional composite transverse tensile and longitudinal shear stress-strain curves to failure, and the corresponding yield zone and crack propagation patterns, will be presented for each of the nine matrix materials in the order they are listed in Table 23. For brevity, no results will be presented here for axial tensile loadings as they were less interesting. The axial tensile stress-strain curves for the first four resin-matrix composites, presented in Reference [1], demonstrated this.

Transverse tensile loading results will be presented in the next subsection, followed by longitudinal shear loading results in the following subsection.

5.4.1 Transverse Tensile Loading

In each of the stress-strain plots presented in this and the following subsection, four curves are included in each plot. These correspond to the four environmental conditions considered in this section, viz, room temperature, dry (RTD), elevated temperature, dry (ETD), room temperature, wet (RTW), and elevated temperature, wet (ETW).

5.4.1.1 AS4/3502 Graphite/Epoxy

The stress-strain curves to failure for the AS4/3502 graphite/epoxy unidirectional composite are plotted in Figure 36. The transverse tensile stress-strain curves for all nine matrix materials are plotted

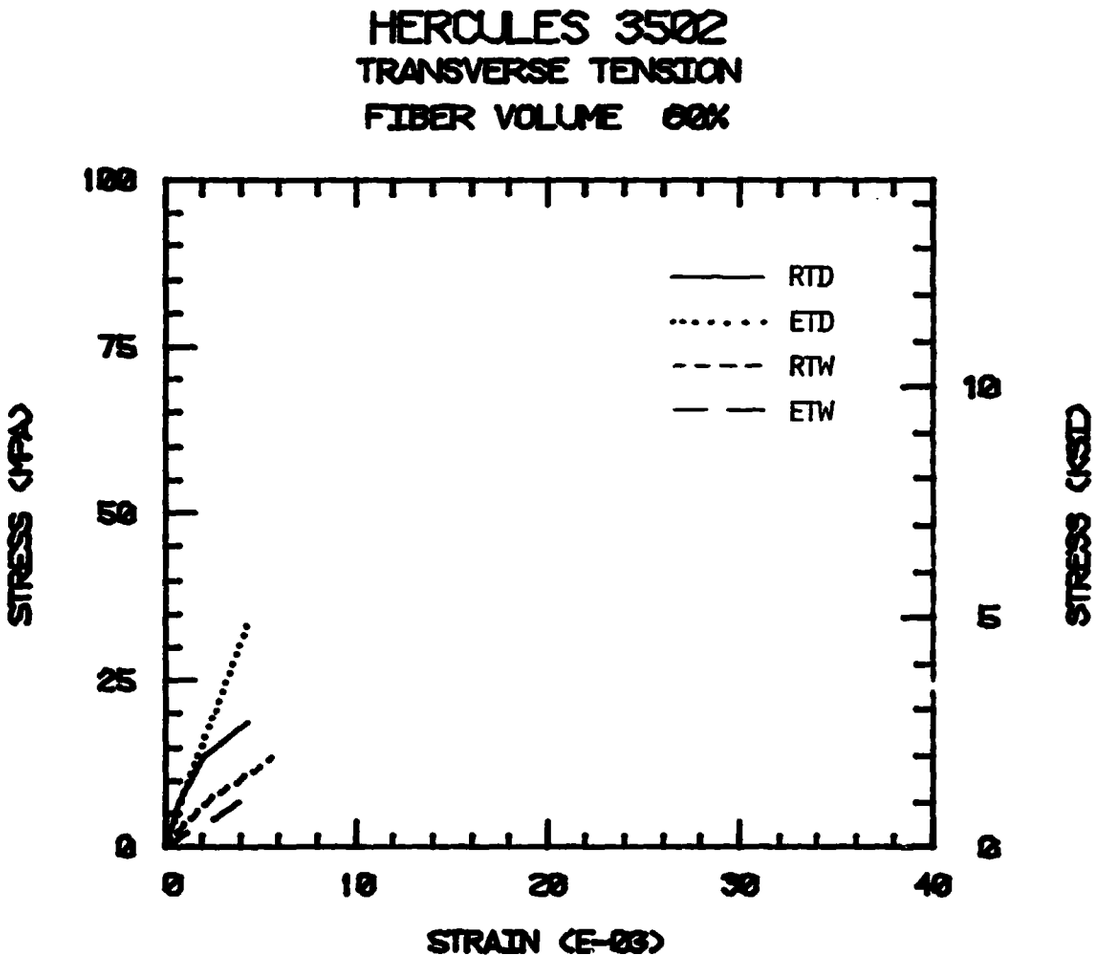

Figure 36. AS4/3502 Graphite/Epoxy Unidirectional Composite, Transverse Tensile Stress-Strain Response.

to the same scale so that comparisons can be readily made. Obviously, the AS4/3502 composite did not exhibit very high transverse tensile strengths and strains to failure relative to some of the other composites, since the stress-strain curves of Figure 36 are crowded near the origin of the plot. The influence of combined temperature and moisture can also be seen, particularly in terms of stiffness reduction.

Figure 37 indicates the extent of matrix material yielding (the shaded regions) and crack propagation (the solid black regions) in the AS4/3502 composite at the RTD condition, for three levels of transverse tensile loading, including zero load. As can be seen, a considerable amount of matrix yielding is predicted to occur during cooldown from the 177°C cure temperature. (It will be noted that the stress distributions, and hence the patterns of yielding and cracking, should always be symmetric prior to mechanical loading, because of the assumed regular square fiber packing array assumed here.) The governing matrix stress-strain curves were presented in Figure 23. At only 14 MPa (Figure 37b) matrix cracking has extended considerably, failure being predicted at 25 MPa (Figure 37c).

The ETD predictions are indicated in Figure 38. No additional yielding occurs during the temperature increase to 100°C (as previously discussed, the cooldown-induced thermal residual stresses are actually relieved somewhat by the temperature increase). Thus, at 21 MPa (Figure 38b), yielding has spread somewhat, but no cracking has yet occurred. Subsequently, a crack pattern similar to that for the RTD case (Figure 37) is predicted, total failure of the composite occurring at 41 MPa (as indicated in the caption of Figure 38). That is, the predicted strength is 64 percent higher at the ETD condition than at the RTD condition, due

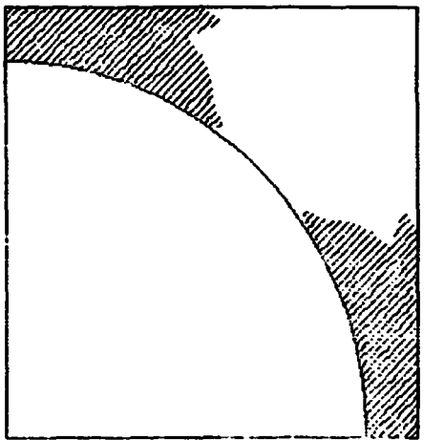

a) No Mechanical Loading

b) $\bar{\sigma}_x$ = 14 MPa (2.0 ksi)

c) $\bar{\sigma}_x$ = 25 MPa (3.6 ksi)

Figure 37. AS4/3502 Graphite/Epoxy Unidirectional Composite, Room Temperature, Dry (RTD), Transverse Tensile Loading: $\bar{\sigma}_x^{ult}$ = 25 MPa (3.6 ksi).

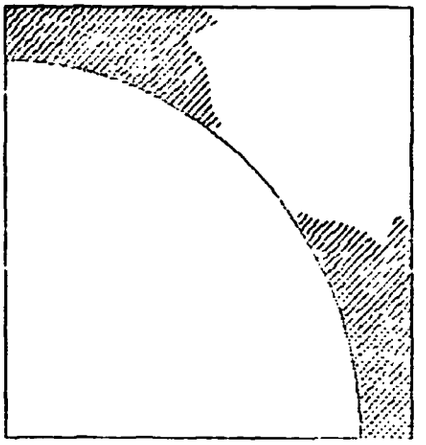

a) No Mechanical Loading

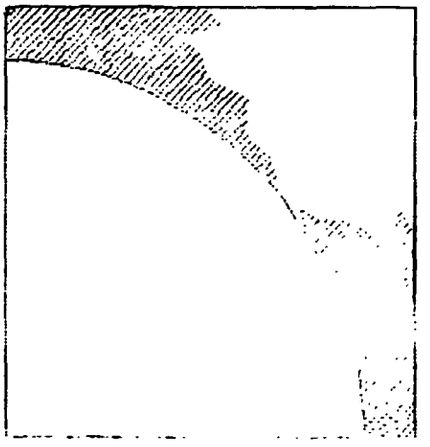

b) $\bar{\sigma}_x$ = 21 MPa (3.0 ksi)

Figure 38. AS4/3502 Graphite/Epoxy Unidirectional Composite, 100°C, Dry (ETD), Transverse Tensile Loading: $\bar{\sigma}_x^{ult}$ = 41 MPa (6.0 ksi).

to the lower thermal residual stresses present before the transverse tensile loading is introduced.

Results for the RTW condition are shown in Figure 39. As can be seen, the addition of 5.0 weight percent moisture to the Hercules 3502 matrix causes almost complete yielding of the matrix, and extensive cracking, prior to mechanical loading (Figure 39a). Failure is predicted at only 20 MPa (Figure 39b). It will be noted that the predicted crack pattern for the RTW case is considerably different than that for the RTD and ETD cases. This should be verifiable by means of scanning electron microscopic examination of the respective fracture surfaces of actual composites. The exposed graphite fiber surfaces for the RTW case should be relatively clean (free of adhering matrix particles), whereas the RTD and ETD specimen fiber surfaces should not. Obviously, experimental data are needed.

Increasing the specimen temperature to 100°C in the moisture-saturated condition does not alter the RTW crack pattern significantly (compare Figure 40a to Figure 39a). Composite failure does occur sooner under transverse tensile loading, however, because of the reduced matrix strength (see Figure 36, or Figure 1 of Section 1).

5.4.1.2 AS4/914 Graphite/Epoxy

The Fibredux 914 epoxy matrix, like the Hercules 3502 discussed above, is not a high strength matrix (see Figure 1 of Section 1, for example). Thus, the predicted transverse tensile strengths of the AS4/914 graphite/epoxy composite are also low at all environmental conditions, as shown in Figure 41. The low RTD strength and high coefficient of thermal expansion (see Table 1 of Section 1) combine to produce total matrix yielding and extensive matrix cracking in the

a) No Mechanical Loading

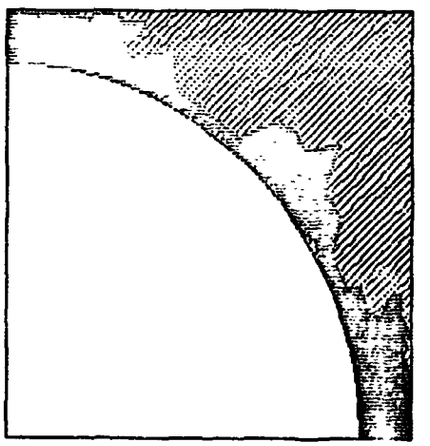

b) $\bar{\sigma}_x$ = 20 MPa (2.9 ksi)

Figure 39. AS4/3502 Graphite/Epoxy Unidirectional Composite, Room Temperature, 5.0% M (RTW), Transverse Tensile Loading: $\bar{\sigma}_x^{ult}$ = 20 MPa (2.9 ksi).

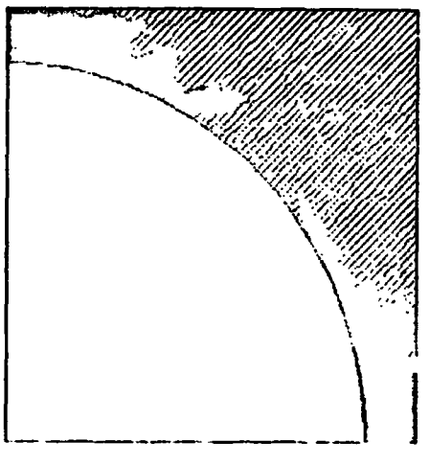

a) No Mechanical Loading

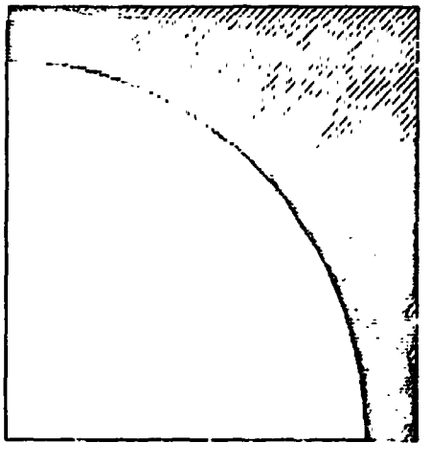

b) $\bar{\sigma}_x$ = 10 MPa (1.5 ksi)

Figure 40. AS4/3502 Graphite/Epoxy Unidirectional Composite, 100°C, 5.0% M (ETW), Transverse Tensile Loading: $\bar{\sigma}_x^{ult}$ = 10 MPa (1.5 ksi).

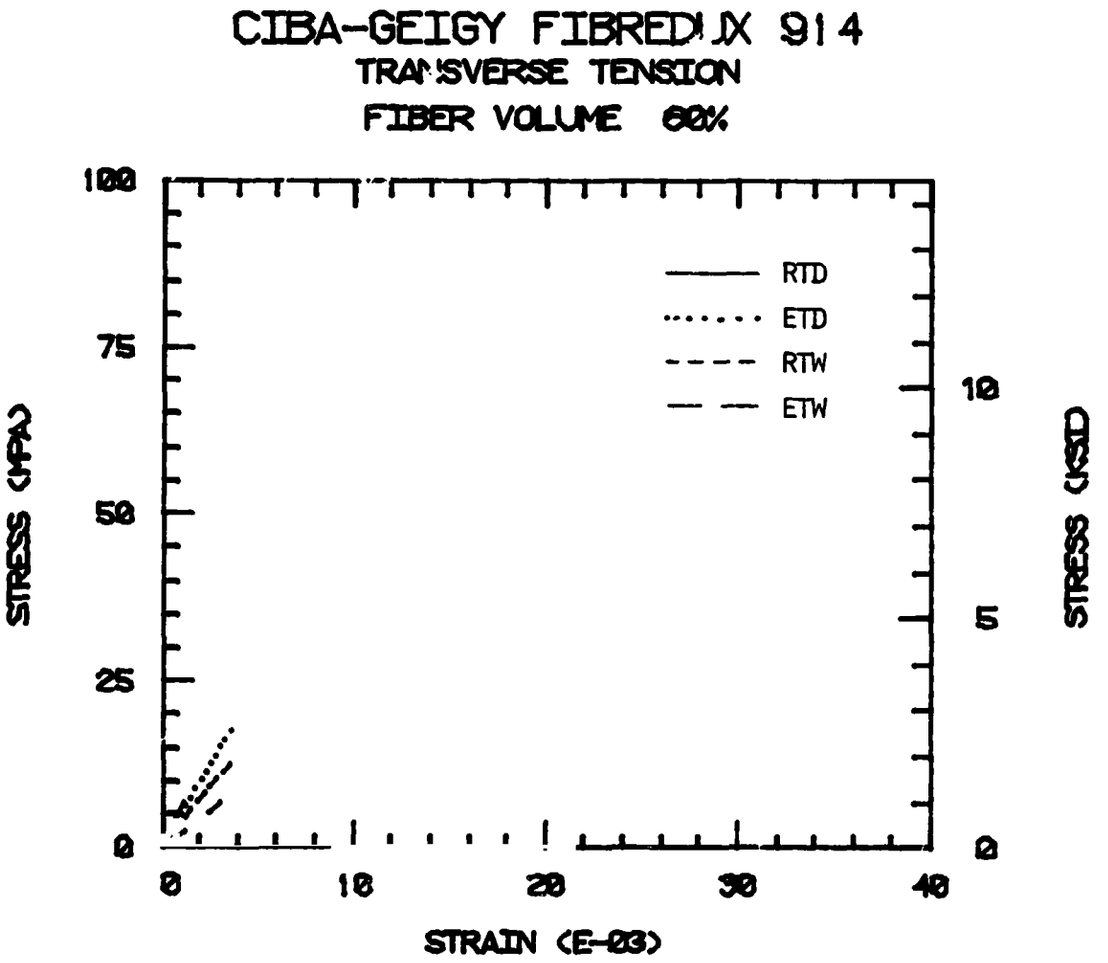

Figure 41. AS4/914 Graphite/Epoxy Unidirectional Composite, Transverse Tensile Stress-Strain Response.

composite prior to mechanical loading, as shown in Figure 42a. Thus, failure due to transverse tensile loading is predicted at only 7 MPa (Figure 42b). The thermal residual stresses are relieved somewhat at the ETD condition, resulting in a somewhat higher composite transverse tensile strength (Figure 41). However, the presence of moisture again degrades the matrix strength, particularly at the elevated temperature, as indicated in Figure 43.

5.4.1.3 AS4/2220-1 Graphite/Epoxy

The predicted transverse tensile stress-strain curves for the AS4/2220-1 graphite/epoxy composite are shown in Figure 44. As can be seen, the predicted strengths at all environmental conditions are considerably higher than for the two previous matrix materials, as are the strains to failure. This matrix material is stronger and tougher than the 3502 and 914 systems. As might be expected, no matrix cracking was predicted at the RTD condition prior to mechanical loading for the AS4/2220-1 composite, although extensive yielding did occur (see Figure 45a). First failure was predicted at about 35 MPa transverse tensile loading, and total failure of the composite at 41 MPa (Figure 45b).

Because of the thermal residual stress relief at 100°C, the ETD strength of this composite was higher than at the RTD condition as was the strain to failure (Figure 44). The predicted crack pattern in the matrix was also different, as can be seen by comparing Figure 46 with Figure 45.

The addition of moisture at room temperature relieves (offsets) the thermal stresses in the composite to some extent, but also reduces the matrix strength (see Figure 1 of Section 1, or Figure 25). The net effect is an only modest increase in composite transverse tensile

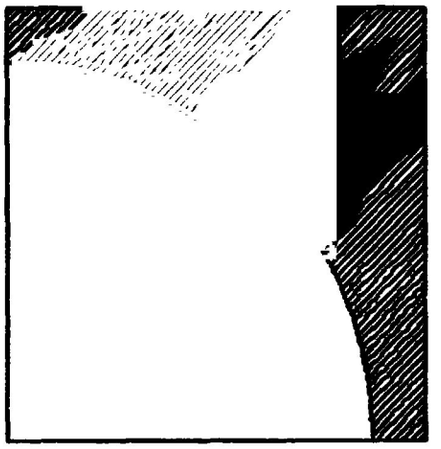

a) No Mechanical Loading

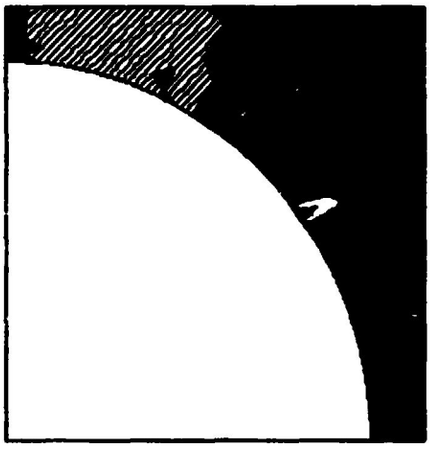

b) $\bar{\sigma}_x$ = 7 MPa (1.0 ksi)

Figure 42. AS4/914 Graphite/Epoxy Unidirectional Composite, Room Temperature, Dry (RTD), Transverse Tensile Loading: $\bar{\sigma}_x^{ult}$ = 7 MPa (1.0 ksi).

a) No Mechanical Loading

b) $\bar{\sigma}_x$ = 13 MPa (1.9 ksi)

Figure 43. AS4/914 Graphite/Epoxy Unidirectional Composite, 100°C, 7.0% M (ETW), Transverse Tensile Loading: $\bar{\sigma}_x^{ult}$ = 13 MPa (1.9 ksi).

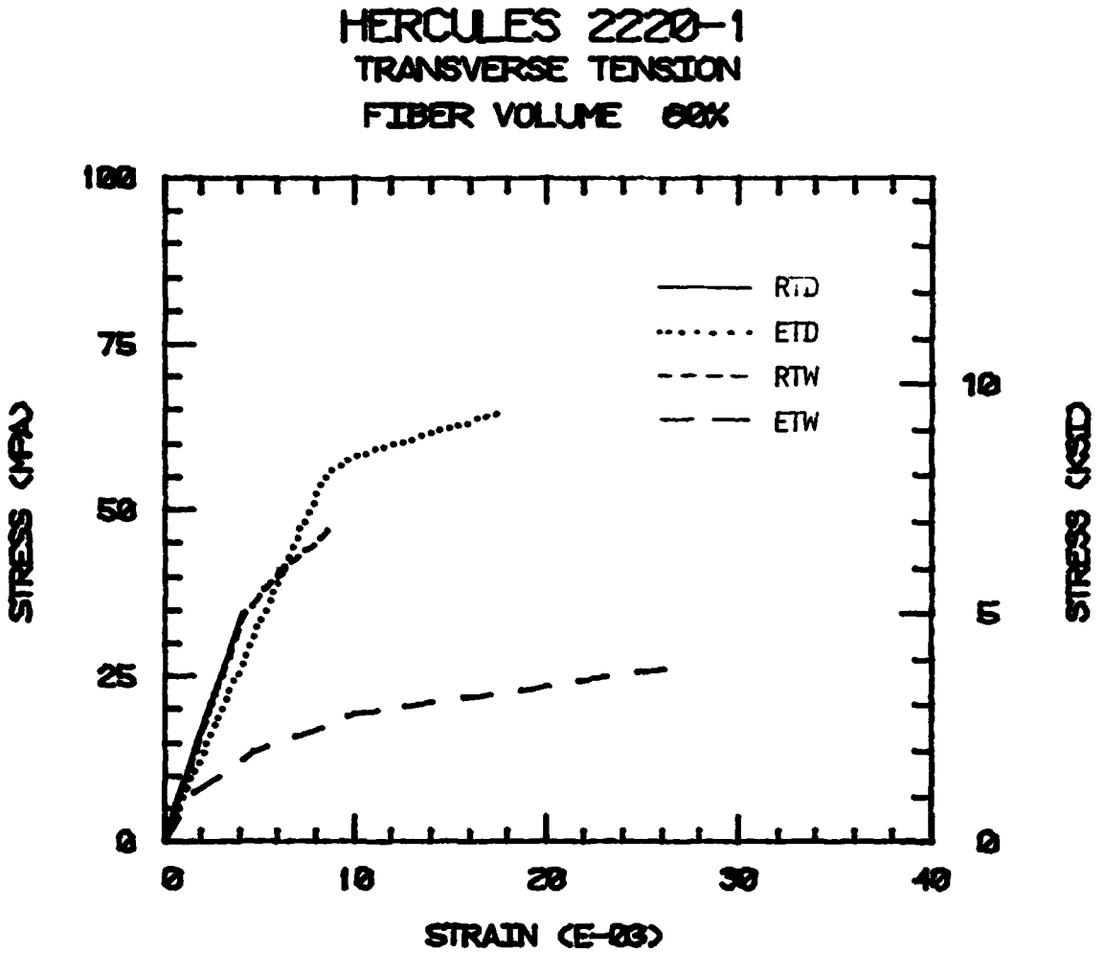

Figure 44. AS4/2220-1 Graphite/Epoxy Unidirectional Composite, Transverse Tensile Stress-Strain Response.

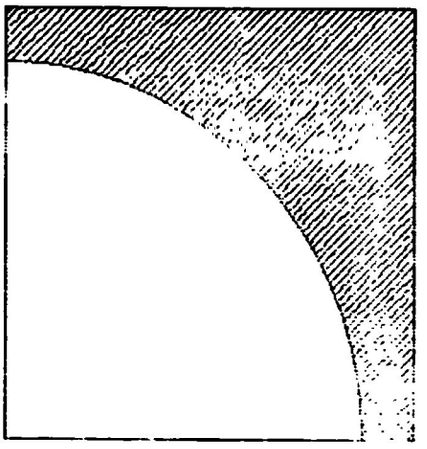

a) No Mechanical Loading

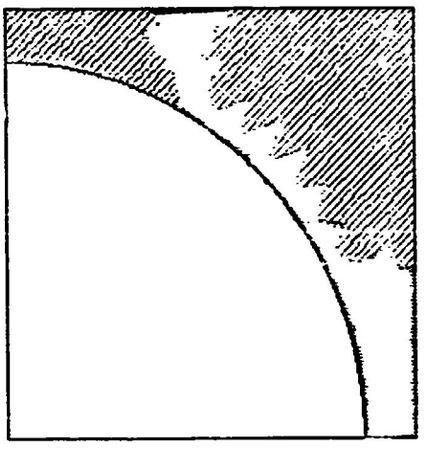

b) $\bar{\sigma}_x$ = 41 MPa (6.0 ksi)

Figure 45. AS4/2220-1 Graphite/Epoxy Unidirectional Composite, Room Temperature, Dry (RTD), Transverse Tensile Loading: $\bar{\sigma}_x^{ult}$ = 41 MPa (6.0 ksi).

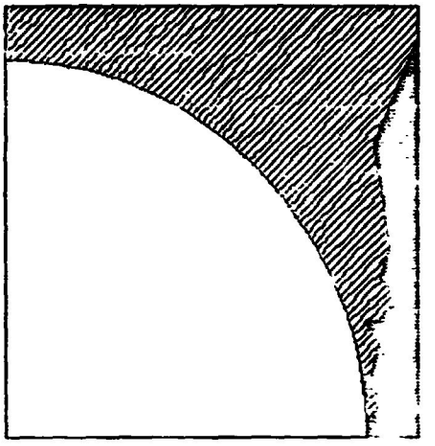

a) $\bar{\sigma}_x$ = 58 MPa (8.4 ksi)

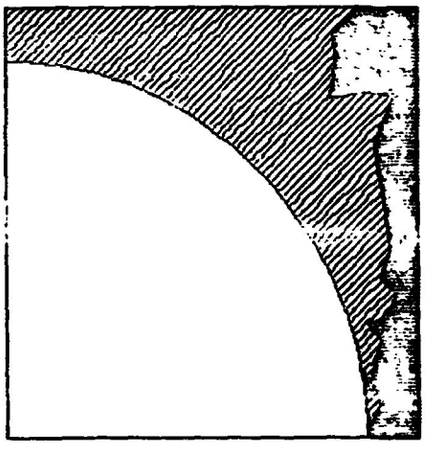

b) $\bar{\sigma}_x$ = 72 MPa (10.4 ksi)

Figure 46. AS4/2220-1 Graphite/Epoxy Unidirectional Composite, 100°C, Dry (ETD), Transverse Tensile Loading: $\bar{\sigma}_x^{ult}$ = 72 MPa (10.4 ksi).

strength at the RTW condition (Figure 44). The predicted crack pattern is somewhat similar to that for the ETD case, as can be seen by comparing Figure 47 with Figure 46. On the other hand, the combined influence of temperature and moisture is a loss of composite transverse tensile strength, and an increase in strain to failure, as shown in Figure 44. The corresponding progression of cracking is shown in Figure 48. Although no cracking occurred prior to mechanical loading (Figure 48a), it was incipient. Matrix cracking did initiate at less than 7 MPa applied stress, having progressed considerably at 14 MPa, as shown in Figure 48b. The final crack pattern (Figure 48c) was generally similar to that for the RTD loading (Figure 45b).

5.4.1.4 AS4/2220-3 Graphite/Epoxy

The predicted composite stress-strain curves are shown in Figure 49. The response would be expected to be generally similar to that for the 2220-1 matrix composite, since the neat resin properties were similar, and this was true (comparing Figure 49 to Figure 44).

The extent of matrix yielding due to cooldown-induced thermal residual stresses was less (comparing Figure 50a to Figure 45a), but the RTD crack propagation pattern due to transverse tensile loading (Figure 50d) was very similar to that for the AS4/2220-1 composite (Figure 45b).

The ETD crack propagation pattern is not shown here as it also was very similar to the ETD pattern for the 2220-1 system. Likewise, the RTW and ETW behaviors were also very similar to their 2220-1 counterparts, including full matrix yielding prior to mechanical loading. This was undoubtedly due to the fact that the 2220-3 epoxy was determined to have a higher coefficient of moisture expansion than the 2220-1 epoxy, and also a higher moisture weight gain (see Table 4 of Section 1).

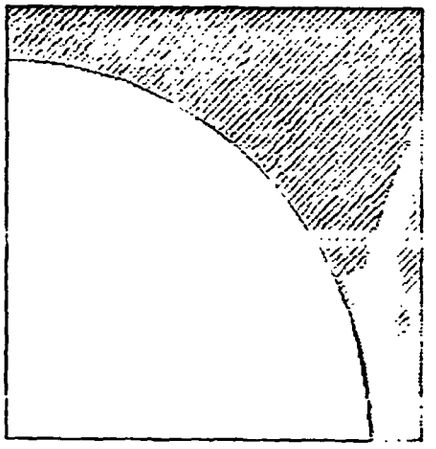

a) $\bar{\sigma}_x$ = 41 MPa (5.9 ksi)

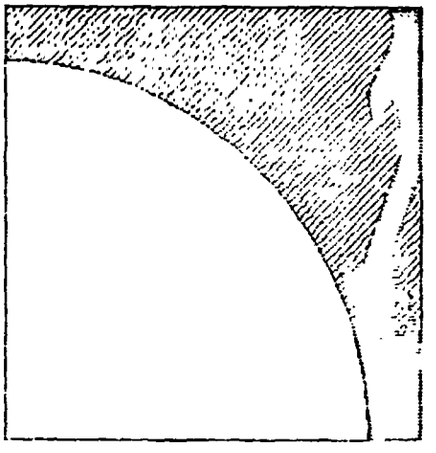

b) $\bar{\sigma}_x$ = 54 MPa (7.9 ksi)

Figure 47. AS4/2220-1 Graphite/Epoxy Unidirectional Composite, Room Temperature, 3.8% M (RTW), Transverse Tensile Loading: $\bar{\sigma}_x^{ult}$ = 54 MPa (7.9 ksi).

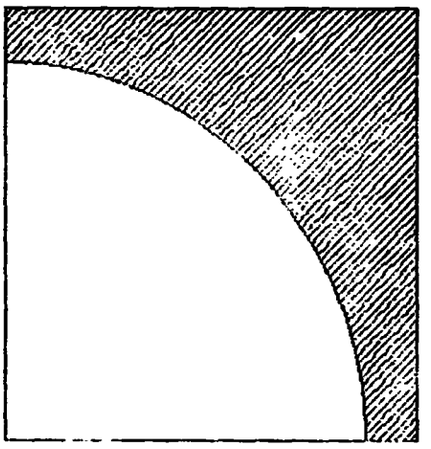

a) No Mechanical Loading

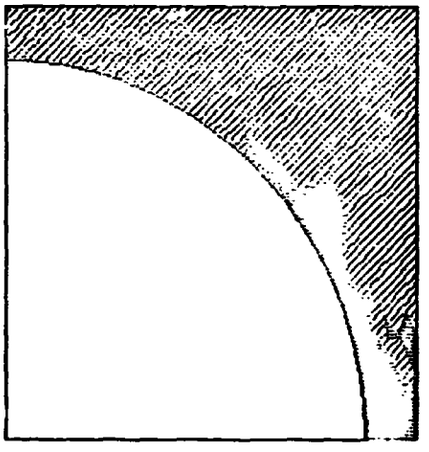

b) $\bar{\sigma}_x$ = 14 MPa (2.0 ksi)

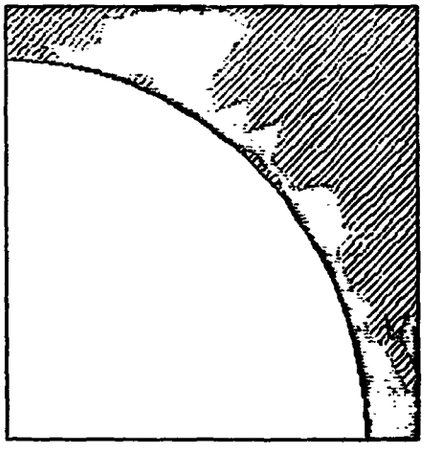

c) $\bar{\sigma}_x$ = 33 MPa (4.8 ksi)

Figure 48. AS4/2220-1 Graphite/Epoxy Unidirectional Composite, 100°C, 3.8% M (ETW), Transverse Tensile Loading: $\bar{\sigma}_x^{ult}$ = 33 MPa (4.8 ksi).

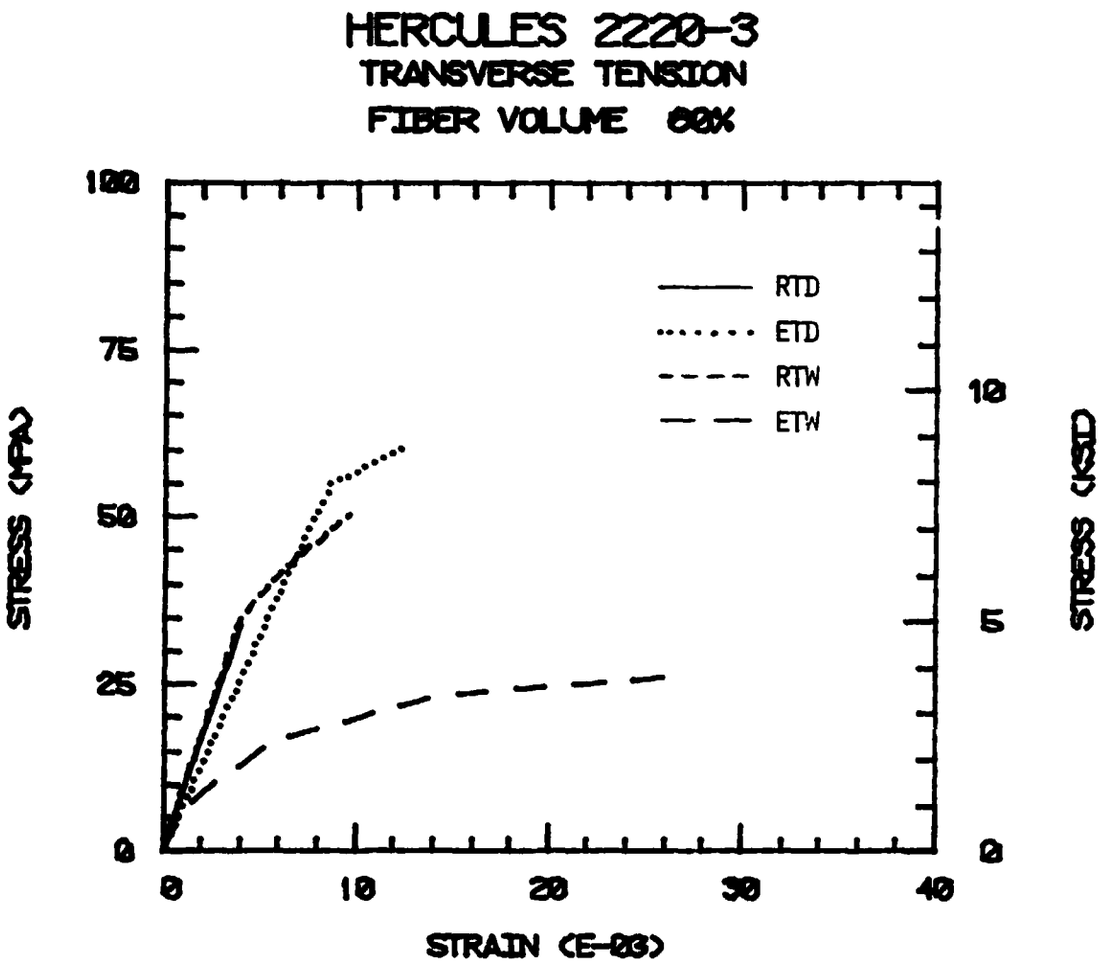

Figure 49. AS4/2220-3 Graphite/Epoxy Unidirectional Composite, Transverse Tensile Stress-Strain Response.

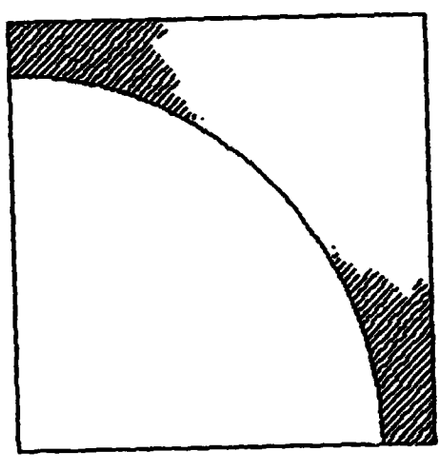

a) No Mechanical Loading

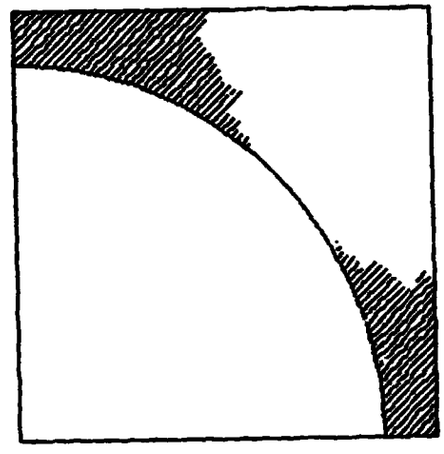

b) $\bar{\sigma}_x$ = 14 MPa (2 ksi)

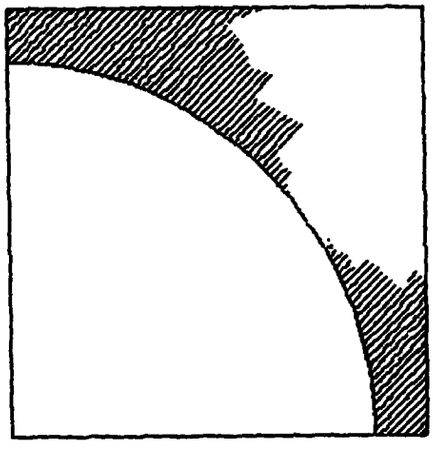

c) $\bar{\sigma}_x$ = 28 MPa (4 ksi)

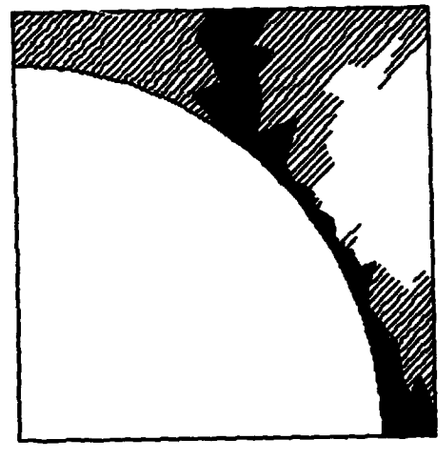

d) $\bar{\sigma}_x$ = 41 MPa (5.9 ksi)

Figure 50. AS4/2220-3 Graphite/Epoxy Unidirectional Composite, Room Temperature, Dry (RTD), Transverse Tensile Loading: $\bar{\sigma}_x^{ult}$ = 41 MPa (5.9 ksi).

5.4.1.5 AS4/3501-6 Graphite/Epoxy

The Hercules 3501-6 epoxy, although a better performer than the Hercules 3502 epoxy, is not as good as the Hercules 2220 systems. This is translated to the composite transverse tensile properties, as seen in Figure 51. In particular, the strains to failure are significantly less than for the AS4/2220 composites. The Hercules 3501-6 has better RTD properties, and hence the extent of matrix yielding prior to loading is less (Figure 52a), and the RTD ultimate strength is higher. The crack propagation pattern at failure (Figure 52c) is almost identical to that for the AS4/2220 composites.

The ETD response is almost identical to the RTD response. However, the RTW response is considerably different, as shown in Figure 53. Matrix cracking was predicted to occur during moisture absorption (Figure 53a), as for the AS4/3502 composite (Figure 39a). Correspondingly, the RTW transverse tensile strength was also predicted to be low (Table 24). At the ETW condition, the response is similar, the matrix cracking being somewhat more extensive at total failure.

5.4.1.6 AS4/HX-1504 Graphite/Epoxy

The transverse tensile stress-strain plots for the AS4/HX-1504 composite are shown in Figure 54. The response is generally similar to that of the two 2220 systems, except that the RTD strength is considerably higher. This is because the RTD strength of the neat resin was much higher, as shown in Figure 1 of Section 1. The extent of yielding and the crack propagation pattern (Figure 55) is very similar to those of the 2220 systems, although first cracking was predicted to not occur until an applied stress of 66 MPa was reached, which is higher than the ultimate strength of either 2220 system. At the ETD condition,

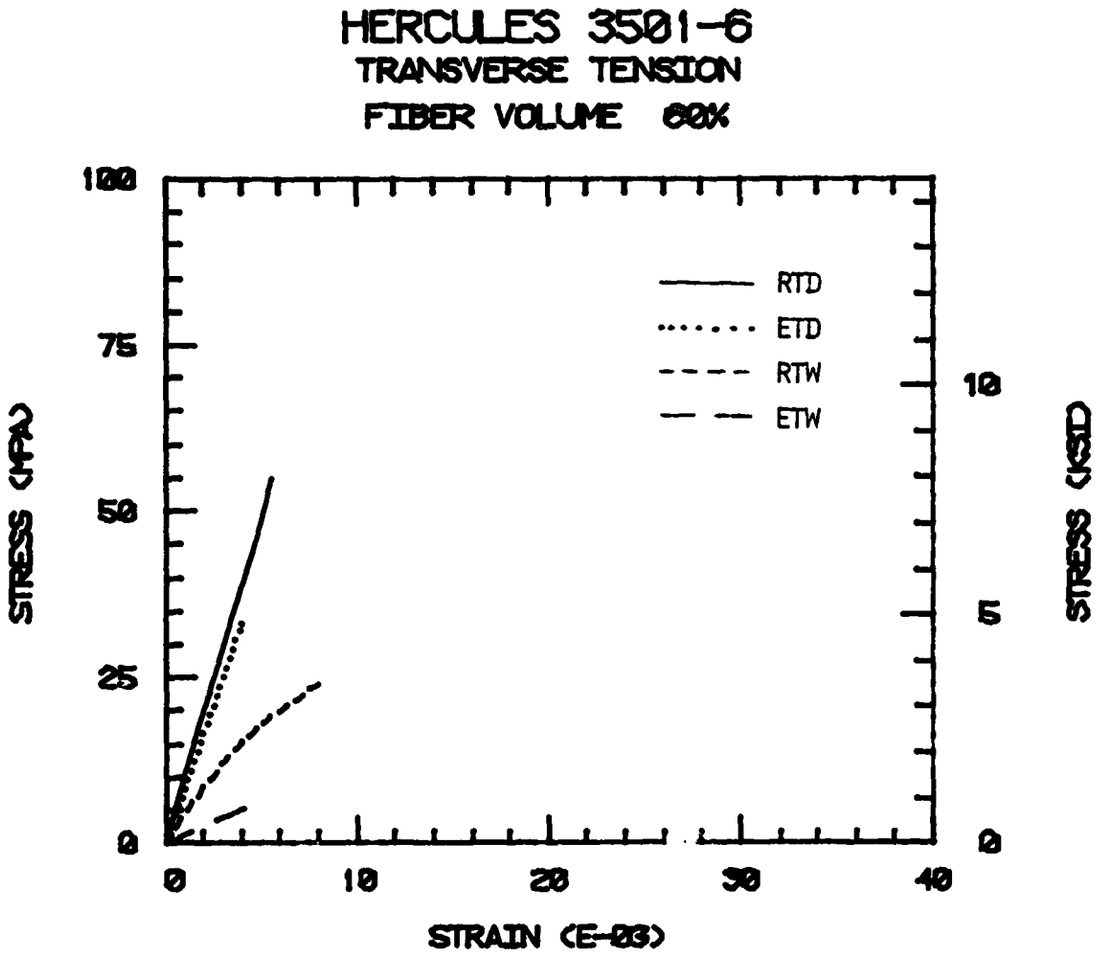

Figure 51. AS4/3501-6 Graphite/Epoxy Unidirectional Composite, Transverse Tensile Stress-Strain Response.

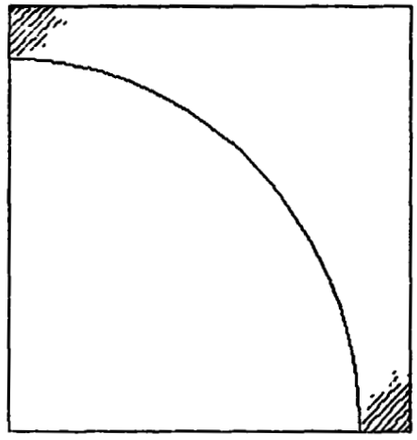

a) No Mechanical Loading

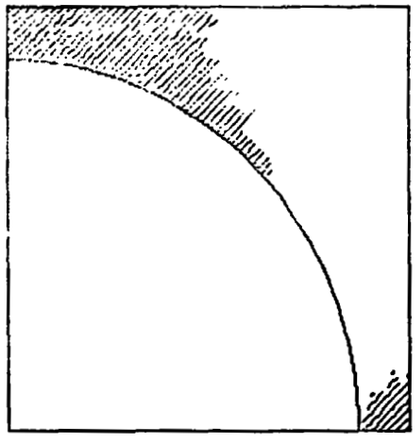

b) $\bar{\sigma}_x$ = 4. ı (6.0 ksi)

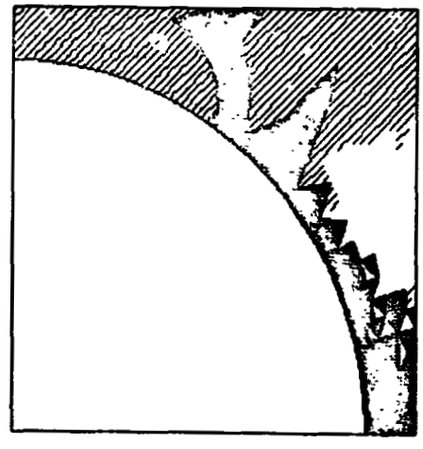

c) $\bar{\sigma}_x$ = 61 MPa (8.9 ksi)

Figure 52. AS4/3501-6 Graphite/Epoxy Unidirectional Composite, Room Temperature, Dry (RTD), Transverse Tensile Loading: $\bar{\sigma}_x^{ult}$ = 61 MPa (8.9 ksi).

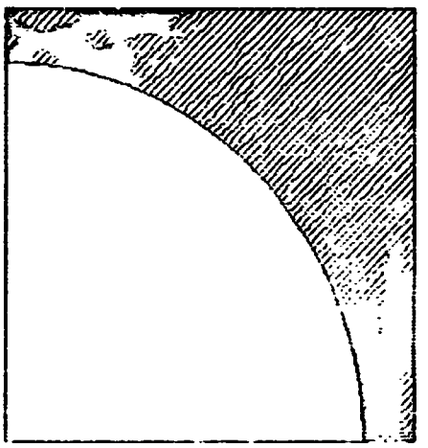

a) No Mechanical Loading

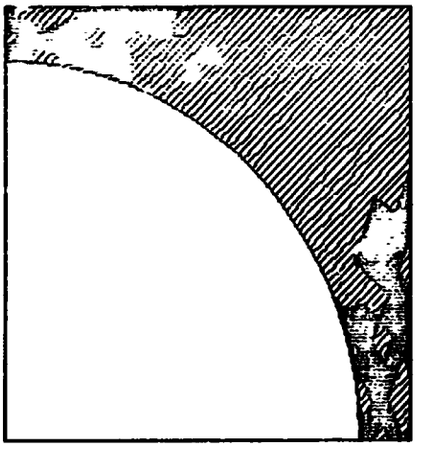

b) $\bar{\sigma}_x$ = 13 MPa (1.8 ksi)

c) $\bar{\sigma}_x$ = 31 MPa (4.4 ksi)

Figure 53. AS4/3501-6 Graphite/Epoxy Unidirectional Composite, Room Temperature, 6.0% M (RTW), Transverse Tensile Loading: $\bar{\sigma}_x^{ult}$ = 31 MPa (4.4 ksi).

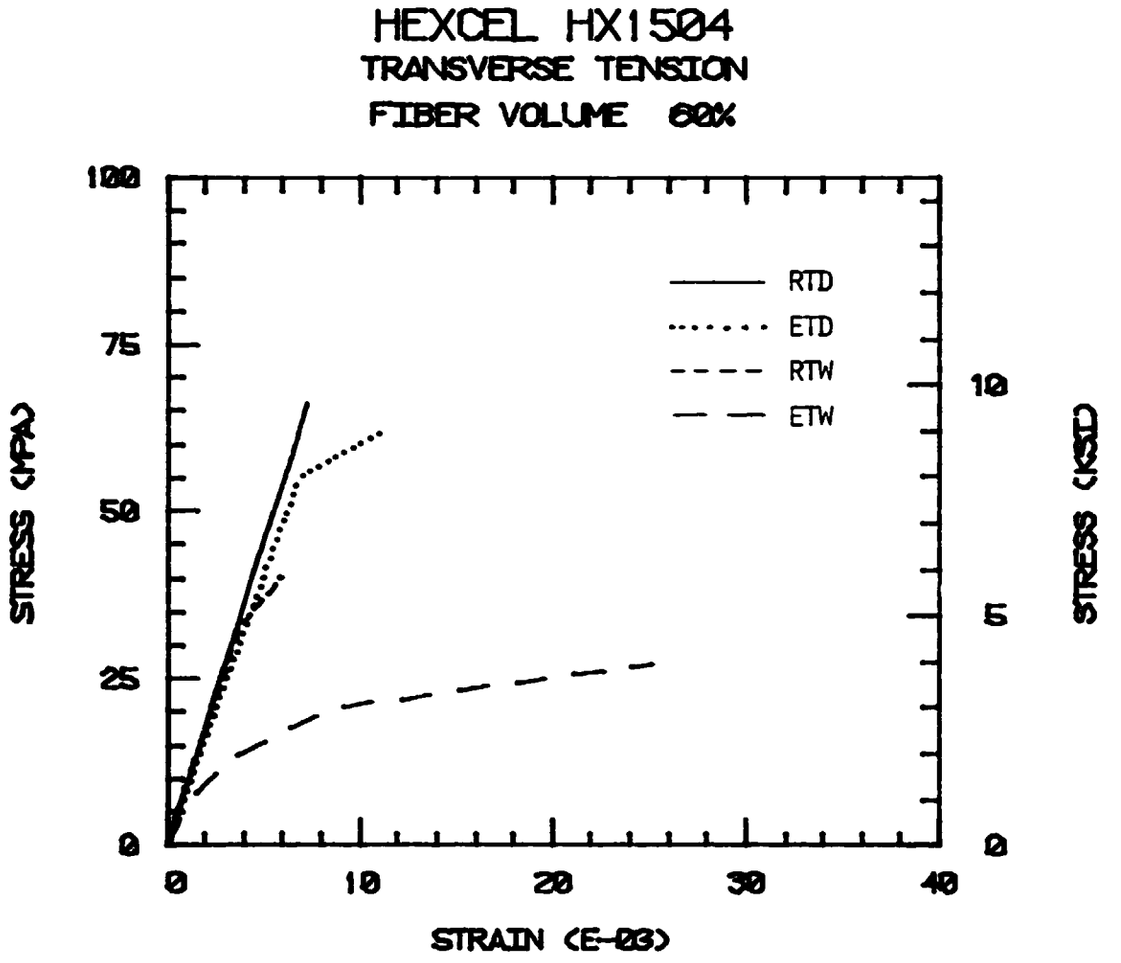

Figure 54. AS4/HX-1504 Graphite/Epoxy Unidirectional Composite, Transverse Tensile Stress-Strain Response.

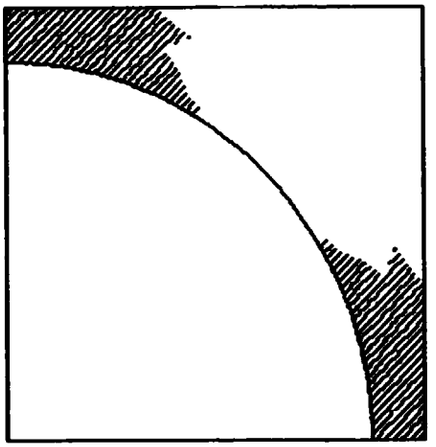

a) No Mechanical Loading

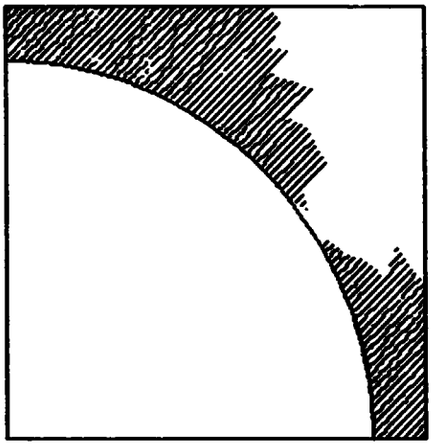

b) $\bar{\sigma}_x$ = 41 MPa (6.0 ksi)

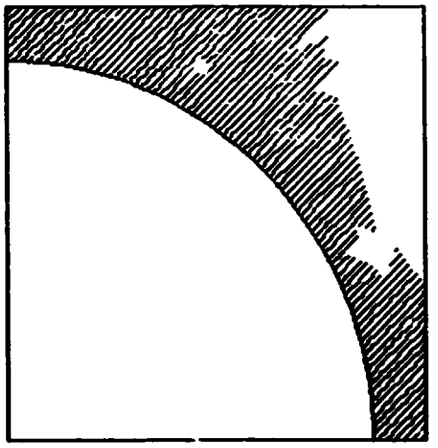

c) $\bar{\sigma}_x$ = 58 MPa (8.4 ksi)

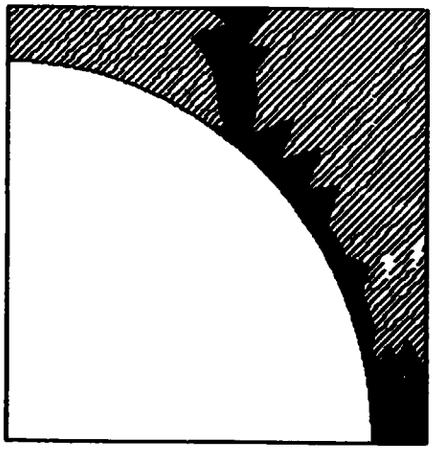

d) $\bar{\sigma}_x$ = 74 MPa (10.8 ksi)

Figure 55. AS4/HX-1504 Graphite/Epoxy Unidirectional Composite, Room Temperature, Dry (RTD), Transverse Tensile Loading: $\bar{\sigma}_x^{ult}$ = 74 MPa (10.8 ksi).

first cracking occurred at 55 MPa.

Yielding and crack patterns for the RTW condition of the AS4/HX-1504 composite are shown in Figure 56. As for the 2220 systems, the RTW crack pattern is predicted to be somewhat different than for the RTD condition, the fiber-matrix interface playing less of a role. Although not shown here, the ETW yield and crack patterns were also similar to those of the 2220 systems with full matrix yield prior to loading, and the first cracking occurring at less than 7 MPa.

5.4.1.7 AS4/5245-C Graphite/Epoxy

The predicted transverse tensile stress-strain curves for the AS4/5245-C unidirectional composite are presented in Figure 57. As can be seen, this matrix system performed well also, exhibiting good strengths at all environmental conditions.

Plots of yielding and crack patterns are shown in Figure 58 for the RTD condition. As can be seen, these are very similar to those for the HX-1504 matrix composite (Figure 55), the extent of yielding being slightly less. First cracking occurred at 58 MPa. The ETD results were similar, first cracking occurring at 55 MPa. Because of the lower moisture expansion and moisture weight gain of the 5245-C matrix relative to the HX-1504 system (see Table 4 of Section 1), its composite properties in the wet condition were better. Matrix yielding was retarded, and first cracking occurred at higher applied loading levels.

5.4.1.8 AS4/CYCOM 907 Graphite/Epoxy

The CYCOM 907 epoxy is a lower modulus, lower strength matrix material than the other systems at the elevated temperature, wet condition. This is reflected in the composite stress-strain curves shown in Figure 59, the RTD properties being quite attractive. The

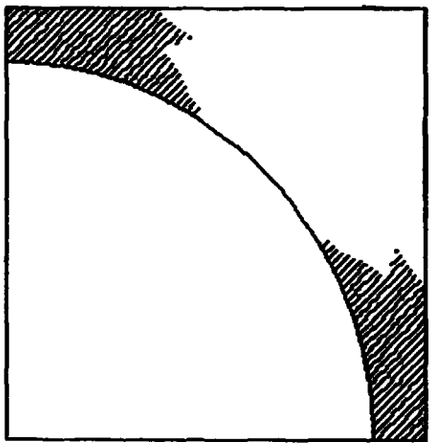

c) No Mechanical Loading

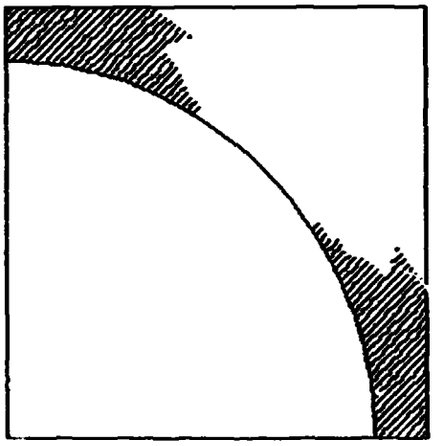

b) $\bar{\sigma}_x$ = 17 MPa (? · ksi)

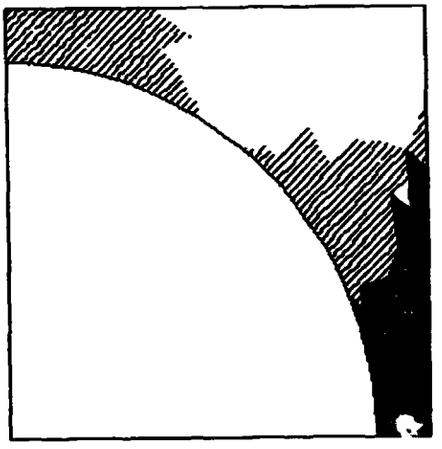

c) $\bar{\sigma}_x$ = 33 MPa (4.8 ksi)

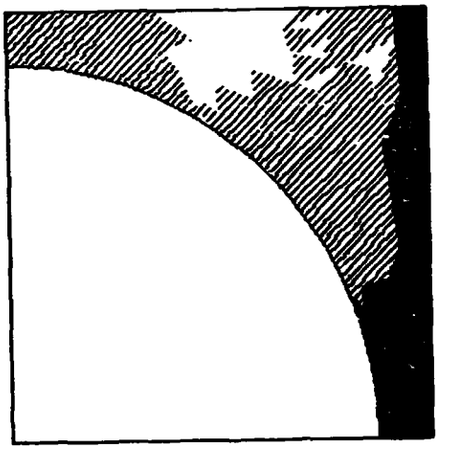

d) $\bar{\sigma}_x$ = 47 MPa (6.8 ksi)

Figure 56. AS4/HX-1504 Graphite/Epoxy Unidirectional Composite, Room Temperature, 3.8% M (RTW), Transverse Tensile Loading: $\bar{\sigma}_x^{ult}$ = 47 MPa (6.8 ksi).

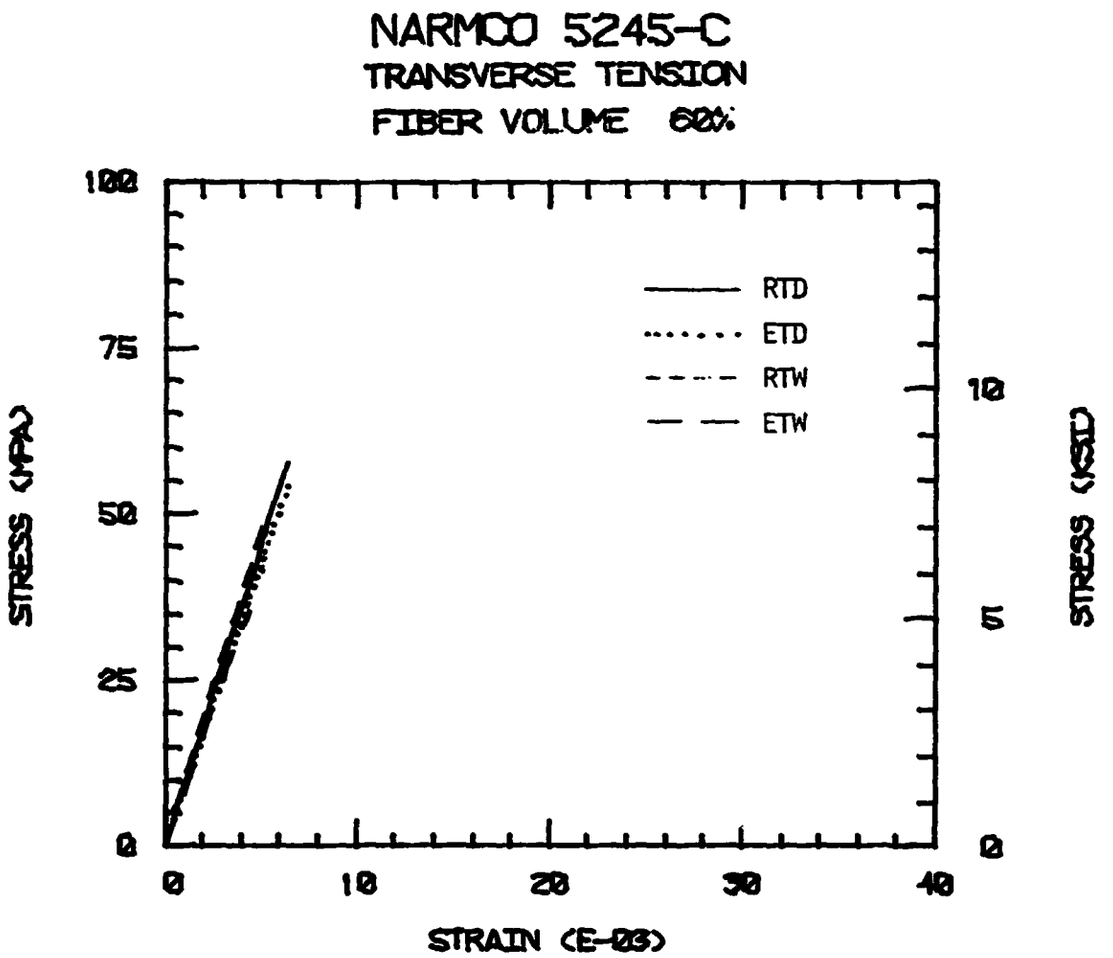

Figure 57. AS4/5245-C Graphite/Epoxy Unidirectional Composite, Transverse Tensile Stress-Strain Response.

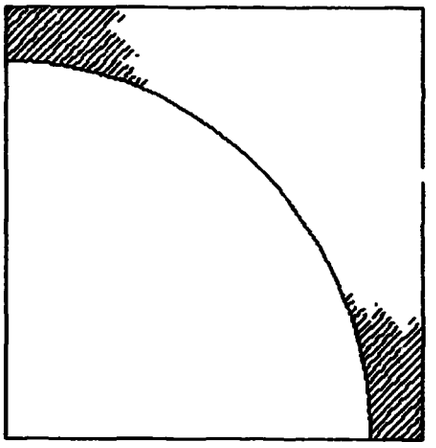

a) No Mechanical Loading

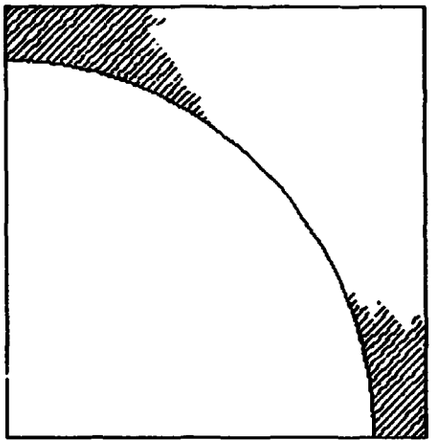

b) $\bar{\sigma}_x$ = 25 MPa (3.6 ksi)

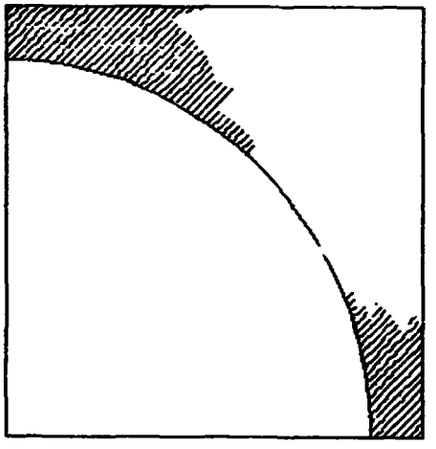

c) $\bar{\sigma}_x$ = 41 MPa (6.0 ksi)

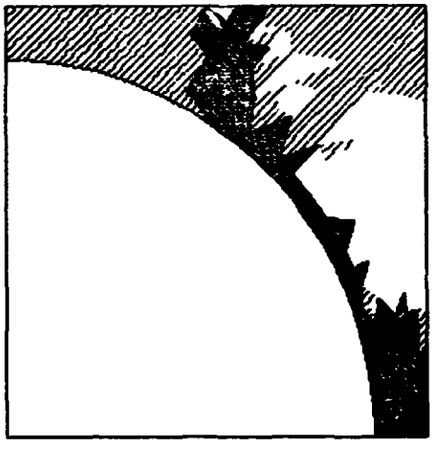

d) $\bar{\sigma}_x$ = 66 MPa (9.6 ksi)

Figure 58. AS4/5245-C Graphite/Epoxy Unidirectional Composite, Room Temperature, Dry (RTD), Transverse Tensile Loading: $\bar{\sigma}_x^{ult}$ = 66 MPa (9.6 ksi).

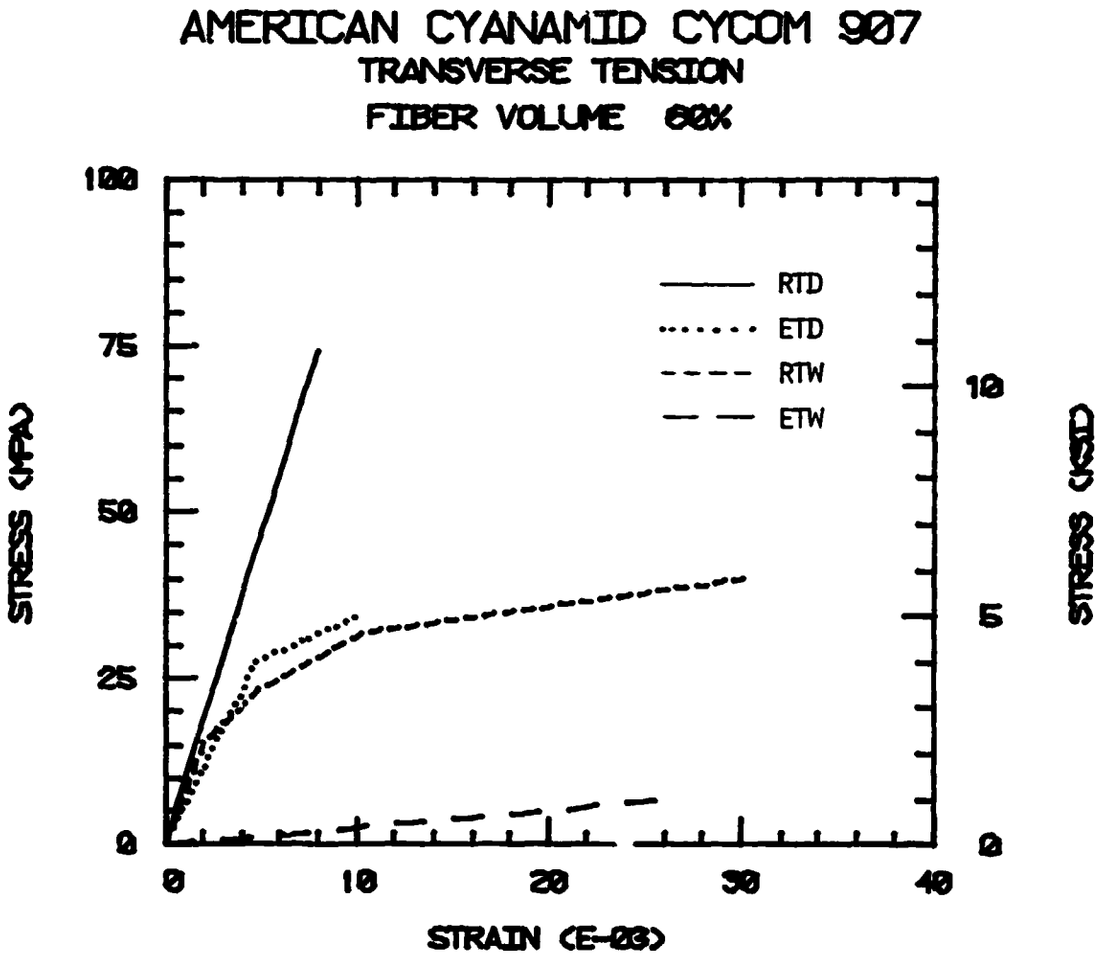

Figure 59. AS4/907 Graphite/Epoxy Unidirectional Composite, Transverse Tensile Stress-Strain Response.

corresponding RTD yield and crack propagation patterns are shown in Figure 60. Although the matrix was fully yielded at cooldown from the cure temperature (Figure 60a), first cracking of the matrix did not occur until 74 MPa, i.e., at about 90 percent of the ultimate strength. Although the crack pattern was similar, first cracking at the ETD condition occurred at only 28 MPa, and the ultimate strength was only half as high (see Table 24).

With the addition of moisture, first cracking occurred much earlier in the transverse tensile loading process, at 16 MPa and 7 MPa for the RTW and ETW conditions, respectively.

5.4.1.9 AS4/ERX-4901A(MDA) Graphite/Epoxy

The composite stress-strain curves are shown in Figure 61. While the RTD strength is high, the ETD strength is not, reflecting the temperature sensitivity of this matrix material. Also, the RTW strength is reasonable, but the ETW strength is very low (Table 16), the corresponding curve not even being shown in Figure 61. The crack patterns were similar to those for the AS4/CYCOM 907 composite.

5.4.2 Longitudinal Shear Loading

Longitudinal shear strengths of unidirectional composites are typically somewhat higher than transverse tensile strengths, as determined experimentally, and this was supported by the micromechanics predictions being presented here (see Table 24). As will be seen in the following figures, yielding of the matrix occurs more readily and the crack propagation patterns are less distinct. That is, the cracking is predicted to be more extensive, and more distributed throughout the matrix. Both of these factors contribute to the predicted nonlinear shear stress-strain response of the composite when subjected to

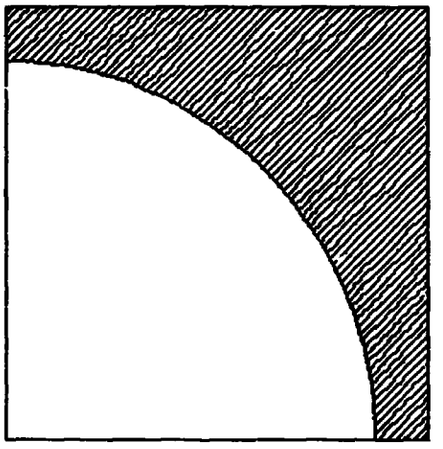

a) No Mechanical Loading

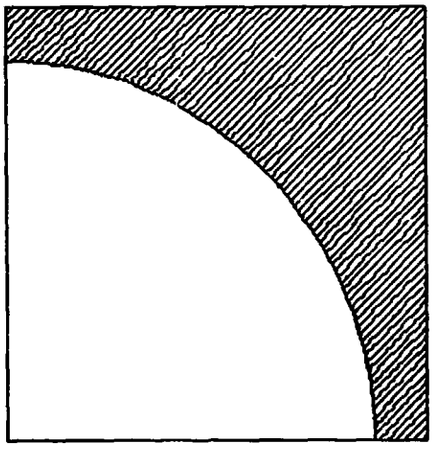

b) $\bar{\sigma}_x$ = 58 MPa (8.4 ksi)

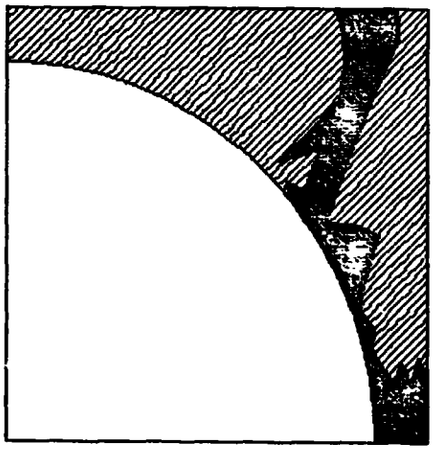

c) $\bar{\sigma}_x$ = 82 MPa (12.0 ksi)

Figure 60. AS4/907 Graphite/Epoxy Unidirectional Composite, Room Temperature, Dry (RTD), Transverse Tensile Loading: $\bar{\sigma}_x^{ult}$ = 82 MPa (12.0 ksi).

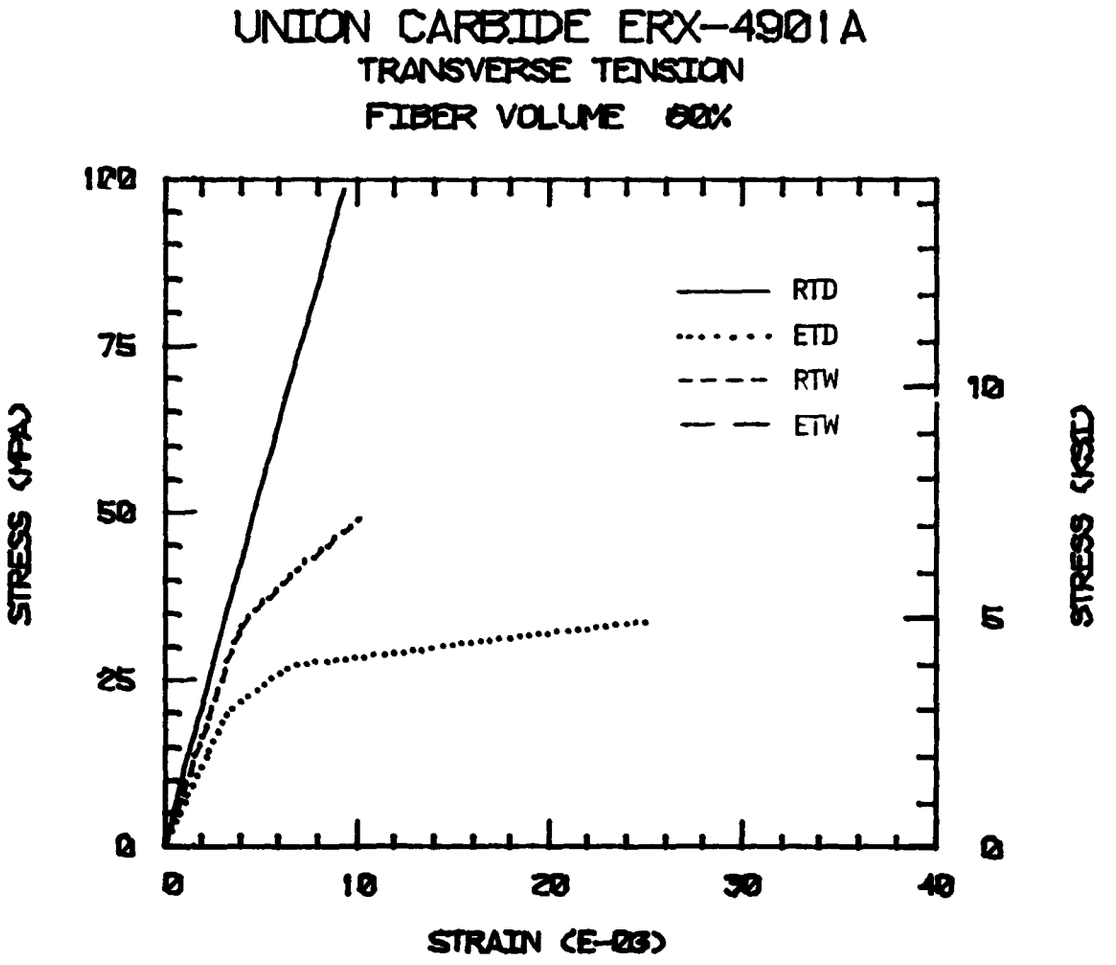

Figure 61. AS4/ERX-4901A(MDA) Graphite/Epoxy Unidirectional Composite, Transverse Tensile Stress-Strain Response.

longitudinal shear loading.

5.4.2.1 AS4/3502 Graphite/Epoxy

The composite longitudinal shear stress-strain curves are shown in Figure 62. This and all of the remaining shear stress-strain curves are plotted to the same scales, for ease of comparisons. The stress scale is also the same as for the transverse normal stress-strain plots of the previous Section 5.4.1. However, the shear strain axis has been expanded from 0.040 full scale to 0.100 full scale i.e., increased by a factor of 2.5, to accommodate the higher predicted shear strain to failure values.

The typical contrast in response due to shear loading (Figure 62) and transverse tensile loading (Figure 36) is obvious, particularly when keeping in mind the differences in the strain scales.

Matrix yield and crack propagation patterns for the AS4/3502 composite subjected to longitudinal shear loading, for all four environmental conditions, are shown in Figures 63 through 66. Comparing, for example, Figure 63 and Figure 37, the RTD condition for shear loading and transverse tensile loading, respectively, demonstrates the more extensive yielding and less well-defined crack patterns typical of the shear loading.

The influence of the failure criterion assumed is particularly evident when comparing Figure 65a to Figure 39a. Both represent no mechanical loading cases for the RTW condition. That is, the composite has not yet been loaded, and hence the condition should be the same in both plots. Yet extensive matrix cracking is indicated in Figure 39a, while no cracking has occurred in Figure 65a. For the transverse tensile loading, a maximum normal stress failure criterion was assumed, which

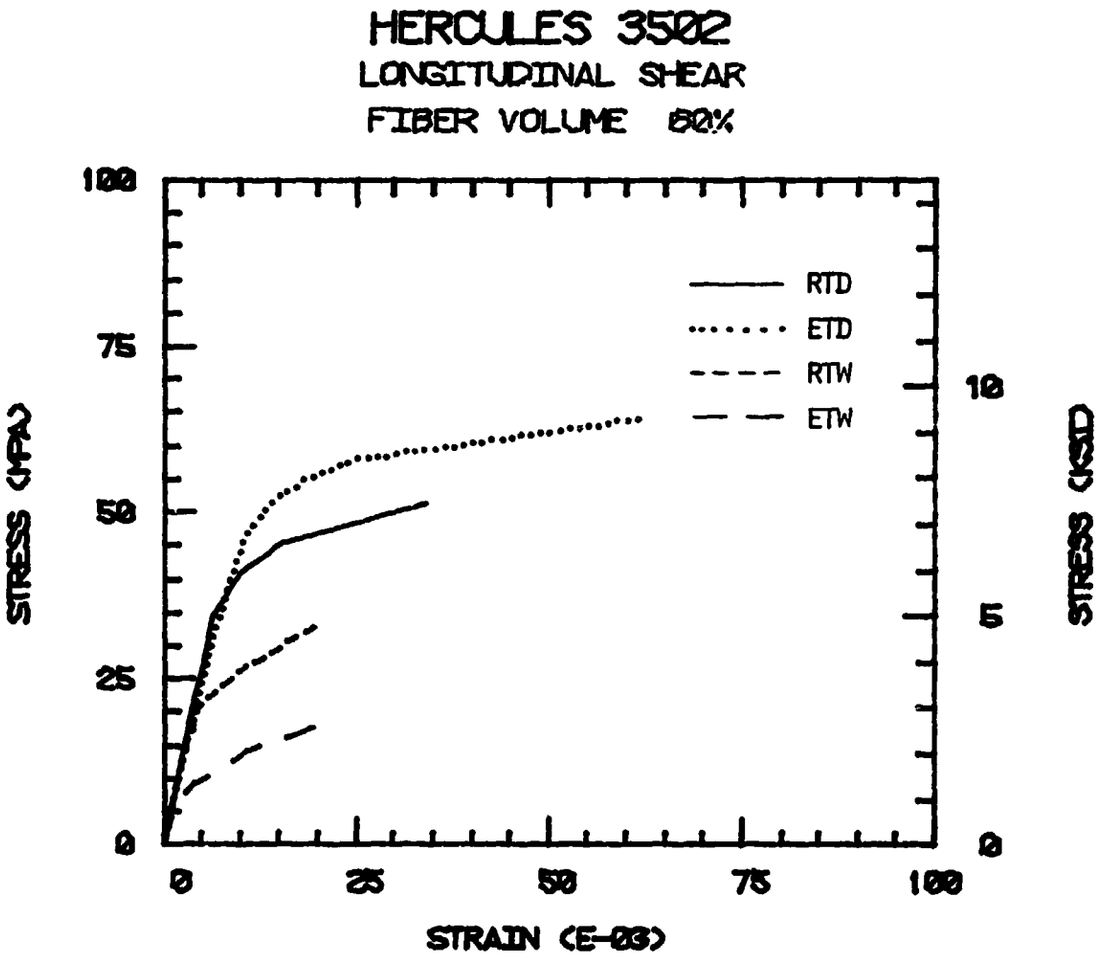

Figure 62. AS4/3502 Graphite/Epoxy Unidirectional Composite, Longitudinal Shear Stress-Strain Response.

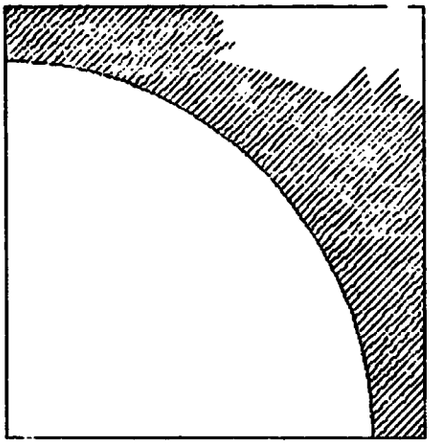

d) $\bar{\tau}_{xz}$ = 27 MPa (4.0 ksi)

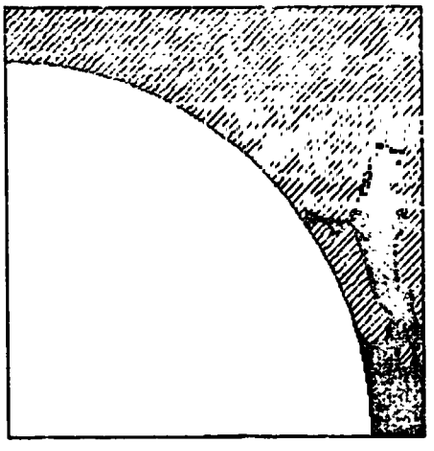

e) τ_{xz} = 41 MPa (5.9 ksi)

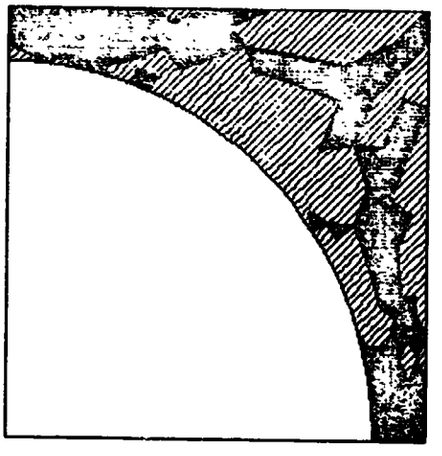

f) $\bar{\tau}_{xz}$ = 52 MPa (7.5 ksi)

Figure 63. AS4/3502 Graphite/Epoxy Unidirectional Composite, Room Temperature, Dry (RTD), Longitudinal Shear Loading: $\bar{\tau}_{xz}^{ult}$ = 58 MPa (8.3 ksi).

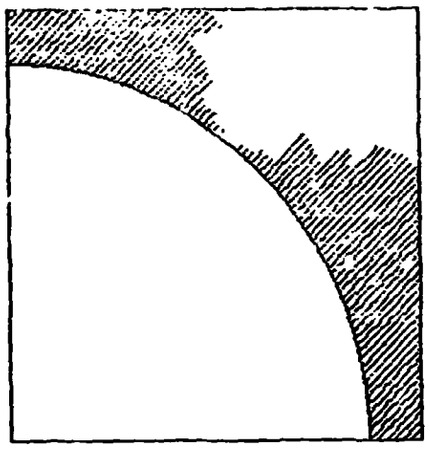

a) $\bar{\tau}_{xz}$ = 21 MPa (3.0 ksi)

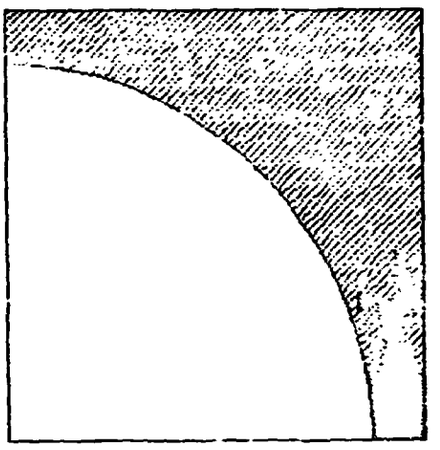

b) $\bar{\tau}_{xz}$ = 46 MPa (6.7 ksi)

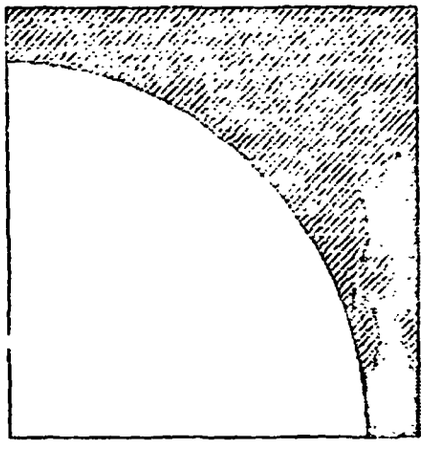

c) $\bar{\tau}_{xz}$ = 52 MPa (7.5 ksi)

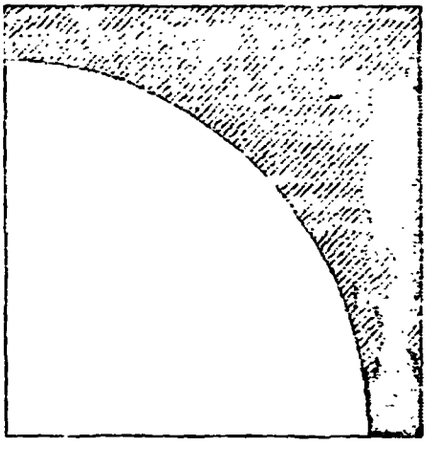

d) $\bar{\tau}_{xz}$ = 58 MPa (8.4 ksi)

Figure 64. AS4/3502 Graphite/Epoxy Unidirectional Composite, 100°C, Dry (ETD), Longitudinal Shear Loading: $\bar{\tau}_{xz}^{ult}$ = 71 MPa (0.3 ksi).

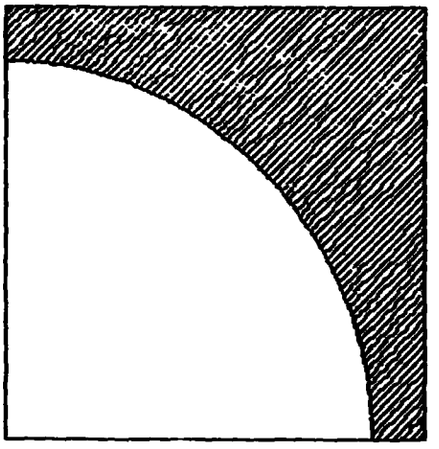

a) No Mechanical Loading

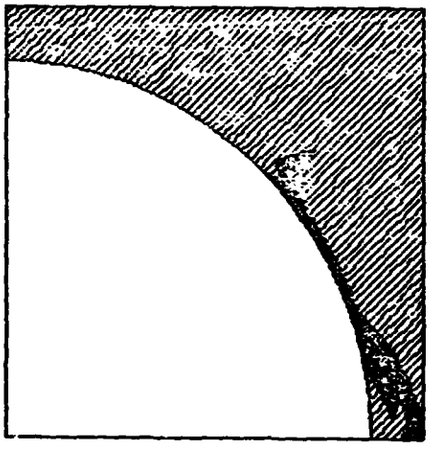

b) $\bar{\tau}_{xz}$ = 26 MPa (3.8 ksi)

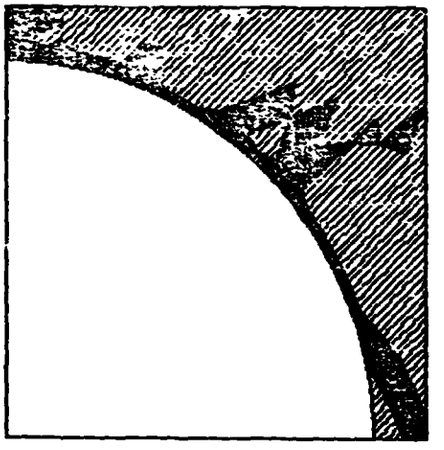

c) $\bar{\tau}_{xz}$ = 34 MPa (4.9 ksi)

Figure 65. AS4/3502 Graphite/Epoxy Unidirectional Composite, Room Temperature, 5.0% M (RTW), Longitudinal Shear Loading: $\bar{\tau}_{xz}^{ult}$ = 34 MPa (4.9 ksi).

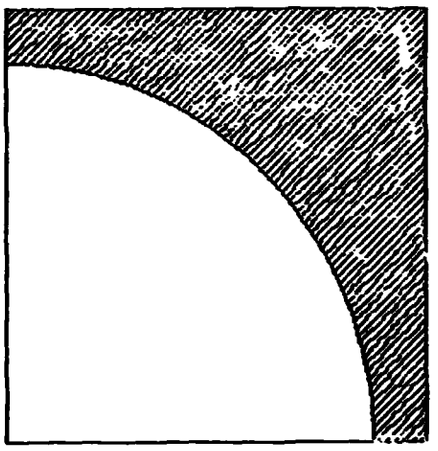

a) No Mechanical Loading

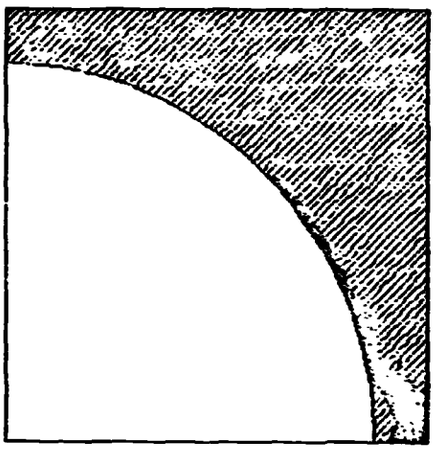

b) $\bar{\tau}_{xz}$ = 7 MPa (1.0 ksi)

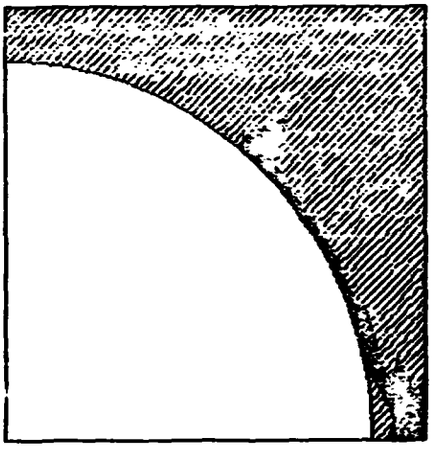

c) $\bar{\tau}_{xz}$ = 14 MPa (2.1 ksi)

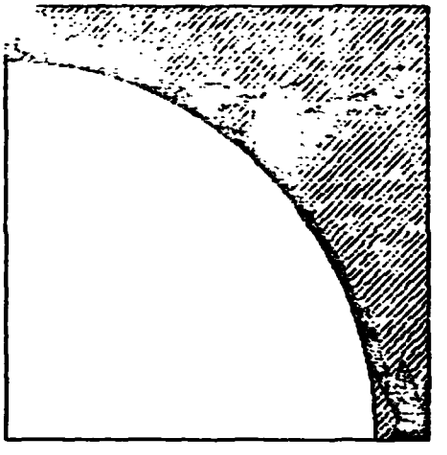

d) $\bar{\tau}_{xz}$ = 19 MPa (2.7 ksi)

Figure 66. AS4/3502 Graphite/Epoxy Unidirectional Composite, 100°C, 5.0%M (ETW), Longitudinal Shear Loading: $\bar{\tau}_{xz}^{ult}$ = 19 MPa (2.7 ksi).

for longitudinal shear loading an octahedral shear failure criterion was assumed, as previously discussed. The former is obviously a more severe criterion in this particular case. The same effect can be seen for the ETW condition, by comparing Figure 66a to Figure 40a.

This influence of assumed failure criterion can be noted for the other matrix systems also, as the following results will demonstrate.

5.4.2.2 AS4/914 Graphite/Epoxy

The composite shear stress-strain curves are presented in Figure 67. The RTD shear strength is about as high and for any of the other composites (see Table 16), but the shear strength drops rapidly with increasing temperature and moisture.

Matrix yielding and crack propagation patterns for the RTD condition are shown in Figure 68. The ETD results were similar. The RTW results shown in Figure 69 are very similar to those for the Hercules 3502 matrix (Figure 65). However, as shown in Figure 70, extensive fiber-matrix interface debonding was predicted at the ETW condition prior mechanical loading; this was not predicted for the AS4/3502 composite (Figure 66a). But matrix failure was obviously imminent. Extensive fiber-matrix debonding occurred at only 7 MPa, and extended rapidly with increasing shear loading (Figure 66). Thus, the ultimate shear strength of the AS4/3502 composite was not significantly higher than that of the AS4/914 composite, viz, 19 MPa versus 13 MPa.

5.4.2.3 AS4/2220-1 Graphite/Epoxy

The composite shear stress-strain curves are shown in Figure 71. This matrix system obviously retains its shear properties better than the two previous systems as a function of temperature and moisture. Matrix yield and crack propagation patterns for three of the four

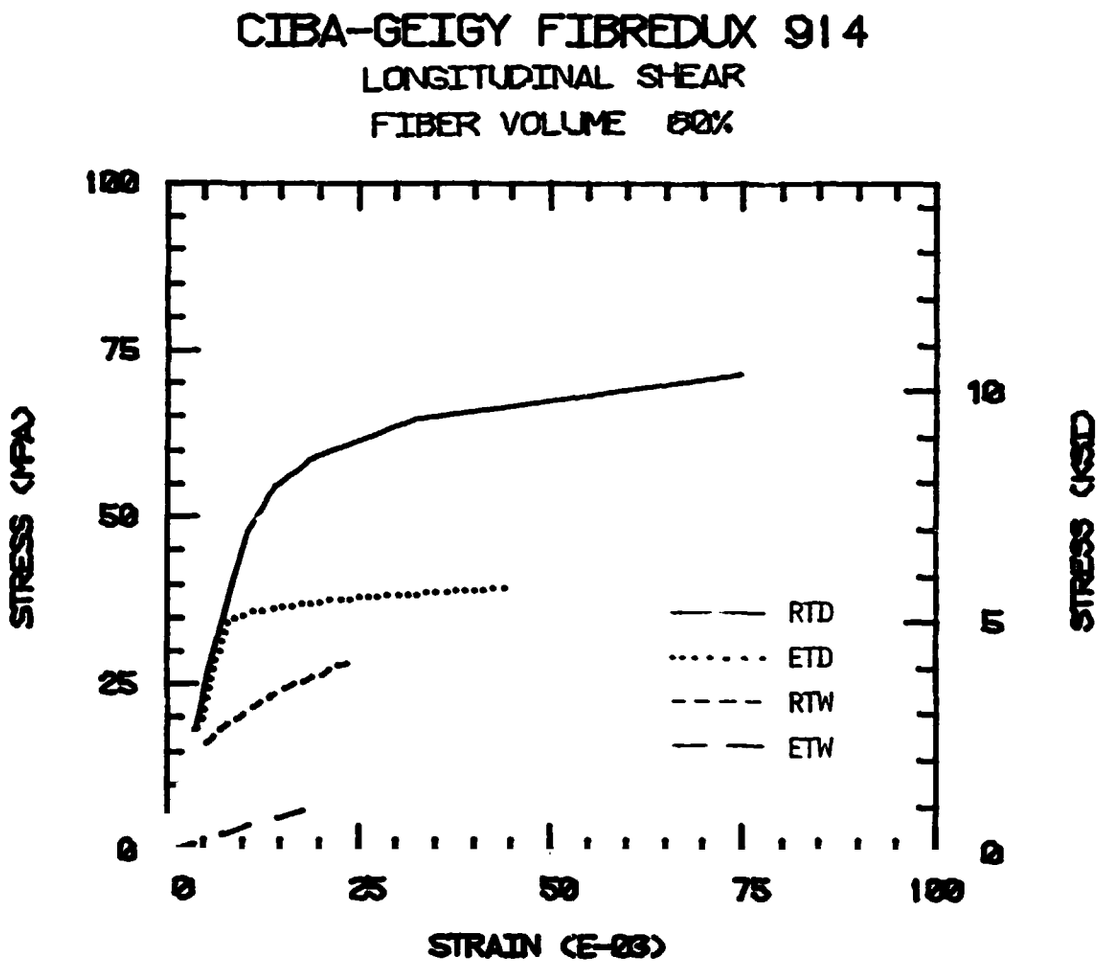

Figure 67. AS4/914 Graphite/Epoxy Unidirectional Composite, Longitudinal Shear Stress-Strain Response.

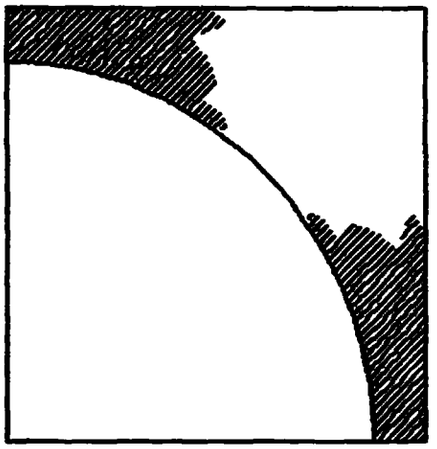

a) No Mechanical Loading

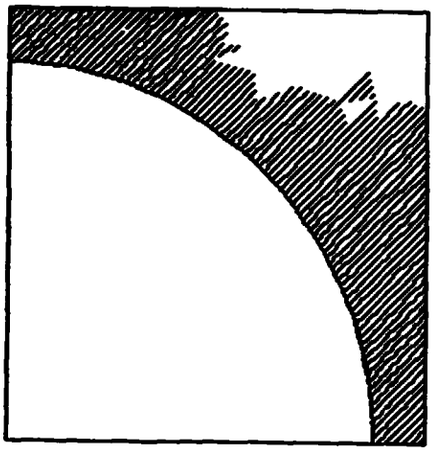

b) $\bar{\tau}_{xz}$ = 17 MPa (4 ksi)

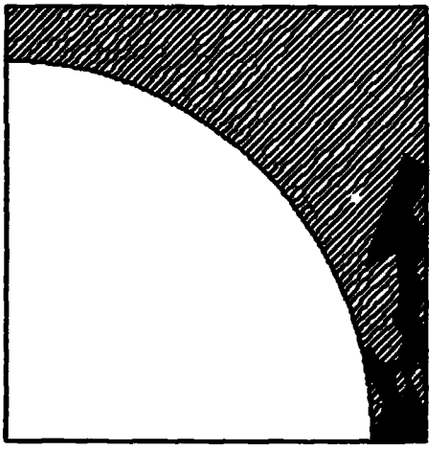

c) $\bar{\tau}_{xz}$ = 55 MPa (7.9 ksi)

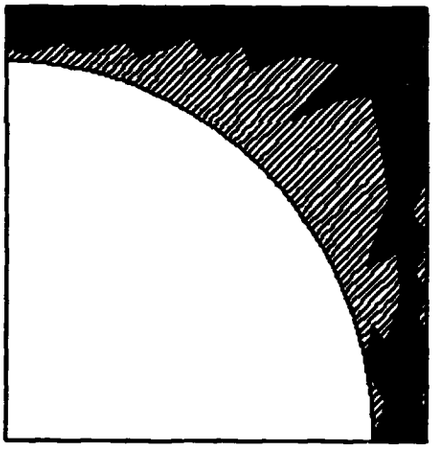

d) $\bar{\tau}_{xz}$ = 77 MPa (11.2 ksi)

Figure 68. AS4/914 Graphite/Epoxy Unidirectional Composite, Room Temperature, Dry (RTD), Longitudinal Shear Loading: $\bar{\tau}_{xz}^{ult}$ = 77 MPa (11.2 ksi).

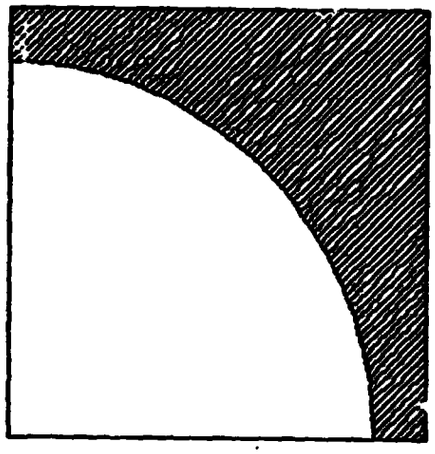

a) No Mechanical Loading

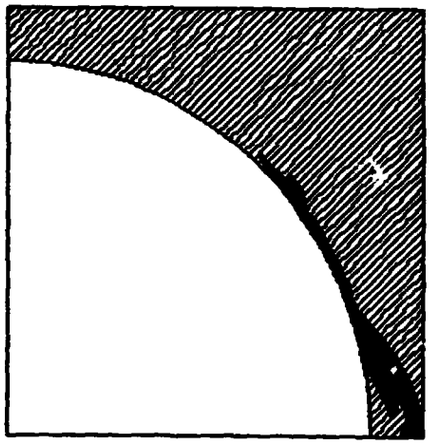

b) $\bar{\tau}_{xz}$ = 18 MPa (2.6 ksi)

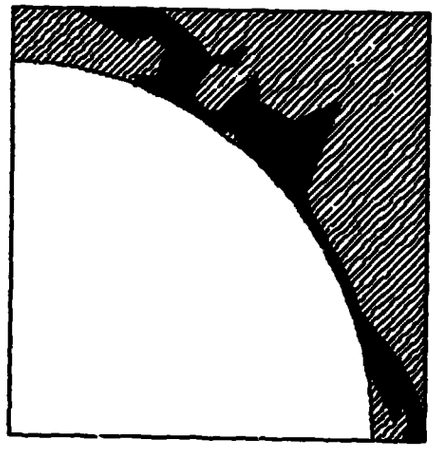

c) $\bar{\tau}_{xz}$ = 29 MPa (4.2 ksi)

Longitudinal Shear Loading: $\bar{\tau}_{xy}^{ult}$ = 30 MPa (4.4 ksi)

Figure 69. AS4/914 Graphite/Epoxy Unidirectional Composite, Room Temperature, 7.0%M (RTW).

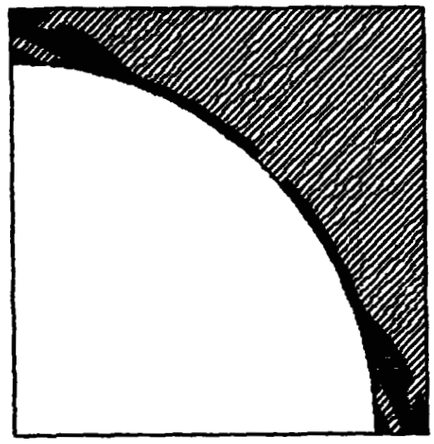

a) No Mechanical Loading

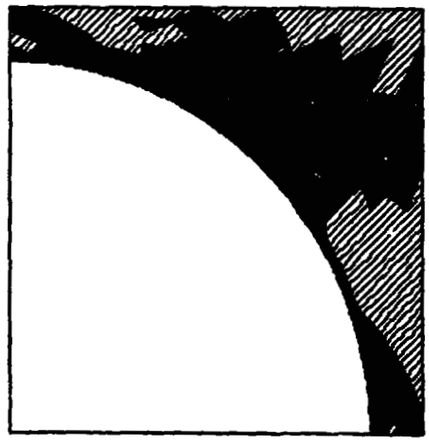

b) $\bar{\tau}_{xz}$ = 13 MPa (1.8 ksi)

Figure 70. AS4/914 Graphite/Epoxy Unidirectional Composite, 100°C, 7.0%M (ETW), Longitudinal Shear Loading: $\bar{\tau}_{xz}^{ult}$ = 13 MPa (1.8 ksi).

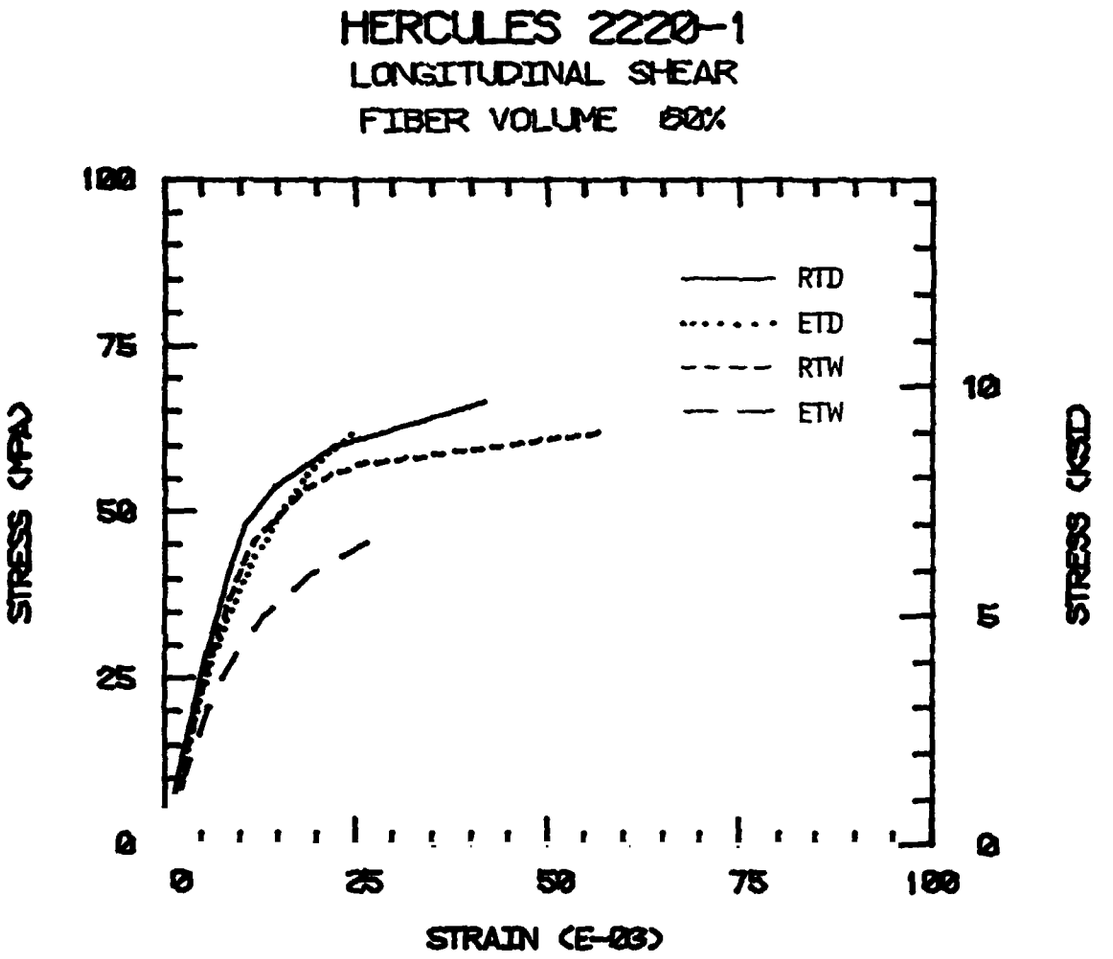

Figure 71. AS4/2220-1 Graphite/Epoxy Unidirectional Composite, Longitudinal Shear Stress-Strain Response.

environmental conditions are shown in Figures 72 through 74. The ETW crack pattern was similar to the RTD pattern (Figure 72). Although full matrix yielding existed prior to loading, no cracks initiated until a shear stress level of 41 MPa was reached. Full failure was predicted at 51 MPa (see Table 24). That is, first cracking did not occur until 80 percent of the ultimate load had been applied. For the RTD condition, first yielding occurred at 48 MPa, which was 65 percent of ultimate.

5.4.2.4 AS4/2220-3 Graphite/Epoxy

The shear stress-strain curves for the AS4/2220-3 composite shown in Figure 75 are similar to those for the AS4/2220-1 composite (Figure 71), as would be expected. The differences are due primarily to the differences in thermal expansion, moisture expansion, and moisture weight gain of the two resins, as indicated in Tables 1 and 4 of Section 1.

The yield and crack propagation patterns were also similar to those for the 2220-1 system. For the RTD condition, for example, the extent of yield to loading was slightly less, but the first cracking initiated sooner, at 41 MPa versus 48 MPa for the AS4/2220-1 composite. The ultimate shear strength was correspondingly lower, as indicated in Table 24. The responses at the three other environmental conditions were generally similar to the 2220-1 response also.

5.4.2.5 AS4/3501-6 Graphite/Epoxy

The shear stress-strain curves are presented in Figure 76. As can be seen, the RTD response is very good, but at the other environmental conditions, the composite does not perform as well as the 2220 systems. The RTD yielding prior to loading was less than for the 2220 systems. However, the general cracking patterns at all conditions were similar.

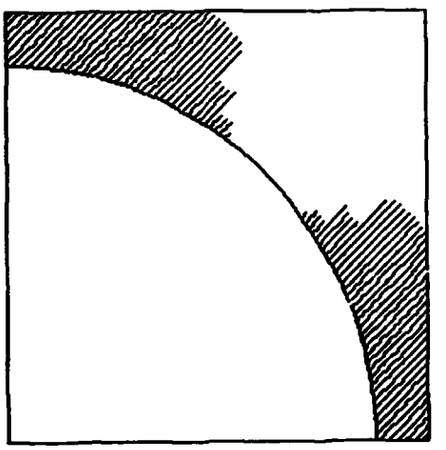

a) No Mechanical Loading

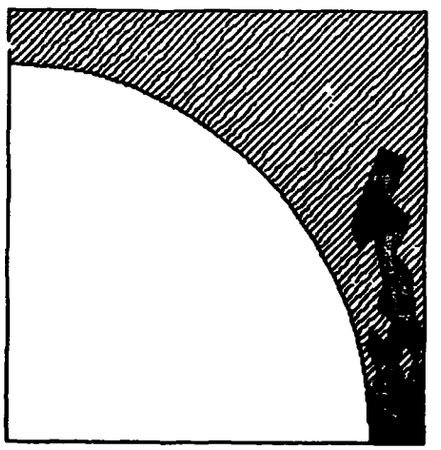

b) $\bar{\tau}_{xz}$ = 54 MPa (7.8 ksi)

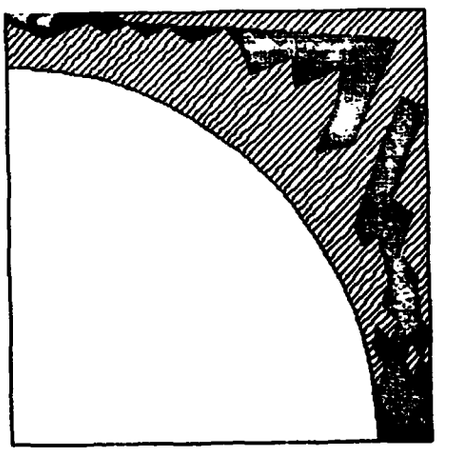

c) $\bar{\tau}_{xz}$ = 67 MPa (9.7 ksi)

Figure 72. AS4/2220-1 Graphite/Epoxy Unidirectional Composite, Room Temperature, Dry (RTD), Longitudinal Shear Loading: $\bar{\tau}^{ult}_{xz}$ = 74 MPa (10.7 ksi).

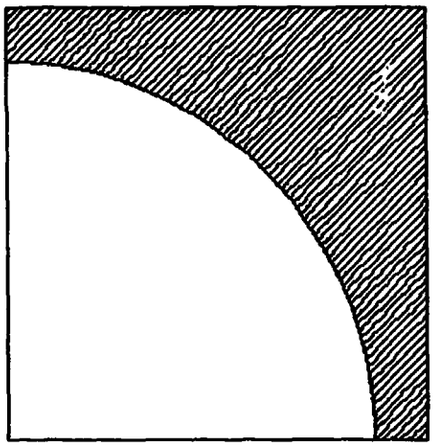

a) $\bar{\tau}_{xz}$ = 62 MPa (9.0 ksi)

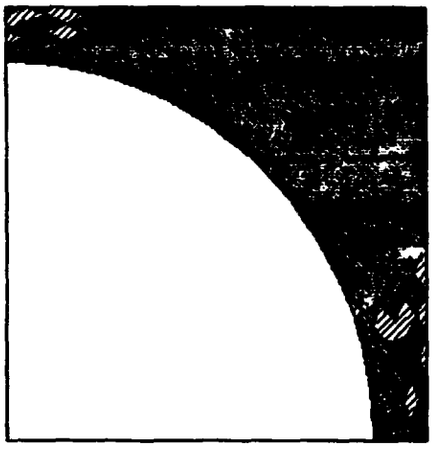

b) $\bar{\tau}_{xz}$ = 69 MPa (10.0 ksi)

Figure 73. AS4/2220-1 Graphite/Epoxy Unidirectional Composite, 100°C, Dry (ETD), Longitudinal Shear Loading: $\bar{\tau}_{xz}^{ult}$ = 69 MPa (10.0 ksi).

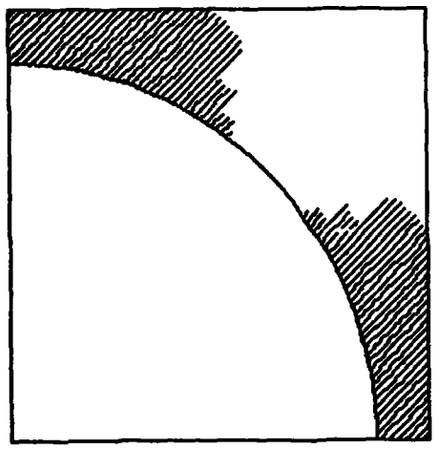

a) No Mechanical Loading

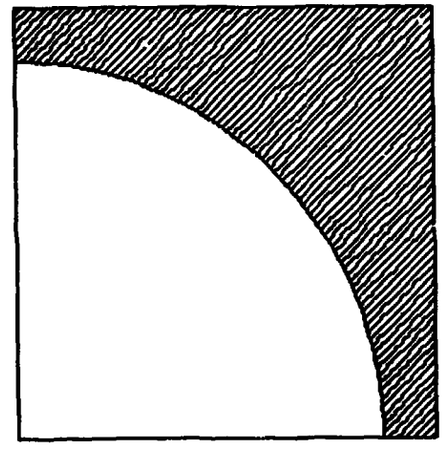

b) $\bar{\tau}_{xz}$ = 41 MPa (6.0 ksi)

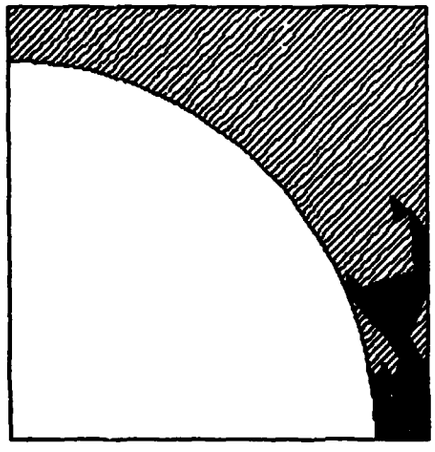

c) $\bar{\tau}_{xz}$ = 49 MPa (7.2 ksi)

d) $\bar{\tau}_{xz}$ = 62 MPa (9.0 ksi)

Figure 74. AS4/2220-1 Graphite/Epoxy Unidirectional Composite, Room Temperature, 3.8%M (RTW), Longitudinal Shear Loading: $\bar{\tau}_{xz}^{ult}$ = 69 MPa (10.0 ksi).

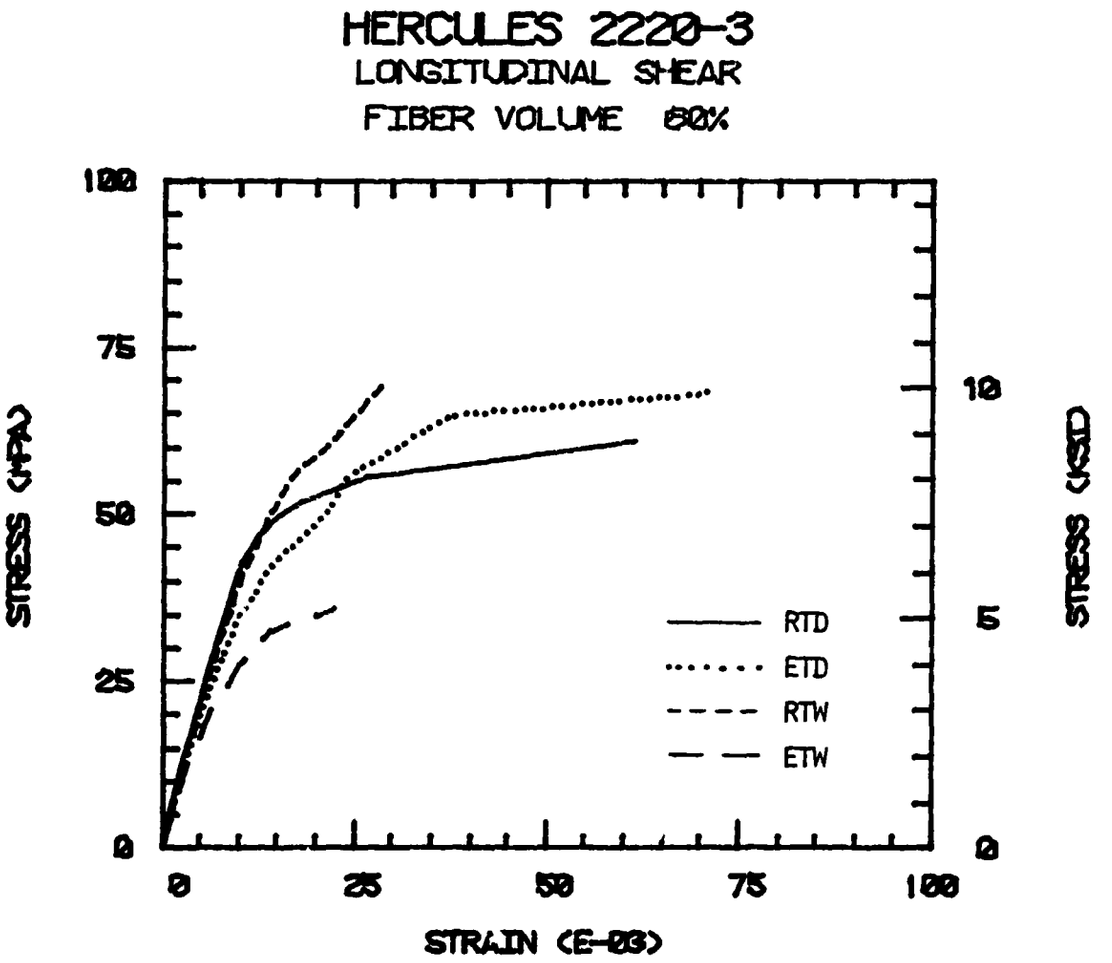

Figure 75. AS4/2220-3 Graphite/Epoxy Unidirectional Composite, Longitudinal Shear Stress-Strain Response.

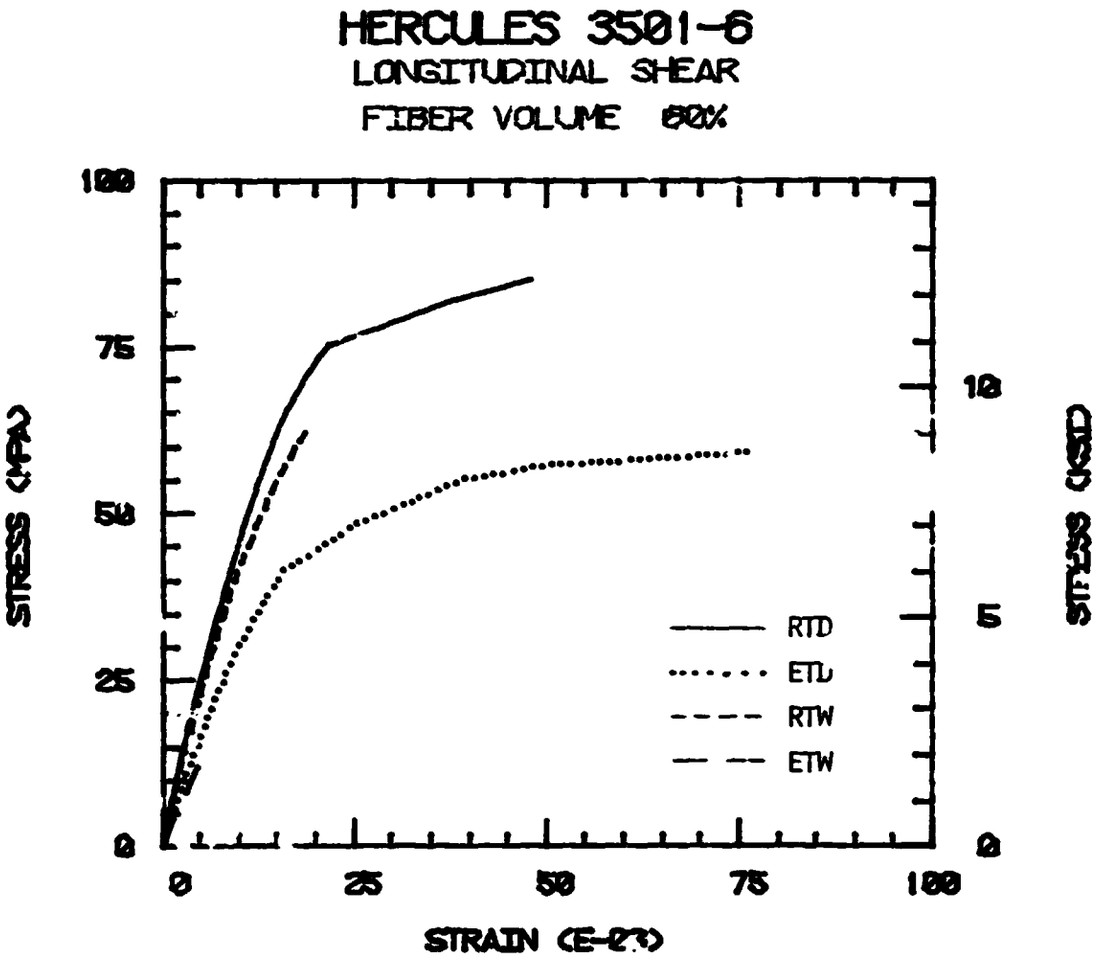

Figure 76. AS4/3501-6 Graphite/Epoxy Unidirectional Composite, Longitudinal Shear Stress-Strain Response.

5.4.2.6 AS4/HX-1504 Graphite/Epoxy

The shear stress-strain curves are shown in Figure 77. The RTD strength is not as high as for the 3501-6 matrix, but at the other conditions it is higher. The yield and crack patterns at all conditions were similar to those for the AS4/3501-6 composite. Specific results are shown in Figures 78 and 79 for the ETD and ETW conditions, respectively.

5.4.2.7 AS4/5245-C Graphite/Epoxy

The AS4/5245-C composite was predicted to perform almost as well in shear as the AS4/HX-1504 composite, as can be seen by comparing Figure 80 with Figure 77. The RTD crack patterns are shown in Figure 81. They were similar for the other three environmental conditions.

5.4.2.8 AS4/CYCOM 907 Graphite/Epoxy

The shear stress-strain curves for the AS4/CYCOM 907 composite are shown in Figure 82. As expected based upon the neat resin properties, this composite was strongly affected by moisture, particularly at levated temperatures.

5.4.2.9 AS4/ERX-4901A(MDA) Graphite/Epoxy

As would be expected, based upon the matrix properties, the RTD shear strength of this composite was much higher than that of any of the other systems. The shear stress-strain curves are shown in Figure 83. The very low ETW response is equally obvious.

The RTD yield and crack patterns for the AS4/ERX-4901A(MDA) composite are shown in Figure 84. As can be seen, cracking is not predicted to occur until a relatively high shear stress has been applied.

5.5 Discussion

The micromechanics predictions presented here are lacking somewhat

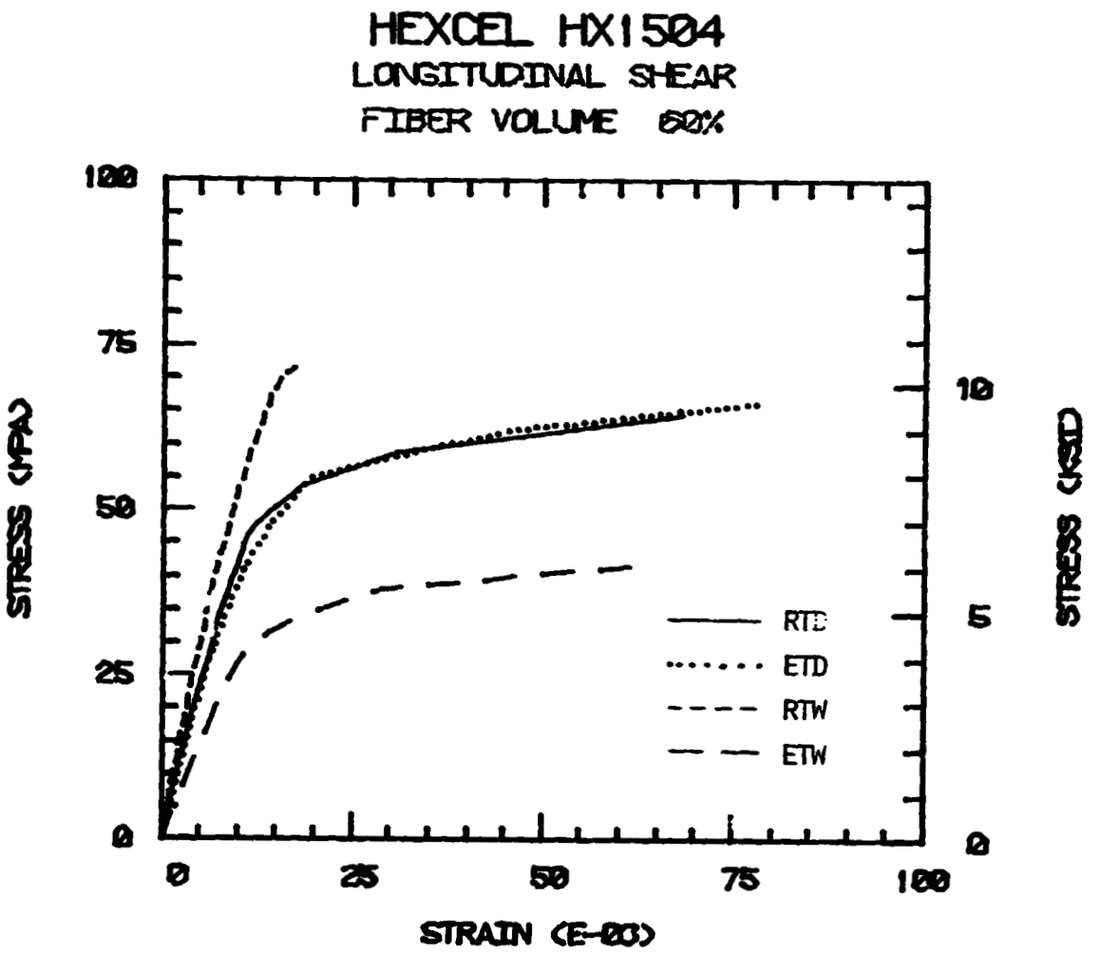

Figure 77. AS4/HX-1504 Graphite/Epoxy Unidirectional Composite, Longitudinal Shear Stress-Strain Response.

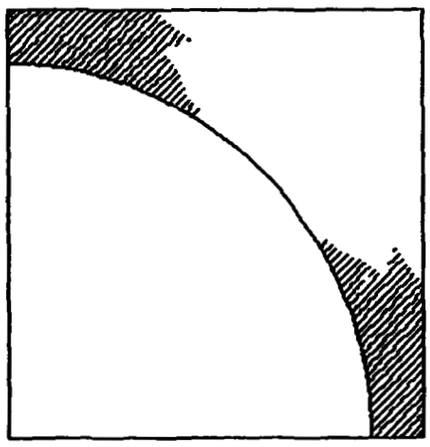

a) No Mechanical Loading

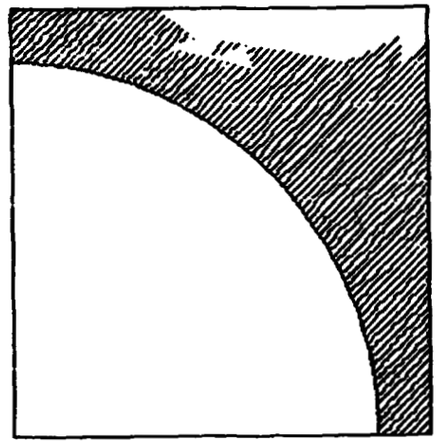

b) $\bar{\tau}_{xz}$ = 41 MPa (6.0 ksi)

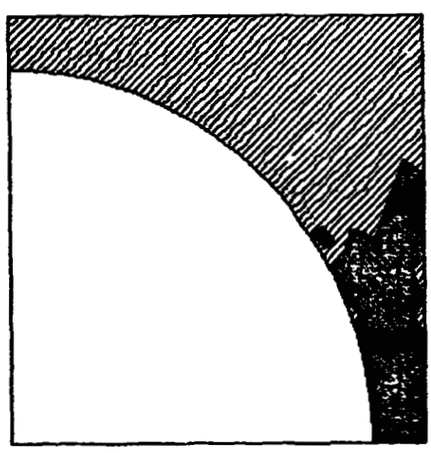

c) $\bar{\tau}_{xz}$ = 55 MPa (8.0 ksi)

d) $\bar{\tau}_{xz}$ = 66 MPa (9.6 ksi)

Figure 78. AS4/HX-1504 Graphite/Epoxy Unidirectional Composite, 100°C, Dry (ETD), Longitudinal Shear Loading: $\bar{\tau}_{xz}^{ult}$ = 72 MPa (10.5 ksi).

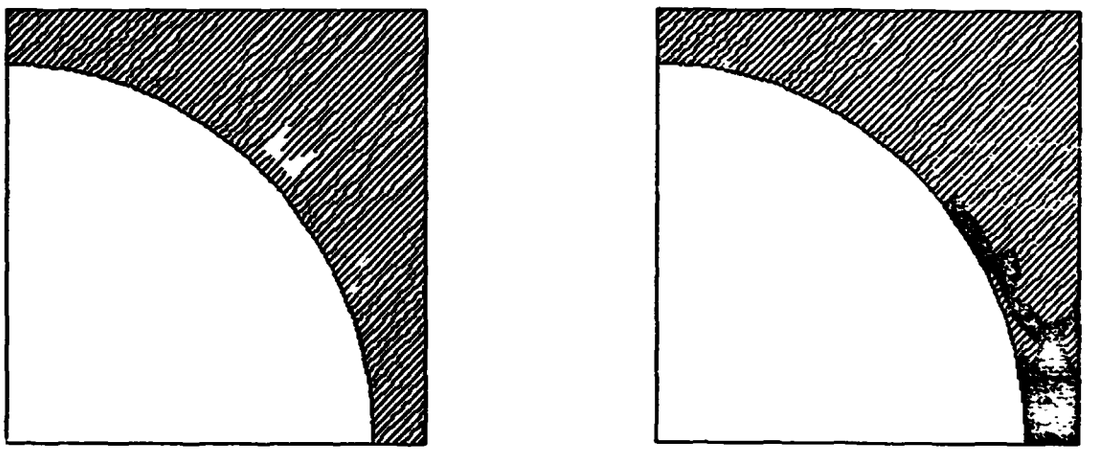

a) No Mechanical Loading

b) $\bar{\tau}_{xz}$ = 32 MPa (4.6 ksi)

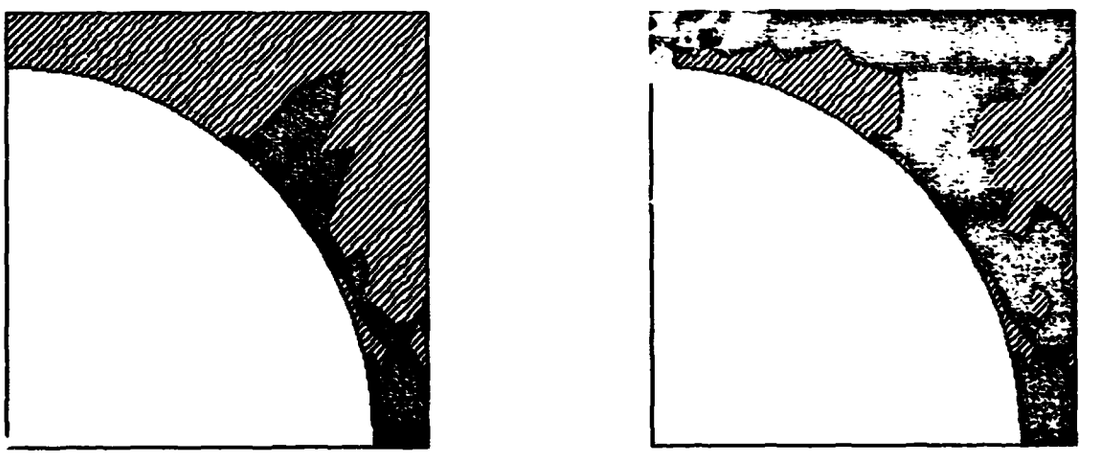

c) $\bar{\tau}_{xz}$ = 38 MPa (5.5 ksi)

d) $\bar{\tau}_{xz}$ = 46 MPa (6.7 ksi)

Figure 79. AS4/HX-1504 Graphite/Epoxy Unidirectional Composite, 100°C, 3.8%M (ETW), Longitudinal Shear Loading: $\bar{\tau}_{xz}^{ult}$ = 46 MPa (6.7 ksi).

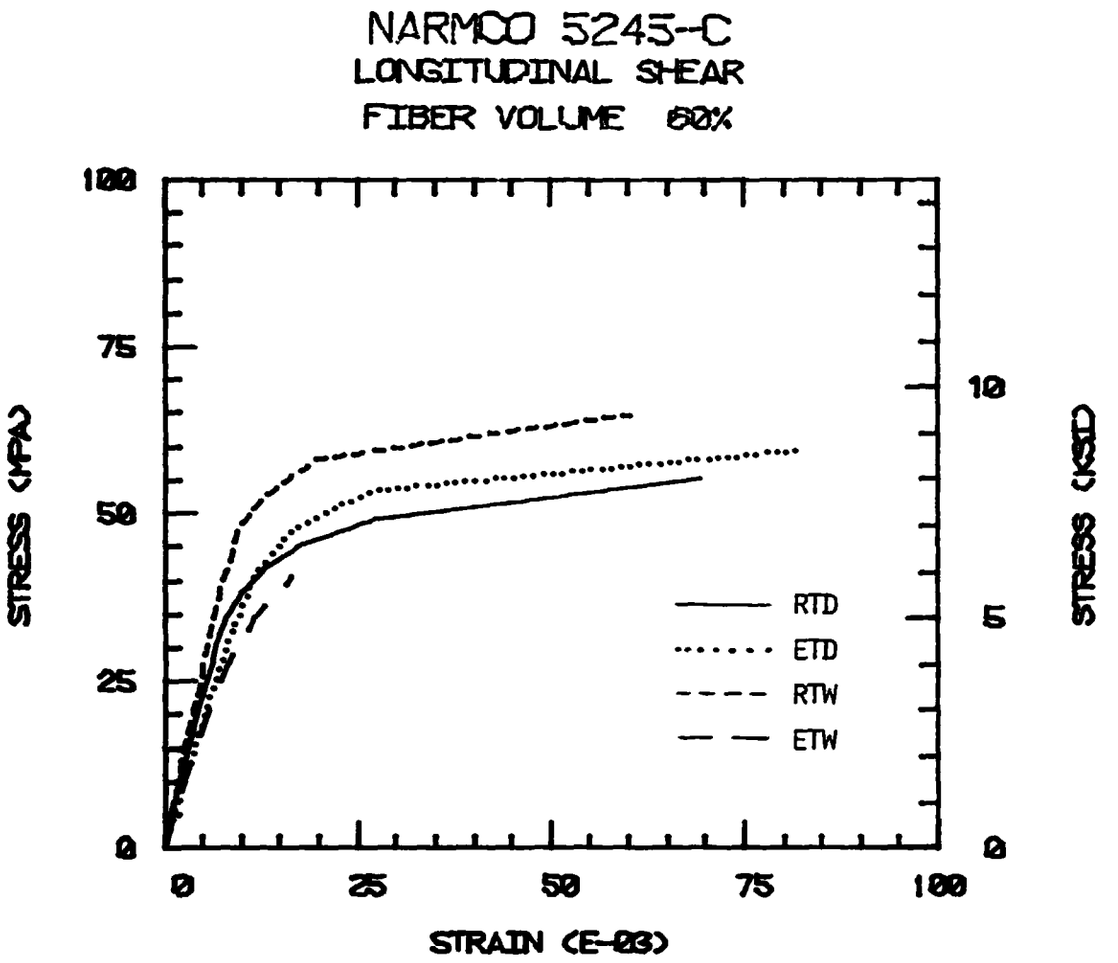

Figure 80. AS4/5245-C Graphite/Epoxy Unidirectional Composite, Longitudinal Shear Stress-Strain Response.

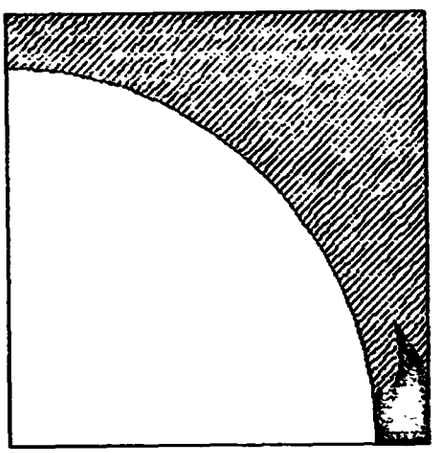

a) $\bar{\tau}_{xz}$ = 31 MPa (4.4 ksi)

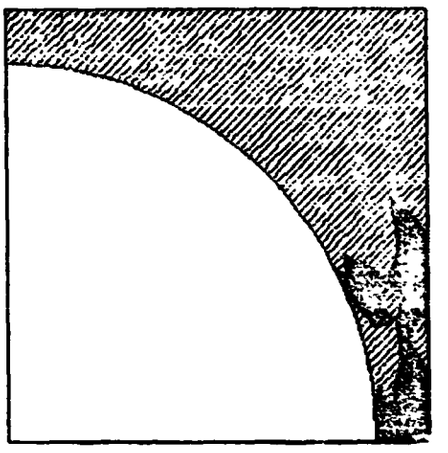

b) $\bar{\tau}_{xz}$ = 39 MPa (5.6 ksi)

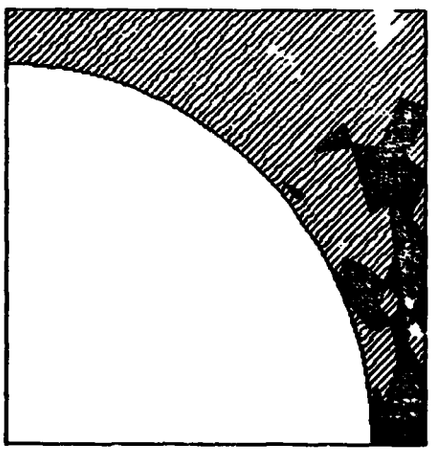

c) $\bar{\tau}_{xz}$ = 45 MPa (6.6 ksi)

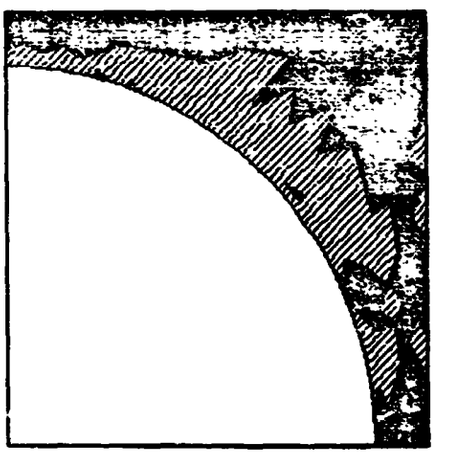

d) $\bar{\tau}_{xz}$ = 61 MPa (8.8 ksi)

Figure 81. AS4/5245-C Gr [illegible] y [illegible] ectional Composite, Room Temperature, [illegible] nal Shear Loading: $\bar{\tau}_{xz}$ ult = 6[illegible]

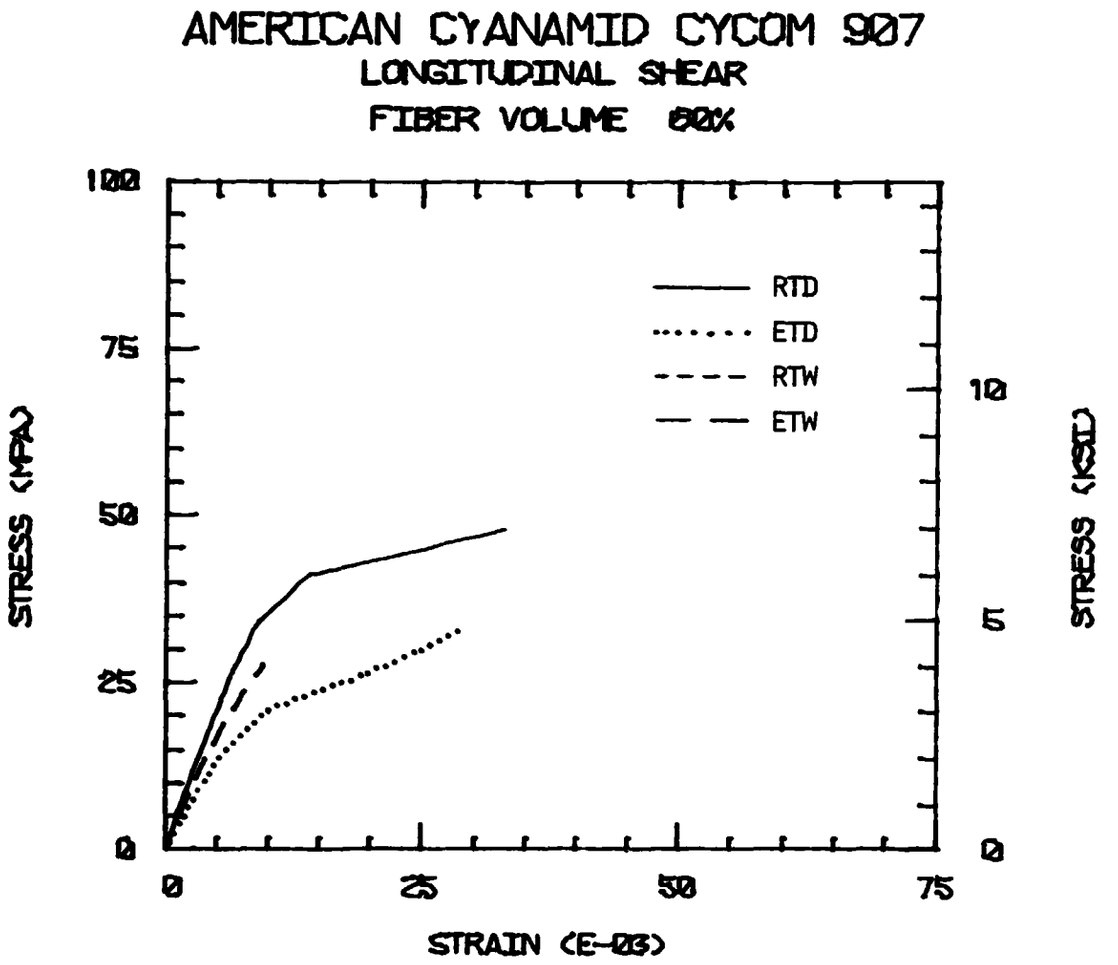

Figure 82. AS4/907 Graphite/Epoxy Unidirectional Composite Longitudinal Shear Stress-Strain Response.

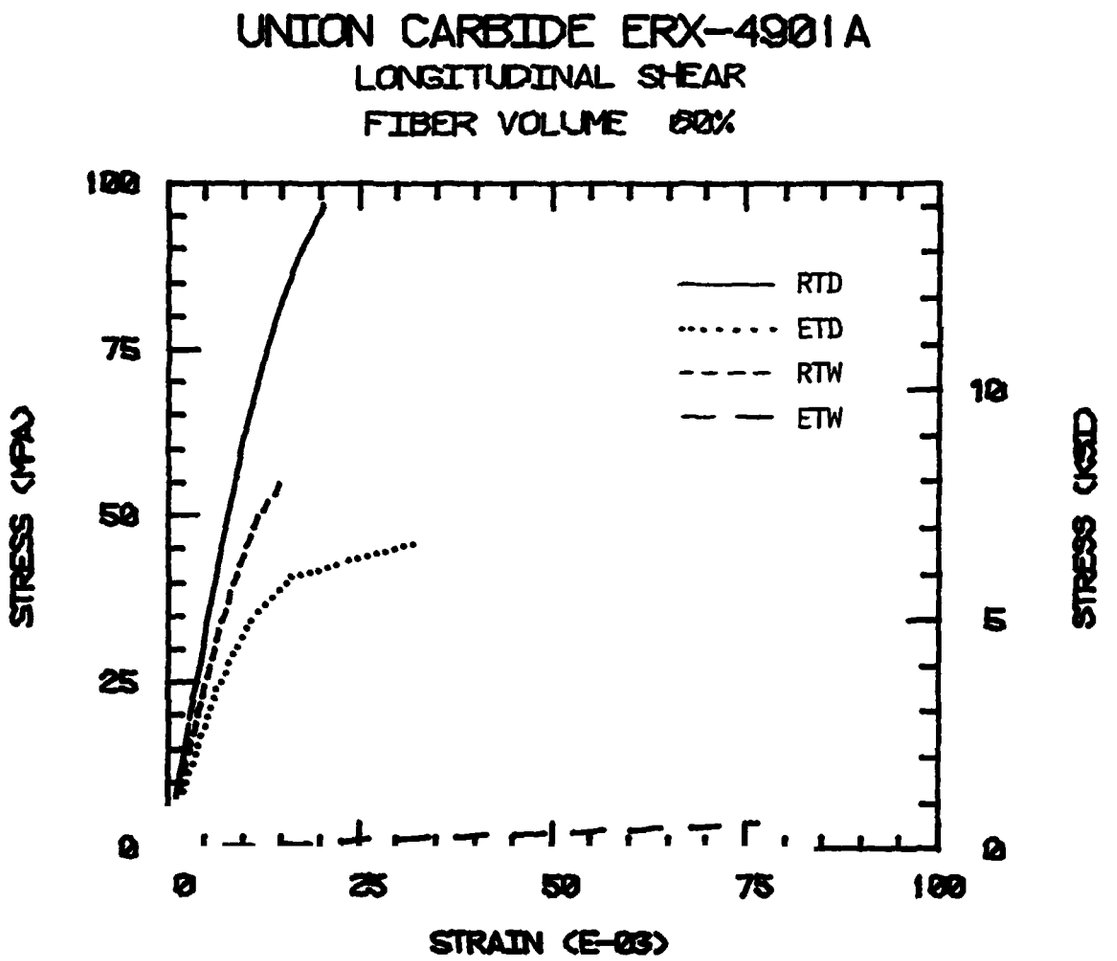

Figure 83. AS4/ERX-4901A(MDA) Graphite/Epoxy Unidirectional Composite, Longitudinal Shear Stress-Strain Response.

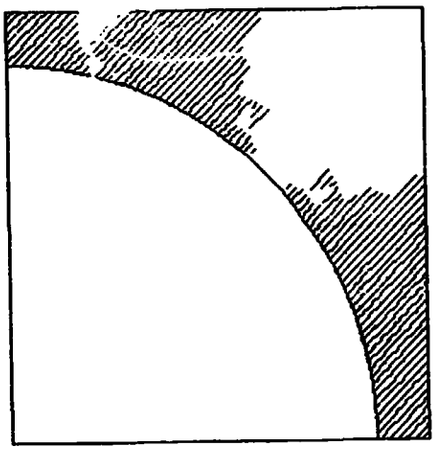

a) No Mechanical Loading

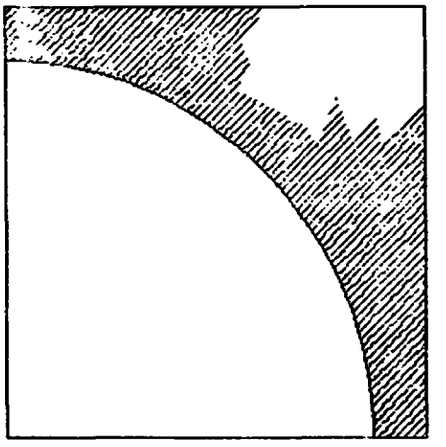

b) $\bar{\tau}_{xz}$ = 41 MPa (6.0 ksi)

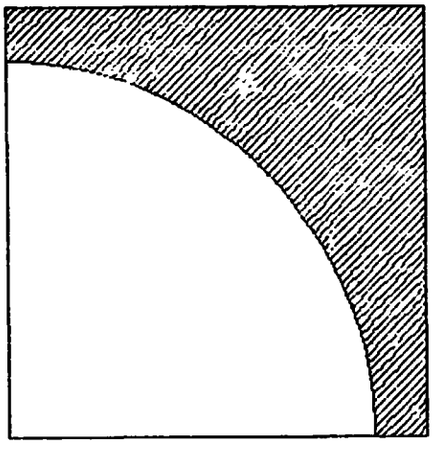

c) $\bar{\tau}_{xz}$ = 83 MPa (12.0 ksi)

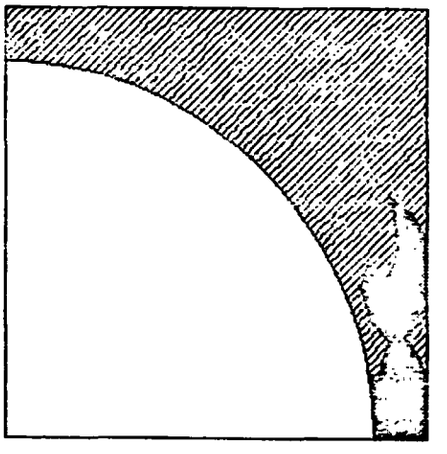

d) $\bar{\tau}_{xz}$ = 97 MPa (14.0 ksi)

Figure 84. AS4/ERX-4901A(MDA) Graphite/Epoxy Unidirectional Composite, Room Temperature, Dry (RTD), Longitudinal Shear Loading: $\bar{\tau}_{xz}^{ult}$ = 114 MPa (16.5 ksi).

in current significant since correlating experimental data are not yet available. Nevertheless, they do serve to demonstrate the potential benefits of using stronger and tougher (higher strain to failure) matrix materials in composites. The present work also represents the first detailed presentation and discussion of predicted matrix yield and crack propagation patterns. Thus, it represents a significant additional step toward the ultimate goal of being able to predict unidirectional composite strength using a rigorous micromechanics analysis, i.e., a physical rather than a phenomenological model of the composite.

During the follow-on study, particular emphasis will be placed on generating experimental data for unidirectional composites incorporating the polymer matrix materials discussed here. Thus, it will hopefully be finally possible to make rigorous correlations between predictions and experiment.

SECTION 6

CONCLUSION

Four additional neat resin systems, viz, Hexcel HX-1504, Narmco 5245-C, American Cyanamid CYCOM 907, and Union Carbide ERX-4901 A(MDA), were successfully cast into test specimens and mechanically characterized. Tension, torsional shear, Iosipescu shear, Single-Edge Notched-Bend fracture toughness, coefficient of thermal expansion, and coefficient of moisture expansion tests were conducted to generate mechanical properties as functions of temperature and moisture. Properties generated for these neat resins were Young's modulus, E, Poisson's ratio, ν, shear modulus, G, tensile ultimate strength σ^u, shear ultimate strength, τ^u, coefficient of thermal expansion, α, and coefficient of moisture expansion, β.

These mechanical properties were input to curve-fit computer programs to reduce each property to an equation describing that property as a function of temperature and moisture. After the curve-fit equations were generated they were incorporated into the Composite Materials Research Group's micromechanics computer program WYO2D and predictions of the composite response of a Hercules AS4 graphite fiber-reinforced composite were made. Correlations of these predictions with actual experimental data will be performed during the next grant year, by first testing various unidirectional composites and then comparing these experimental results with the finite element micromechanics predictions of material behavior.

Processability of the four systems was quite varied. The two ACEE material systems, i.e., HX-1504 and 5245-C, were fairly easily cast into the necessary test specimens, with the 5245-C being slightly more

viscous and therefore more difficult to cast than the HX-1504. The CYCOM 907 was very difficult to cast into neat resin specimens, with a great deal of time spent under vacuum to remove air bubbles. It was never successfully cast into the torsion dogbone configuration, making it necessary to perform Iosipescu shear testing instead of torsional shear testing on this material. The ERX-4901A(MDA) was formulated (mixed) just prior to being cast into test specimens and was extremely easy to handle. It exhibited the viscosity of water during initial handling and casting, which did necessitate some careful sealing of molds to prevent the resin from leaking out. It also required a much longer cure cycle than the other three neat resins, the duration being nearly four times as long.

Overall, the four materials chosen for the present second-year grant study performed at least as well as better than the four first-year materials. The HX-1504 and 5245-C exhibited comparable strengths and moduli when compared to the Hercules 2220-1 and 2220-3 matrix materials of the first-year program [1]. The 5245-C performed better at the 121°C test temperature, but was about equal to the HX-1504 at room temperature for all tests performed. The 5245-C absorbed the least amount of moisture of the four systems tested this year, with the moisture absorption of the HX-1504 being almost equal to that of the 2220-1 and -3 epoxies of the first year. The CYCOM 907 and ERX-4901A(MDA) absorbed higher percentages of moisture, and their properties degraded extremely rapidly when tested at hot/wet conditions.

The ERX-4901A(MDA) exhibited the highest room temperature, dry Young's modulus for any polymer tested to date in this program, viz, 4.8 GPa (0.70 Msi). It also exhibited the highest tensile and shear

strengths at the room temperature, dry condition, viz, 109 MPa (15.8 ksi) and 123 MPa (17.8 ksi) respectively. At the room temperature, wet condition the ERX-4901A(MDA) performed as well or better in tension and shear than the other three systems tested this year. Unfortunately, the hot/wet properties of ERX-4901A(MDA) are extremely poor even at 82°C.

The two ACEE resin systems, the HX-1504 and 5245-C, were judged to be quite good matrix material candidates. They processed readily, and performed as well or better than the four resins tested previously in the first-year study [1]. The CYCOM 907 and ERX-4901A(MDA) are interesting model systems, but lack the high temperature, wet performance required for most aerospace composite applications. The ERX-4901A, being cured at only 160°C, could possibly be improved in terms of its environmental performance by increasing the cure temperature slightly, which should raise its T_g. The ERX-4901A(MDA) would be a good candidate for compression or shear loading applications if use at elevated temperatures was restricted, and moisture levels were minimized, because of its high stiffness.

The already extensive collection of fracture surface photographs and scanning electron microphotographs generated during the first-year study [1] was added to. This should prove to be very valuable as a data base for future work.

The lack of general agreement of the neat resin experimental data with the isotropic relation relating the stiffness parameters E, ν and G, i.e., Young's modulus, Poisson's ratio, and shear modulus, respectively, as discussed in the first-year report [1], was fully confirmed. Similar trends were observed for all eight matrix materials which have now been characterized. In addition, independent experimental measurements of bulk modulus K, performed to support the present study by

DuPont [16], further supported these findings. Thus, this is obviously an important subject for additional study also.

Finally, the rigorous finite element micromechanics analysis results presented in detail here and in the first-year report [1] have clearly demonstrated the utility of such a predictive capability. It is anticipated that significant additional progress in this area will be made during the next year, as unidirectional composite experimental data become available for correlation purposes.

REFERENCES

1. R. S. Zimmerman, D. F. Adams and D. E. Walrath, "Investigation of the Relations Between Neat Resin and Advanced Composite Mechanical Properties," NASA Report No. NASA CR-172303, Volume I-Results, Volume II-Appendices; Mechanical Engineering Department, University of Wyoming, Report No. UWME-DR-301-101-1, May 1983.

2. D. F. Adams and B. G. Schaffer, "Analytical/Experimental Correlations of Stiffness Properties of Unidirectional Composites," Composites Technology Review, Vol. 4, No. 2, Summer 1982, pp. 45-48.

3. G. C. Grimes and D. F. Adams, "Investigation of Compression Fatigue Properties of Advanced Composites," Northrop Technical Report NOR 79-17, Naval Air Systems Command Contract N00019-77-C-0519, October 1979.

4. G. C. Grimes, D. F. Adams and E. G. Dusablon, "The Effects of Discontinuities on Compression Fatigue Properties of Advanced Composites," Northrop Technical Report NOR 80-158, Naval Air Systems Command Contract N00019-79-C-0276, October 1980.

5. D. F. Adams and D. A. Crane, "Combined Loading Micromechanical Analysis of a Unidirectional Composite," Composites, Vol. 15, No. 3, July 1984, pp. 181-192.

6. D. S. Cairns and D. F. Adams, "Moisture and Thermal Expansion Properties of Unidirectional Composite Materials and the Epoxy Matrix," Journal of Reinforced Plastics and Composites, Vol. 2, No. 4, October 1983, pp. 239-255.

7. D. F. Adams and D. E. Walrath, "Iosipescu Shear Properties of SMC Composite Materials," Proceedings of the Sixth Conference on Composite Materials: Testing and Design," ASTM STP 787, Phoenix, Arizona, May 1981, pp. 19-33.

8. D. E. Walrath and D. F. Adams, "The Iosipescu Shear Test as Applied to Composite Materials," Experimental Mechanics, Vol. 23, No. 1, March 1983, pp. 105-110.

9. D. E. Walrath and D. F. Adams, "Analysis of the Stress State in an Iosipescu Shear Test Specimen," Report UWME-DR-301-102-1, Department of Mechanical Engineering, University of Wyoming, June 1983.

10. D. E. Walrath and D. F. Adams, "Verification and Application of the Iosipescu Shear Test Method," Report UWME-DR-401-103-1, Department of Mechanical Engineering, University of Wyoming, June 1984.

11. I. S. Sokolnikoff, Mathematical Theory of Elasticity, Second Edition, McGraw-Hill Book Company, New York, 1956.

12. D. A. Crane and D. F. Adams, "Finite Element Micromechanical Analysis of a Unidirectional Composite Including Longitudinal Shear Loading," Report UWME-DR-101-101-1, Department of Mechanical Engineering, University of Wyoming, February 1981.

13. Communication with Eugene T. Camponeschi, Jr., Advanced Composites, David Taylor Naval Ship Research and Development Center, Annapolis, Maryland, April 1984.

14. S. G. Lekhnitski, Theory of Elasticity of an Anisotropic Elastic Body, Holden-Day, San Francisco, 1963.

15. R. M. Jones, Mechanics of Composite Materials, McGraw-Hill Book Company, New York, 1975, pp. 52-54.

16. P. Zoller, Unpublished Bulk Moduli Data for Four Neat Resin Systems, Central Research and Development Department, E. I. duPont de Nemours Co., Wilmington, Delaware, 1984.

17. D. F. Adams, R. L. Ramkumar and D. E. Walrath, "Analysis of Porous Laminates in the Presence of Ply Drop-Offs and Fastener Holes," Northrop Technical Report NOR 84-10, Naval Air Systems Command Contract N00019-82-C-0063, May 1984.

18. "Standard Test Method for Plane-Strain Fracture Toughness of Metallic Materials," ASTM E399, Part 7, American Society for Testing Materials, 1981.

19. W. D. Bascom, G. W. Bullman, D. L. Hunston, and R. M. Jensen, "The Width-Tapered Double Cantilever Beam for Interlaminar Fracture Testing," Proceedings of the 29th National SAMPE Symposium, Reno, Nevada, April 1984, pp. 970-978.

20. D. F. Adams and D. A. Crane, "Finite Element Micromechanical Analysis of a Unidirectional Composite Including Longitudinal Shear Loading," Computers and Structures, Vol. 18, No. 6, 1984, pp. 1153-1165.

21. D. F. Adams, "High Performance Composite Materials for Vehicle Construction, An Elastoplastic Analysis of Crack Propagation in a Unidirectional Composite," Report R-1070-PR, The Rand Corporation, March 1973.

22. D. F. Adams and D. P. Murphy, "Analysis of Crack Propagation as an Energy Absorption Mechanism in Metal Matrix Composites," Report UWME-DR-101-102-1, Department of Mechanical Engineering, University of Wyoming, February 1981.

23. D. F. Adams, "Elastoplastic Crack Propagation in a Transversely Loaded Unidirectional Composite," Journal of Composite Materials, Vol. 8, January 1974, pp. 38-54.

24. D. F. Adams, "A Micromechanical Analysis of Crack Propagation in an Elastoplastic Composite Material," Fibre Science and Technology, Vol. 7, No. 4, October 1974, pp. 237-256.

25. "Hercules Product Data Sheet No. 847-3: Magnamite Graphite Fiber Type AS4," Hercules, Inc., Magna, Utah, August 1981.

26. D. S. Cairns and D. F. Adams, "Moisture and Thermal Expansion of Composite Materials," Report UWME-DR-101-104-1, Department of Mechanical Engineering, University of Wyoming, November 1981.

27. D. F. Adams and M. M. Monib, "Moisture Expansion and Thermal Expansion Coefficients of a Polymer-Matrix Composite Material," Proceedings of the Fourth Conference on Fibrous Composites in Structural Design, San Diego, California, November 1978.

28. R. M. Richard and J. M. Blacklock, "Finite Element Analysis of Inelastic Structures," AIAA Journal, Vol. 7, No. 3, March 1969, pp. 432-438.

29. D. F. Adams and D. E. Walrath, "Hygrothermal Response of Polymer Matrix Composite Materials," Report UWME-DR-901-102-1, Department of Mechanical Engineering, University of Wyoming, September 1979.

APPENDIX A

Tables of Individual Test Specimen Results for the Various Neat Resins

TABLE A1

NEAT RESIN TENSILE TESTING OF FIRST-YEAR RESIN SYSTEMS AT 121°C, DRY CONDITION

Resin System	Specimen No.		Ultimate Stress (MPa)	Ultimate Stress (ksi)	Ultimate Strain	Tensile Modulus (GPa)	Tensile Modulus (Msi)	Poisson's Ratio
3502	LTDM	31	59.3	8.6	0.023	2.69	0.39	0.466
		32	39.3*	5.7*	0.014	2.83	0.41	0.474
		33	49.6	7.2	0.019	2.62	0.38	0.458
		34	44.1	6.4	0.016	2.83	0.41	0.458
		35	59.3	8.6	0.023	2.69	0.39	0.460
		36	55.2	8.2	0.020	2.96	0.43	0.461
	Average		53.8	7.8	0.019	2.76	0.40	0.463
	Standard Deviation		6.9	1.0	0.004	0.14	0.02	0.006
914	LTDN	31	18.6	2.7	0.069	0.62	0.09	0.451
		32	15.1*	2.2*	0.071	0.34*	0.05*	0.424
		33	20.0	2.9	0.054*	0.69	0.10	0.408
		34	19.3	2.8	0.059	0.76	0.11	0.442
		35	20.0	2.9	0.071	0.76	0.11	0.458
		36	19.3	2.8	0.073	0.55	0.08	0.435
	Average		19.3	2.8	0.069	0.67	0.10	0.436
	Standard Deviation		0.6	0.1	0.006	0.09	0.03	0.018

TABLE A1 (CONTINUED)

NEAT RESIN TENSILE TESTING OF FIRST-YEAR RESIN SYSTEMS AT 121°C, DRY CONDITION

Resin System	Specimen No.	Ultimate Stress (MPa)	Ultimate Stress (ksi)	Ultimate Strain	Tensile Modulus (GPa)	Tensile Modulus (Msi)	Poisson's Ratio
2220-1	LTDL 31	59.3	8.6	0.044	2.07	0.30	0.421
	32	60.0	8.7	0.049	2.14	0.31	0.376
	33	64.1	9.3	0.047	2.28	0.33	0.426
	34	59.3	8.6	0.038	2.21	0.32	0.424
	35	57.9	8.4	0.035	2.28	0.33	0.430
	Average	60.0	8.7	0.043	2.21	0.32	0.415
	Standard Deviation	2.1	0.3	0.006	0.07	0.01	0.022
2220-3	LTDK 31	65.5	9.5	0.049	2.21	0.32	0.401
	32	63.4	9.2	0.043	2.21	0.32	0.395
	33	64.1	9.3	0.051	2.21	0.32	0.395
	34	63.4	9.2	0.051	2.21	0.32	0.377
	35	54.5	7.9	0.032*	2.21	0.32	0.355
	36	62.7	9.1	0.042	1.93	0.28	0.410
	37	62.0	9.0	0.051	2.14	0.31	0.394
	Average	62.3	9.0	0.048	2.16	0.31	0.390
	Standard Deviation	3.6	0.5	0.004	0.10	0.01	0.018

* Not included in average

TABLE A2

NEAT RESIN TENSILE TESTING OF FIRST-YEAR RESIN SYSTEMS AT 121°C, MOISTURE-SATURATED CONDITIONS

Resin System	Specimen No.		Ultimate Stress (MPa)	(ksi)	Ultimate Strain	Tensile Modulus (GPa)	(Msi)	Poisson's Ratio
3502	LTWM	31	13.8	2.0	0.007	1.86	0.27	0.442
		32	13.8	2.0	0.008	1.86	0.27	0.470
		33	22.7*	3.3*	0.013*	1.93	0.28	0.462
		34	14.5	2.1	0.008	1.93	0.28	0.435
		35	19.3	2.8	0.011	1.93	0.28	0.446
	Average		15.3	2.2	0.009	1.90	0.28	0.451
	Standard Deviation		2.6	0.4	0.002	0.04	0.01	0.014
914	LTWN	31	8.3	1.2	0.065	0.28	0.04	
		32	8.3	1.2	0.070	0.28	0.04	
		33	7.6	1.1	0.057*	0.21	0.03	
		34	8.8	1.2	0.072	0.28	0.04	
		35	9.0	1.3	0.074	0.28	0.04	
	Average		8.3	1.2	0.070	0.27	0.04	
	Standard Deviation		0.5	0.1	0.004	0.03	0.01	

* Not included in average

TABLE A2 (CONTINUED)

NEAT RESIN TENSILE TESTING OF FIRST-YEAR RESIN SYSTEMS AT 121°C, MOISTURE-SATURATED CONDITIONS

Resin System	Specimen No.		Ultimate Stress (MPa)	Ultimate Stress (ksi)	Ultimate Strain	Tensile Modulus (GPa)	Tensile Modulus (Msi)	Poisson's Ratio
2220-1	LTWL	31	24.1	3.5	0.050	1.24*	0.18*	0.585
		32	23.4	3.4	0.054	1.03	0.15	0.559
		33	22.7	3.3	0.050	1.10	0.16	0.568
		34	23.4	3.4	0.047	0.90*	0.13*	0.559
		35	24.1	3.5	0.060	1.03	0.15	0.560
	Average		23.4	3.4	0.052	1.02	0.15	0.566
	Standard Deviation		0.6	0.1	0.005	0.08	0.01	0.012
2220-3	LTWK	31	20.7	3.0	0.071	0.96	0.14	
		32	19.3	2.8	0.056*	0.76	0.11	
		33	20.0	2.9	0.075	0.89	0.13	
		34	22.0	3.2	0.092*	0.89	0.13	
		35	22.0	3.2	0.079	0.82	0.12	
	Average		20.8	3.0	0.075	0.86	0.13	
	Standard Deviation		1.2	0.2	0.004	0.08	0.01	

* Not included in average

TABLE A3

HEXCEL HX-1504 NEAT RESIN TENSILE TESTS - DRY

Specimen No.		Test Temperature (°C)	Ultimate Stress (MPa)	Ultimate Stress (ksi)	Ultimate Strain	Tensile Modulus (GPa)	Tensile Modulus (Msi)	Poisson's Ratio
LTDJ	11	23	69.6	10.1	0.019	3.79	0.55	0.360
	12		82.7	12.0	0.023	3.79	0.55	0.368
	13		83.4	12.1	0.024*	3.93	0.57	0.363
	14		59.3*	8.6*	0.015*	4.00	0.58	0.379
	15		69.6	10.1	0.015*	3.86	0.56	0.374
	16		80.6	11.7	0.019	4.00	0.58	0.372
	Average		77.2	11.2	0.020	3.86	0.57	0.369
	Standard Deviation		7.0	1.0	0.002	0.07	0.01	0.007
LTDJ	21	82	75.8	11.0	0.030*	3.03	0.44	0.366
	22		66.1	9.6	0.017*	3.45	0.50	0.336
	23		54.5	7.9*	0.017*	3.31	0.48	0.373
	24		66.8	9.7	0.022	3.38	0.49	0.368
	25		69.6	10.1	0.023	3.24	0.47	0.362
	26		75.1	10.9	0.027	3.24	0.47	0.352
	Average		70.3	10.3	0.024	3.31	0.48	0.360
	Standard Deviation		4.1	0.6	0.003	0.14	0.02	0.014
LTDJ	31	121	64.8	9.4	0.041	2.62	0.38	0.359
	32		54.5*	7.9*	0.025*	2.69	0.39	0.362
	33		61.3	8.9	0.030	2.76	0.40	0.354
	34		63.4	9.2	0.037	2.76	0.40	0.360
	35		60.0	8.7	0.030	2.62	0.38	0.377
	36		61.4	8.9	0.044*	2.69	0.39	0.390
	Average		62.0	9.0	0.035	2.69	0.39	0.367
	Standard Deviation		0.3	2.1	0.005	0.07	0.01	0.014

* Not included in average

TABLE A4

HEXCEL HX-1504 NEAT RESIN TENSILE TESTS - MOISTURE-SATURATED

Specimen No.		Test Temperature (°C)	Ultimate Stress (MPa)	(ksi)	Ultimate Strain	Tensile Modulus (GPa)	(Msi)	Poisson's Ratio
LTWJ	1	23	45.5	6.6	0.013*	3.44	0.50	0.401
	2		57.9	8.4	0.018*	3.44	0.50	0.399
	3		41.3*	6.0*	0.013*	3.58	0.52	0.364
	4		47.5	6.9	0.014	4.06	0.59	0.398
	5		54.4	7.9	0.016	3.44	0.50	0.395
	6		53.0	7.7	0.016	3.31	0.48	0.405
	7		53.0	7.7	0.016	3.44	0.50	0.409
	Average		51.0	7.4	0.016	3.51	0.51	0.396
	Standard Deviation		4.0	0.6	0.001	0.21	0.03	0.015
LTWJ	20	82	47.5	6.9	0.019	2.96	0.43	0.416
	21		43.4*	6.3*	0.018	2.69	0.39	0.410
	22		48.2	7.0	0.019	2.82	0.41	0.407
	23		46.8	6.8	0.022	2.55	0.37	0.407
	24		48.9*	7.1*	0.022	2.69	0.39	0.410
	25		46.2	6.7	0.021	0.42	2.89	0.411
	Average		47.5	6.9	0.020	0.40	2.76	0.410
	Standard Deviation		0.9	0.1	0.001	0.02	0.14	0.003
LTWJ	31	121	2.0	13.8	0.041*	0.89	0.13	
	32		8.9*	1.3*	0.072	0.41*	0.06*	
	34		17.9	2.6	0.082#	1.38*	0.20*	
	35		16.5	2.4	0.082#	0.89	0.13	
	36		15.8	2.3	0.082#	0.76	0.11	
	37		15.5	2.4	0.082#	0.89	0.13	
	Average		15.8	2.3	0.079	0.89	0.13	
	Standard Deviation		1.4	0.2	0.004	0.76	0.11	

* Not included in average

Strain amplifier saturated; specimen failed soon afterward

TABLE A5

HEXCEL HX-1504 NEAT RESIN TORSION TESTS - DRY

Specimen No.		Test Temperature (°C)	Ultimate Shear Stress (MPa)	(ksi)	Ultimate Shear Strain	Shear Modulus (GPa)	(Msi)
LSDJ	01	23	98.6	14.3	0.105*	1.52*	0.22*
	02		86.9	12.6	0.048*	1.79	0.26
	03		106.8	15.5	0.082	1.86	0.27
	04		102.0	14.8	0.095	1.59	0.23
	05		102.0	14.8	0.084	2.00	0.29
	06		89.6	13.0	0.064	2.14*	0.31*
	Average		97.9	14.2	0.081	1.79	0.26
	Standard Deviation		7.6	1.1	0.013	0.21	0.03
LSDJ	10	82	79.3	11.5	0.135	1.38	0.20
	11		78.6	11.4	0.085	1.72	0.25
	12		68.9	10.0	0.057*	1.65	0.24
	13		81.4	11.8	0.134	1.99*	0.29*
	14		78.6	11.4	0.146*	1.03*	0.15*
	15		72.4	10.5	0.086	1.24	0.18
	Average		76.5	11.1	0.110	1.51	0.22
	Standard Deviation		4.8	0.7	0.028	0.20	0.03
LSDJ	20	121	41.4*	6.0*	0.128	1.10	0.16
	21		44.1	6.4	0.139	1.03	0.15
	22		57.9	8.4	0.102*	1.45*	0.21*
	23		57.2	8.3	0.105	1.03	0.15
	24		56.5	8.2	0.119	1.24*	0.18*
	Average		53.8	7.8	0.117	1.10	0.16
	Standard Deviation		6.9	1.0	0.012	0.07	0.01

* Not included in average

TABLE A6

HEXCEL HX-1504 NEAT RESIN TORSION TESTS - MOISTURE-SATURATED

Specimen No.	Test Temperature (°C)	Ultimate Shear Stress (MPa)	Ultimate Shear Stress (ksi)	Ultimate Shear Strain	Shear Modulus (GPa)	Shear Modulus (Msi)
LSWJ 01	23	71.7	10.4	0.074	1.10	0.16
02		62.0	9.0	0.049	1.31	0.19
03		69.6	10.1	0.069	1.10	0.16
04		60.0	8.7	0.027	2.34	0.34
05		51.0*	7.4*	0.017*	2.90*	0.42*
06		86.2*	12.5	0.073	1.58	0.23
Average		65.8	9.6	0.058	1.52	0.22
Standard Deviation		5.7	0.8	0.020	0.55	0.08
LSWJ 10	82	64.1	9.3	0.103	0.90	0.13
11		67.6*	9.8*	0.090	0.96	0.14
12		64.8	9.4	0.068	1.65	0.24
13		54.5*	7.9*	0.092	0.69	0.10
14		57.9	8.4	0.033*	2.34*	0.34*
Average		62.3	9.0	0.088	1.03	0.15
Standard Deviation		3.8	0.6	0.015	0.41	0.06
LSWJ 20	121	38.6	5.6	0.080	0.34	0.05
21		15.8*	2.3*	0.223*	0.28*	0.04*
22		34.5	5.0	--	--	--
23		53.1*	7.7*	0.087	0.55	0.08
24		41.4	6.0	0.071	1.10*	0.16*
25		34.5	5.0	0.026*	0.96	0.14
Average		37.2	5.4	0.079	0.62	0.09
Standard Deviation		3.4	0.5	0.008	0.28	0.04

*Not included in average

TABLE A7

NARMCO 5245-C NEAT RESIN TENSION TESTS - DRY

Specimen No.	Test Temperature (°C)	Ultimate Stress (MPa)	Ultimate Stress (ksi)	Ultimate Strain	Tensile Modulus (GPa)	Tensile Modulus (Msi)	Poisson's Ratio
LTDO 07	23	67.6	9.8	0.019	3.79	0.55	0.391
08		78.6	11.4	0.022	3.79	0.55	0.383
09		75.2	10.9	0.021	3.72	0.54	0.388
Average		73.8	10.7	0.021	3.75	0.54	0.387
Standard Deviation		5.6	0.8	0.002	0.04	0.01	0.004
LTDO 11	82	46.2*	6.7*	0.014*	3.38	0.49	0.381*
12		64.1	9.3	0.020	3.38	0.49	0.392
13		82.7*	12.0*	0.028	3.45	0.50	0.411*
14		59.3	8.6	0.017	3.72*	0.54*	0.400
15		86.2*	12.5*	0.031*	3.31	0.48	0.380*
16		63.4	9.2	0.019	3.65	0.53	0.397
Average		62.0	9.0	0.021	3.45	0.50	0.396
Standard Deviation		2.8	0.4	0.005	0.14	0.02	0.004
LTDO 21	121	69.6	10.1	0.030	3.03	0.44	0.384*
22		59.3*	8.6*	0.023*	2.96	0.43	0.388
23		77.2	11.2	0.056	3.24	0.47	0.412
24		78.6	11.4	0.057	3.45*	0.50*	0.424*
25		76.5	11.1	0.057	2.48*	0.36*	0.399
Average		75.8	11.0	0.050	3.10	0.45	0.400
Standard Deviation		4.1	0.6	0.013	0.14	0.02	0.012

*Not included in average

TABLE A8

NARMCO 5245-C NEAT RESIN TENSION TESTS - MOISTURE-SATURATED

Specimen No.	Test Temperature (°C)	Ultimate Stress (MPa)	Ultimate Stress (ksi)	Ultimate Strain	Tensile Modulus (GPa)	Tensile Modulus (Msi)	Poisson's Ratio
LTWO 01	23	62.7	9.1	0.016	4.07	0.59	0.385
02		73.8*	10.7*	0.019	4.07	0.59	0.377*
03		45.5	6.6	--	3.45*	0.50*	0.398
04		31.0	4.5	0.008*	4.00	0.58	0.424*
05		49.0	7.1	0.013	3.93	0.57	0.420*
06		26.9*	3.9*	--	--	--	0.393
Average		46.9	6.8	0.016	4.00	0.58	0.392
Standard Deviation		13.1	1.9	0.003	0.07	0.01	0.006
LTWO 11	82	54.5	7.9	0.057*	2.83*	0.41*	0.412
12		57.2	8.3	0.050	3.03	0.44	0.448*
13		57.9	8.4	0.041	3.03	0.44	0.437
14		47.6*	6.9*	0.018*	3.17	0.46	0.425
15		58.6	8.5	0.040	3.17	0.46	0.421
16		53.8	7.8	0.024	3.03	0.44	0.411*
Average		56.5	8.2	0.039	3.10	0.45	0.424
Standard Deviation		2.1	0.3	0.011	0.07	0.01	0.010
LTWO 21	121	29.0*	4.2*	0.082#	1.31*	0.16*	
22		28.3	4.1	0.082#	0.97	0.14	
23		28.3	4.1	0.082#	0.90	0.13	
24		27.6	4.0	0.082#	0.90	0.13	
25		27.6	4.0	0.082#	--	--	
Average		27.6	4.0	0.082#	0.90	0.13	
Standard Deviation		0.7	0.1	--	0.04	0.01	

*Not included in average
#Strain amplifier saturation

TABLE A9

NARMCO 5245-C NEAT RESIN TORSION TESTS - DRY

Specimen No.	Test Temperature (°C)	Ultimate Shear Stress (MPa)	Ultimate Shear Stress (ksi)	Ultimate Shear Strain	Shear Modulus (GPa)	Shear Modulus (Msi)
LSDO 01	23	31.8*	4.6*	0.030*	1.03	0.15
02		55.8	8.1	0.064	0.90	0.13
03		62.7	9.1	0.053	1.17	0.17
04		72.4*	10.5*	0.024*	3.10*	0.45*
05		46.9	6.8	0.059	0.96	0.14
06		57.9	8.4	0.070*	0.83	0.12
Average		55.8	8.1	0.059	0.96	0.14
Standard Deviation		6.9	1.0	0.006	0.14	0.02
LSDO 10	82	82.0	11.9	0.073	1.31	0.19
11		70.3	10.2	0.024	0.96*	0.14*
12		97.2*	14.1*	0.069	1.79	0.26
13		62.7	9.1	0.024*	2.48*	0.36*
14		46.9*	6.8*	0.033	1.45	0.21
15		50.3	7.3	0.045	1.24	0.18
Average		66.2	9.6	0.059	1.45	0.21
Standard Deviation		13.1	1.9	0.019	0.23	0.04
LSDO 20	121	61.4	8.9	0.060	1.03	0.15
21		67.6	9.8	0.138*	1.84*	0.28*
22		71.7	10.4	0.081	1.24	0.18
23		89.6	13.0	0.041*	1.17	0.17
24		57.9*	8.4*	0.066	0.90	0.13
25		67.6	9.8	0.099	0.76	0.11
Average		66.9	9.7	0.076	1.03	0.15
Standard Deviation		4.1	0.6	0.017	0.21	0.03

*Not included in average

TABLE A10

NARMCO 5245-C NEAT RESIN TORSION TESTS - MOISTURE-SATURATED

Specimen No.	Test Temperature (°C)	Ultimate Shear Stress (MPa)	Ultimate Shear Stress (ksi)	Ultimate Shear Strain	Shear Modulus (GPa)	Shear Modulus (Msi)
LSWO 01	23	73.1	10.6	0.051	1.45	0.21
02		67.6	9.8	0.020*	1.38	0.20
03		62.7	9.1	0.081*	0.90*	0.13*
04		73.8	10.7	0.073*	1.03	0.15
05		43.4*	6.3*	0.017*	1.03	0.15
06		88.2*	12.8*	0.067	1.72	0.25
07		70.3	10.2	0.043	1.65	0.24
08		57.9	8.4	0.034	2.07*	0.30*
Average		67.6	9.8	0.049	1.38	0.20
Standard Deviation		6.2	0.9	0.014	0.28	0.04
LSWO 11	82	68.3*	9.9*	0.056	1.93*	0.28*
12		60.7*	8.8*	0.057	1.24	0.18
13		63.4	9.2	0.060	1.31	0.19
14		64.1	9.3	0.060	1.58	0.23
15		66.9	9.7	0.076*	1.31	0.19
Average		64.8	9.4	0.058	1.38	0.20
Standard Deviation		2.1	0.3	0.002	0.14	0.02
LSWO 21	121	31.0	4.5	0.128	0.55*	0.08*
22		36.5	5.3	0.097*	1.52*	0.22*
23		35.2	5.1	0.163	0.69	0.10
24		33.1	4.8	0.120	0.90	0.13
25		68.3*	9.9*	0.151	1.10	0.16
Average		33.8	4.9	0.141	0.90	0.13
Standard Deviation		2.8	0.	0.020	0.21	0.03

*Not included in average

TABLE A11

AMERICAN CYANAMID CYCOM 907 NEAT RESIN TENSION TESTS - DRY

Specimen No.	Test Temperature (°C)	Ultimate Stress (MPa)	Ultimate Stress (ksi)	Ultimate Strain	Tensile Modulus (GPa)	Tensile Modulus (Msi)	Poisson's Ratio
LTDP 07	23	82.0	11.9	0.031	3.24	0.47	0.418
08		95.8	13.9	0.051	3.24	0.47	0.416
09		80.7	11.7	0.030	3.31	0.48	0.414
Average		86.2	12.5	0.037	3.26	0.47	0.416
Standard Deviation		8.3	1.2	0.012	0.04	0.06	0.002
LTDP 11	82	68.3	9.9	0.050	2.83	0.41	0.435*
12		65.5	9.5	0.069	2.69	0.39	0.414
13		66.9	9.7	0.054	2.83	0.41	0.430
14		66.2	9.6	0.057	2.69	0.39	0.409*
15		60.7*	8.8*	0.029*	2.76	0.40	0.427
Average		66.9	9.7	0.054	2.76	0.40	0.424
Standard Deviation		1.4	0.2	0.004	0.07	0.01	0.008
LTDP 21	121	11.0	1.6	0.082#	0.55	0.08	0.313*
22		10.3*	1.5*	0.082#	0.28*	0.04*	0.440*
23		14.5	2.1	0.082#	1.03	0.15	0.350
24		15.8	2.3	0.082#	0.97	0.14	0.385
25		13.8	2.0	0.082#	0.76	0.11	0.391
Average		13.8	2.0	0.082#	0.83	0.12	0.375
Standard Deviation		2.1	0.3	--	0.22	0.03	0.022

*Not included in average

#Strain amplifier saturation, specimen failed soon afterward

TABLE A12

AMERICAN CYANAMID CYCOM 907 NEAT RESIN TENSION TESTS - MOISTURE-SATURATED

Specimen No.	Test Temperature (°C)	Ultimate Stress (MPa)	Ultimate Stress (ksi)	Ultimate Strain	Tensile Modulus (GPa)	Tensile Modulus (Msi)	Poisson's Ratio
LTWP 01	23	57.9	8.4	0.026	2.90	0.42	0.428
02		49.0*	7.1*	0.018*	2.90	0.42	0.417
03		56.5	8.2	0.026	3.03*	0.44*	0.435
04		57.9	8.4	0.022	2.96	0.43	0.432
05		57.9	8.4	0.028	2.90	0.42	0.427
Average		57.9	8.4	0.026	2.90	0.42	0.430
Standard Deviation		0.7	0.1	0.002	0.03	0.01	0.004
LTWP 11	82	3.45	0.5	0.082#	0.07	0.01	
12		2.07	0.3	0.082#	0.07	0.01	
13		1.38	0.2	0.082#	0.07	0.01	
14		0.69	0.1	0.082#	0.07	0.01	
15		3.45	0.5	0.082#	0.28*	0.04	
Average		2.07	0.3	0.082#	0.07	0.01	
Standard Deviation		1.38	0.2	--	0.00	0.00	
	121	NOT TESTED					

*Not included in average

#Strain amplifier saturated; specimen failed soon afterward

TABLE A13

AMERICAN CYANAMID CYCOM 907 NEAT RESIN IOSIPESCU SHEAR TESTS - DRY

Specimen No.	Test Temperature (°C)	Ultimate Shear Stress (MPa)	(ksi)	Ultimate Shear Strain	Shear Modulus (GPa)	(Msi)
LIDP 01	23	27.6*	4.0*	0.023	1.24	0.18
02		33.8	4.9	0.030	1.31	0.19
03		53.1	7.7	0.049	1.17	0.17
04		34.5	5.0	0.030	1.17	0.17
05		58.6*	8.5*	0.082*	1.03	0.15
Average		40.7	5.9	0.033	1.18	0.17
Standard Deviation		11.0	1.6	0.011	0.10	0.02
LIDP 14	82	46.9	6.8	0.095#	1.17*	0.17*
15		46.9	6.8	0.095#	1.03	0.15
16		46.2	6.7	0.095#	0.96	0.14
17		44.8	6.5	0.095#	0.96	0.14
18		43.4*	6.3*	0.095#	0.96	0.14
Average		46.2	6.7	0.095#	0.98	0.14
Standard Deviation		0.7	0.1		0.04	0.01
LIDP 21	121	24.1*	3.5*	0.114	0.69	0.10
22		28.3	4.1	0.095#	0.83	0.12
23		27.6	4.0	0.095#	0.76	0.11
24		29.0	4.2	0.095#	0.76	0.11
25		29.0	4.2	0.095#	0.83	0.12
Average		28.3	4.1	0.095#	0.77	0.11
Standard Deviation		0.7	0.1		0.06	0.01

*Not included in average

#Strain amplifier saturated

TABLE A14

AMERICAN CYANAMID CYCOM 907 NEAT RESIN IOSIPESCU SHEAR TESTS - MOISTURE-SATURATED

Specimen No.	Test Temperature (°C)	Ultimate Shear Stress (MPa)	(ksi)	Ultimate Shear Strain	Shear Modulus (GPa)	(Msi)
LIWP 01	23	46.9*	6.8*	0.103	0.96	0.14
02		43.4	6.3	0.050	1.10	0.16
03		44.8	6.5	0.053	1.17	0.17
04		40.7*	5.9*	0.044	1.03	0.15
05		44.8	6.5	0.077	1.10	0.16
Average		44.1	6.4	0.056	1.10	0.16
Standard Deviation		0.7	0.1	0.014	0.07	0.01
LIWP 11	82	4.8	0.7	0.116#	0.14	0.02
12		4.8	0.7	0.116#	0.07	0.01
13		4.8	0.7	0.116#	0.34	0.05
14		4.8	0.7	0.116#	0.14	0.02
15		6.9*	1.0*	0.116#	0.34	0.05
Average		4.8	0.7	0.116#	0.21	0.03
Standard Deviation		0.0	0.0	-	0.14	0.02
	121	NOT TESTED				

*Not included in average

#Strain amplifier saturated

TABLE A15

UNION CARBIDE ERX-4901A(MDA) NEAT RESIN TENSION TESTS - DRY

Specimen No.	Test Temperature (°C)	Ultimate Stress (MPa)	Ultimate Stress (ksi)	Ultimate Strain	Tensile Modulus (GPa)	Tensile Modulus (Msi)	Poisson's Ratio
LTDQ 00	23	120.0	17.4	0.028	5.10*	0.74*	0.413
01		85.5	12.4	--	4.76	0.69	0.407
02		117.9	17.1	--	4.83	0.70	0.418*
03		115.8	16.8	--	4.90	0.71	0.408
04		71.7*	10.4*	0.015	4.76	0.69	0.405
05		104.1	15.1	0.020	4.76	0.69	0.391*
Average		108.9	15.8	0.021	4.83	0.70	0.408
Standard Deviation		14.5	2.1	0.006	0.01	0.01	0.003
LTDQ 11	82	62.0*	9.0*	0.082#	2.90	0.42	0.416*
12		57.9	8.3	0.082#	2.76	0.40	0.436
13		55.8	8.1	0.082#	3.03*	0.44*	0.435
14		55.8	8.1	0.082#	2.83	0.41	0.452*
15		51.7*	7.5*	0.082#	2.55*	0.37*	0.448
Average		56.5	8.2	0.082	2.83	0.41	0.440
Standard Deviation		1.4	0.2	--	0.07	0.01	0.007
LTDQ 21	121	10.3	1.5	0.082#	0.41	0.06	0.257*
22		9.0	1.3	0.082#	0.62	0.09	0.337
23		13.1*	1.9*	0.082#	0.76*	0.11*	0.414*
24		8.3	1.2	0.082#	0.21*	0.03*	0.361
25		9.6	1.4	0.082#	0.48	0.07	0.341
Average		9.6	1.4	0.082#	0.48	0.07	0.346
Standard Deviation		0.7	0.1	--	0.10	0.02	0.013

*Not included in average

#Strain amplifier saturation, specimen failed soon afterward

TABLE A16

UNION CARBIDE ERX-4901A(MDA) NEAT RESIN TENSION TESTS - MOISTURE-SATURATED

Specimen No.	Test Temperature (°C)	Ultimate Stress (MPa)	Ultimate Stress (ksi)	Ultimate Strain	Tensile Modulus (GPa)	Tensile Modulus (Msi)	Poisson's Ratio
LTWQ 01	23	60.6*	8.8*	0.021*	3.51	0.51	0.402
02		75.1	10.9	0.029	3.58	0.52	0.374*
03		79.2	11.5	0.055	3.51	0.51	0.411*
04		82.7	12.0	0.054	4.00*	0.58*	0.391
05		79.9	11.6	0.045	3.58	0.52	0.398
Average		79.2	11.5	0.046	3.58	0.52	0.396
Standard Deviation		2.8	0.4	0.012	0.04	0.01	0.006
LTWQ 11	82	3.44	0.5	0.079	0.14	0.02	
12		2.77	0.4	0.082	0.07	0.01	
13		2.77	0.4	--	--	--	
14		2.07	0.3	0.071	0.07	0.01	
15		2.77	0.4	0.082	0.07	0.01	
16		2.77	0.4	0.059*	0.14	0.02	
Average		2.77	0.4	0.079	0.07	0.01	
Standard Deviation		0.41	0.06	0.005	0.00	0.00	
LTWQ	121	NOT TESTED					

*Not included in average

#Strain amplifier saturation

TABLE A17

UNION CARBIDE ERX-4901A(MDA) NEAT RESIN TORSION TESTS - DRY

Specimen No.	Test Temperature (°C)	Ultimate Shear Stress (MPa)	(ksi)	Ultimate Shear Strain	Shear Modulus (GPa)	(Msi)
LSDQ B1	23	122.0	17.7	0.076	1.65*	0.24*
03		100.9*	14.5*	0.052	1.86	0.27
04		122.7	17.8	0.113	2.14	0.31
05		123.4	17.9	--	1.93	0.28
06		123.4	17.9	--	2.21	0.32
Average		122.8	17.8	0.080	2.00	0.29
Standard Deviation		0.7	0.1	0.031	0.14	0.02
LSDQ 11	82	75.2	10.9	0.080	1.58	0.23
12		74.5	10.8	0.072	1.45	0.21
13		75.2	10.9	0.016	0.90*	0.13*
14		73.8	10.7	0.074	1.31	0.19
15		71.7*	10.4*	0.073	1.79*	0.26*
Average		74.5	10.8	0.075	1.45	0.21
Standard Deviation		0.7	0.1	0.004	0.14	0.02
LSDQ 21	121	30.3	4.4	0.071	0.90	0.13
22		29.6	4.3	0.065	0.76	0.11
23		35.2	5.1	0.045	1.10	0.16
24		31.7	4.6	0.038*	1.24*	0.18*
25		22.1*	3.2*	0.084*	0.69*	0.10*
Average		31.7	4.6	0.060	0.90	0.13
Standard Deviation		2.8	0.4	0.014	0.14	0.02

*Not included in average

TABLE A18

UNION CARBIDE ERX-4901A(MDA) NEAT RESIN TORSION TESTS - MOISTURE-SATURATED

Specimen No.	Test Temperature (°C)	Ultimate Shear Stress (MPa)	Ultimate Shear Stress (ksi)	Ultimate Shear Strain	Shear Modulus (GPa)	Shear Modulus (Msi)
LSWQ 01	23	64.1	9.3	0.053	1.31	0.19*
02		57.9*	8.4*	0.043*	1.52	0.22
03		74.4	10.8	0.081	1.65	0.24
04		75.8	11.0	0.112	2.27*	0.33*
05		80.6	11.7	0.205*	1.79	0.26
06		81.3*	11.8*	0.180*	1.72	0.25
07		72.3	10.5	0.062	1.52	0.22
Average		73.7	10.7	0.077	1.65	0.24
Standard Deviation		6.2	0.9	0.026	0.14	0.02
LSWQ 11	82	6.2	0.9	0.201*	0.07	0.01
12		2.1*	0.3*	0.088	0.07	0.01
13		7.6*	1.1*	0.054*	0.34	0.05
14		5.5	0.8	0.089	0.28	0.04
15		4.1	0.6	0.144	0.07	0.01
16		3.4	0.5	0.140	0.14	0.02
Average		4.8	0.7	0.115	0.16	0.02
Standard Deviation		1.4	0.2	0.031	0.12	0.01
	121	NOT TESTED				

*Not included in average

TABLE A19

CRITICAL ENERGY RELEASE RATES FOR THE HX-1504, 5245-C, CYCOM 907, AND ERX-4901A(MDA) MATRIX MATERIALS, DRY CONDITION

Material System	Specimen No.	Strain Energy Release Rate, G_{IC} (J/m^2)		
		23°C	82°C	121°C
HX-1504	LFDJ 01	467*	688*	225*
	2	477*	--	925*
	3	--	799*	776*
	4	473*	1007*	63
	5	152	661	842
	6	355	508	934*
	Average	253	600	727
	Standard Deviation	--	--	--
5245-C	LFDO 01	462	289	340
	2	422	322	606*
	3	527	547*	176
	4	1255*	803*	824*
	5	978*	282	728*
	6	607*	--	683
	Average	470	298	258
	Standard Deviation	53	21	--
CYCOM 907	LFDP 01	1070	3944*	4615
	2	1544	9920*	25861*
	3	1486	3081	46964*
	4	3444*	3970*	14990*
	5	1075	3389	11282*
	6	1290	3388	14621*
	Average	1293	3286	4615
	Standard Deviation	222	178	--
ERX-4901A(MDA)	LFDQ 01	1248*	973	26320*
	2	115*	459	17940*
	3	146	1293*	17502*
	4	406	1022*	568
	5	1772*	1016*	1513
	6	880*	--	24038*
	Average	275	716	1040
	Standard Deviation	--	--	--

*Not included in average

TABLE A20

CRITICAL ENERGY RELEASE RATES FOR THE HX-1504, 5245-C, CYCOM 907, AND ERX-4901A(MDA) MATRIX MATERIALS, MOISTURE-SATURATED CONDITION

Material System	Specimen No.	Strain Energy Release Rate, G_{IC} (J/m^2)		
		23°C	82°C	121°C
HX-1504	LFWJ 01	918	2243*	2119
	2	812	1264	3211
	3	772	863	4509
	4	902	639	7790*
	5	610	1250	5587*
	6	969*	1485	7679*
	Average	803	1100	3280
	Standard Deviation	124	341	1196
5245-C	LFWO 01	2325*	5265*	2837
	2	1954*	3949*	2704
	3	460	768	1433
	4	1309*	2467*	4283*
	5	724	6671*	7176*
	6	2586*	796	14503*
	Average	592	782	2325
	Standard Deviation	--	--	775
CYCOM 907	LFWP 01	6659*	80054*	#
	2	2594	131843*	
	3	4638*	47108	
	4	3606*	231456*	
	5	2914	202282*	
	6	3013	--	
	Average	2840	47108	
	Standard Deviation	219	--	
ERX-4901A(MDA)	LFWQ 01	3573*	15516*	#
	2	2098	19652*	
	3	1761	7593*	
	4	2098	23790*	
	5	1663	2690	
	6	1147	1610	
	Average	1753	2150	
	Standard Deviation	392	--	

*Not included in average

#Not measured

APPENDIX B

Individual Stress-Strain Curves for the Various Neat Resin Test Specimens

HEXCEL 1504 EPOXY 23C DRY TENSION

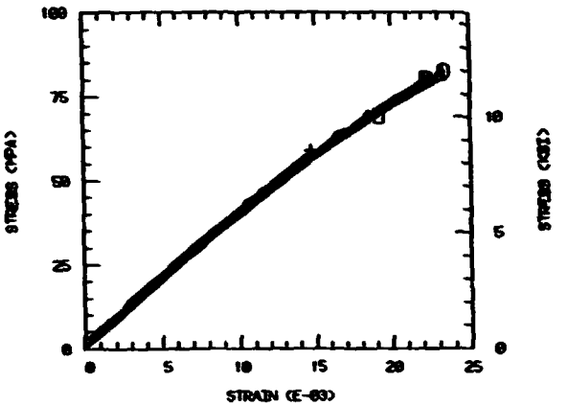

HEXCEL 1504 EPOXY 82C DRY TENSION

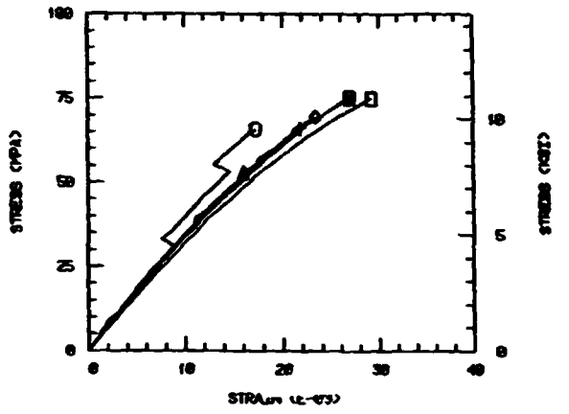

HEXCEL 1534 EPOXY 121C DRY TENSION

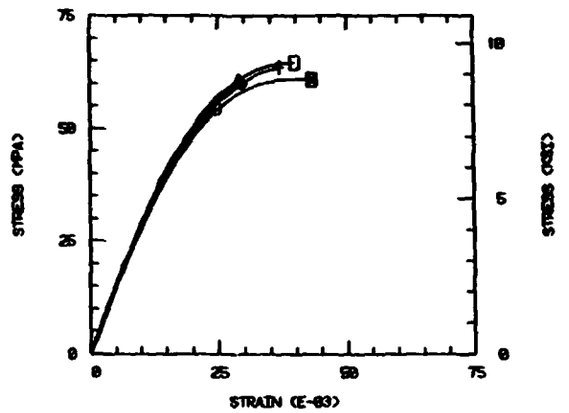

HEXCEL 1504 EPOXY 23C WET TENSION

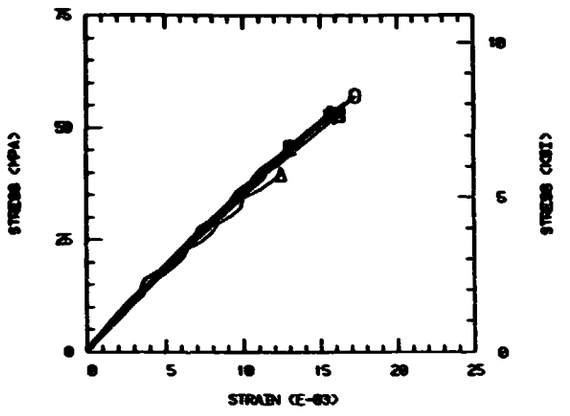

HEXCEL 1504 EPOXY 82C WET TENSION

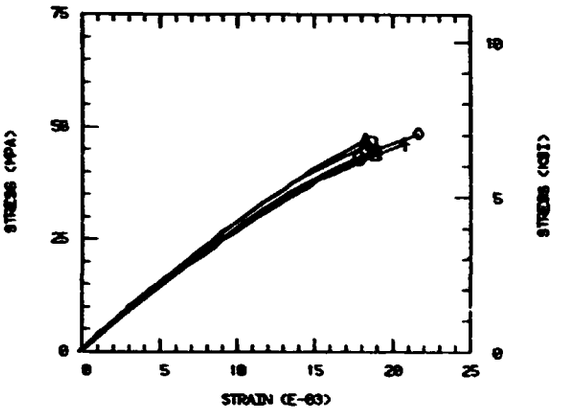

HEXCEL 1504 EPOXY 121C WET TENSION

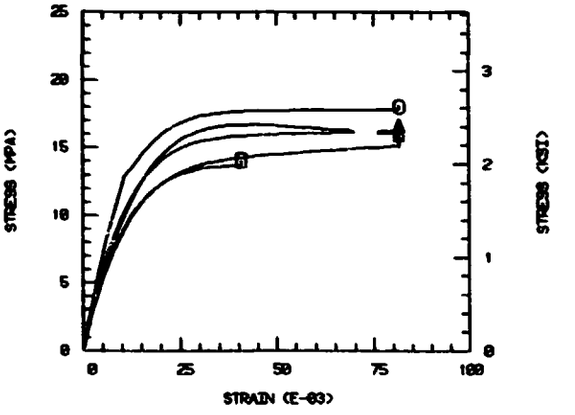

HEXCEL 1504 EPOXY 23C DRY TORSION SHEAR

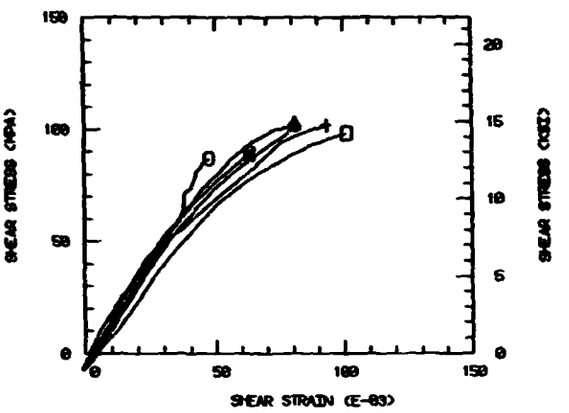

HEXCEL 1504 EPOXY 82C DRY TORSION SHEAR

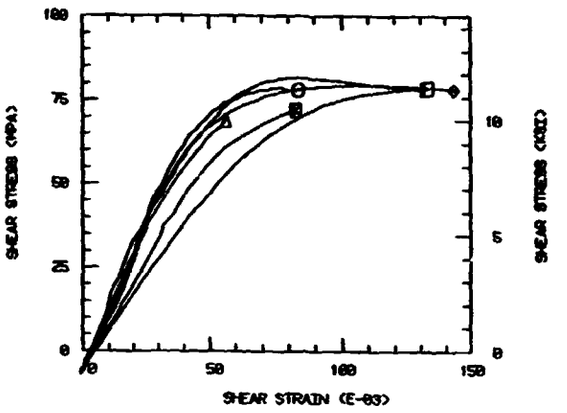

HEXCEL 1504 EPOXY 121C DRY TORSION SHEAR

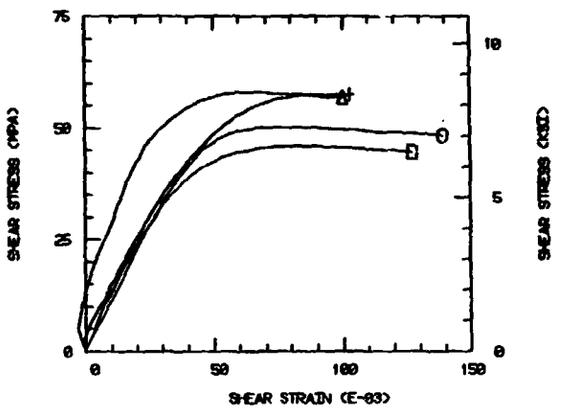

HEXCEL 150 ' EPOXY 23C WET SHEAR

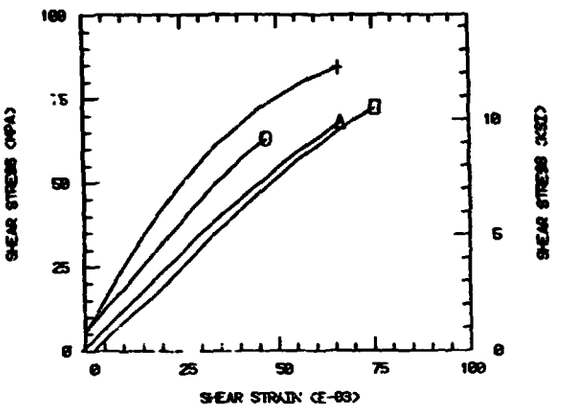

HEXCEL 1504 EPOXY 82C WET SHEAR

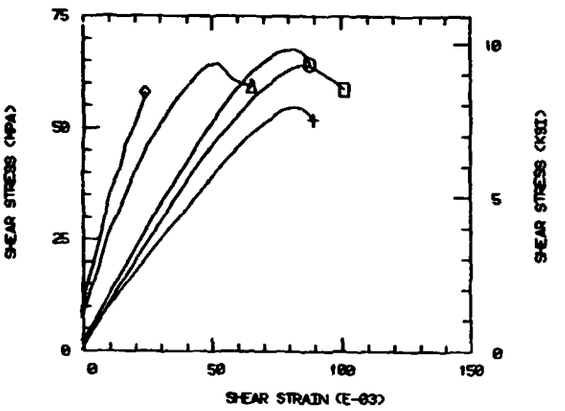

HEXCEL 1504 EPOXY 121C WET SHEAR

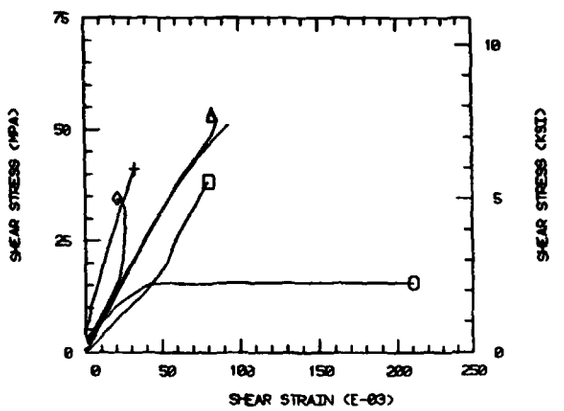

NARMCO 5245-C 23C DRY TENSION

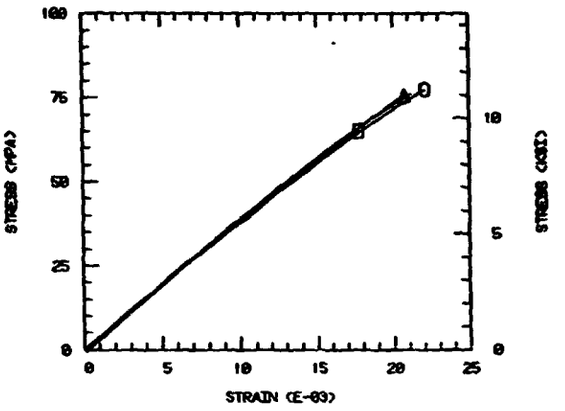

NARMCO 5245-C 82C DRY TENSION

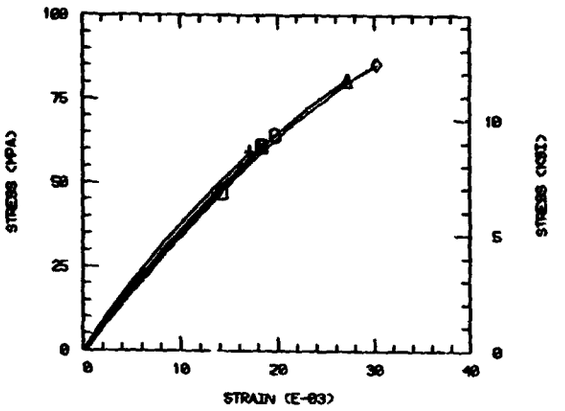

NARMCO 5245-C 121C DRY TENSION

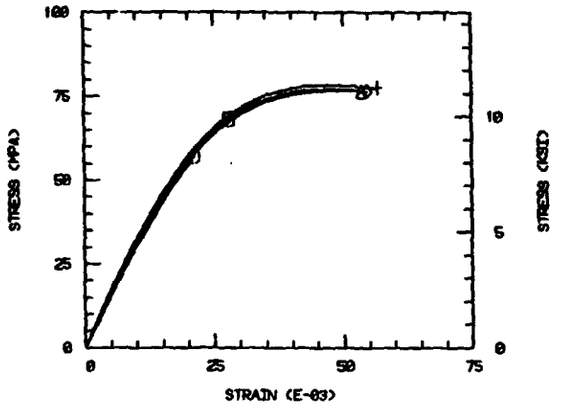

NARMCO 5245-C 23C WET TENSION

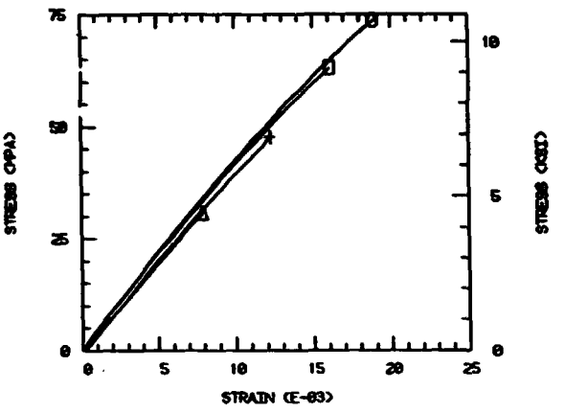

NARMCO 5245-C 82C WET TENSION

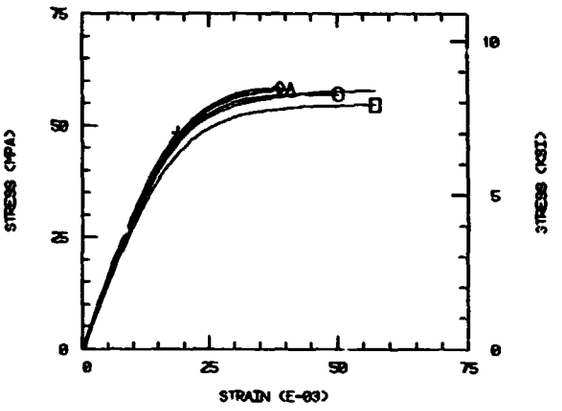

NARMCO 5245-C 121C WET TENSION

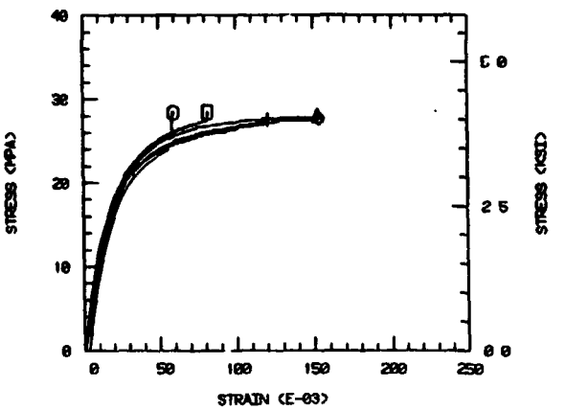

NARMCO 5245-C 23C DRY TORSION SHEAR

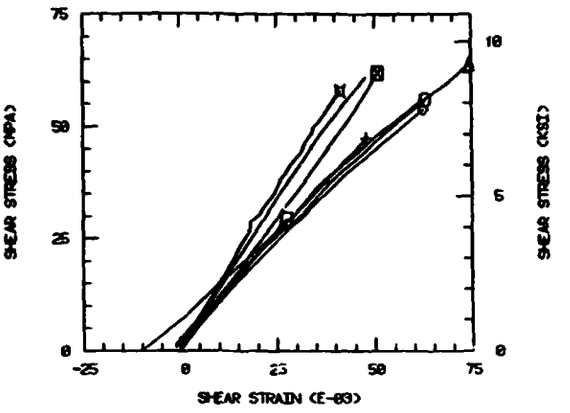

NARMCO 5245-C 82C DRY TORSION SHEAR

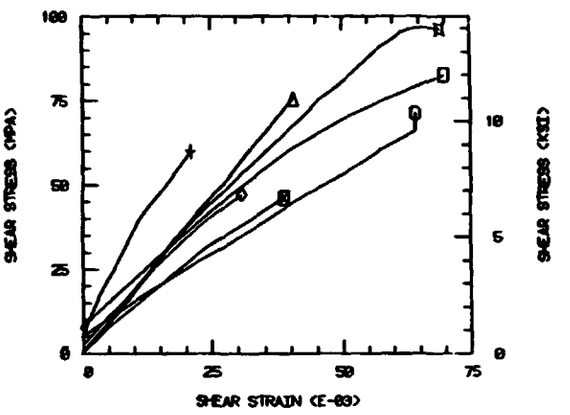

NARMCO 5245-C 121C DRY TORSION SHEAR

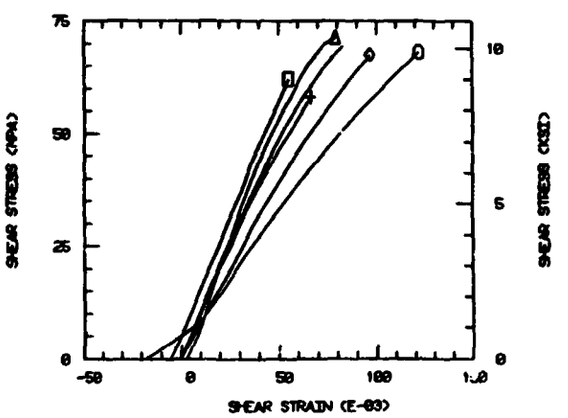

NARMCO 5245-C 23C WET TORSION SHEAR

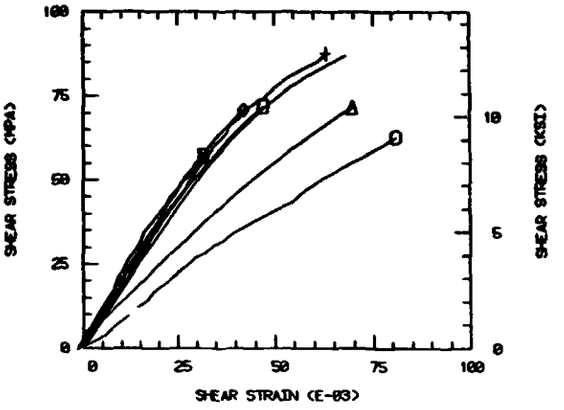

NARMCO 5245-C 82C WET TORSION SHEAR

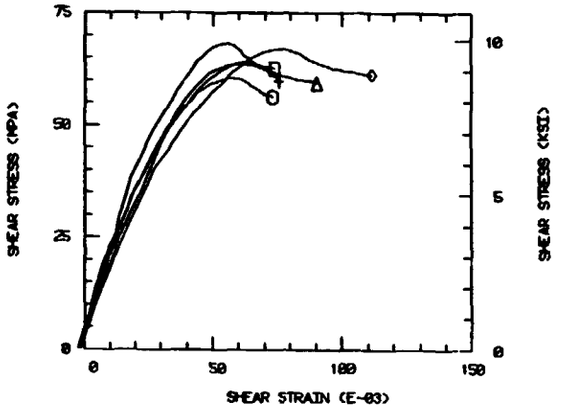

NARMCO 5245-C 121C WET TORSION SHEAR

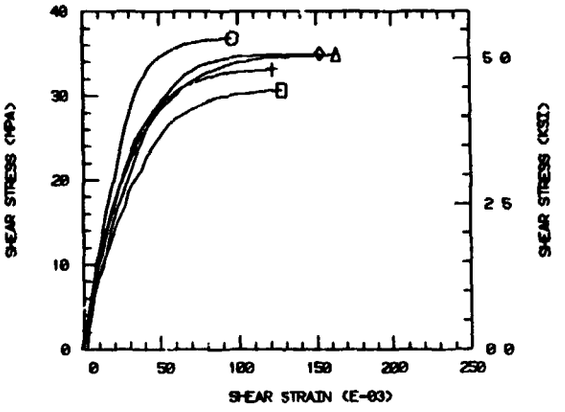

CYCOM 907 EPOXY 23C DRY TENSION

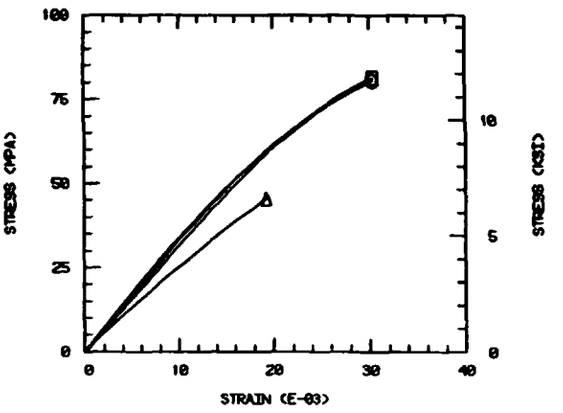

CYCOM 907 EPOXY 82C DRY TENSION

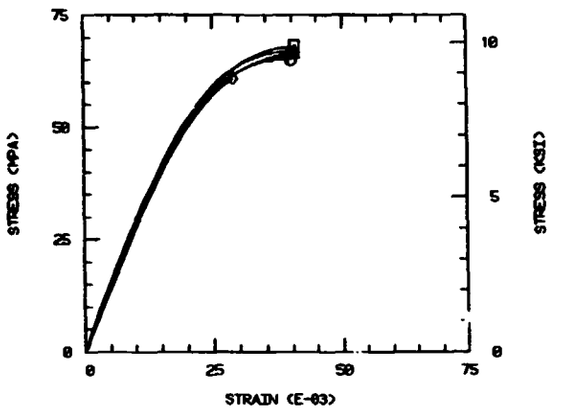

CYCOM 907 EPOXY 121C DRY TENSION

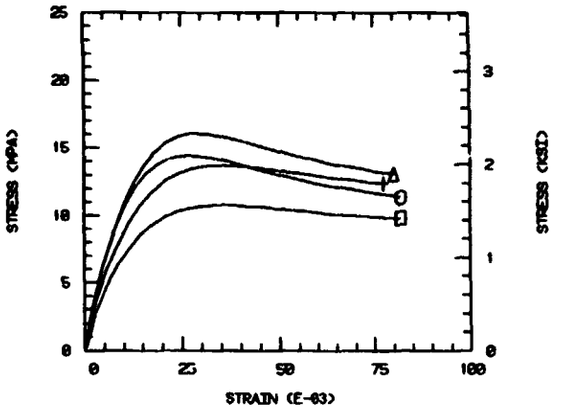

CYCOM 907 EPOXY 23C WET TENSION

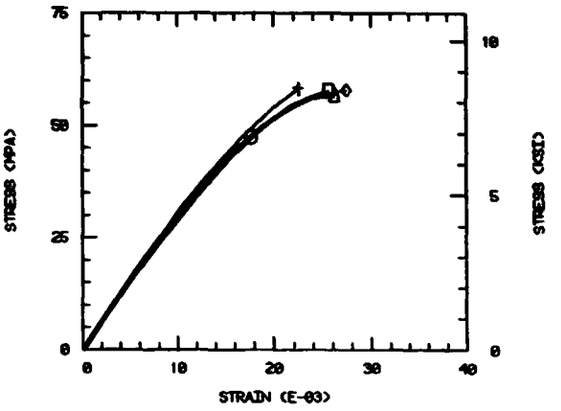

CYCOM 907 EPOXY 82C WET TENSION

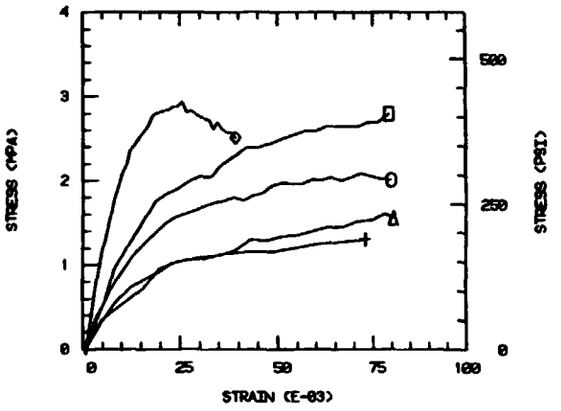

CYCOM 907 EPOXY 23C DRY IOSIPESCU SHEAR

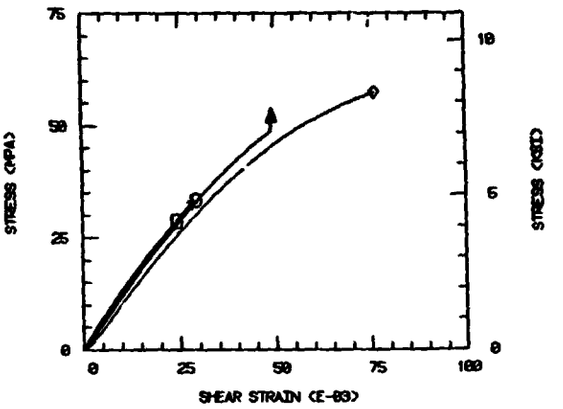

CYCOM 907 EPOXY 82C DRY IOSIPESCU SHEAR

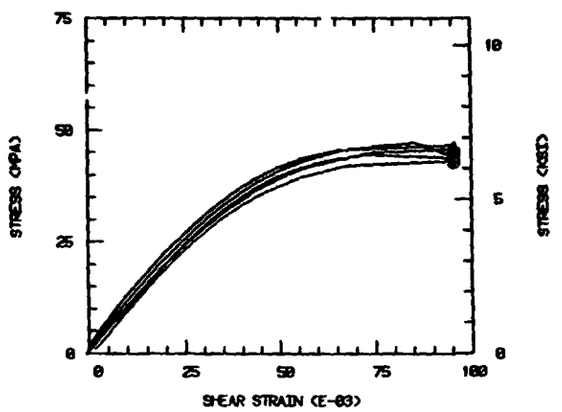

CYCOM 907 EPOXY 121C DRY IOSIPESCU SHEA

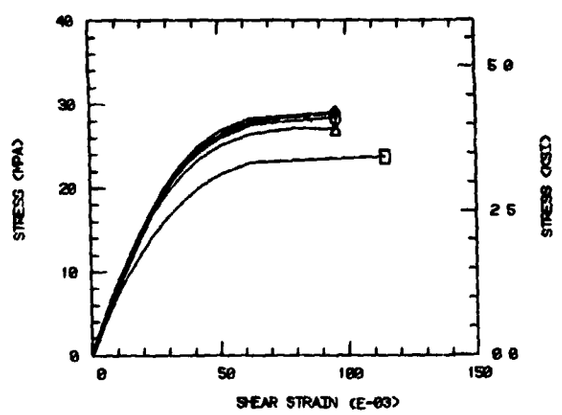

CYCOM 907 EPOXY 23C WET IOSIPESCU SHEAR

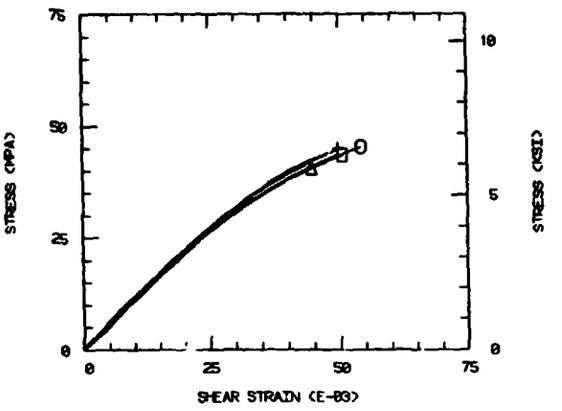

CYCOM 907 EPOXY 82C WET IOSIPESCU SHEAR

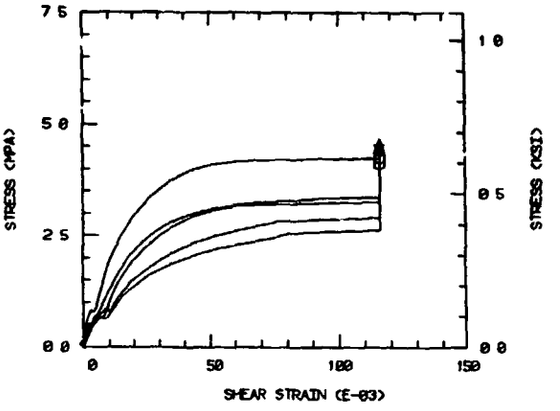

UNION CARBIDE ERX-4901A 23C DRY TENSION

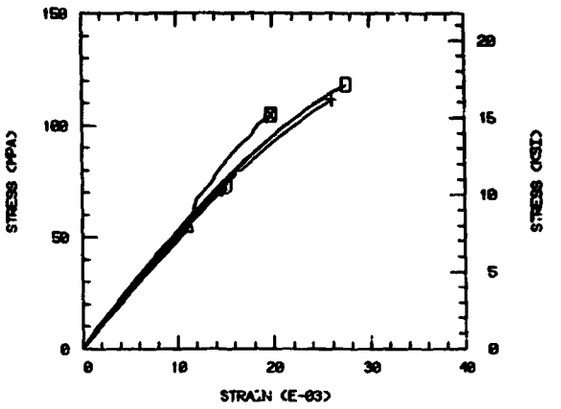

UNION CARBIDE ERX-4901A 82C DRY TENSION

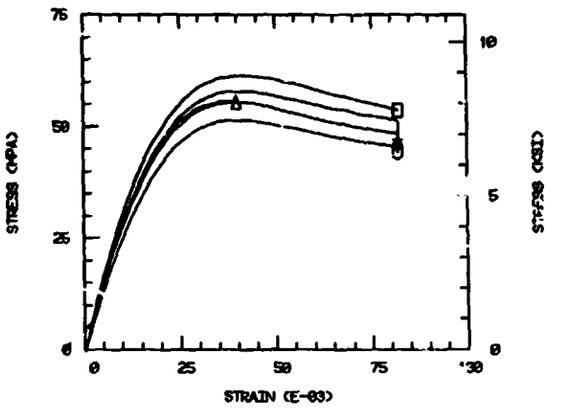

UNION CARBIDE ERX-4901A 121C DRY TENSION

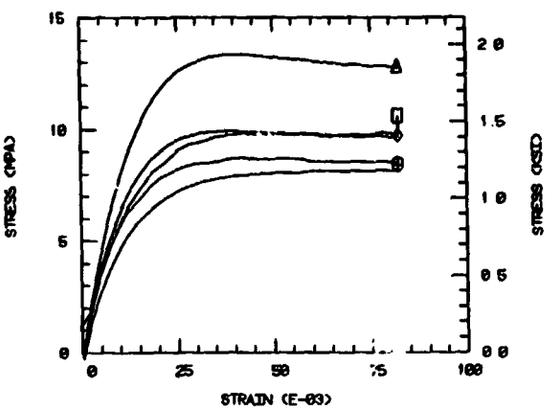

UNION CARBIDE ERX-4901A 23C DRY TENSION

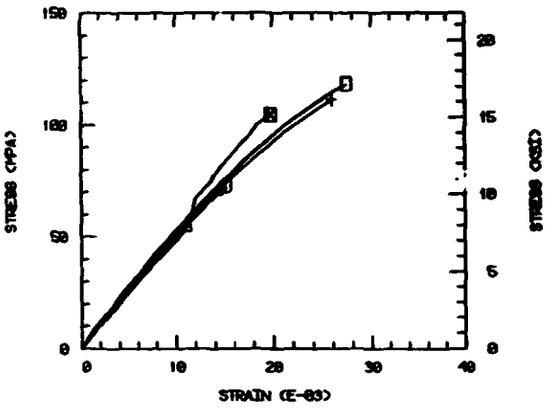

UNION CARBIDE ERX-4901A 82C WET TENSION

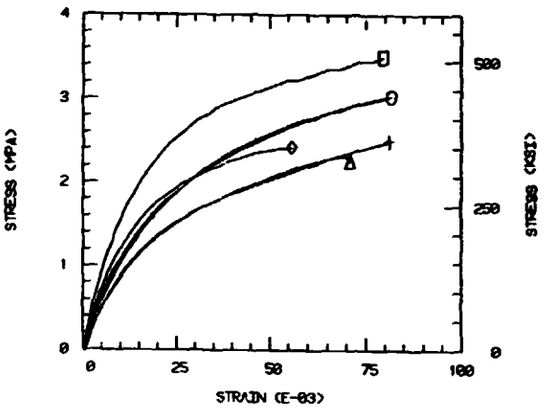

UNION CARBIDE ERY-4901A 23C DRY SHEAR

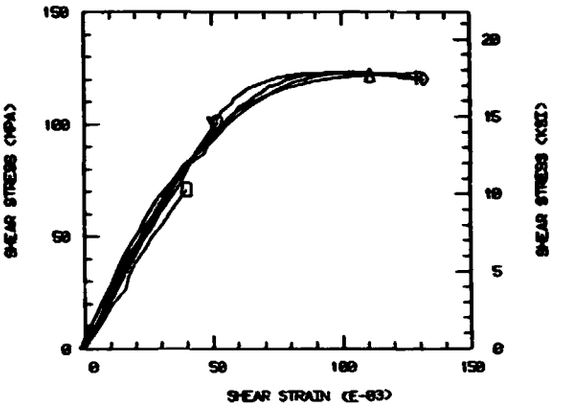

UNION CARBIDE ERX-4901A 82C DRY SHEAR

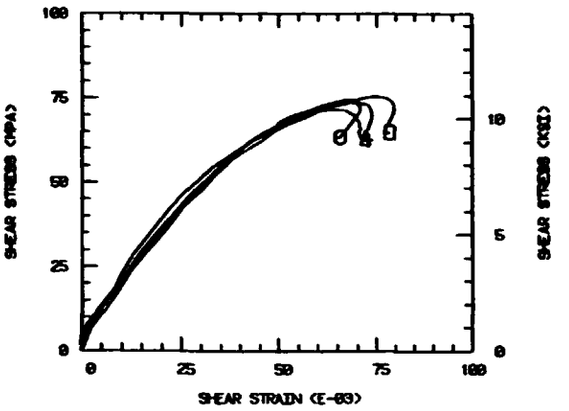

UNION CARBIDE ERX-4901A 121C DRY SHEAR

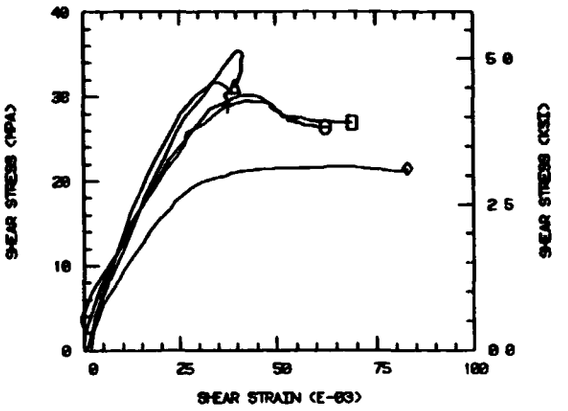

UNION C. . IDE ERX-4901A 23C WET SHEAR

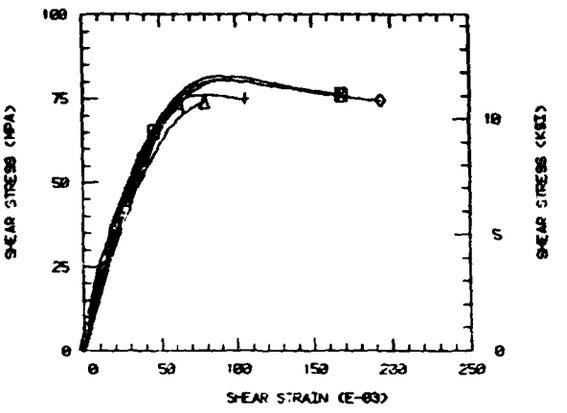

UNION CARBIDE ERX-4901A 82C WET SHEAR

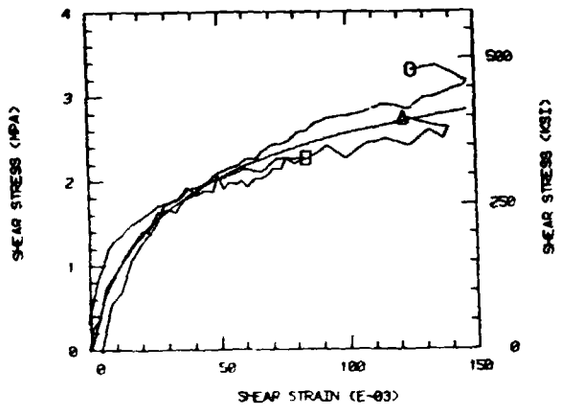

3502 EPOXY 121C DRY TENSION

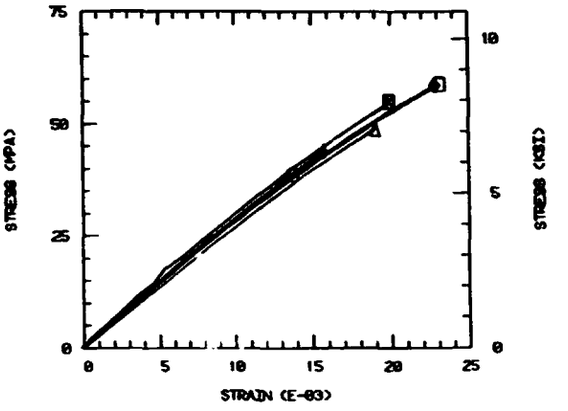

FIBREDUX 914 EPOXY 121C DRY TENSION

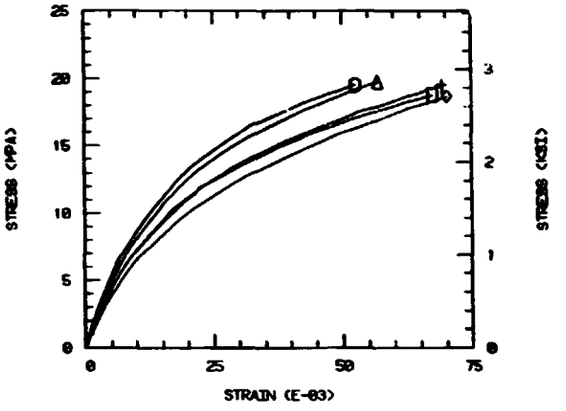

2220-1 EPOXY 121C DRY TENSION

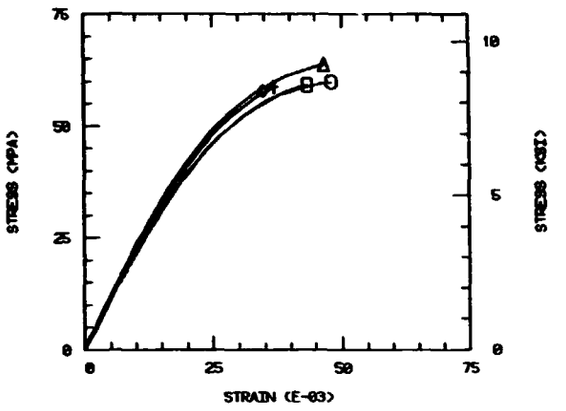

2220-3 EPOXY 121C DRY TENSION

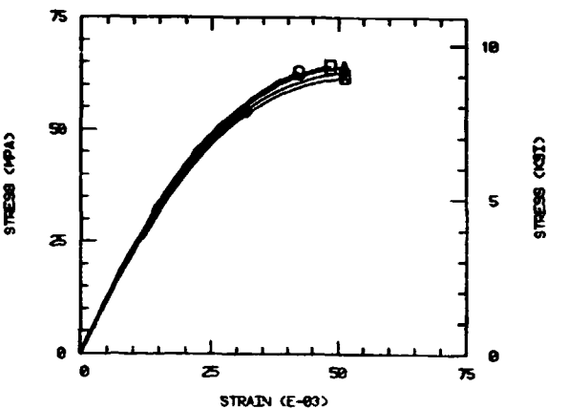

APPENDIX C

Fracture Surfaces of the Various Neat Resin Fracture Toughness Specimens

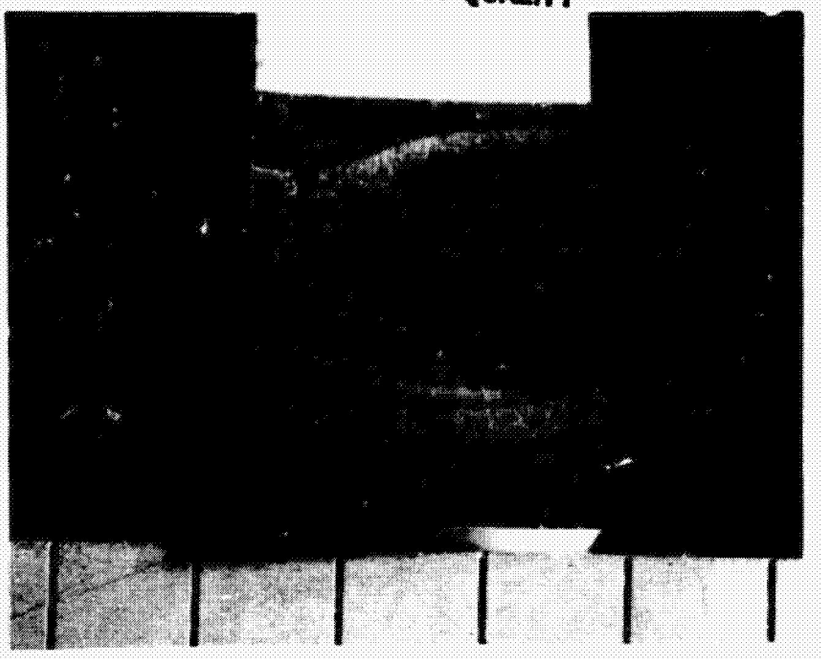

Figure C1. Hexcel HX-1504 Epoxy Fracture Toughness Specimen No. LFDJ01, 23°C, Dry.

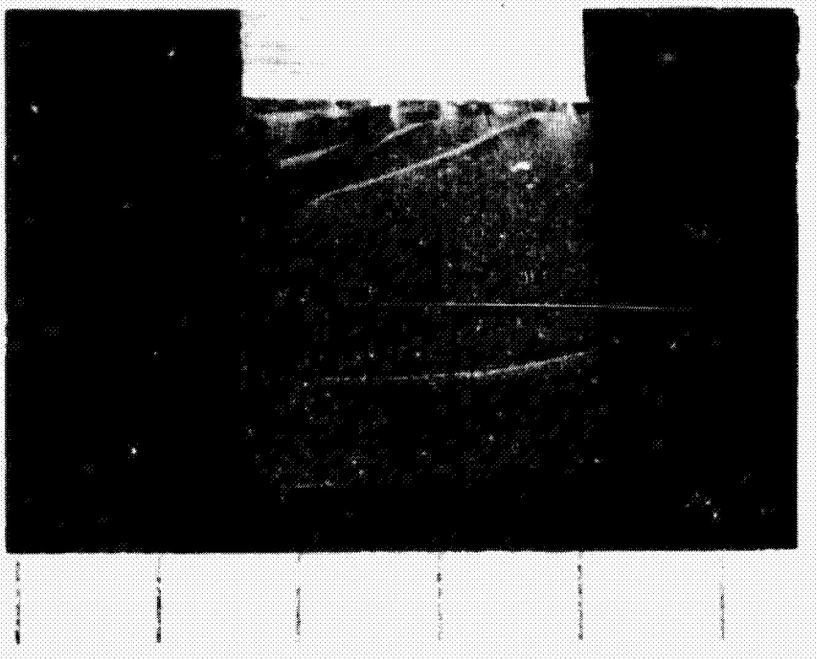

Figure C2. Hexcel HX-1504 Epoxy Fracture Toughness Specimen No. LFDJ16, 82°C, Dry.

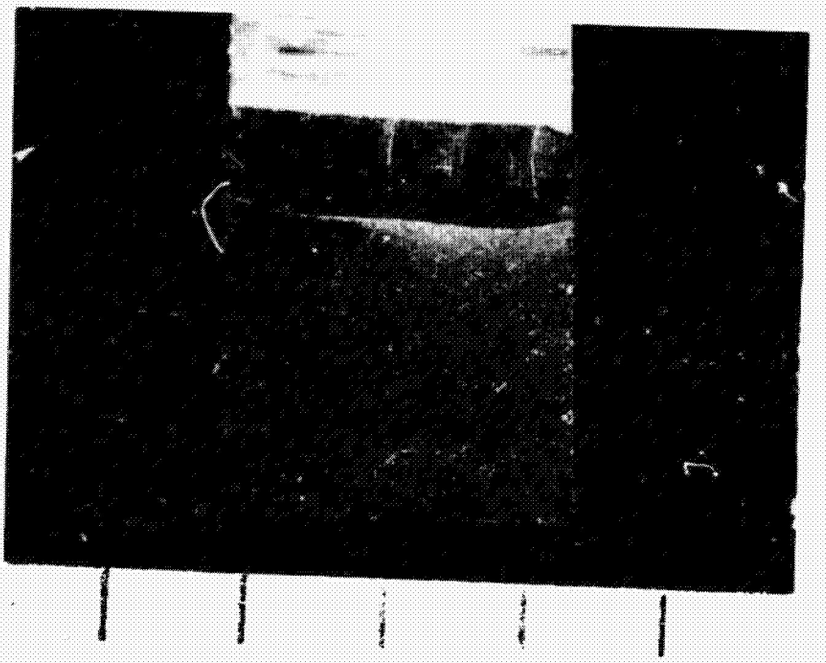

Figure C3. Hexcel HX-1504 Epoxy Fracture Toughness Specimen No. LFDJ25, 121°C, Dry.

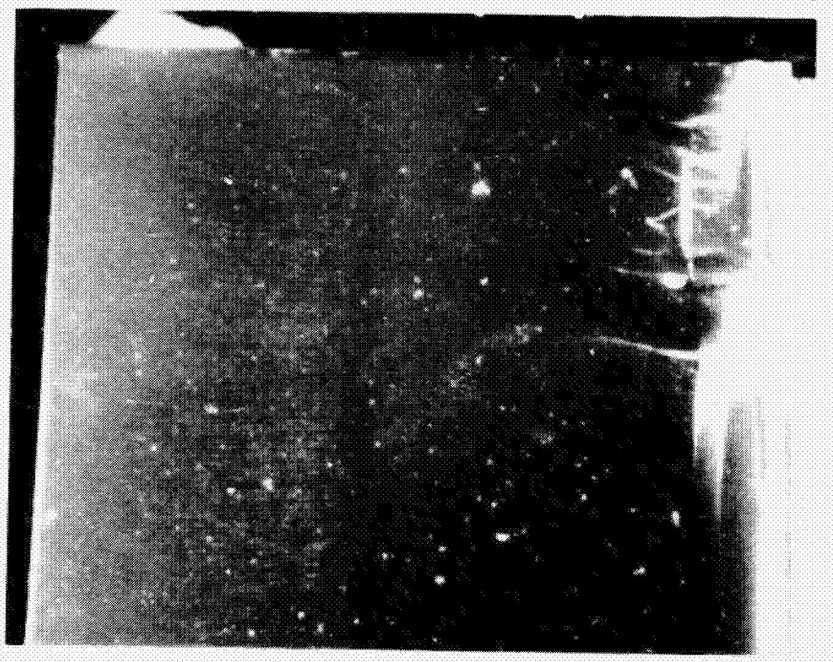

Figure C4. Narmco 5245-C Bismaleimide/Epoxy Fracture Toughness Specimen No. LFD002, 23°C, Dry.

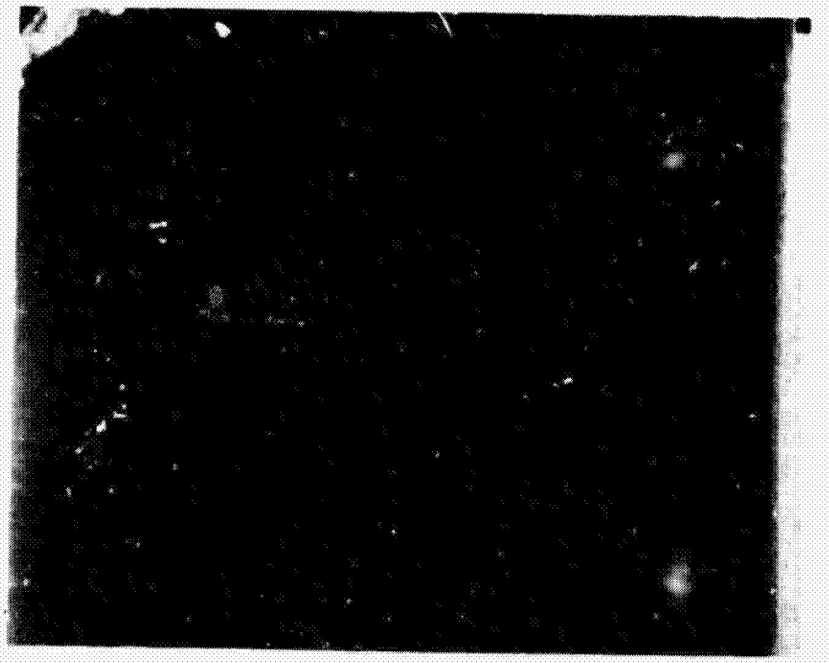

Figure C5. Narmco 5245-C Bismaleimide/Epoxy Fracture Toughness Specimen No. LFD016, 82°C, Dry.

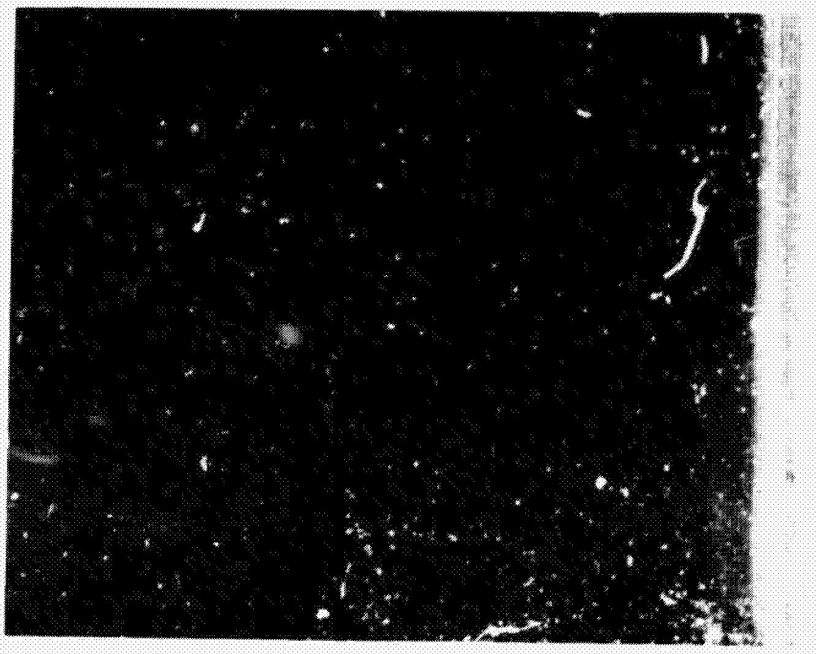

Figure C6. Narmco 5245-C Bismaleimide/Epoxy Fracture Toughness Specimen No. LFD023, 121°C, Dry.

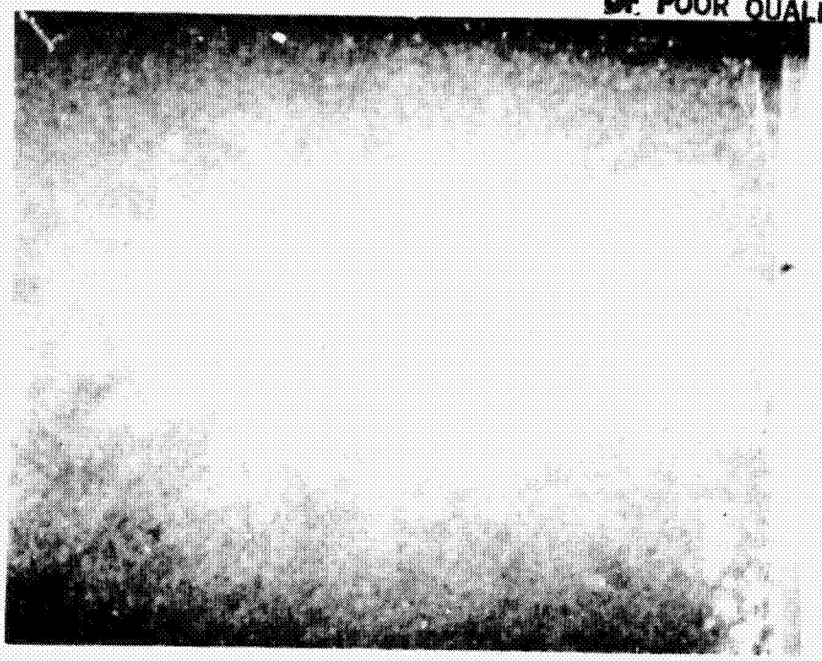

Figure C7. CYCOM 907 Epoxy Fracture Toughness Specimen No. LFDP01, 23°C, Dry.

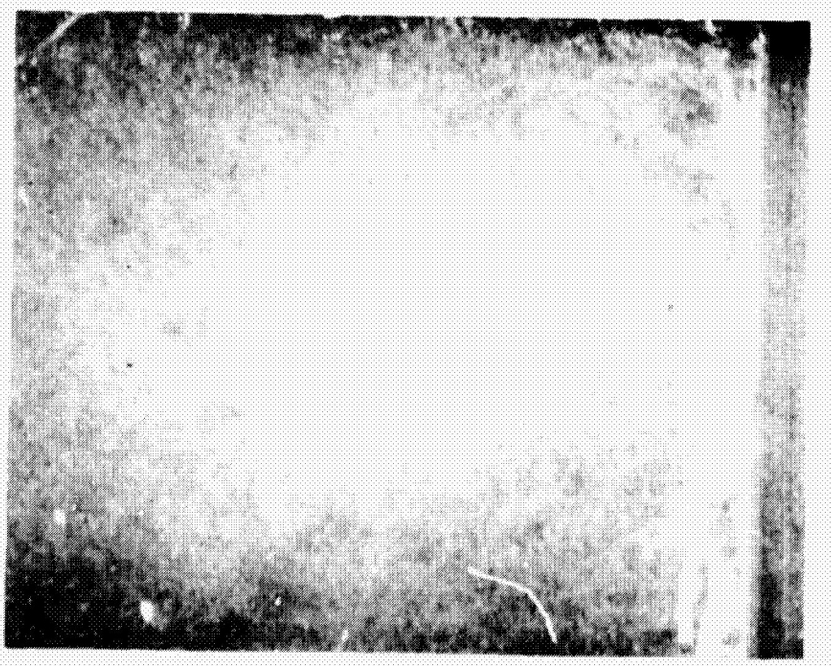

Figure C8. CYCOM 907 Epoxy Fracture Toughness Specimen No. LFDP13, 82°C, Dry.

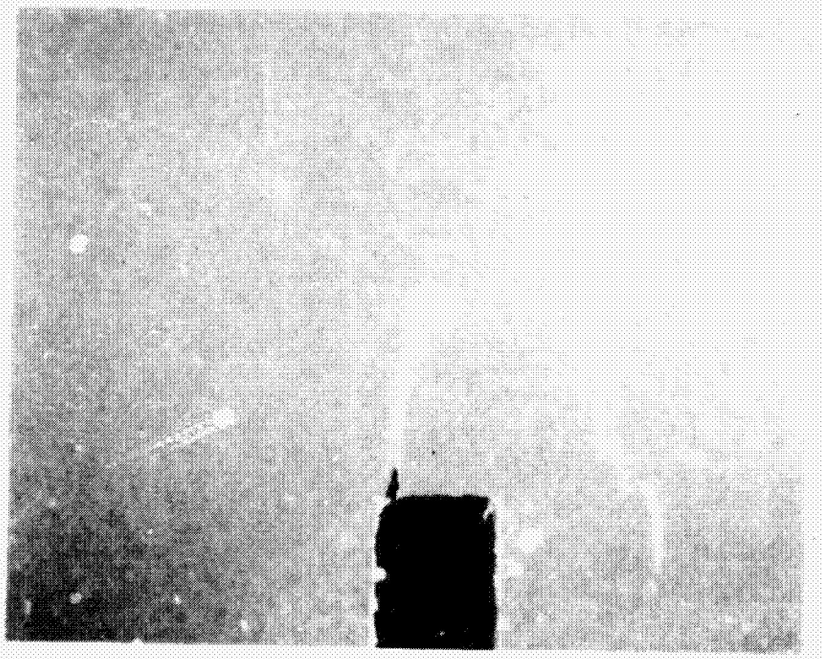

Figure C9. CYCOM 907 Epoxy Fracture Toughness Specimen No. LFDP25, 121°C, Dry (Side View of Notch Root).

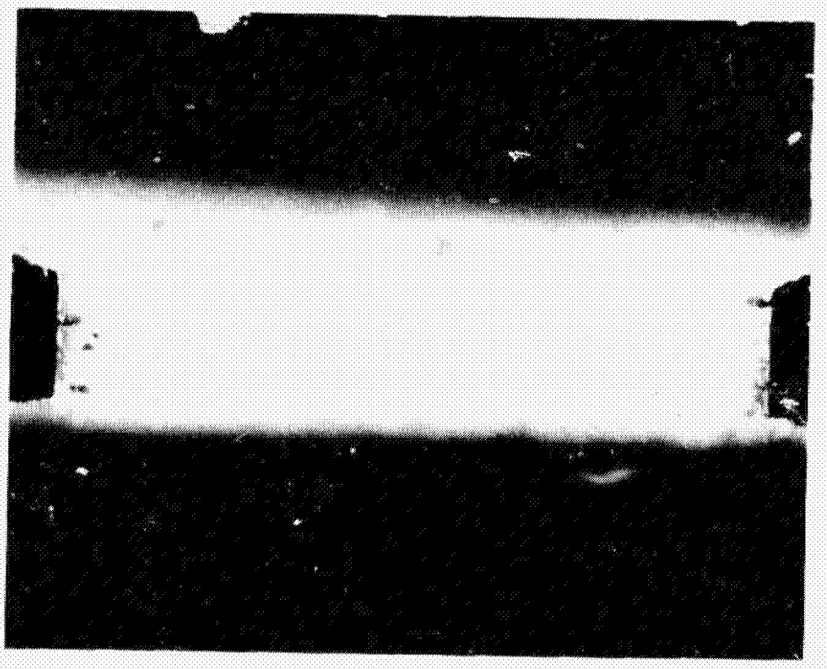

Figure C10. CYCOM 907 Epoxy Fracture Toughness Specimen No. LFDP25, 121°C, Dry (Looking Down the Sawcut Notch at the Razor Blade Cut).

Figure C11. ERX-4901A(MDA) Epoxy Fracture Toughness Specimen No. LFD003, 23°C, Dry.

Figure C12. ERX-4901A(MDA) Epoxy Fracture Toughness Specimen No. LFD012, 82°C, Dry.

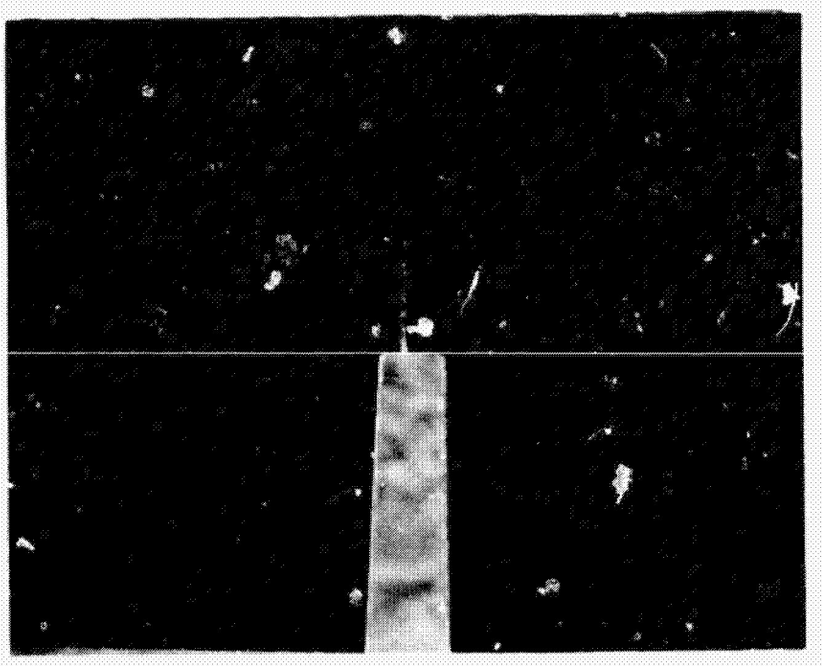

Figure C13. ERX-4901A(MDA) Epoxy Fracture Toughness Specimen No. LFDQ2, 121°C, Dry (Side View of Notch Root).

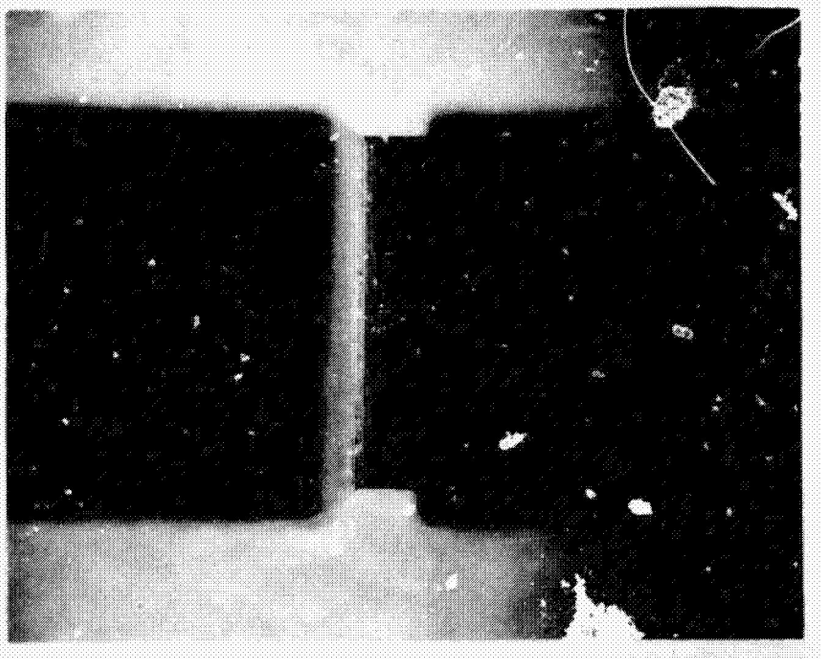

Figure C14. ERX-4901A(MDA) Epoxy Fracture Toughness Specimen No. LFDQ2, 121°C, Dry (Looking Down the Sawcut Notch at the Razor Blade Cut).

APPENDIX D

Scanning Electron Microphotographs of Fracture Surfaces of the Various Neat Resin Systems

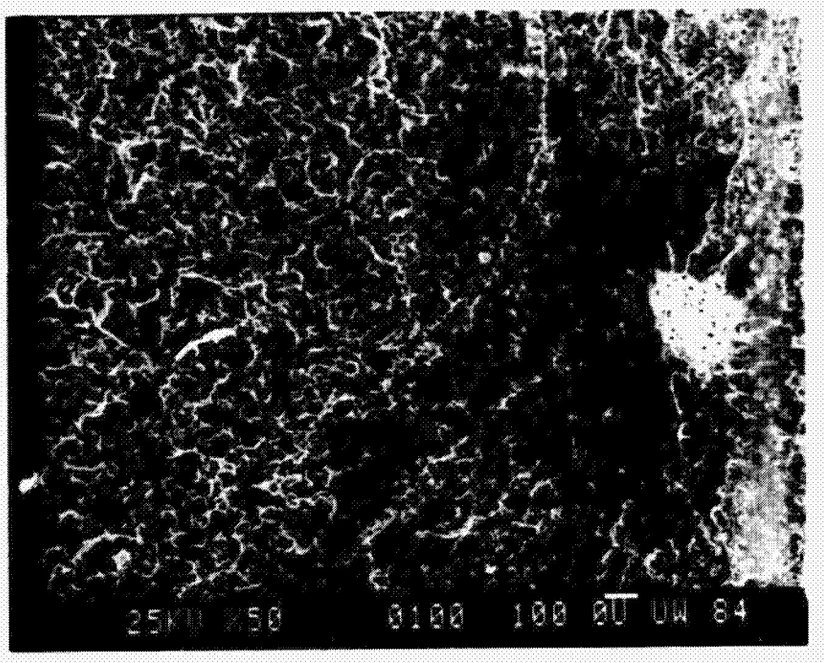

Figure D1. Hexcel HX-1504 Epoxy Tension Specimen No. LTDJ26, 82°C, Dry.

This SEM photograph shows an overall view of the initiation site, a small (smooth) transition region, and the surrounding rough region.

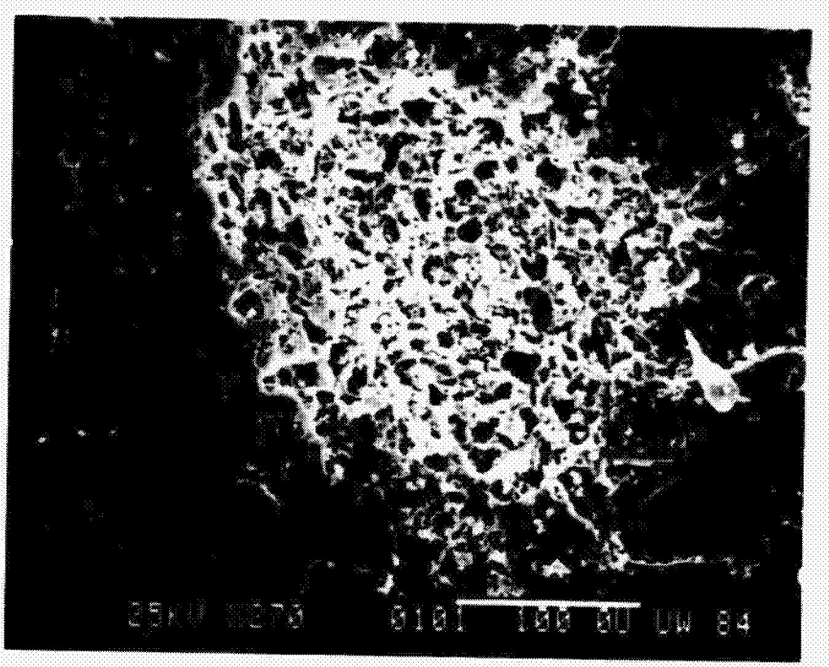

Figure D2. Hexcel HX-1504 Epoxy Tension Specimen No. LTDJ26, 82°C, Dry.

This close-up of Figure D1 shows the initiation site to be a large collection of voids in the epoxy.

Figure D3. Hexcel HX-1504 Epoxy Tension Specimen No. LTWJ32, 121°C, Moisture-Saturated.

This photograph is an overall view of the fracture surface, with no apparent initiation site, the whole surface being relatively rough.

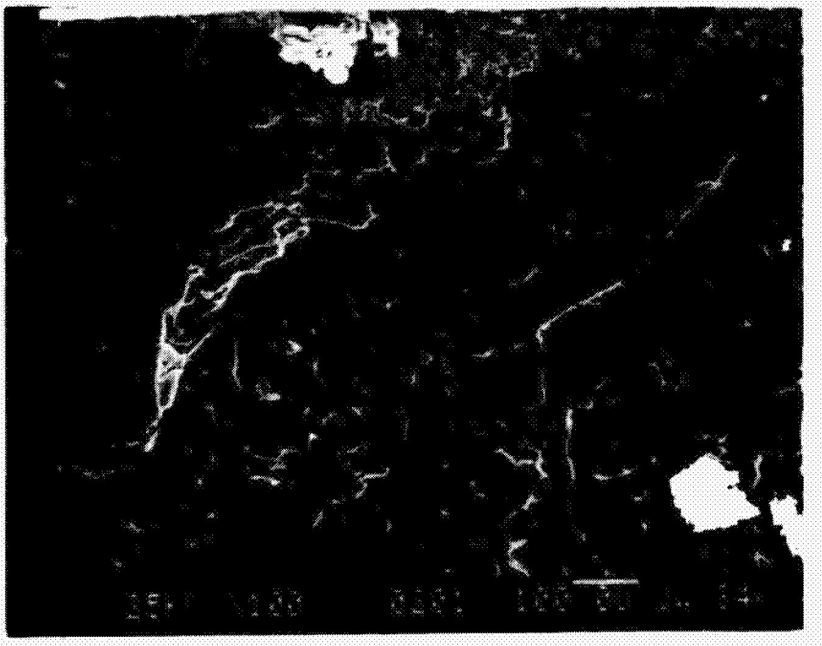

Figure D4 . Hexcel HX-1504 Epoxy Tension Specimen No. LTWJ32, 121°C, Moisture-Saturated.

This close-up of Figure D3 shows an area on the surface of the specimen where failure could have begun. The flaking and rough appearance of the surrounding region will be noted, suggesting the void formation was due to the coallescing of smaller defects in the specimen.

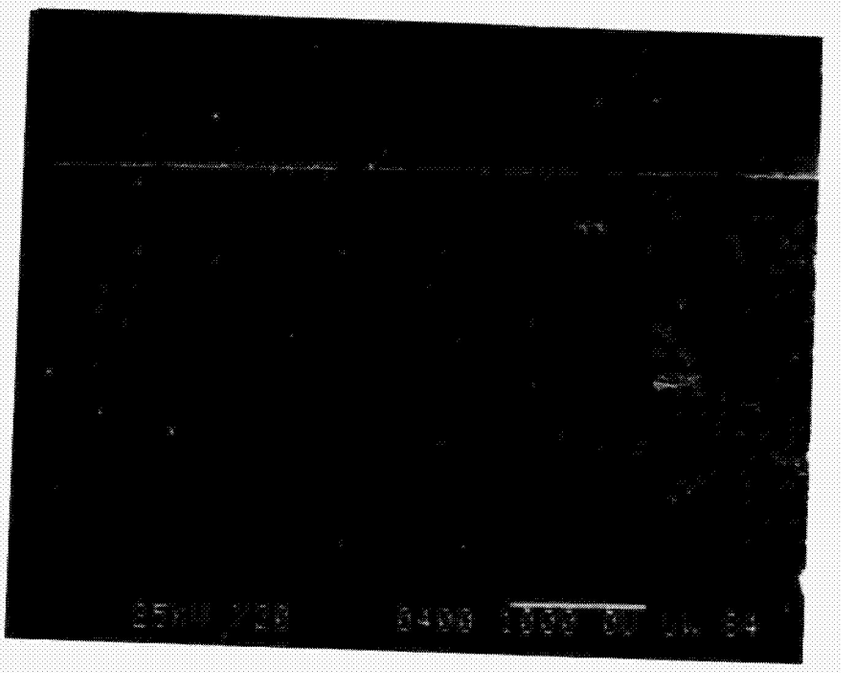

Figure D5. Narmco 5245-C Bismaleimide/Epoxy Tension Specimen No. LTD024, 121°C, Dry.

This SEM photograph shows the failure initiation zone and transition region, surrounded by a not so coarse rough region.

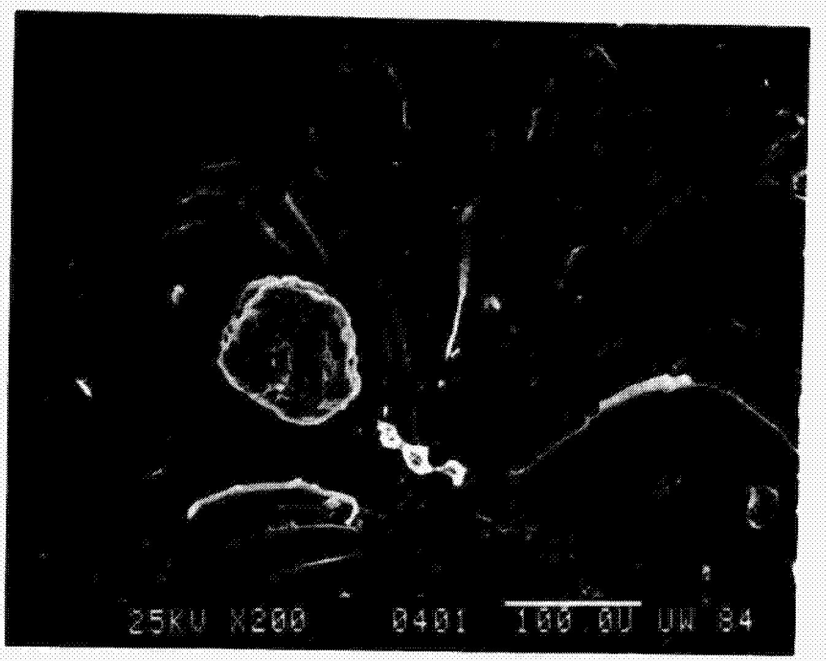

Figure D6. Narmco 5245-C Bismaleimide/Epoxy Tension Specimen No. LTD024, 121°C, Dry.

This close-up of the initiation site of Figure D5 shows some flaking evident, but no apparent inclusion present to cause the failure. A dust particle on the surface is seen to the upper left of the failure initiation site.

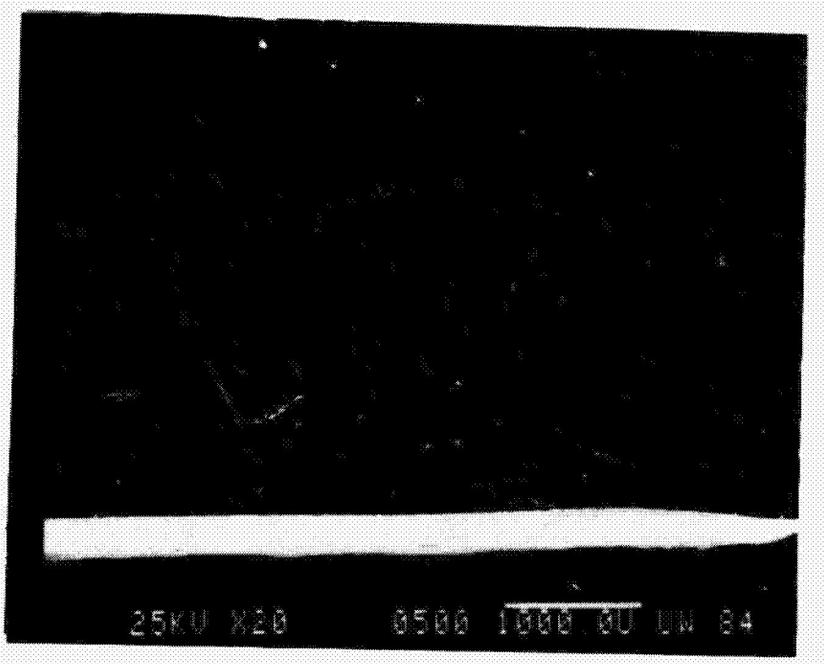

Figure D7. Narmco 5245-C Bismaleimide/Epoxy Tension Specimen No. LTW023, 121°C, Moisture-Saturated.

This overall view of the failure plane shows a slightly coarser surface than observed in the dry specimens, and a larger flaking appearance.

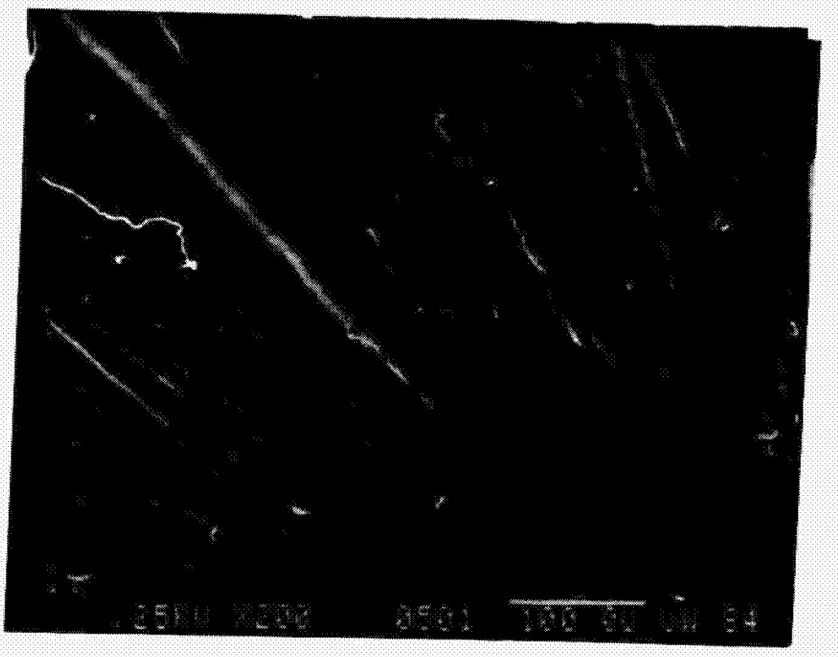

Figure D8. Narmco 5245-C Bismaleimide/Epoxy Tension Specimen No. LTW023, 121°C, Moisture-Saturated.

This close-up of Figure D7 shows no inclusion at the apparent failure initiation site. No coalesced voids are present but the flaky appearance of the surface is quite evident.

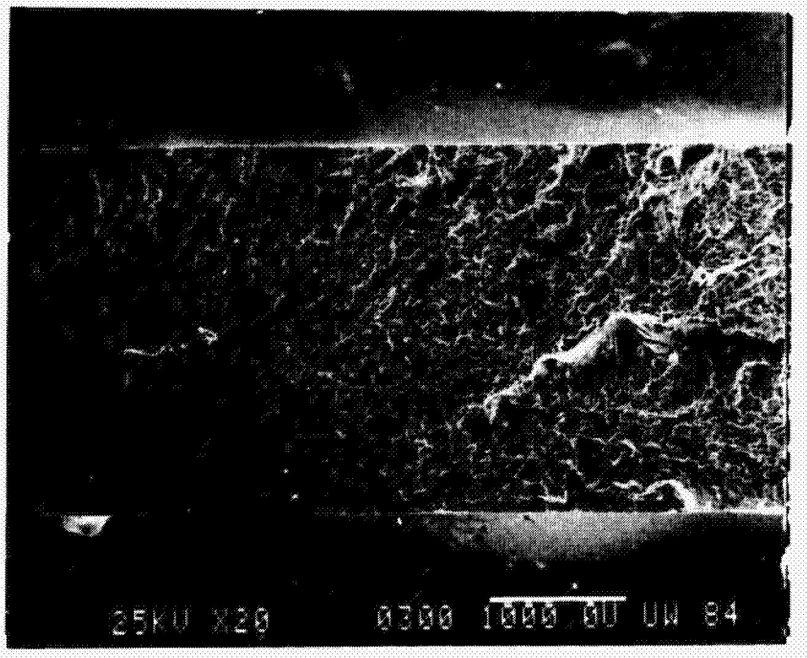

Figure D9. CYCOM 907 Epoxy Tension Specimen No. LTDP05, 23°C, Dry.

An initiation site is apparent near the lower left corner of the specimen. The remainder of the specimen surface appears fairly rough.

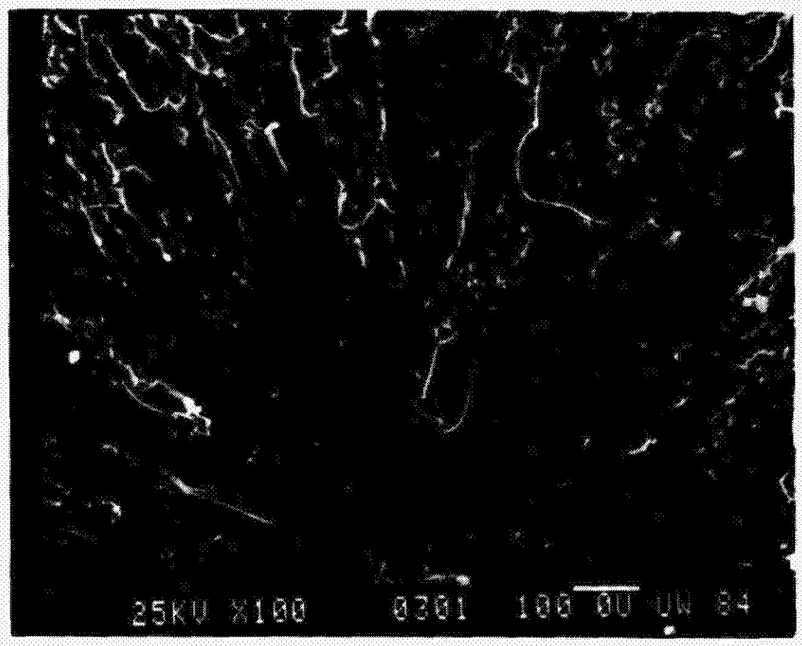

Figure D10. CYCOM 907 Epoxy Tension Specimen No. LTDP05, 23°C, Dry.

This close-up of Figure D9 shows a very small transition area around a particle near the surface of the specimen. The flaky appearance also seen in Figure D4 is apparent and a small number of coalesced voids can be identified.

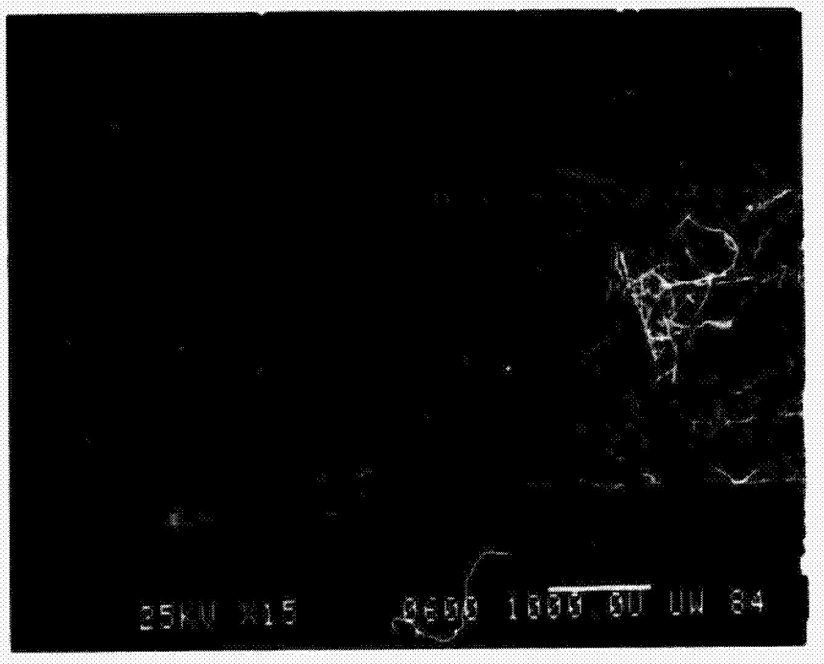

Figure D11. CYCOM 907 Epoxy Tension Specimen No. LTWP05, 23°C, Moisture-Saturated.

This photograph is similar to the dry tensile specimen shown in Figure D5, but appears less rough. The initiation region is near the lower left corner of the specimen. The light colored fibrous material in the upper right is debris on the surface.

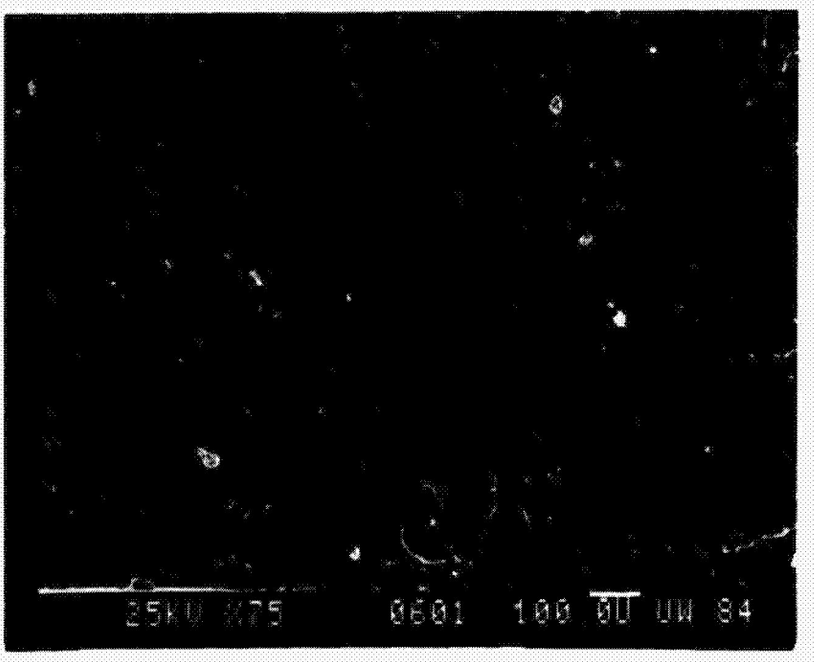

Figure D12. CYCOM 907 Epoxy Tension Specimen No. LTWP05, 23°C, Moisture-Saturated.

This close-up of the initiation site of Figure D11 shows no apparent feature which caused the failure. More voids and less prominent flaky regions are seen when compared to the dry specimen for this resin system (see Figure D10).

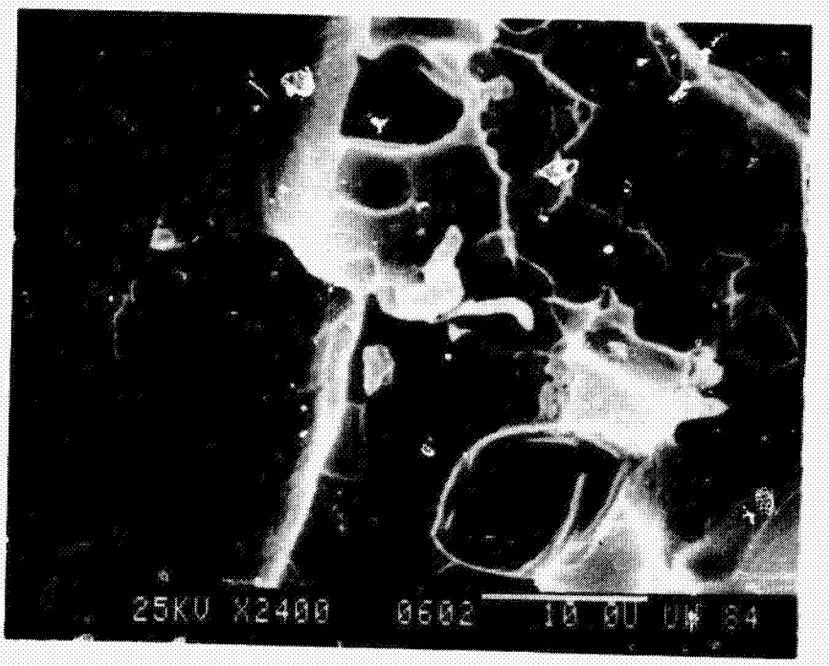

Figure D13. CYCOM 907 Epoxy Tension Specimen No. LTWPC5, 23°C, Moisture-Saturated.

This higher magnification of a typical region of voids in Figure D12 shows that these holes could have been formed by the opening of much smaller defects, or by a coalescing of numerous small defects.

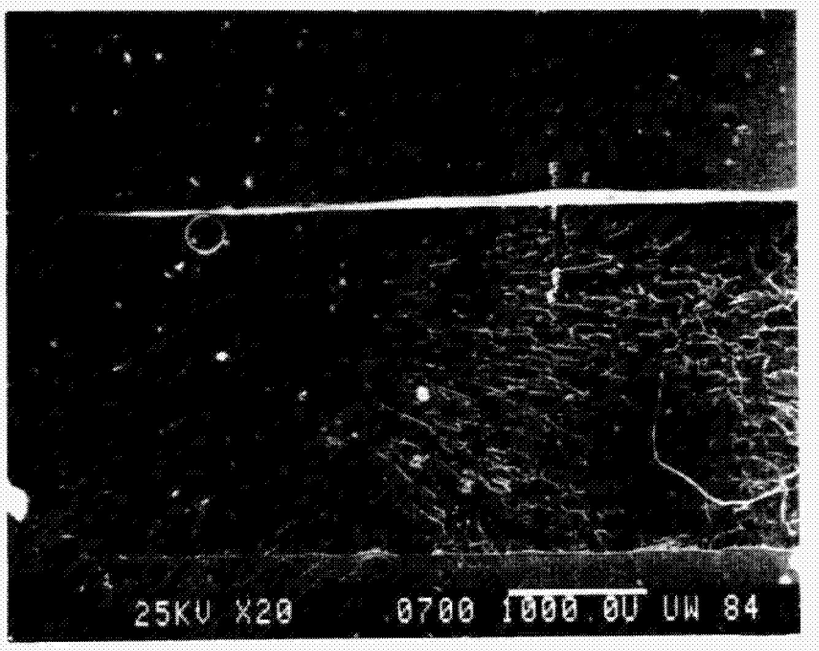

Figure D14. ERX-4901A (MDA) Epoxy Tension Specimen No. LTDQ15, 82°C, Dry.

This overall view shows a spherical particle at the failure initiation site, and a double transition zone from smooth to rough before the gross rough region was created.

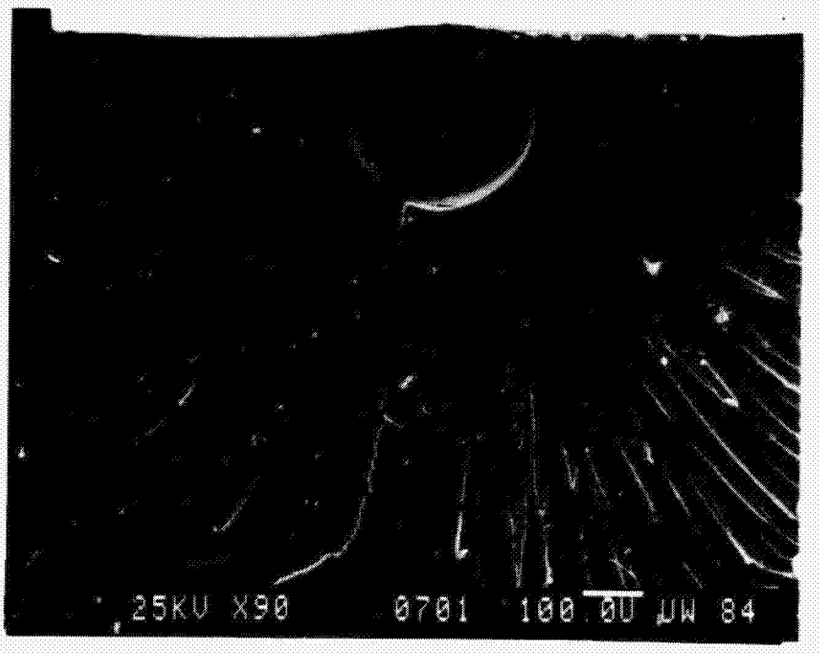

Figure D15. ERX-4901A(MDA) Epoxy Tension Specimen No. LTDQ15, 82°C, Dry.

This close-up of the spherical particles of Figure D14 shows some flaking appearing surrounding the particle. The particle is probably an undissolved crystal of curing agent.

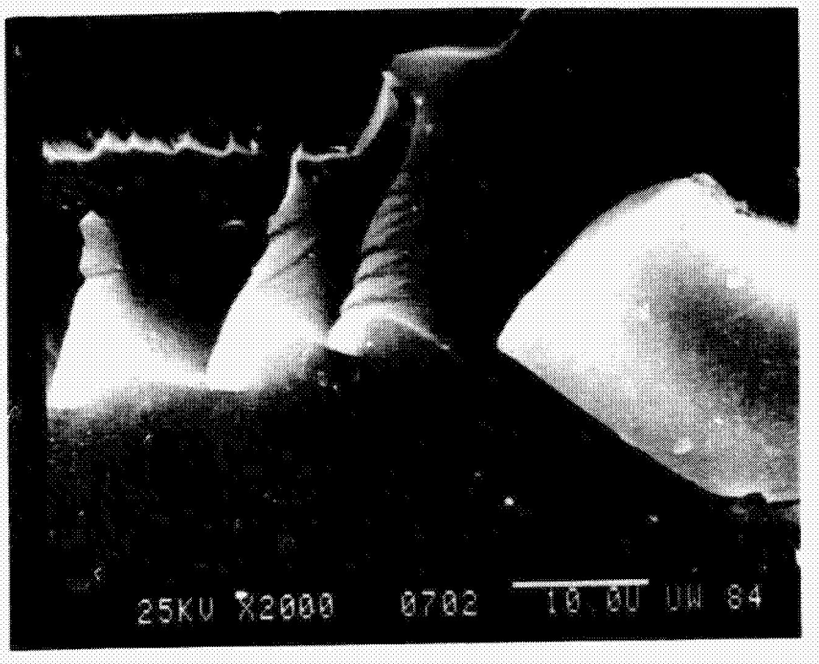

Figure D16. ERX-4901A(MDA) Epoxy Tension Specimen No. LTDQ15, 82°C, Dry.

This close-up of the flaking transition region of Figure D15 shows the scalloped surface and crack. It indicates that the flaking region is more of a scalloped surface, where the resin fails by crack propagation and arrest, and then jumps to a different area which must be weaker than the bulk resin surrounding it.

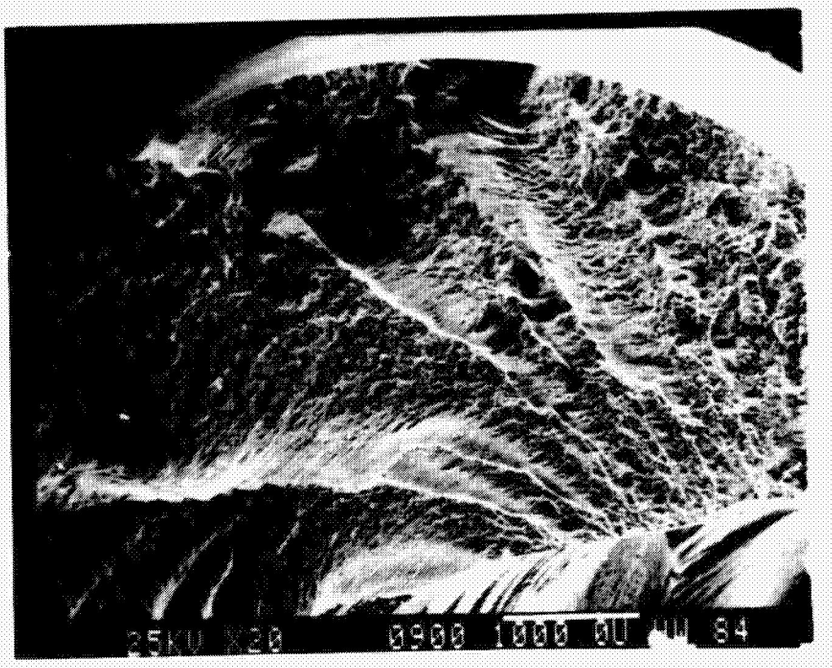

Figure D17. Hexcel HX-1504 Torsion Specimen No. LSDJ24, 121°C, Dry.

This overall view of the shear fracture surface shows the similarity in appearance with the tensile fracture for this resin as seen in Figures D1 and D3.

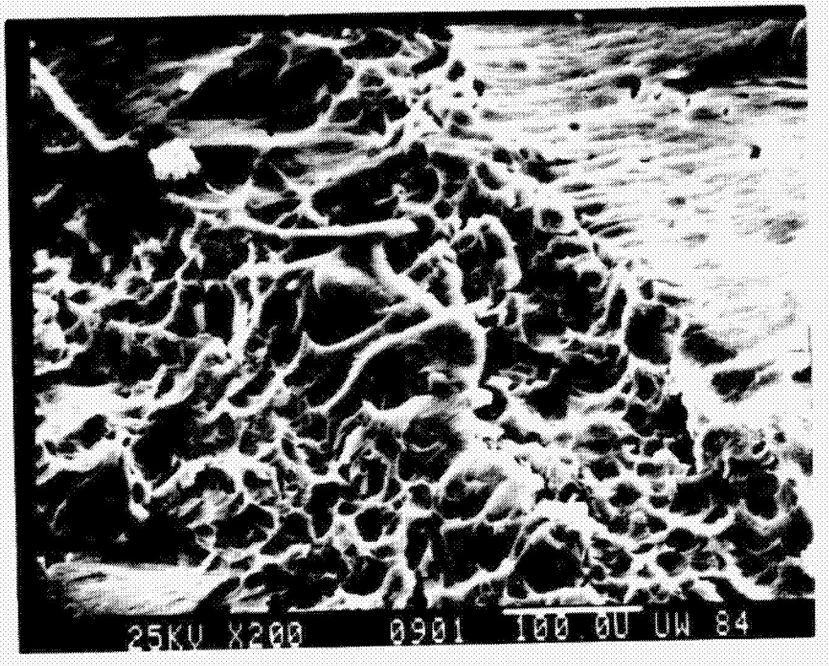

Figure D18. Hexcel HX-1504 Torsion Specimen No. LSDJ24, 121°C, Dry.

This close-up of a local region of Figure D17 shows small flakes and possibly a group of coalesced voids in the specimen, which may have contributed to the failure.

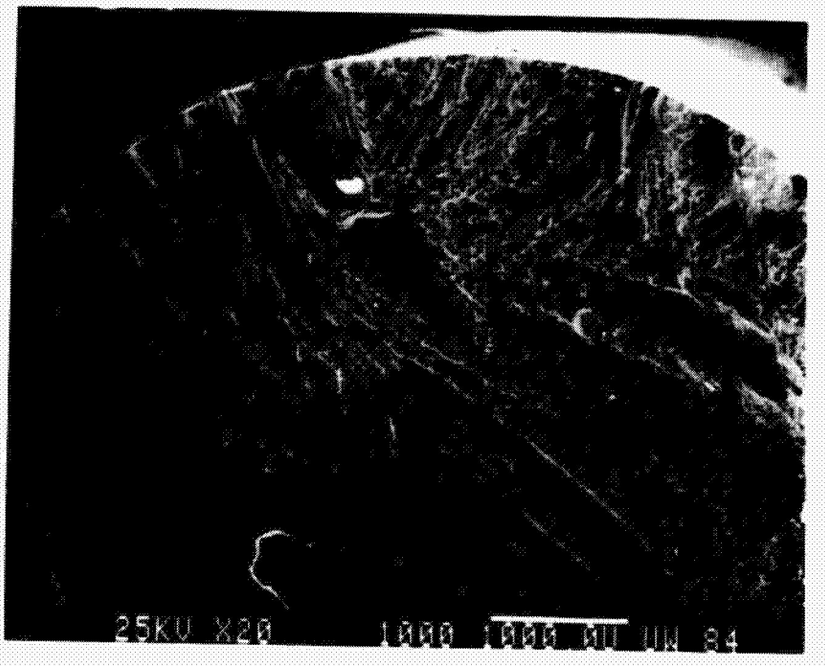

Figure D19. Hexcel HX-1504 Torsion Specimen No. LSWJ22, 121°C, Moisture-Saturated.

This overall view appears very similar to the fracture surface seen in Figure D3 for this same resin system, although perhaps slightly less coarse.

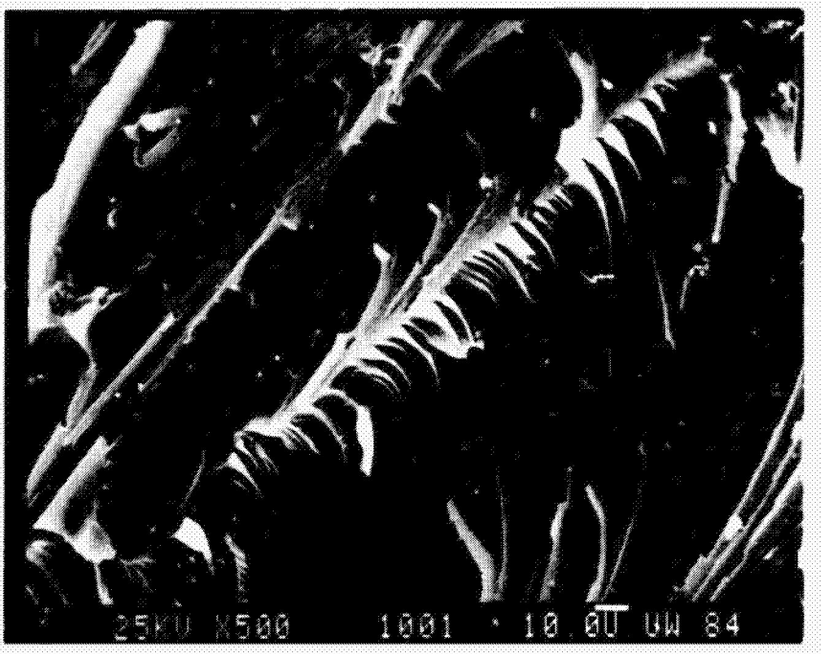

Figure D20. Hexcel HX-1504 Torsion Specimen No. LSWJ22, 121°C, Moisture-Saturated.

This close-up of Figure D19 shows the scalloped ridges seen in some previous tensile failures also.

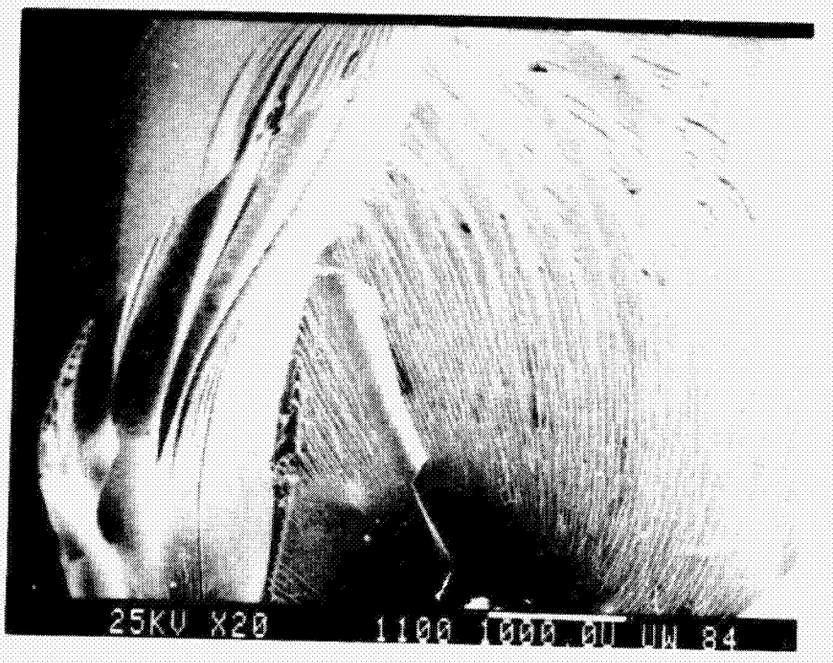

Figure D21. Narmco 5245-C Bismaleimide/Epoxy Torsion Specimen No. LSD005, 23°C, Dry.

This photograph shows the swirl pattern seen in many torsional failures of neat resin.

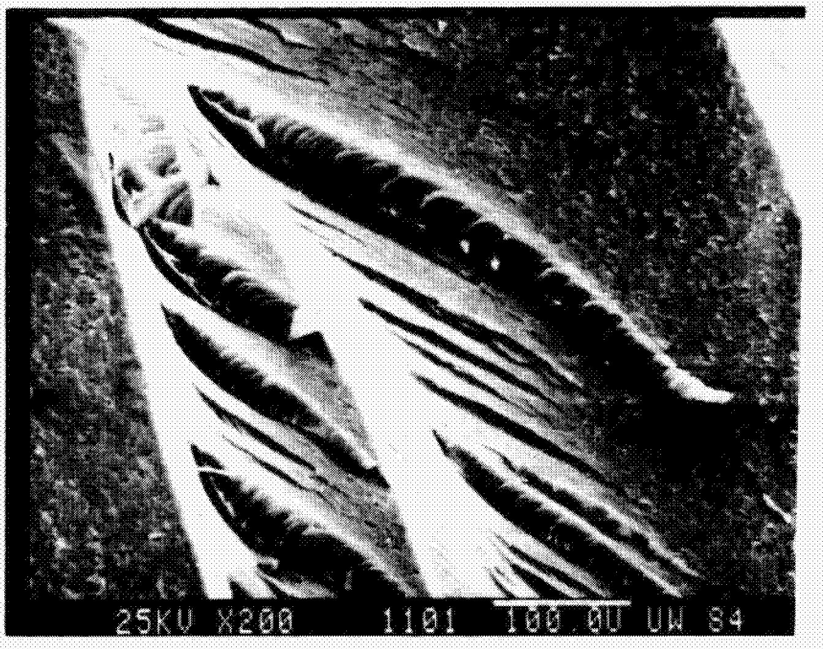

Figure D22. Narmco 5245-C Bismaleimide/Epoxy Torsion Specimen No. LSD005, 23°C, Dry.

This close-up of a region of the swirl pattern of Figure D21 shows some cracking and flaking present from the torsion failure.

Figure D23. Narmco 5245-C Bismaleimide/Epoxy Torsion Specimen No. LSW011, 82°C, Moisture-Saturated.

This torsion specimen exhibited the same general appearance seen in many tensile failures, with the initiation site being surrounded by a transition zone and then a coarse zone. The flaking appearance in a radial pattern will also be noted.

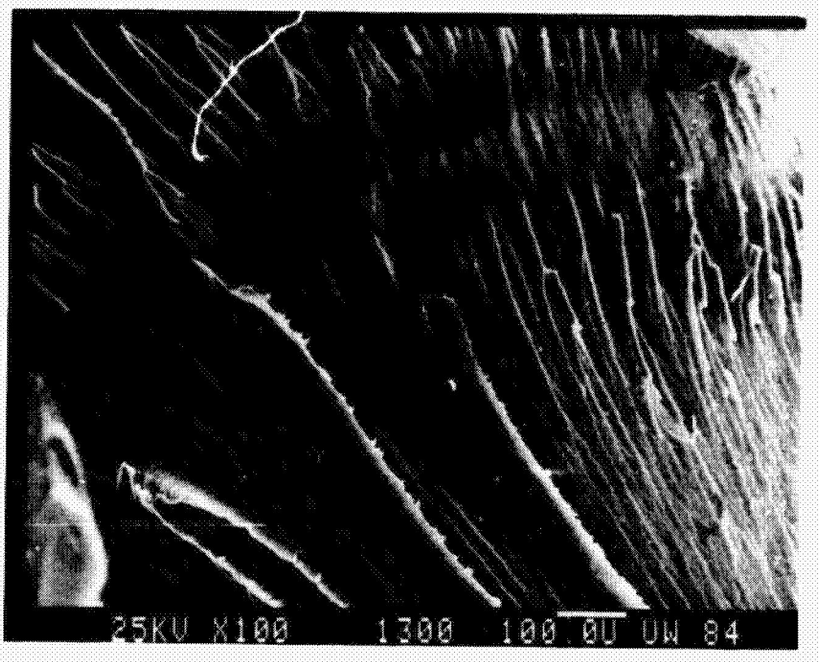

Figure D24. Narmco 5245-C Bismaleimide/Epoxy Torsion Specimen No. LSW011, 82°C, Moisture-Saturated.

This close-up of Figure D23 shows the flaking pattern in greater detail.

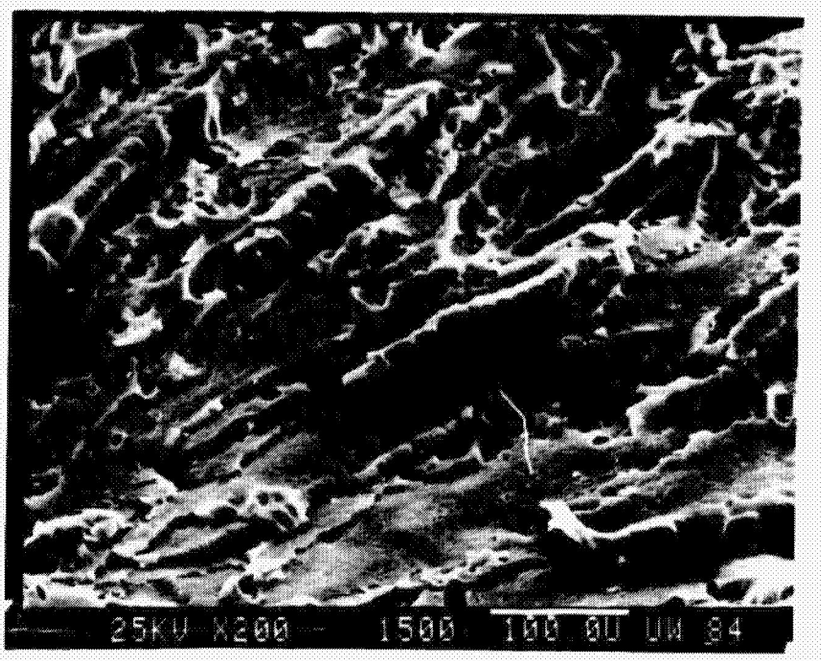

Figure D25. CYCOM 907 Epoxy Iosipescu Shear Specimen No. LIDP05, 23°C, Dry.

This photograph was taken near the notch root region and shows some flaking and coalesced voids in the surface.

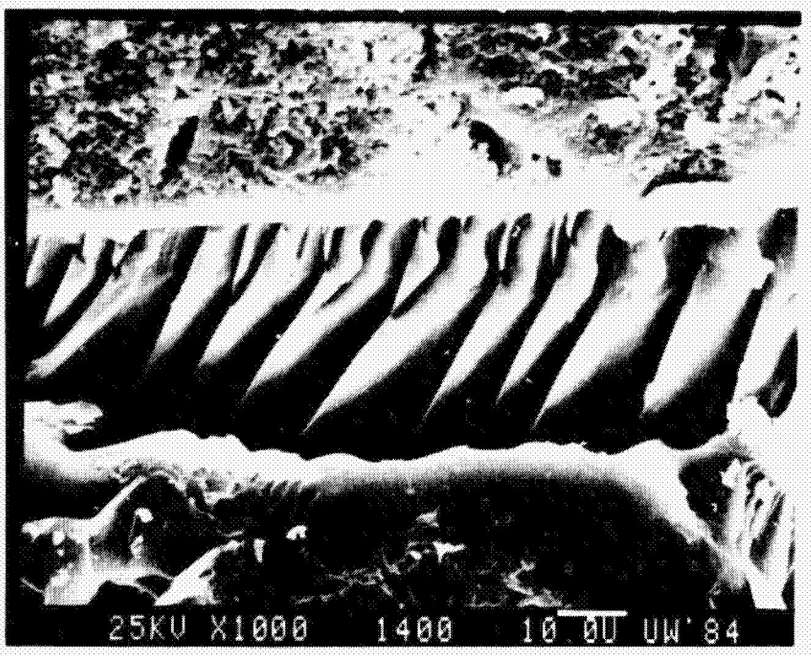

Figure D26. CYCOM 907 Epoxy Iosipescu Shear Specimen No. LIWP04, 23°C, Moisture-Saturated.

This photograph was taken near the notch root region and shows the shear lacerations seen in many shear failures viewed in the SEM.

Figure D27. ERX-4901A(MDA) Epoxy Torsion Specimen No. LSDQ15, 82°C, Dry.

Some flaking can be seen near the right side of the specimen. A large crack in the center of the specimen is also obvious.

Figure D28. EE?-4901A(MDA) Epoxy Torsion Specimen No. LSPQ15, 82°C, Dry.

This close-up of the large crack in the center of Figure D27 shows some swirling pattern, and a remnant sticking out caused by the fracture of the specimen.

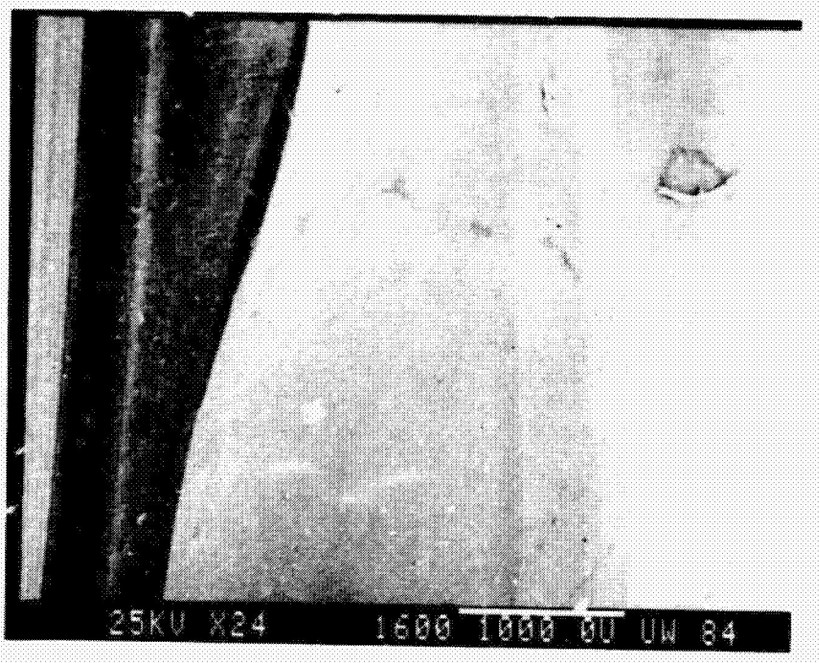

Fig. D29. Hexcel HX-1504 Epoxy Fracture Toughness Specimen No. LFDJ01, 23°C, Dry.

The saw notch is at the left of the photograph. The crack propagated toward the right and possibly arrested at the ridge near the notch. Some coarseness can be seen between the notch and the first ridge.

Figure D30. Hexcel HX-1504 Epoxy Fracture Toughness Specimen No. LFDJ16, 82°C, Dry.

The saw notch is again at the left of the photograph. Little difference can be seen between the room temperature fracture indicated in Figure D29 and the 82°C specimen fracture shown in this photograph.

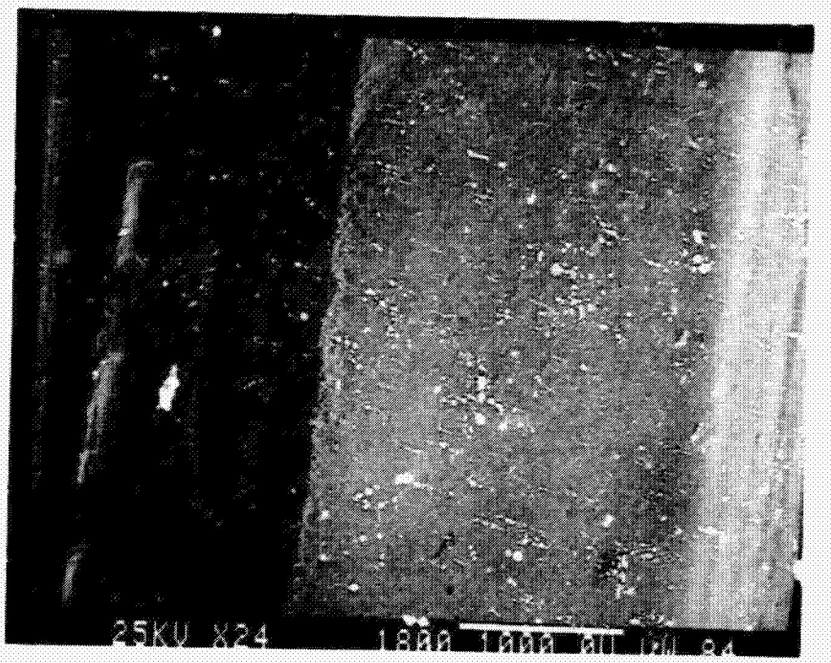

Figure D31. Hexcel HX-1504 Epoxy Fracture Toughness Specimen No. LFDJ25, 121°C, Dry.

With the notch at the left, some cracking is seen between it and the ridge near the center of the specimen. Some coarseness is also apparent to the right of the ridge, where the crack could have arrested and then continued to propagate.

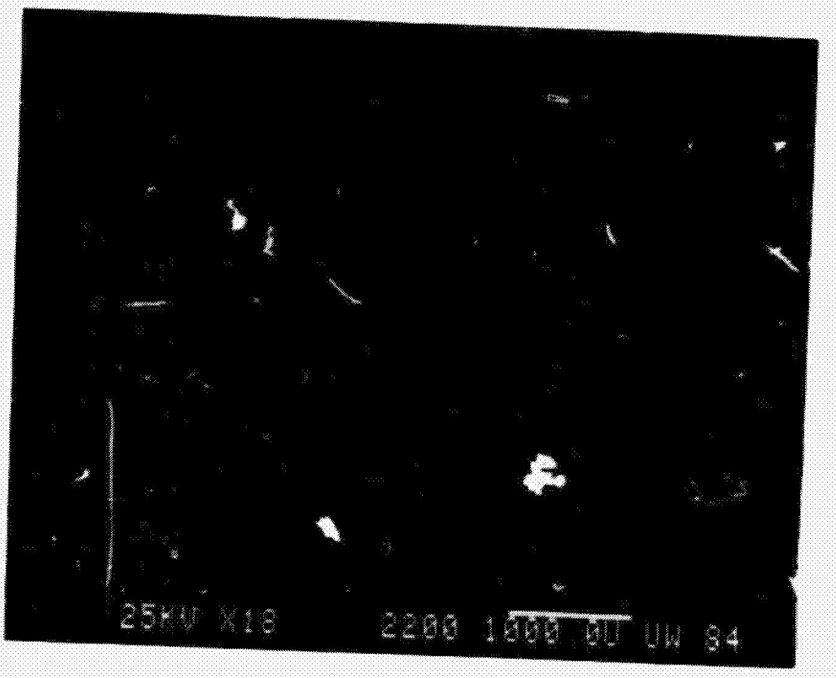

Figure D32. Narmco 5245-C Bismaleimide/Epoxy Fracture Toughness Specimen No. LFD002, 23°C, Dry.

The saw notch is at the left. Possible crack arrest is indicated near the notch, but appears to have propagated unstably afterwards.

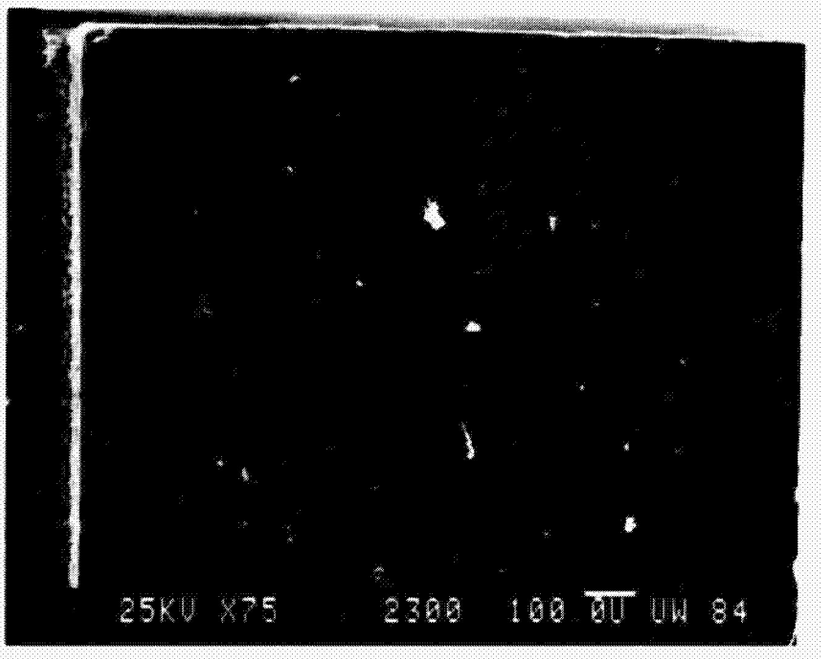

Figure D33. Narmco 5245-C Bismaleimide/Epoxy Fracture Toughness Specimen No. LFD016, 82°C, Dry.

The saw notch is at the left. Several transition regions with varying surface appearances are seen emanating from it.

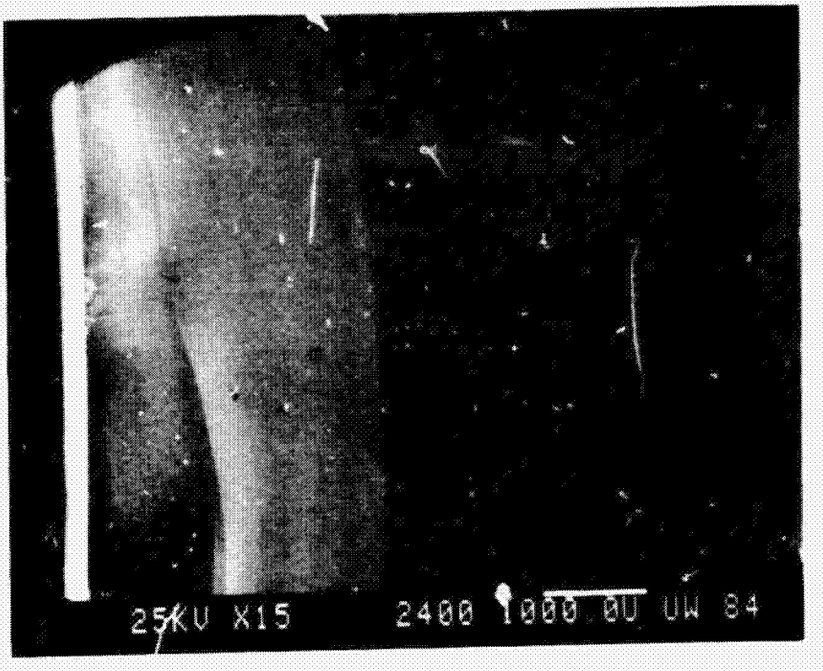

Figure D34. Narmco 5245-C Bismaleimide/Epoxy Fracture Toughness Specimen No. LFD023, 121°C, Dry.

Numerous ridge areas are seen in this photograph, which could be areas where the crack slowed or arrested its movement, or where the crack attempted to move off of the specimen centerline before returning to center.

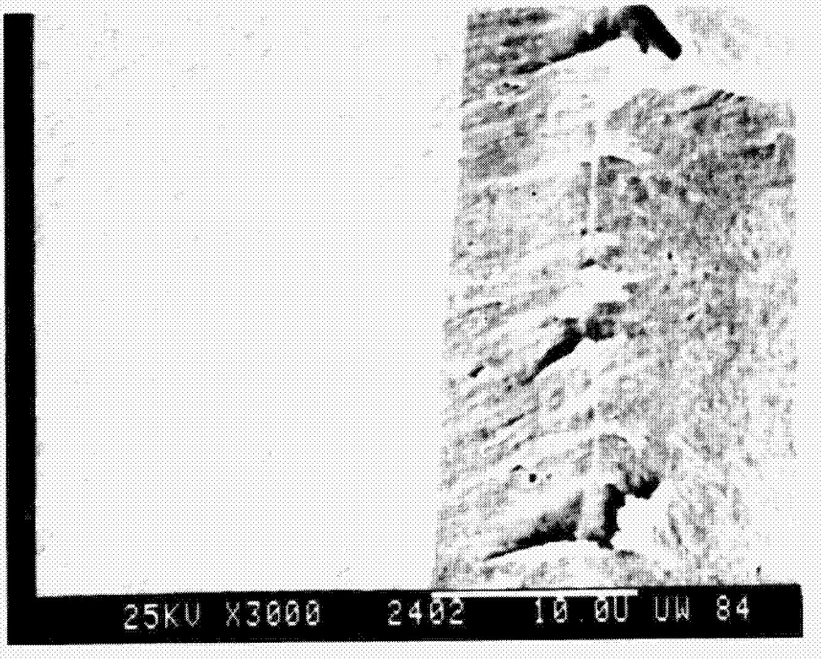

Figure D35. Narmco 5245-C Bismaleimide/Epoxy Fracture Toughness Specimen No. LFD023, 121°C, Dry.

This close-up of the large ridges in Figure D34 shows two different surface features on either side of the ridge where possible crack arrest occurred.

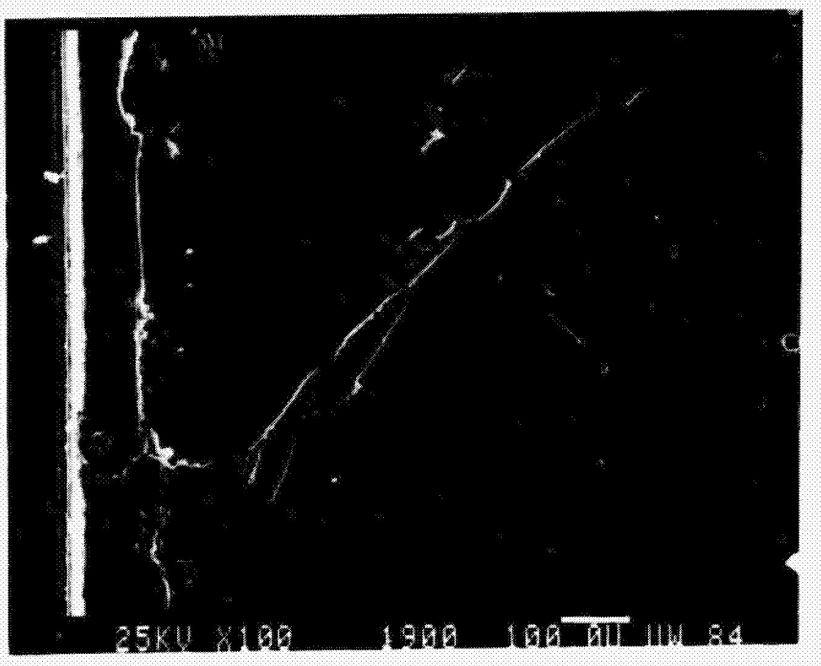

Figure D36. CYCOM 907 Epoxy Fracture Toughness Specimen No. LFDP02, 23°C, Dry.

The saw notch is at the left with the razor blade cut adjacent to it. Much porosity is seen but no evidence of crack arrest.

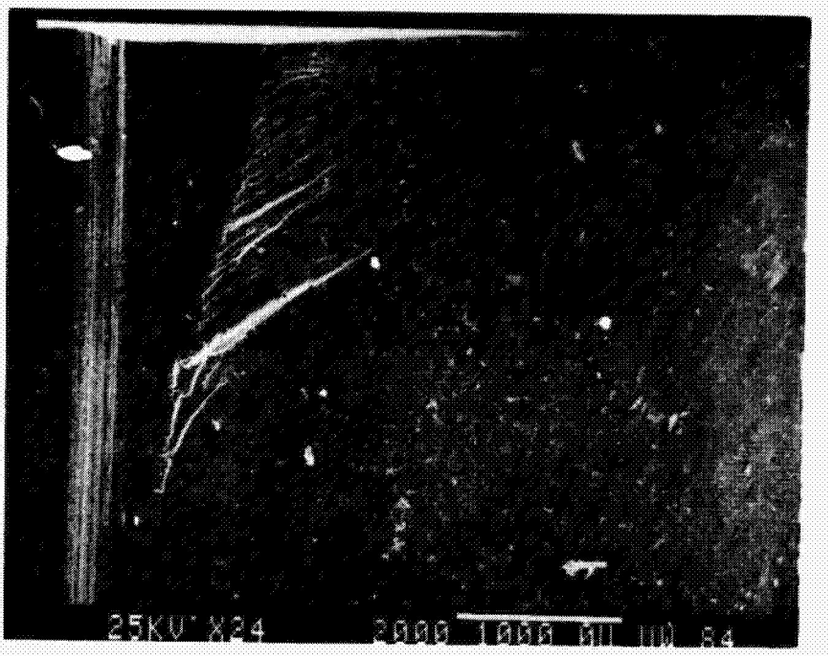

Figure D37. CYCOM 907 Epoxy Fracture Toughness Specimen No. LFDP13, 82°C, Dry.

The saw notch is at the left of the photograph. There appears to be no significance of the large ridge near the notch.

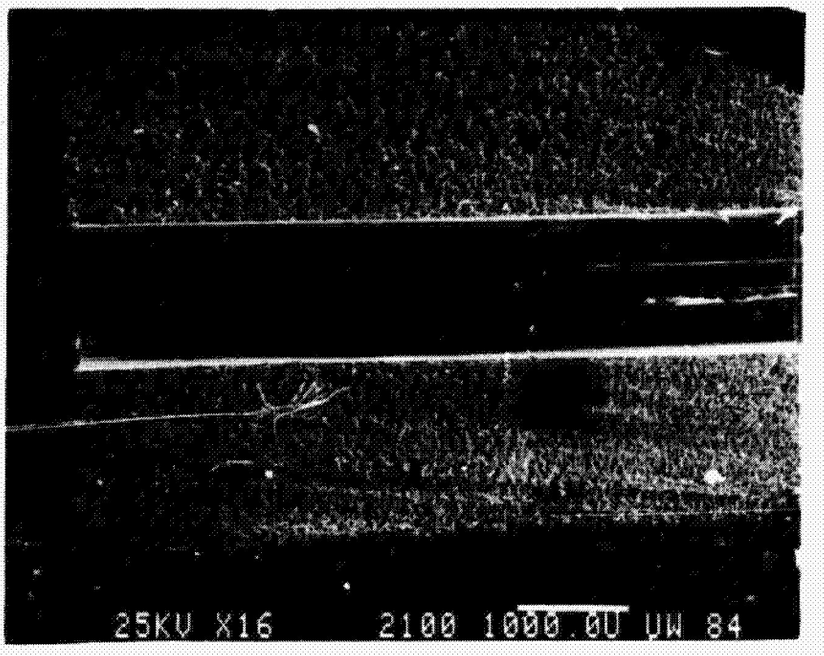

Figure D38. CYCOM 907 Epoxy Fracture Toughness Specimen No. LFDP25, 121°C, Dry.

This overall view looking down the saw notch and razor blade cut shows how the elevated temperature caused strongly plastic behavior for this material.

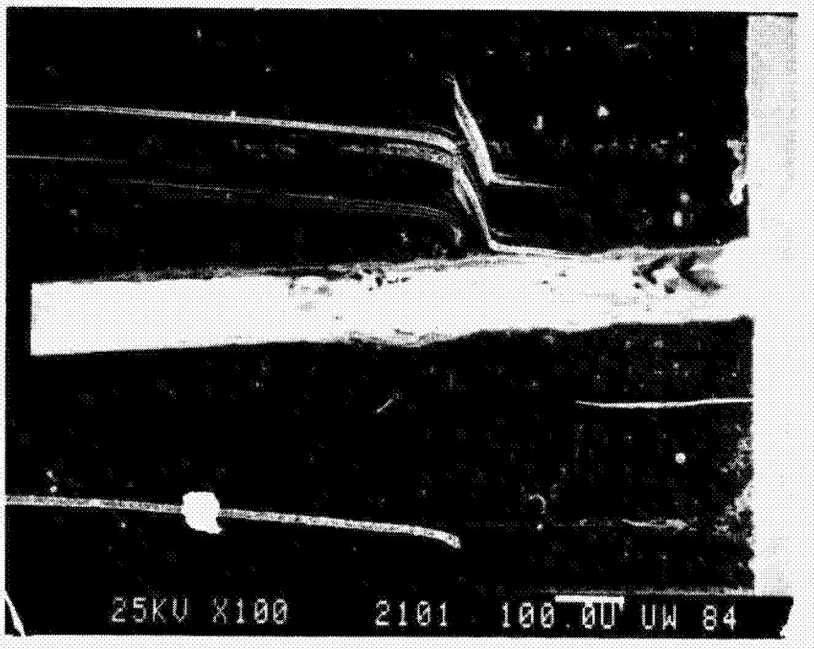

Figure D39. CYCOM 907 Epoxy Fracture Toughness Specimen No. LFDP25, 121°C, Dry.

This close-up of the razor blade starter crack of Figure D38 shows how the crack opened at the elevated temperature.

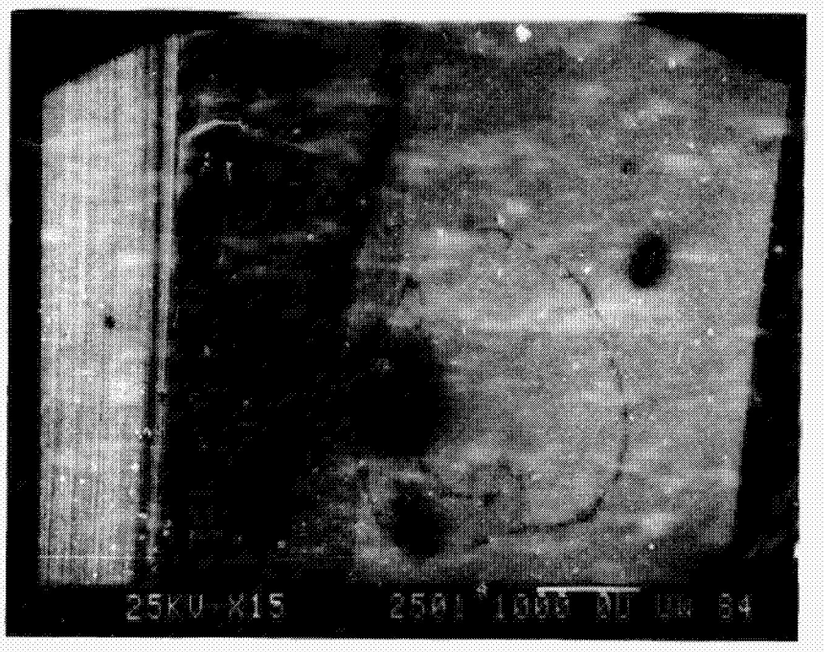

Figure D40. ERX-4901A(MDA) Epoxy Fracture Toughness Specimen No. LFDQ03, 23°C, Dry.

The saw notch is at the left. A large ridge is seen in the center of the photograph and may be a region of crack arrest.

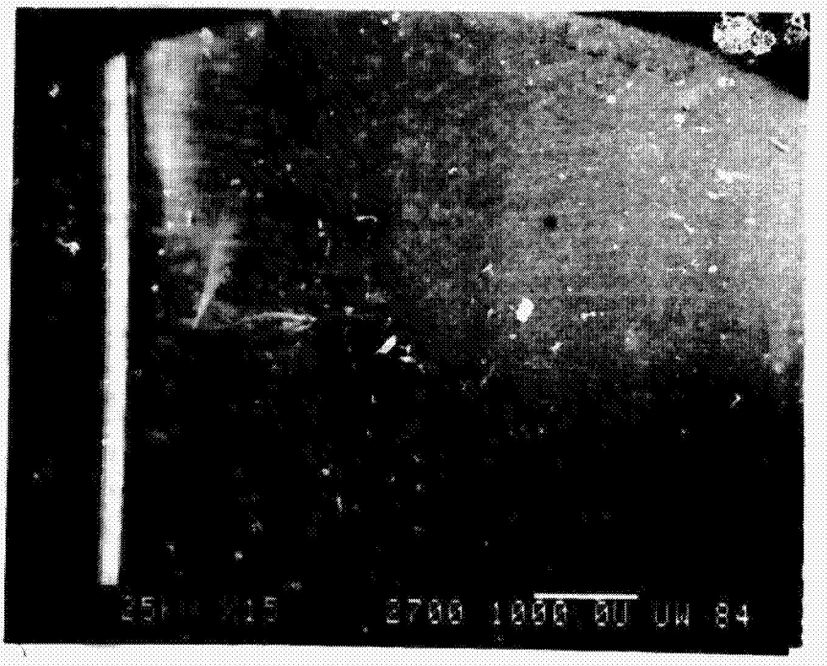

Figure D41. ERX-4901A(MDA) Epoxy Fracture Toughness Specimen No. LFDQ12, 82°C, Dry.

The saw notch is at the left. No distinct fracture surface features were seen for this resin at this test temperature.

1. Report No.	2. Government Accession No.	3. Recipient's Catalog No.
NASA CR-177970		

4. Title and Subtitle	5. Report Date
Mechanical Properties Testing of Candidate Polymer Matrix Materials for Use in High Performance Composites	December 1985
	6. Performing Organization Code

7. Author(s)	8. Performing Organization Report No
Richard S. Zimmerman Donald F. Adams	UWME-DR-401-104-1
	10. Work Unit No.

9. Performing Organization Name and Address	11. Contract or Grant No.
Composite Materials Research Group University of Wyoming Laramie, Wyoming 82071	NAG1-277
	13. Type of Report and Period Covered Contractor Report May 1983-May 1984
12. Sponsoring Agency Name and Address	14. Sponsoring Agency Code
National Aeronautics and Space Administration Washington, D. C. 20546	505-33-33-02

15. Supplementary Notes

Langley Technical Monitor:
Dr. Norman J. Johnston

16. Abstract

The mechanical properties of four candidate neat resin systems for use in graphite/epoxy composites were characterized. This included tensile and shear stiffnesses and strengths, coefficients of thermal and moisture expansion, and fracture toughness. Tests were conducted on specimens in the dry state and moisture-saturated, at temperatures of 23°C, 82°C and 121°C. The neat resins tested were Hexcel HX-1504, Narmco 5245-C, American Cyanamid CYCOM 907, and Union Carbide ERX-4901A (MDA). Results were compared with those obtained for four other epoxy resins tested in a prior program, viz, Hercules 3502, 2220-1, and 2220-3, and Ciba-Geigy Fibredux 914, as well as with available Hercules 3501-6 data.

Scanning electron microscopic examination of fracture surfaces was performed, to permit the correlation of observed failure modes with the environmental test conditions.

A finite element micromechanics analysis was used to predict unidirectional composite response under various test conditions, using the measured neat resin properties as input data.

17. Key Words (Suggested by Author(s))	18. Distribution Statement
polymer matrices toughened epoxies mechanical properties micromechanics predictions	Unclassified, Unlimited Subject category 24

19. Security Classif. (of this report)	20. Security Classif. (of this page)	21. No. of Pages	22. Price*
Unclassified	Unclassified	301	A14

*For sale by the National Technical Information Service, Springfield, Virginia 22161